MASS SPECTROMETRY OF FLUORINATED METAL β-DIKETONATES AND MONOTHIO-β-DIKETONATES

by

Mark Lindsay John Reimer

B.Sc.(Hons.), University of Manitoba, 1981

A Thesis

Submitted to the Faculty of Graduate Studies

in partial fulfillment of the requirements

for the degree of

Doctor of Philosophy

University of Manitoba

Winnipeg, Manitoba

February, 1988.

MASS SPECTROMETRY OF FLUORINATED METAL B-DIKETONATES AND MONOTHIO-B-DIKETONATES

BY

MARK LINDSAY JOHN REIMER

A thesis submitted to the Faculty of Graduate Studies of the University of Manitoba in partial fulfillment of the requirements of the degree of

DOCTOR OF PHILOSOPHY

C. RESULTS

1. General Remarks

The number codes and IUPAC names of the fifteen β-diketones and twelve monothio-β-diketones used as ligands in this study are shown in Table 6. Table 7 provides a list of the Al(III), Ga(III), Co(III), Ni(II), Pd(II), Cu(II) and Zn(II) complexes for which mass spectra have been obtained. Initial consideration will be given to the β-diketonates on a "metal-by-metal" basis, followed by an analogous treatment of the monothio-β-diketonate complexes. Discussion will focus upon the major metal-containing ions; analysis of organic fragments will be undertaken only when pertinent to the elucidation of decomposition pathways involving metal-containing ions.

Results are tabulated as percent relative abundances (%RA; most abundant ion in spectrum normalized to 100.0), m/z values (in parentheses), and percentages of the total ion current (%TIC). The %RA values are normally based on the most abundant isotope of each element; exceptions include ions containing chlorine and/or metal atoms, in which case contributions from all isotopes of these atoms are considered. Values of m/z refer to the most abundant isotope of each element. Abundance measurements for peaks differing by only one or two mass units (eg. $[Met(L-H)]^+$, $[MetL]^+$ and $[MetHL]^+$) are corrected for contributions due to both metal and nonmetal isotopes using the post-acquisition routine ISO on the VG Analytical 11-250 data system (software release B1.0).

Table 6. Numbering system and IUPAC names of ligands.

$C_6H_5CXCH_2COCHF_2$	$C_4H_3SCXCH_2COCHF_2$	$C_6H_5CXCH_2COCF_3$
1	**2**	**3**
a: X=O	**a:** X=O	**a:** X=O
		b: X=S
$C_6H_4CH_3CXCH_2COCF_3$	$C_6H_4FCXCH_2COCF_3$	$C_6H_4ClCXCH_2COCF_3$
4	**5**	**6**
a: X=O	**a:** X=O	**a:** X=O
b: X=S	**b:** X=S	
$C_6H_4OCH_3CXCH_2COCF_3$	$C_4H_3SCXCH_2COCF_3$	$C_4H_2SCH_3CXCH_2COCF_3$
7	**8**	**9**
	a: X=O	**a:** X=O
b: X=S	**b:** X=S	**b:** X=S
$C_4H_2SClCXCH_2COCF_3$	$C_4H_3OCXCH_2COCF_3$	$C_{10}H_7CXCH_2COCF_3$
10	**11**	**12**
a: X=O	**a:** X=O	**a:** X=O
$C_6H_5CXCH_2COC_2F_5$	$C_4H_3SCXCH_2COC_2F_5$	$C_{10}H_7CXCH_2COC_2F_5$
13	**14**	**15**
a: X=O	**a:** X=O	
b: X=S	**b:** X=S	**b:** X=S
$C_6H_5CXCH_2COC_3F_7$	$C_4H_3SCXCH_2COC_3F_7$	$C_{10}H_7CXCH_2COC_3F_7$
16	**17**	**18**
a: X=O	**a:** X=O	
b: X=S	**b:** X=S	**b:** X=S

Table 6. (continued).

1a. 1,1-difluoro-4-phenyl-2,4-butanedione

2a. 1,1-difluoro-4-(2'-thienyl)-2,4-butanedione

3a. 1,1,1-trifluoro-4-phenyl-2,4-butanedione
b. 1,1,1-trifluoro-4-mercapto-4-phenyl-but-3-en-2-one

4a. 1,1,1-trifluoro-4-(4'-methylphenyl)-2,4-butanedione
b. 1,1,1-trifluoro-4-mercapto-4-(4'-methylphenyl)-but-3-en-2-one

5a. 1,1,1-trifluoro-4-(4'-fluorophenyl)-2,4-butanedione
b. 1,1,1-trifluoro-4-mercapto-4-(4'-fluorophenyl)-but-3-en-2-one

6a. 1,1,1-trifluoro-4-(4'-chlorophenyl)-2,4-butanedione

7b. 1,1,1-trifluoro-4-mercapto-4-(4'-methoxyphenyl)-but-3-en-2-one

8a. 1,1,1-trifluoro-4-(2'-thienyl)-2,4-butanedione
b. 1,1,1-trifluoro-4-mercapto-4-(2'-thienyl)-but-3-en-2-one

9a. 1,1,1-trifluoro-4-(5'-methyl-2'-thienyl)-2,4-butanedione
b. 1,1,1-trifluoro-4-mercapto-4-(5'-methyl-2'-thienyl)-but-3-en-2-one

10a. 1,1,1-trifluoro-4-(5'-chloro-2'-thienyl)-2,4-butanedione

11a. 1,1,1-trifluoro-4-(2'-furyl)-2,4-butanedione

12a. 1,1,1-trifluoro-4-(2'-naphthyl)-2,4-butanedione

13a. 1,1,1,2,2-pentafluoro-5-phenyl-3,5-pentanedione
b. 1,1,1,2,2-pentafluoro-5-mercapto-5-phenyl-pent-4-en-3-one

14a. 1,1,1,2,2-pentafluoro-5-(2'-thienyl)-3,5-pentanedione
b. 1,1,1,2,2-pentafluoro-5-mercapto-5-(2'-thienyl)-pent-4-en-3-one

15b. 1,1,1,2,2-pentafluoro-5-mercapto-5-(2'-naphthyl)-pent-4-en-3-one

16a. 1,1,1,2,2,3,3-heptafluoro-6-phenyl-4,6-hexanedione
b. 1,1,1,2,2,3,3-heptafluoro-6-mercapto-6-phenyl-hex-5-en-4-one

17a. 1,1,1,2,2,3,3-heptafluoro-6-(2'-thienyl)-4,6-hexanedione
b. 1,1,1,2,2,3,3-heptafluoro-6-mercapto-6-(2'-thienyl)-hex-5-en-4-one

18b. 1,1,1,2,2,3,3-heptafluoro-6-mercapto-6-(2'-naphthyl)-hex-5-en-4-one

Table 7. Listing of metal β-diketonates and monothio-β-diketonates.

See Table 6 for explanation of number codes.

β-diketonates:	**Al–1a, –2a, –3a, –4a, –5a, –8a, –9a**
	Ga–1a, –2a, –3a, –4a, –5a, –8a, –12a
	Co–1a, –2a, –3a, –4a, –6a, –8a, –10a, –11a, –12a, –13a, –14a, –16a, –17a
	Ni–1a, –2a, –3a, –8a, –9a, –13a, –14a, –16a, –17a
	Pd–3a, –8a, –13a, –14a, –16a, –17a
	Cu–1a, –2a, –3a, –8a, –9a, –11a, –12a, –13a, –14a, –16a, –17a
	Zn–1a, –2a, –3a, –8a, –9a, –13a, –14a, –16a, –17a
Monothio-β-diketonates:	**Co–13b, –14b, –15b, –16b, –17b, –18b**
	Ni–3b, –5b, –7b, –8b, –9b, –13b, –14b, –15b, –16b, –17b, –18b
	Pd–3b, –7b, –8b, –13b, –14b, –15b, –16b, –17b, –18b
	Cu–3b, –4b, –5b, –8b, –13b, –16b
	Zn–3b, –5b, –7b, –8b, –9b

All of the mass spectra (Figures 29-127) depict monoisotopic data.

Metastable transitions shown in the tabulated data that are not attributable to linked-scanning experiments have been obtained through work performed on the Hitachi single-focusing mass spectrometer and are calculated by means of the standard relationship: $m^* = (m_d)^2/m_p$, where m^* is the metastable mass, m_d is the mass of the daughter ion, and m_p is the parent ion mass.

Many of the conventions concerning the representation of structure and bonding in metal-containing ions proposed by Westmore (106,173) have been adopted here. For instance, whenever possible, ions are depicted as even-electron (EE^+) structures accommodated by appropriate changes in the formal oxidation state of the metal. In other cases, the symbol $\rceil^{+\cdot}$ is used when the location of the charge and unpaired electron is not specified. An arrow originating from a donor atom to the metal represents a coordinate bond where both electrons are formally associated with, and donated by, the ligand (no formal change in metal oxidation state required), while a dash "—" represents a bond formed by equal sharing of electrons (a formal unit increase of metal oxidation state required). Half-headed ("fishhook") and full-headed arrows originating from a bond or a site of non-bonded electrons indicate the movement of one or two electrons, respectively. Other general symbols include $[M]^{+\cdot}$ = molecular ion, L = ligand and Met = metal (if not specified).

For purposes of clarity and ease of reading, all tables, figures and schemes pertaining to a given set of metal chelates are grouped together at the end of each section.

2. Mass Spectra of β-diketonates

(a) Al(III) β-diketonates

Relative abundance data for the seven Al(III) β-diketonates studied appear in Tables 8-10. Plots of their corresponding EI mass spectra are presented in Figures 29-35. A linked-scanning, metastable study was conducted on **Al-3a.** The mass spectrum of one of the chelates (**Al-3a**) has been previously reported (128).

The fragmentations of the complexes possessing a trifluoromethyl substituent (R' = CF_3; Tables 8 and 9) are very similar, so their spectra will be discussed together. Suggested decomposition pathways for these chelates are given in Scheme 16. The most abundant ion in all spectra is the EE^+ ion $[Al(III)L_2]^+$; metastable evidence confirms that it is formed via the direct loss of an intact ligand radical ($L^{\cdot}$) from the molecular ion $[Al(III)L_3]^{+\cdot}$. Elimination of the $OE^{\cdot}$ neutral $F^{\cdot}$ from $[M]^{+\cdot}$ is observed in all but one complex (**Al-9a**), albeit the relative abundance of this ion is very low (<2%). Subsequent fragmentation of $[Al(III)L_2]^+$ leads primarily to daughter ions formed via the loss of EE^o neutrals (CF_2, (L-R')). These observations are consistent with the valency-change concept of Lacey and Shannon (109) as well as Westmore's axiom (106) regarding the preferred fragmentation pathways of a metal β-diketonate in which the metal is not amenable to either an increase or decrease in oxidation state. Hence aluminum chelates, stable only in the Al^{3+} oxidation state, are

restricted to losses of EE^{o} fragments after an initial OE· radical loss.

Possible mechanisms for the elimination of CF_2 and (L-R') from $[Al(III)L_2]^+$ are given in Scheme 17. Facile fluorine transfer to the aluminum center is predicted by HSAB theory; Al(III) is a hard acid and F is a hard base. The alternative pathway from $[Al(III)L_2]^+$ to $[Al(III)FL]^+$ shown in Scheme 17 involves the migration of a fluorine atom to the metal followed by the elimination of the remainder of the ligand. The EE^{o} neutral species (L-F) lost in this process can be pictured as having a cyclic structure:

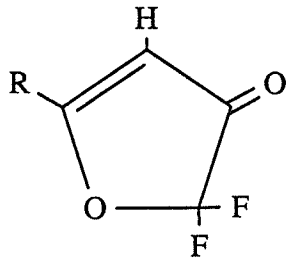

(L-F)

Metastable evidence indicates that the loss of (L-F) is also prevalent in the formation of $[Al(III)F_2(L-R')]^+$ from $[Al(III)FL(L-R')]^+$. This process is illustrated in Scheme 18.

The decomposition of $[Al(III)FL]^+$ to yield $[Al(III)F_2(L-R')]^+$ (Scheme 19) involves fluorine transfer and the elimination of CF_2 in a manner similar to that described in Scheme 17.

Two trends in hard-soft/acid-base behavior can be discerned from these spectra, both of which correlate the hardness of an acceptor as a function of the other groups bonded to it. The first case involves the

transfer of fluorine to a "bare" aluminum center:

$$[Al(III)L_2]^+ \longrightarrow [Al(III)FL(L\text{-}R')]^+$$

versus the migration of fluorine to an aluminum center that already has a fluorine bonded to it:

$$[Al(III)FL]^+ \longrightarrow [Al(III)F_2(L\text{-}R')]^+$$

A comparison of the %TIC carried by $[Al(III)FL(L\text{-}R')]^+$ (average 3.2%) and $[Al(III)F_2(L\text{-}R')]^+$ (average 5.5%) suggests that for these five complexes, fluorine transfer occurs more readily when a fluorine is already bonded to the aluminum. This phenomenon can be viewed as an example of the symbiotic effect described by Jorgensen (157) in which the presence of hard groups on an acceptor facilitates the addition of other hard substituents to it. The second relationship involves the nature of the chelate ring substituents (R groups), which also appears to play a role in the relative ease of fluorine migration. An examination of the %TIC carried by the three types of fluorine transfer ions ($[Al(III)FL(L\text{-}R')]^+$, $[Al(III)FL]^+$ and $[Al(III)F_2(L\text{-}R')]^+$) for each of the five aryl-substituted complexes reveals a progression in ion stabilities based on the type of R group present (average %TIC in parentheses): R = 4-methylphenyl (2.5) < phenyl (4.2) = 5-methyl-2-thienyl (4.3) < 4-fluorophenyl (5.1) < 2-thienyl (6.0). In terms of HSAB theory, the introduction of a methyl substituent into the R group (ie. R = $C_6H_4CH_3$, $C_4H_2SCH_3$) results in a softer, more polarizable moiety as compared to the non-methylated analog. As a consequence, the aluminum center is softened and fluorine transfer declines in significance. Conversely, the addition of a strongly electron-

withdrawing fluorine atom to the phenyl group (R = C_6H_4F) effects a concomitant hardening of the metal, yielding a higher %TIC for the three fluorine-transfer ions.

The losses of a ligand radical and a fluorine radical from $[Al(III)L_2]^+$ (leading to the formation of $[Al(III)L]^{+\cdot}$ and $[Al(III)L(L-F)]^{+\cdot}$, respectively) observed in compounds **Al-3a** and **Al-5a** represent clear exceptions to the 'even-electron rule' (174). These processes are also difficult to rationalize using the concepts of metal valency change, as aluminum oxidation states other than +3 are extremely rare. It must be noted however, that the relative abundances of $[Al(III)L]^{+\cdot}$ and $[Al(III)L(L-F)]^{+\cdot}$ are very low (<1.5%) and as such may be regarded as relatively minor fragmentation products.

Proposed fragmentation pathways for the difluoromethyl-substituted Al(III) β-diketonates **Al-1a** and **Al-2a** (Table 10) are shown in Scheme 20. As was seen in the trifluoromethyl derivatives, the molecular ion is only moderately abundant, while $[Al(III)L_2]^+$ is the base peak in both spectra. Many of the remaining aluminum-containing ions are the result of EE^o neutral losses (CO, CHF, (L-F)) from $[Al(III)L_2]^+$. Suggested mechanisms for the formation of $[Al(III)FL(L-COF)]^+$ in **Al-2a** and $[Al(III)FL(L-R')]^+$ and $[Al(III)FL]^+$ in complexes **Al-1a** and **Al-2a** are depicted in Schemes 21 and 22, respectively, while the formation of $[Al(III)F_2(L-R')]^+$ from $[Al(III)FL(L-R')]^+$ (Scheme 18) and from $[Al(III)FL]^+$ (Scheme 19) has already been discussed. Although fluorine transfer to the metal is proposed in each of these four mechanisms, the resultant ions are considerably lower in abundance than those derived from fluorine migrations in the corresponding CF_3-substituted

complexes. Two plausible explanations for this behavior can be suggested. First, the migration of fluorine to aluminum in the formation of $[Al(III)FL(L\text{–}CHF_2)]^+$ involves the loss of a CHF moiety, which is a considerably less stable neutral product than the CF_2 group generated in the fluorine transfer:

$$[Al(III)L_2]^+ \longrightarrow [Al(III)FL(L\text{–}CF_3)]^+$$

found in the CF_3 derivatives. In fact, CF_2 has a strongly resonance-stabilized structure (99). And secondly, as viewed from a purely statistical standpoint, the opportunities for fluorine transfer are diminished in CHF_2 (2 fluorine atoms) as compared to CF_3 (3 fluorine atoms).

Scheme 23 outlines a proposed mechanism for the elimination of $Al(III)F_3$ from $[Al(III)F_2(L\text{–}COF)]^+$ in **Al–1a** and **Al–2a.** Although unconfirmed by metastable evidence, this process has a precedent in the mass spectra of Al(III) hexafluoroacetylacetonates (124). The formation of $[Al(III)F_2(L\text{–}COF)]^+$ from $[Al(III)FL]^+$ is comparable to the formation of$[Al(III)FL(L\text{–}COF)]^+$ from $[Al(III)L_2]^+$ as shown in Scheme 21. The two metal-based fluorines in $[Al(III)F_2(L\text{–}COF)]^+$ "harden" the acceptor characteristics of the aluminum center, thereby allowing a third fluorine transfer process to occur. The result is the expulsion of $Al(III)F_3$ and the creation of the EE^+ organic fragment $[L\text{–}COF_2]^+$.

The origins and identities of the ions at m/z 268 in **Al–2a** (possibly $[Al(III)F_2L]^{+\cdot}$) and m/z 258 in **Al–1a** are not established.

Table 8. 70 eV-EI mass spectra of compounds **A1-3a, A1-4a** and **A1-5a.**

	A1-3a			**A1-4a**			**A1-5a**		
R =	$-C_6H_5$			$-C_6H_4CH_3$			$-C_6H_4F$		
R'=	$-CF_3$			$-CF_3$			$-CF_3$		
ION	%RA	m/z	%TIC	%RA	m/z	%TIC	%RA	m/z	%TIC
$[AlL_3]^+$ (a)	13.5	(672)	8.7	14.1	(714)	7.3	16.6	(726)	8.6
$[AlL_2(L-F)]^+$	0.9	(653)	0.6	0.8	(695)	0.4	1.6	(707)	0.8
$[AlL_2]^+$ (b)	[a]100.0	(457)	64.3	[a]100.0	(485)	52.0	[a]100.0	(493)	51.6
$[AlL(L-F)]^+$	[b]1.2	(438)	0.8	-	(466)	-	1.4	(474)	0.7
$[AlFL(L-R')]^+$(c)	[b]7.0	(407)	4.5	[b]3.7	(435)	1.9	[b]7.3	(443)	3.8
$[AlFL]^+$ (d)	[b,c]6.2	(261)	4.0	4.9	(275)	2.5	9.8	(279)	5.1
$[AlL]^+$	[b]0.8	(242)	0.5	-	(256)	-	1.3	(260)	0.7
$[AlF_2(L-R')]^+$	[c,d]6.6	(211)	4.2	5.8	(225)	3.0	12.2	(229)	6.3
$[HL]^+$	-	(216)	-	3.5	(230)	1.8	1.2	(234)	0.6
$[HL-R']^+$	-	(147)	-	4.9	(161)	2.5	1.9	(165)	1.0
$[RCO]^+$	[c]13.0	(105)	8.4	28.8	(119)	15.0	28.1	(123)	14.5
$[R]^+$	4.5	(77)	2.9	12.5	(91)	6.5	6.6	(95)	3.4
$[R']^+$	1.8	(69)	1.2	13.4	(69)	7.0	2.8	(69)	1.4

[a] Identified metastable transitions are indicated by superscripts which relate the daughter ion to its precursor as labelled in column 1.

Table 9. 70 eV-EI mass spectra of compounds **A1–8a** and **A1–9a.**

	A1–8a			**A1–9a**		
R =	$-C_4H_3S$			$-C_4H_2SCH_3$		
R'=	$-CF_3$			$-CF_3$		
ION	%RA	m/z	%TIC	%RA	m/z	%TIC
$[AlL_3]^+$	22.3	(690)	11.8	7.4	(732)	3.8
$[AlL_2(L-F)]^+$	1.5	(671)	0.8	-	(713)	-
$[AlL_2]^+$	100.0	(469)	53.1	100.0	(497)	51.5
$[AlFL(L-R')]^+$	7.2	(419)	3.8	4.1	(447)	2.1
$[AlFL]^+$	11.4	(267)	6.1	9.8	(281)	5.1
$[AlF_2(L-R')]^+$	15.2	(217)	8.1	11.3	(231)	5.8
$[HL]^+$	-	(222)	-	1.6	(236)	0.8
$[HL-R']^+$	-	(153)	-	2.2	(167)	1.1
$[RCO]^+$	24.4	(111)	13.0	40.0	(125)	20.6
$[R]^+$	-	(83)	-	2.5	(97)	1.3
$[R']^+$	6.2	(69)	3.3	7.3	(69)	3.8

Table 10. 70 eV-EI mass spectra of compounds **A1-1a** and **A1-2a.**

	A1-1a	**A1-2a**
R =	$-C_6H_5$	$-C_4H_3S$
R'=	$-CHF_2$	$-CHF_2$

ION	%RA	m/z	%TIC	%RA	m/z	%TIC
$[AlL_3]^+$	15.3	(618)	7.1	6.0	(636)	2.7
$[AlL_2]^+$	100.0	(421)	46.4	100.0	(433)	45.1
$[AlFL(L-COF)]^+$	-	(393)	-	1.7	(405)	0.8
$[AlFL(L-R')]^+$	-	(389)	-	1.5	(401)	0.7
$[AlF_2L]^+$	-	(262)	-	1.2	(268)	0.5
	3.5	(258)	1.6	-	(264)	-
$[AlFL]^+$	1.5	(243)	0.7	1.9	(249)	0.9
$[AlL]^+$	1.4	(224)	0.7	1.2	(230)	0.5
$[AlF_2(L-COF)]^+$	2.8	(215)	1.3	7.0	(221)	3.2
$[AlF_2(L-R')]^+$	1.8	(211)	0.8	1.3	(217)	0.5
$[HL-R']^+$	10.3	(147)	4.8	2.4	(153)	1.1
$[L-COF_2]^+$	7.6	(131)	3.5	13.1	(137)	5.9
$[RCO]^+$	36.7	(105)	17.0	55.6	(111)	25.1
$[RC_2H_2]^+$	13.8	(103)	6.4	16.5	(109)	7.4
$[RCCH]^+$	4.5	(102)	2.1	4.7	(108)	2.1
$[R]^+$	11.5	(77)	5.3	2.7	(83)	1.2
$[C_3HO_2]^+$	6.4	(69)	3.0	4.6	(69)	2.1

Figure 29.

Normalized 70 eV-EI mass spectrum of

tris[1,1,1-trifluoro-4-phenyl-2,4-butanedionato]Al(III)

{**Al-3a**}.

m/z $[M]^{+\cdot}$ = 672, $[L]^{+}$ = 215

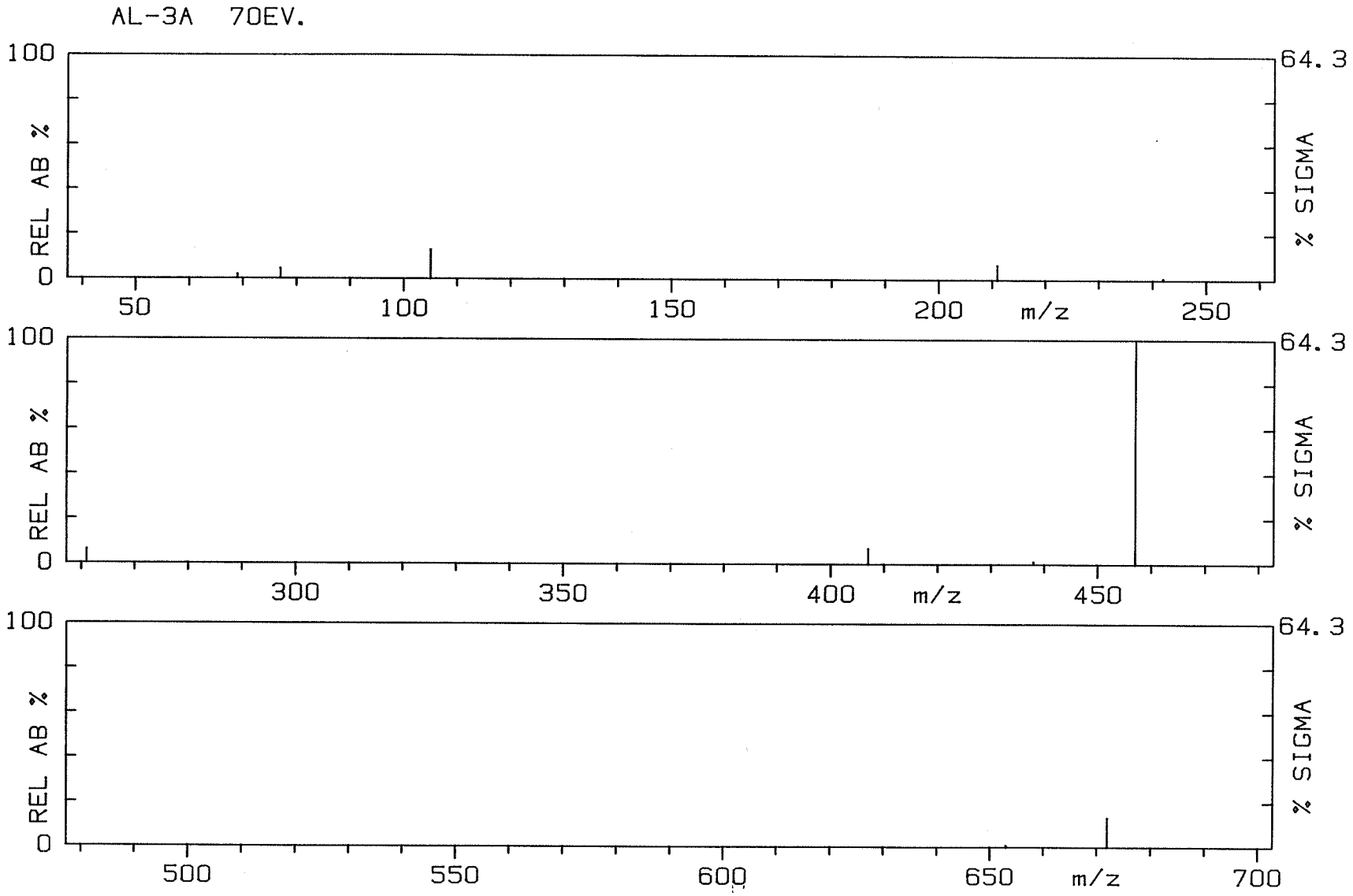
AL-3A 70EV.
100
REL AB %
0
50
100
150
200
m/z
250
64.3
% SIGMA
100
REL AB %
0
300
350
400
m/z
450
64.3
% SIGMA
100
REL AB %
0
500
550
600
650
m/z
700
64.3
% SIGMA

Figure 30.

Normalized 70 eV-EI mass spectrum of

tris[1,1,1-trifluoro-4-(4'-methylphenyl)-2,4-butanedionato]Al(III)

{**Al-4a**}.

m/z $[M]^{+\cdot}$ = 714, $[L]^{+}$ = 229

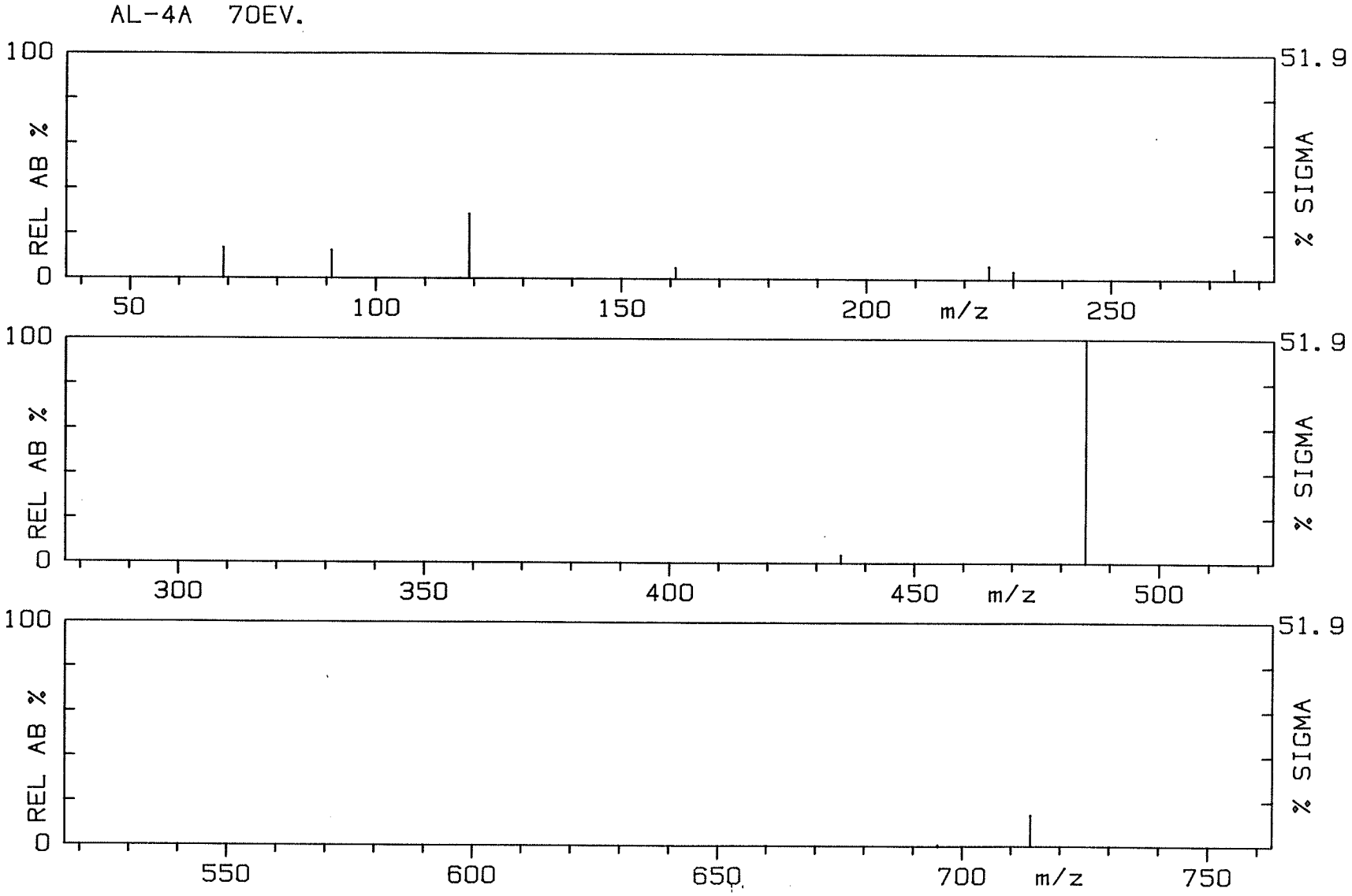
AL-4A 70EV.
100
0
REL AB %
51.9
% SIGMA
50
100
150
200
m/z
250
300
350
400
450
500
550
600
650
700
750

Figure 31.

Normalized 70 eV-EI mass spectrum of

tris[1,1,1-trifluoro-4-(4'-fluorophenyl)-2,4-butanedionato]Al(III)

{Al-5a}.

m/z $[M]^{+\cdot}$ = 726, $[L]^{+}$ = 233

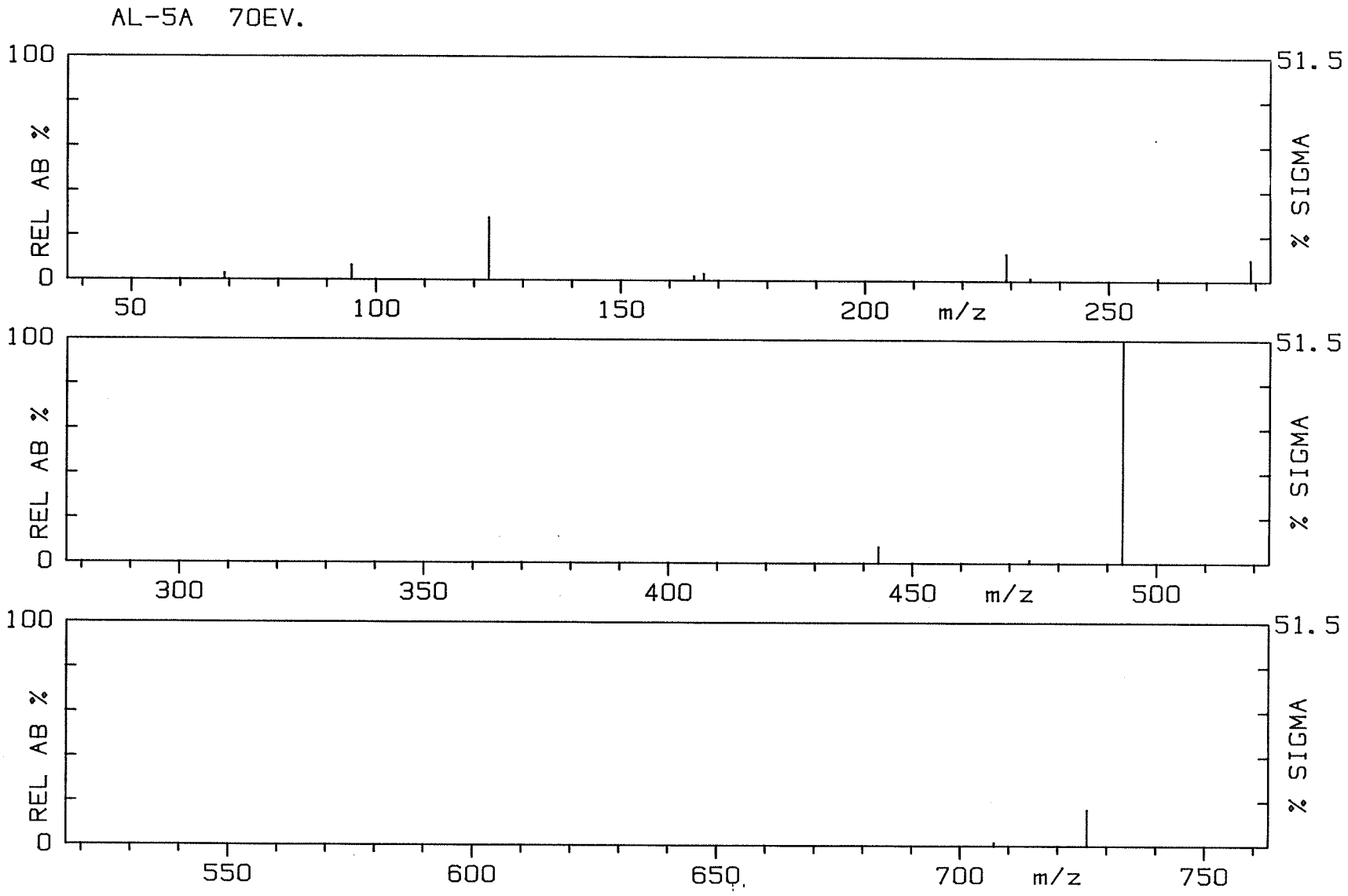
AL-5A 70EV.
100
REL AB %
0
50
100
150
200
m/z
250
51.5
% SIGMA
100
REL AB %
0
300
350
400
450
m/z
500
51.5
% SIGMA
100
REL AB %
0
550
600
650
700
m/z
750
51.5
% SIGMA

Figure 32.

Normalized 70 eV-EI mass spectrum of

tris[1,1,1-trifluoro-4-(2'-thienyl)-2,4-butanedionato]Al(III)

(**Al-8a**).

m/z $[M]^{+\cdot}$ = 690, $[L]^{+}$ = 221

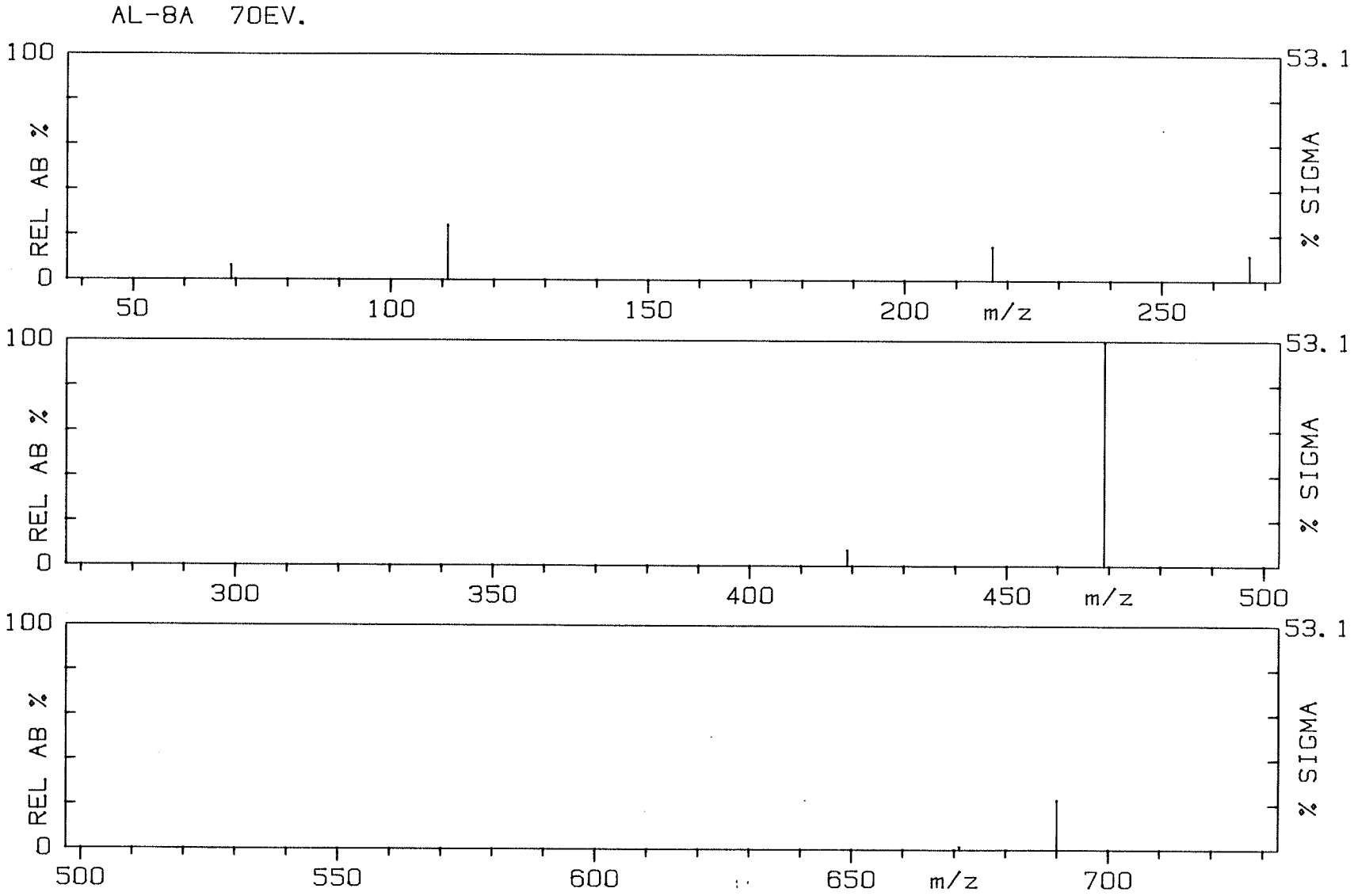
AL-8A 70EV.
100
0
REL AB %
53.1
% SIGMA
50
100
150
200
m/z
250
300
350
400
450
500
550
600
650
700

Figure 33.

Normalized 70 eV-EI mass spectrum of

tris[1,1,1-trifluoro-4-(5'-methyl-2'-thienyl)-2,4-butanedionato]Al(III)

{**Al-9a**}.

m/z $[M]^{+\cdot}$ = 732, $[L]^{+}$ = 235

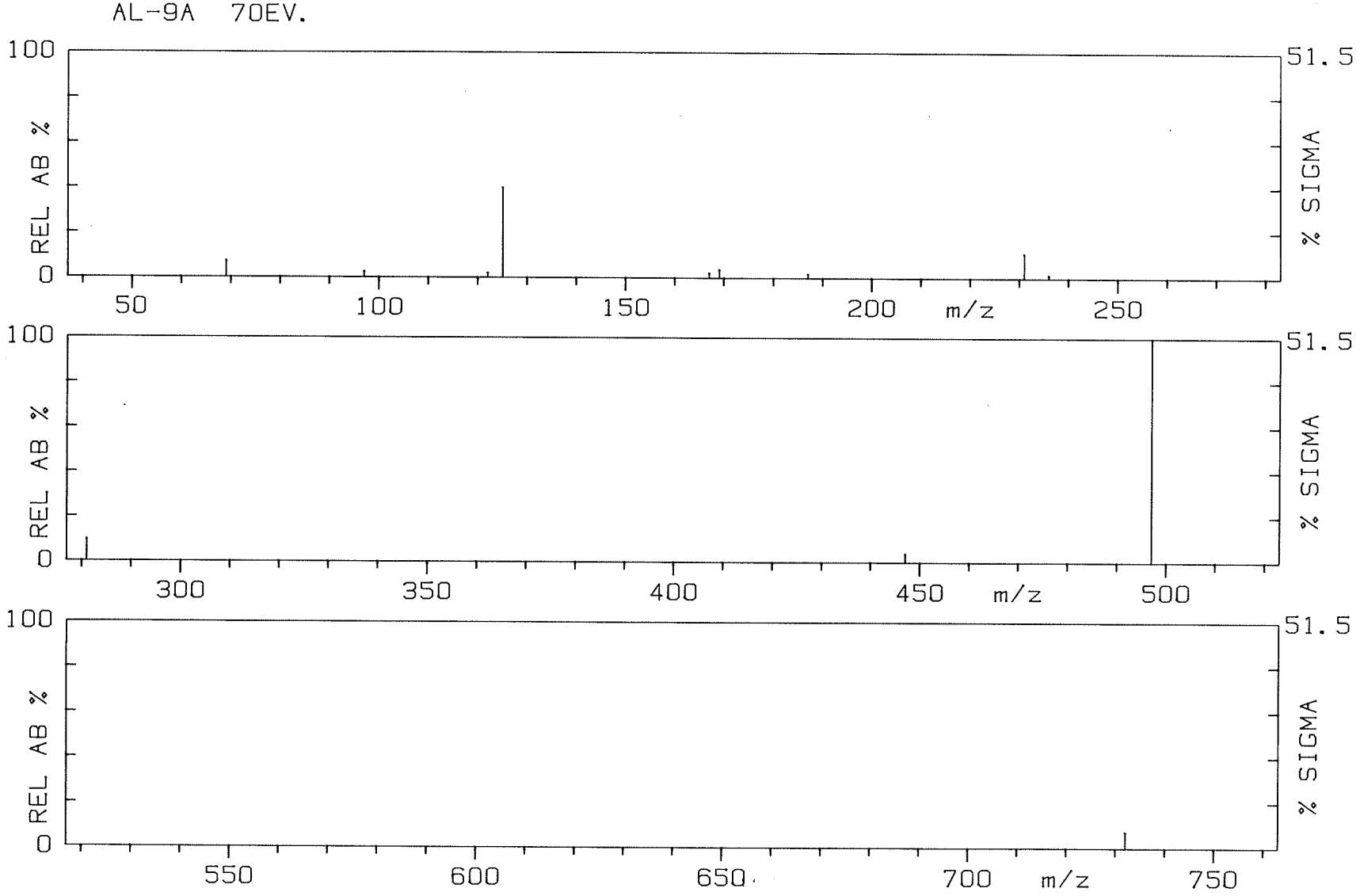
AL-9A 70EV.
100
REL AB %
0
51.5
% SIGMA
50
100
150
200
m/z
250
100
REL AB %
0
51.5
% SIGMA
300
350
400
450
m/z
500
100
REL AB %
0
51.5
% SIGMA
550
600
650
700
m/z
750

Figure 34.

Normalized 70 eV-EI mass spectrum of

tris[1,1,-difluoro-4-phenyl-2,4-butanedionato]Al(III)

{**Al-1a**}.

m/z $[M]^{+\cdot}$ = 618, $[L]^{+}$ = 197

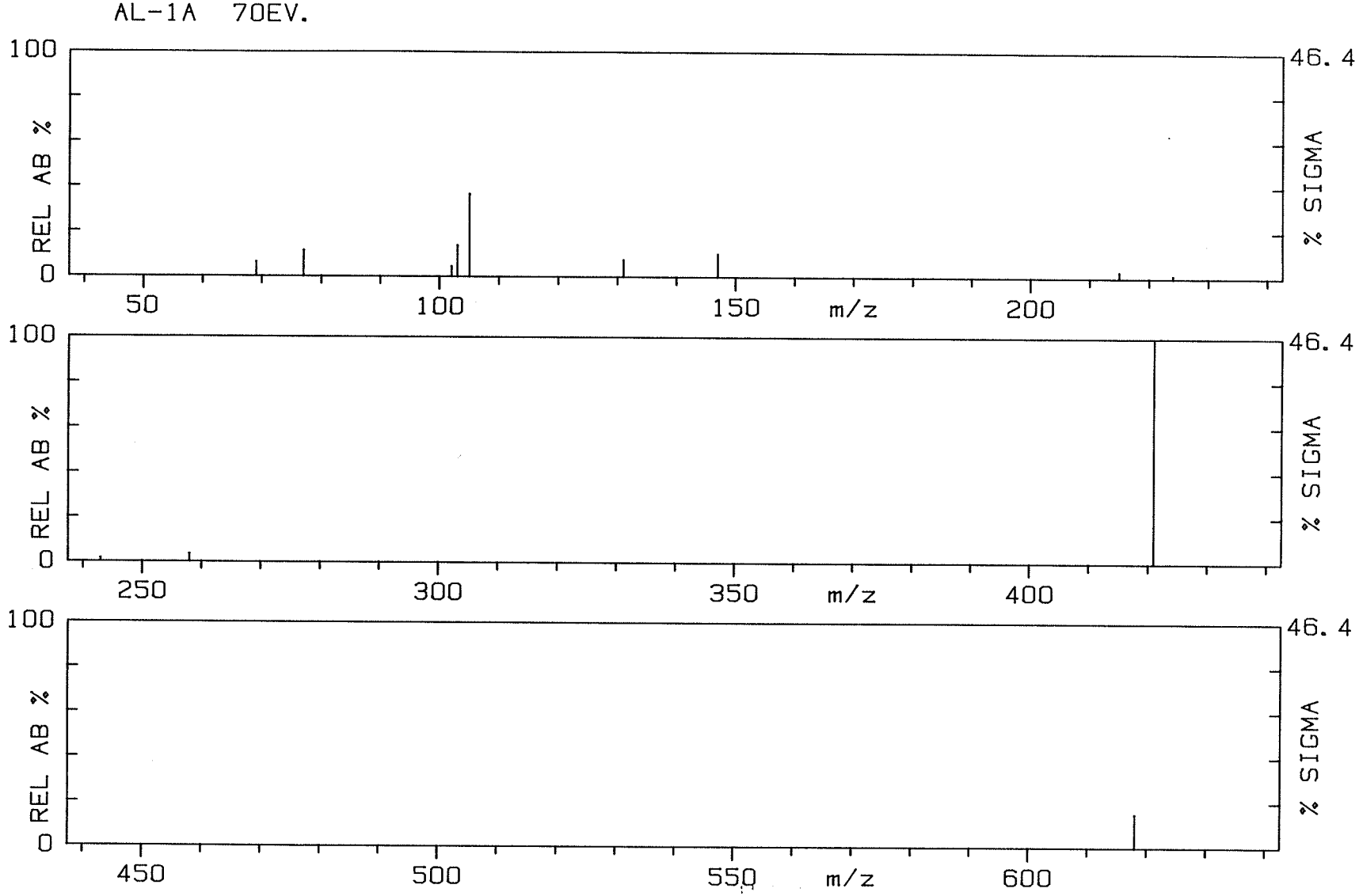
AL-1A 70EV.
100
REL AB %
0
50
100
150
m/z
200
46.4
% SIGMA
100
REL AB %
0
250
300
350
m/z
400
46.4
% SIGMA
100
REL AB %
0
450
500
550
m/z
600
46.4
% SIGMA

Figure 35.

Normalized 70 eV-EI mass spectrum of

tris[1,1,-difluoro-4-(2'-thienyl)-2,4-butanedionato]Al(III)

{**Al-2a**}.

m/z $[M]^{+\cdot}$ = 636, $[L]^{+}$ = 203

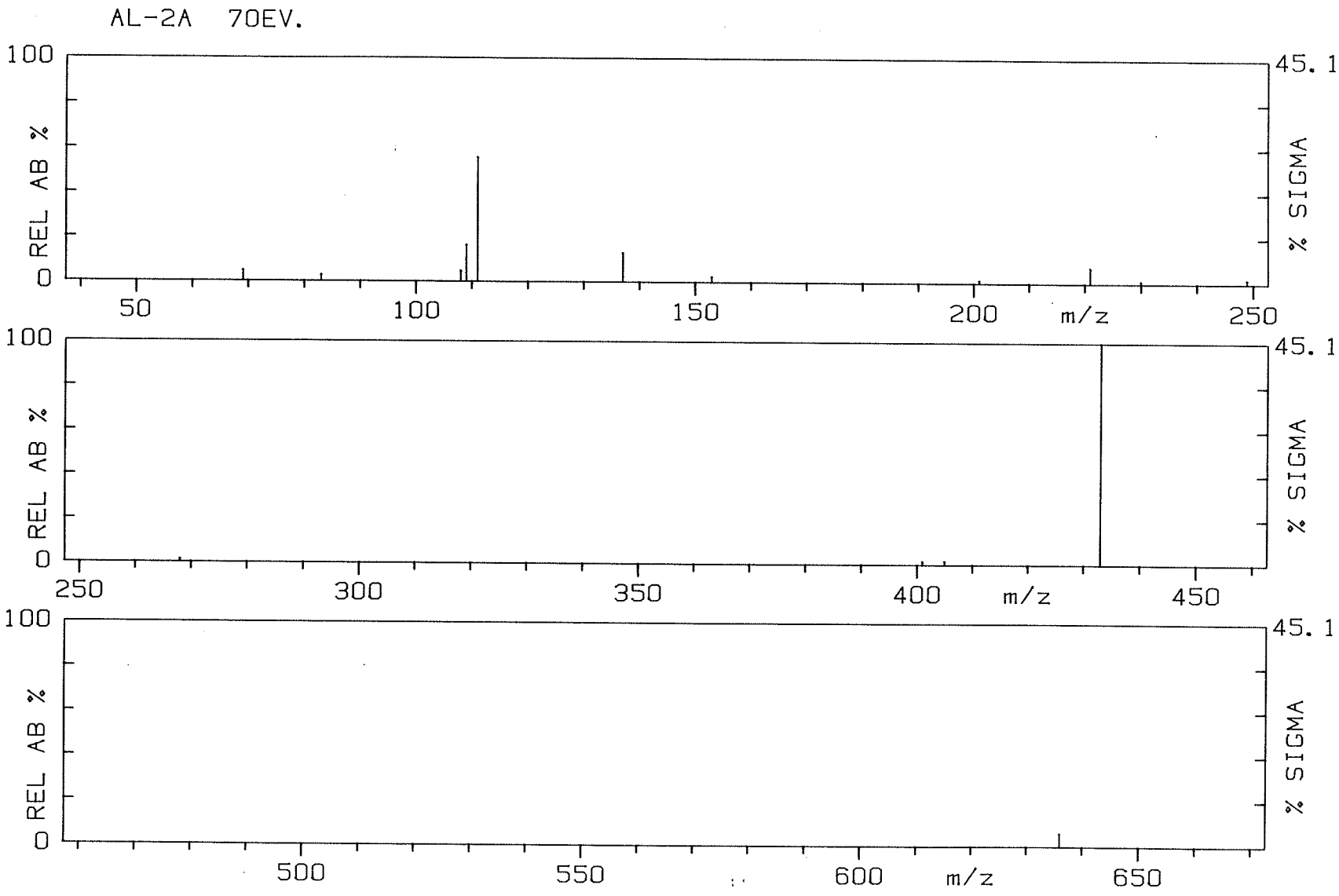
AL-2A 70EV.
100
0
REL AB %
45.1
% SIGMA
50
100
150
200
m/z
250
250
300
350
400
m/z
450
500
550
600
m/z
650

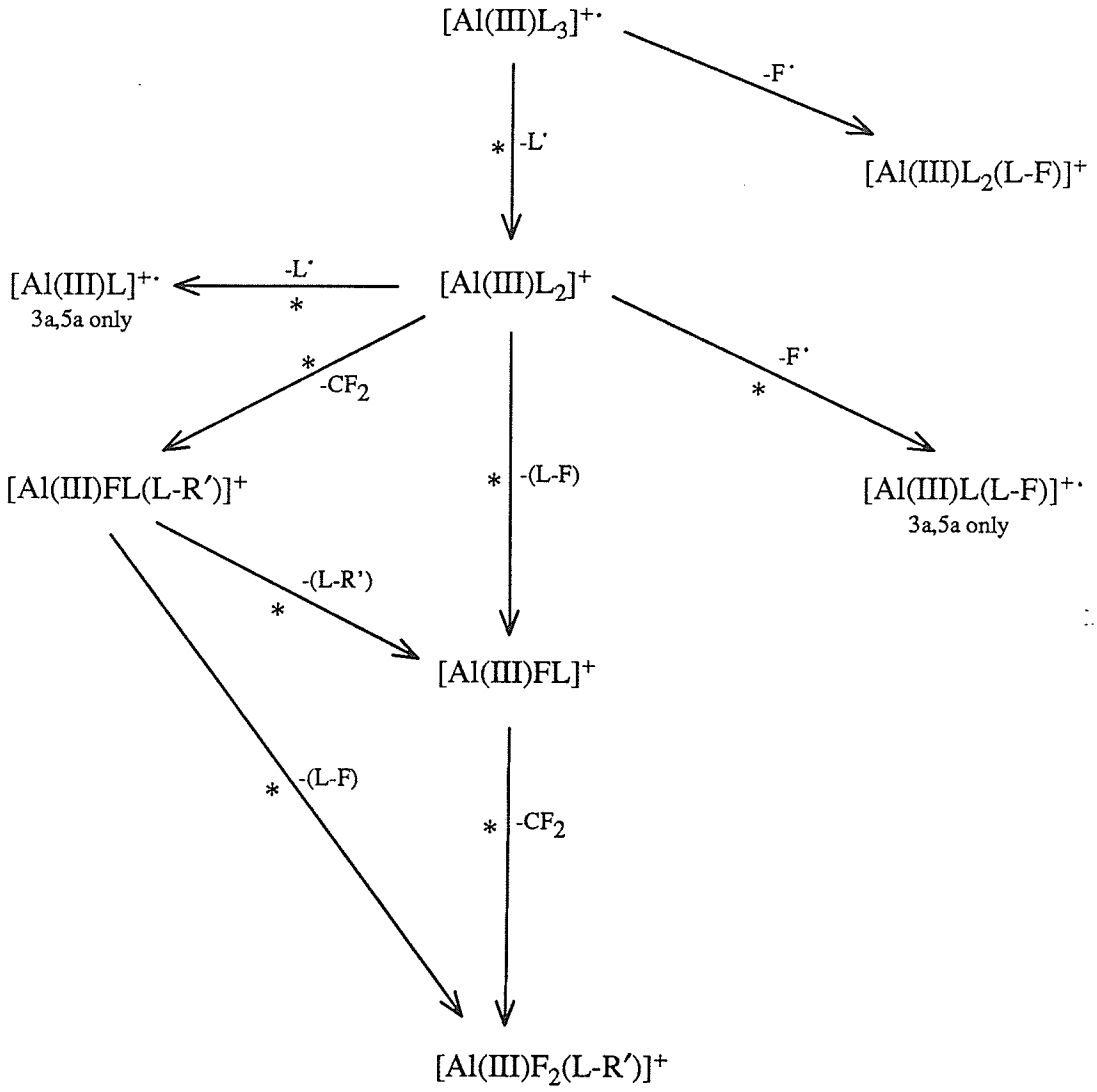

* process confirmed by the observation of a metastable transition in at least one of the complexes.

Scheme 16. Proposed fragmentation pathways for Al(III) β-diketonates where R' = CF_3 (**Al-3a, -4a, -5a, -8a** and **-9a**). Pathways are commmon to all complexes except where noted.

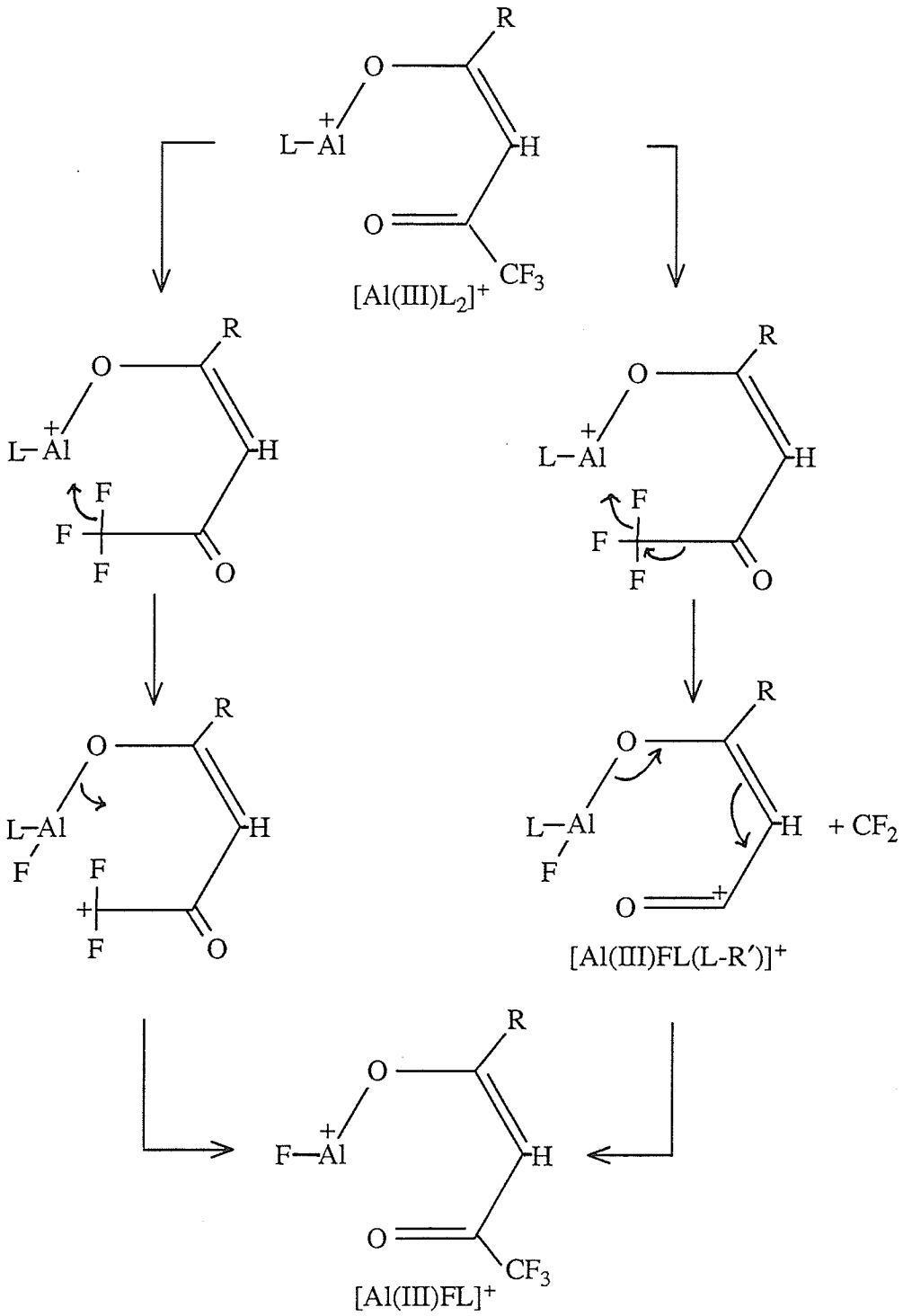

Scheme 17. Suggested mechanisms for the formation of $[Al(III)FL(L\text{-}R')]^+$ and $[Al(III)FL]^+$ in **Al-3a, -4a, -5a, -8a** and **-9a.**

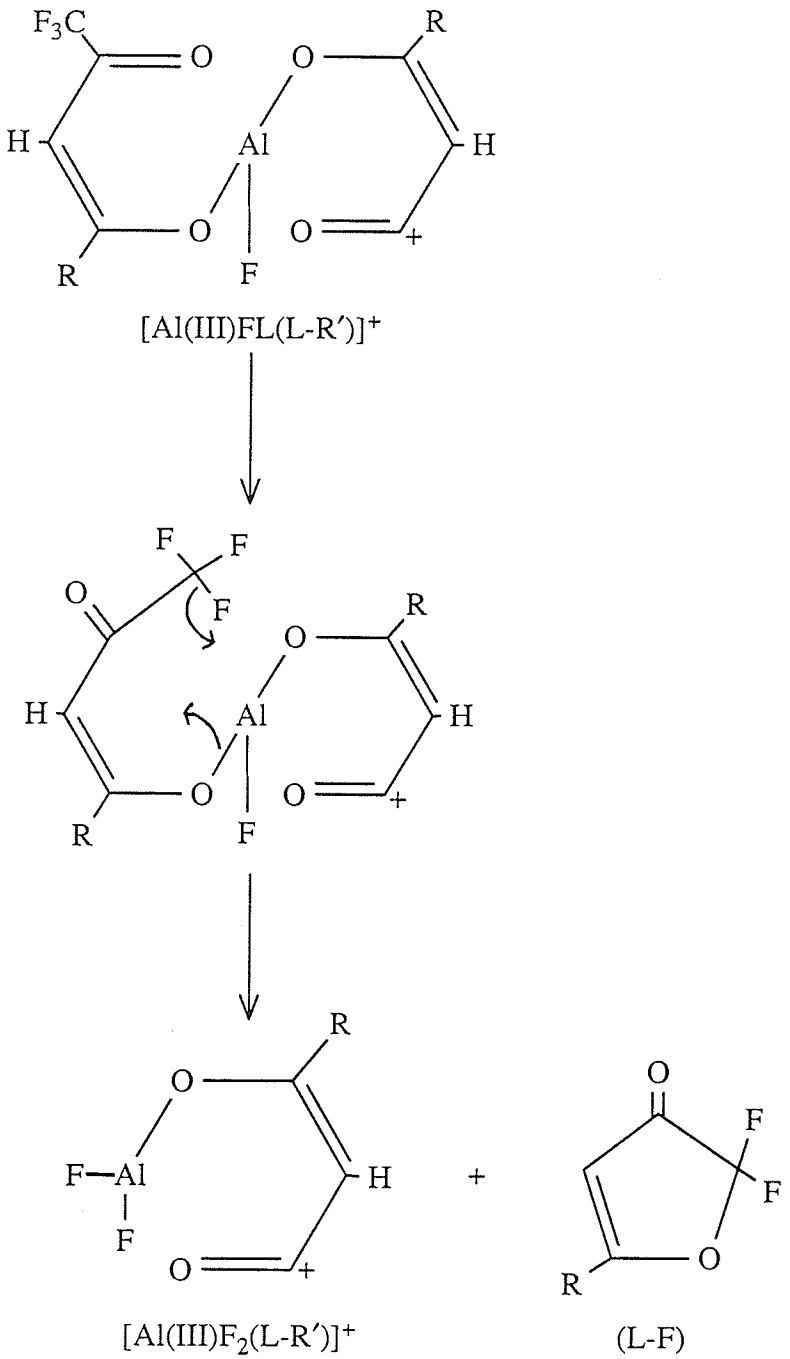

Scheme 18. Suggested mechanism for the formation of $[Al(III)F_{2(L-R')}]^+$ from $[Al(III)FL(L-R')]^+$ in **Al-3a, -4a, -5a, -8a** and **-9a.**

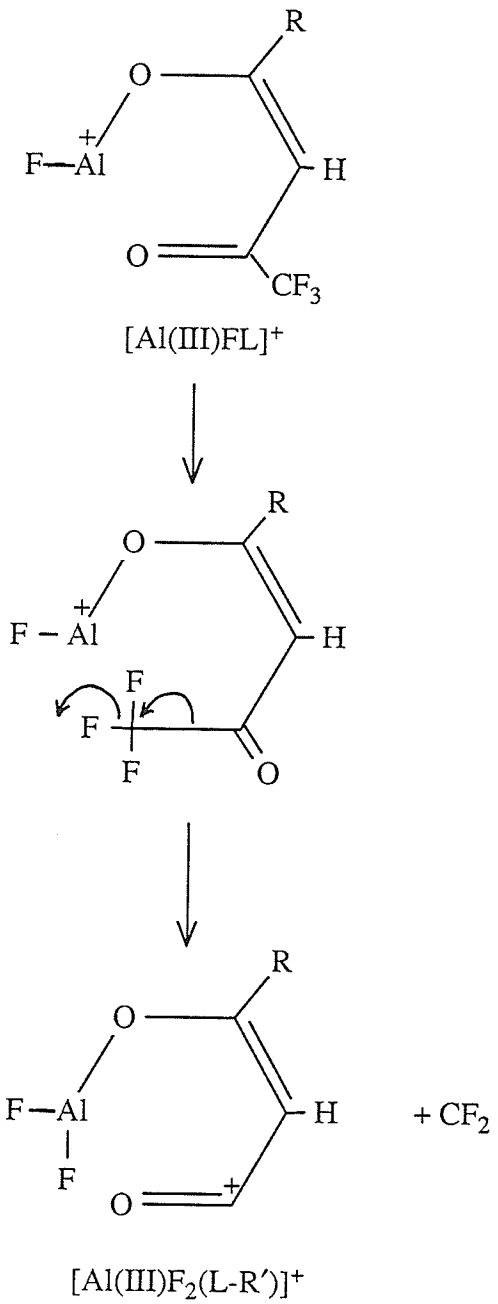

Scheme 19. Suggested mechanism for the formation of $[Al(III)F_{2(L-R')}]^+$ in **Al-3a, -4a, -5a, -8a** and **-9a.**

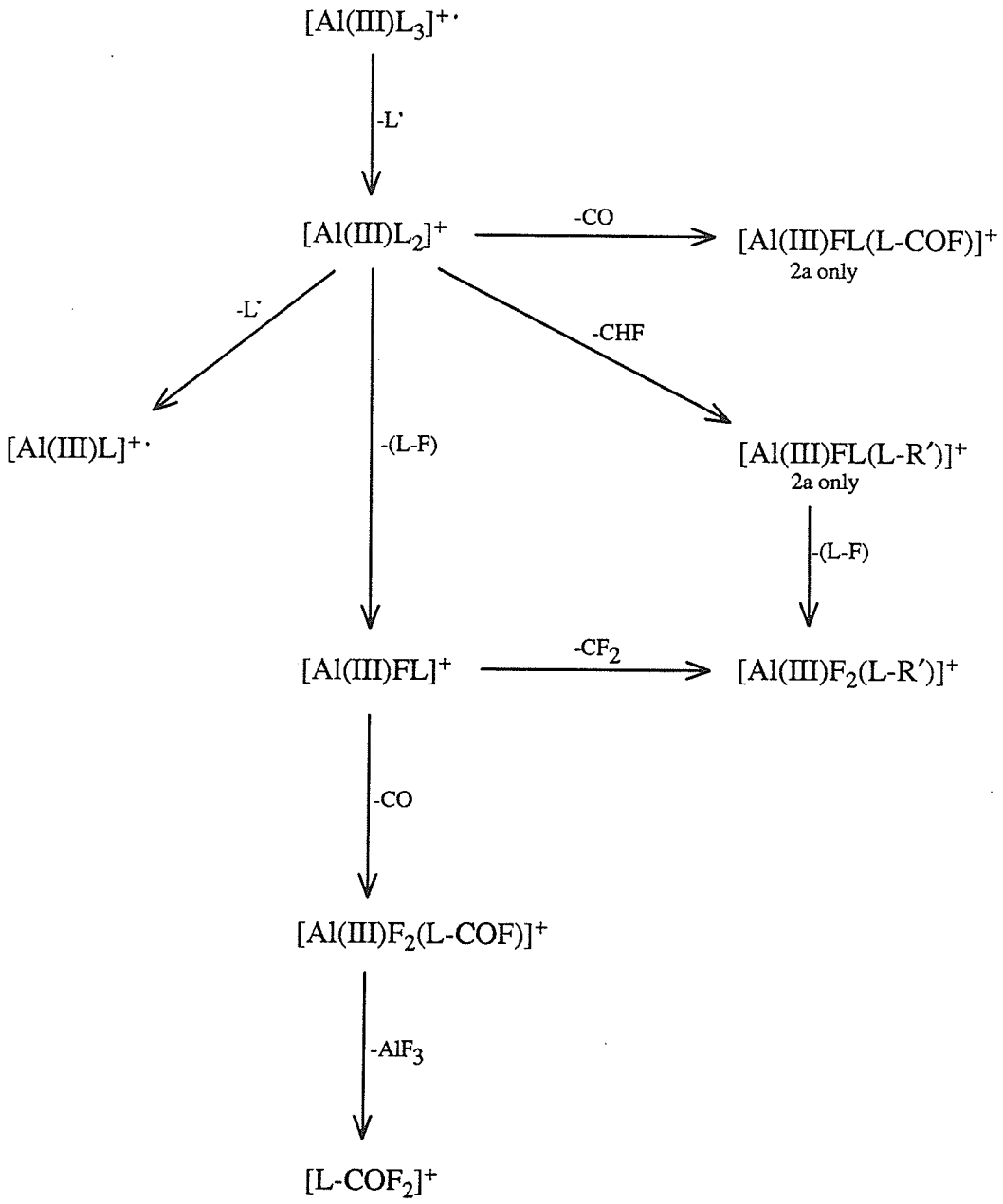

Scheme 20. Proposed fragmentation pathways for Al(III) β-diketonates where R' = CHF_2 (**Al-1a** and **-2a**). Pathways are common to both complexes except where noted.

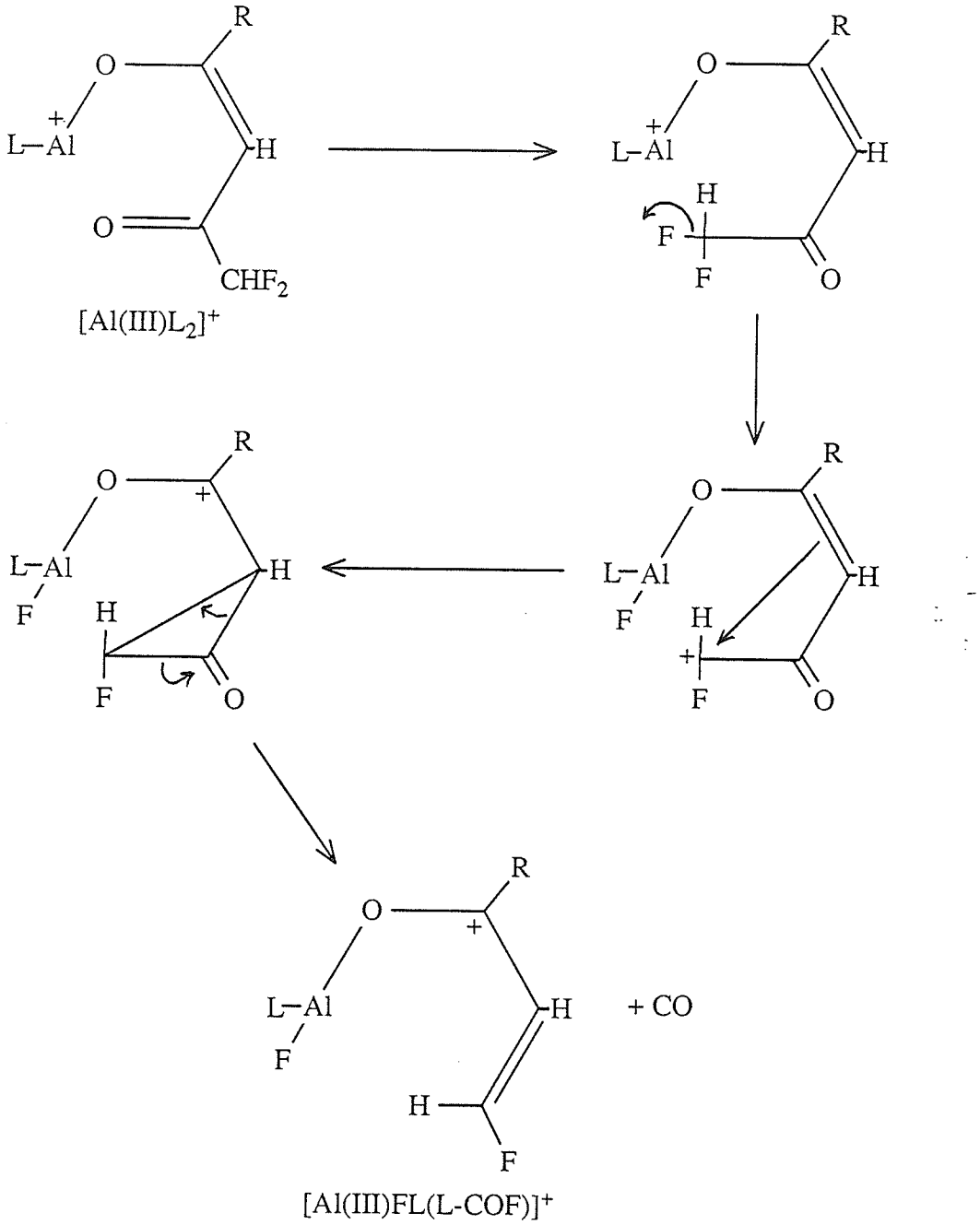

Scheme 21. Suggested mechanism for the formation of [Al(III)FL(L-COF)]+ in **Al-2a.**

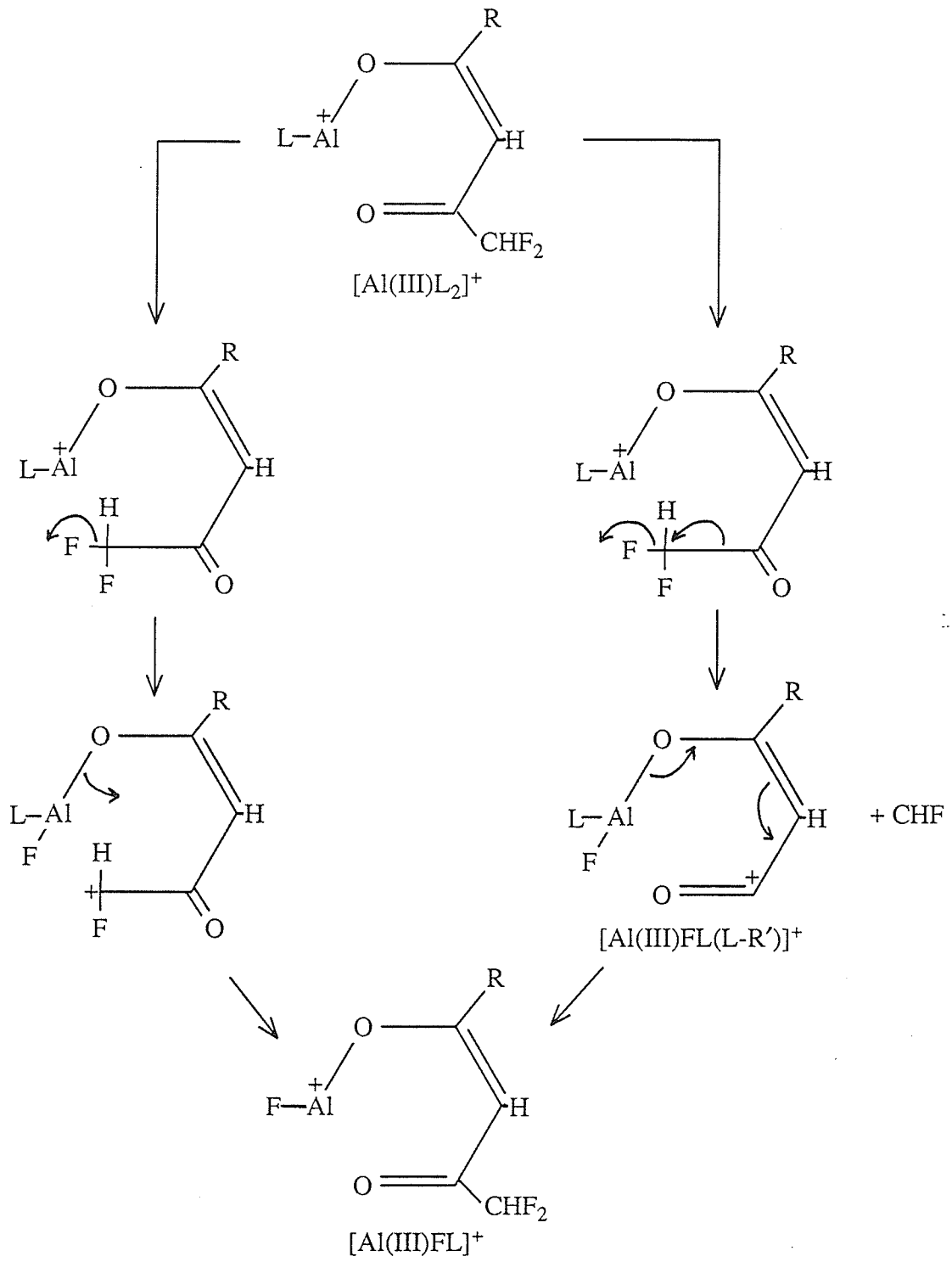

Scheme 22. Suggested mechanisms for the formation of $[Al(III)FL]^+$ in **Al-1a** and **-2a.**

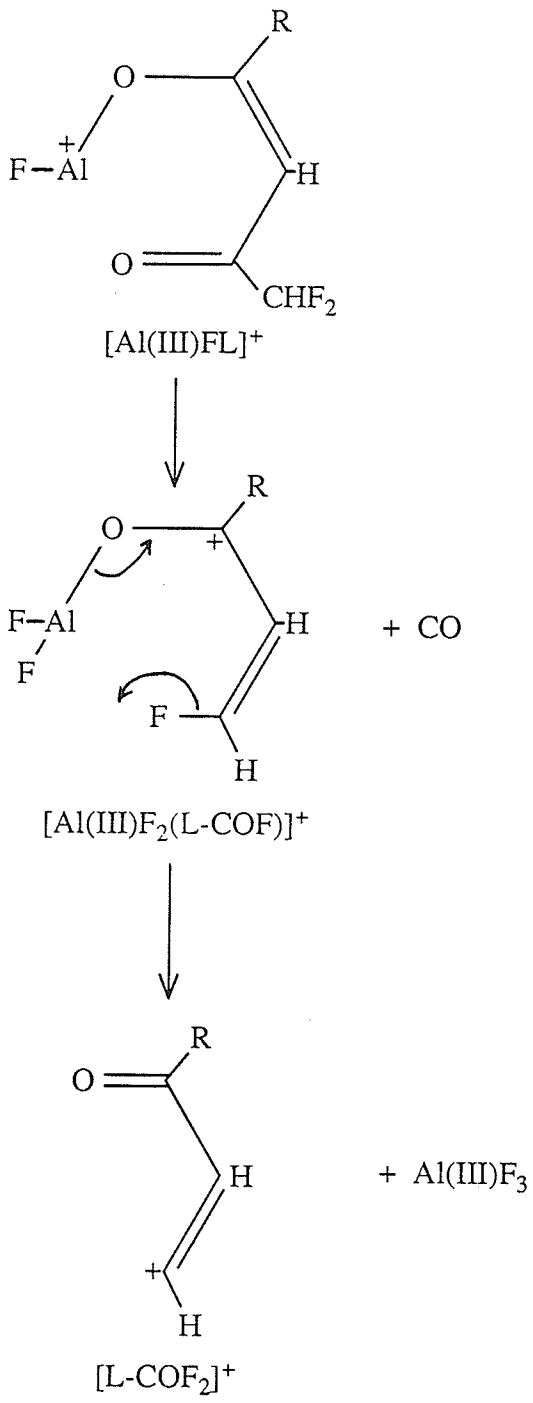

Scheme 23. Suggested mechanism for the elimination of Al(III)F_3 in **Al-1a** and **-2a**.

(b) Ga(III) β-diketonates

Relative abundance data for the seven Ga(III) β-diketonates studied appear in Tables 11-13. Plots of the EI mass spectra are depicted in Figures 36-42. Metastable evidence was obtained through a linked-scanning study of **Ga-5a**. Das (141) has published a brief report on the mass spectra of the trifluoromethyl derivatives **Ga-3a**, **Ga-4a**, **Ga-5a**, **Ga-8a** and **Ga-12a**.

Suggested decomposition pathways for the Ga(III) β-diketonate complexes possessing a difluoromethyl substituent (R' = CHF_2; Table 11) are shown in Scheme 24. The base peak in both **Ga-1a** and **Ga-2a** is the EE^+ species $[Ga(III)L_2]^+$, while the molecular ion is of comparatively low abundance. This behavior mimics that found in the Al(III) chelates. However, the existence of the bare metal ion $[Ga(I)]^+$ appears to be unique, and is believed to arise through the concerted elimination of two ligand radicals from $[Ga(III)L_2]^+$ as shown in Scheme 25. The loss of each L occurs with the transfer of an electron to the metal, reducing its oxidation state from +3 to +1. Such a process was initially proposed by Charalambous et al. (116) in their study of the mass spectra of Ga(III) acetylacetonate and trifluoroacetylacetonate. The ready availability of the Ga(I) oxidation state is in contrast to the absence of bare metal ions in the spectra of other trivalent metal

chelates (e.g. Met = Al(III), V(III), Fe(III) and Cr(III)), metals which do not possess stable +1 oxidation states. High resolution (R.P. 5000) mass spectrometry was used to confirm the presence of $[Ga(I)]^+$, since at least three ions having a nominal mass of 69u ($[Ga(I)]^+$, $[C_3HO_2]^+$ and $[CF_3]^+$) appeared plausible:

Ion	Mass (calc)	Mass (expt)	Δm (mmu)
$[^{69}Ga(I)]^+$	68.9256	68.9245	1.1
$[C_3HO_2]^+$	68.9977	68.9245	73.2
$[CF_3]^+$	68.9952	68.9245	70.7

The characteristic doublet at m/z 69 and 71 (intensity ratio 3:2) aided in the interpretation.

The migration of the R group to the metal in $[Ga(III)L_2]^+$ results in the loss of the EE^o neutral (L-R) and the formation of the EE^+ fragment ion $[Ga(III)RL]^+$. Mechanisms based on four- and six-membered cyclic transition states (120) are illustrated in Scheme 26. Although depicted as concerted processes, the sequence of reactions leading to the formation of $[Ga(III)RL]^+$ could entail a series of consecutive, step-wise decompositions, possibly commencing with the migration of the aryl group to the positively-charged gallium.

The mechanisms involved in the fragmentation sequence

$$[Ga(II)L_2]^+ \longrightarrow [Ga(III)FL]^+ \longrightarrow [Ga(III)F_2(L\text{-}COF)]^+ \longrightarrow [L\text{-}COF_2]^+$$

shown in Scheme 24 can be described by analogy to Schemes 22 and 23 discussed earlier. The propensity for EE^o neutral losses in these

chelates is consistent with the established stability of the +3 oxidation state of gallium. A decomposition pathway leading to the elimination of neutral $Ga(III)F_3$ is found in the reaction

$$[Ga(III)FL]^+ \longrightarrow [L-2F]^+$$

A proposed mechanism for this process is given in Scheme 27. Once again, the "hardening" influence of a fluorine atom(s) on the metal facilitates the subsequent migration of another fluorine to the same acceptor.

The fragmentation pathways for the Ga(III) β-diketonate complexes possessing a trifluoromethyl substituent (R' = CF_3; Tables 12 and 13) are shown in Scheme 28. Metastable transitions confirm the loss of a ligand radical from $[M]^+$ to give $[Ga(III)L_2]^+$, which is again the base peak in all five spectra. Many of the decomposition reactions emanating from $[Ga(III)L_2]^+$ have, in some form, been previously discussed. For instance, the mechanisms involved in the consecutive elimination of EE^o neutrals CF_2, (L-R') and CF_2 in the sequence

$$[Ga(III)L_2]^+ \longrightarrow [Ga(III)FL(L-R')]^+ \longrightarrow$$
$$[Ga(III)FL]^+ \longrightarrow [Ga(III)F_2(L-R')]^+$$

as well as the direct loss of (L-F) in

$$[Ga(III)L_2]^+ \longrightarrow [Ga(III)FL]^+$$

can be described by Schemes 17 and 19. The loss of (L-F) is also seen in the decomposition:

$$[Ga(III)FL(L\text{-}R')]^+ \longrightarrow [Ga(III)F_2(L\text{-}R')]^+$$

which presumably follows a mechanism analogous to that depicted in Scheme 18. Meanwhile, the generation of the bare $[Ga(I)]^+$ ion through the loss of two ligand radicals from $[Ga(III)L_2]^+$ can be rationalized by the mechanism shown in Scheme 25, and the R-group transfer product $[Ga(III)RL]^+$ can arise by processes illustrated in Scheme 26 (confirmed by a metastable transition). The decomposition:

$$[Ga(III)RL]^+ \longrightarrow [Ga(III)R_2]^+$$

observed in the spectrum of **Ga-8a** also parallels the migration/fragmentation in

$$[Ga(III)L_2]^+ \longrightarrow [Ga(III)RL]^+$$

described in Scheme 26 for the difluoromethyl-substituted Ga(III) chelates.

The trends in hard/soft acid/base behavior applied earlier to the CF_3-substituted Al(III) β-diketonates can be extended to their Ga(III) counterparts. However, the distinctions are not as clear in the gallium complexes, possibly because of the lower ion currents carried by the metal-containing ions. Nevertheless, it can be seen that fluorine transfer in ions which already have a metal-bonded fluorine ($[Ga(III)FL]^+ \longrightarrow [Ga(III)F_2(L\text{-}R')]^+$; average %TIC = 0.8) is favored over fluorine migration to gallium where no fluorines are present ($[Ga(III)L_2]^+ \longrightarrow [Ga(III)FL(L\text{-}R')]^+$; average %TIC = 0.3). An examination of the %TIC carried by the gallium-fluorine bonded

fragments ($[Ga(III)FL(L\text{-}R')]^+$, $[Ga(III)FL]^+$ and $[Ga(III)F_2(L\text{-}R')]^+$) for each of the five complexes reinforces the concept of ion stability as a function of the electron-donating qualities of the various aryl substituents (average %TIC in parentheses): R = 4-methylphenyl (0.4) < phenyl (0.7) = 2-naphthyl (0.7) < 4-fluorophenyl (0.9) < 2-thienyl (1.1). These trends parallel those reported for the corresponding aluminum complexes and indicate that the hardness of an acceptor is dependent upon the other groups to which it is bound.

Table 11. 70 eV-EI mass spectra of compounds **Ga-1a** and **Ga-2a.**

	Ga-1a	**Ga-2a**
R =	$-C_6H_5$	$-C_4H_3S$
R'=	$-CHF_2$	$-CHF_2$

ION	%RA	m/z	%TIC	%RA	m/z	%TIC
$[GaL_3]^+$	2.5	(660)	1.0	2.6	(678)	0.8
$[GaL_2]^+$	100.0	(463)	38.7	100.0	(475)	30.6
$[GaRL]^+$	3.6	(343)	1.4	10.3	(355)	3.2
[GaFL]+	13.0	(285)	5.0	10.3	(291)	3.2
$[GaF_2(L\text{-}COF)]^+$	3.0	(257)	1.2	3.6	(263)	1.1
$[Ga]^+$	7.7	(68.9)	3.0	11.9	(68.9)	3.6
$[HL]^+$	3.2	(198)	1.2	4.0	(204)	1.2
$[L\text{-}F]^+$	4.8	(178)	1.9	7.2	(184)	2.2
$[L\text{-}2F]^+$	3.8	(159)	1.5	3.1	(165)	0.9
$[HL\text{-}R']^+$	12.2	(147)	4.7	7.5	(153)	2.3
$[L\text{-}COF_2]^+$	14.7	(131)	5.7	10.7	(137)	3.3
$[L\text{-}R]^+$	5.8	(120)	2.2	27.6	(126)	8.5
$[RCO]^+$	40.2	(105)	15.6	88.8	(111)	27.2
$[RC_2H_2]^+$	15.3	(103)	5.9	9.9	(109)	3.0
$[RCCH]^+$	6.7	(102)	2.6	9.5	(108)	2.9
$[R]^+$	16.5	(77)	6.4	9.9	(83)	3.0
$[C_3HO_2]^+$	5.5	(69)	2.1	9.5	(69)	2.9

Table 12. 70 eV-EI mass spectra of compounds **Ga-3a**, **Ga-4a** and **Ga-5a**.

	Ga-3a			**Ga-4a**			**Ga-5a**		
R =	$-C_6H_5$			$-C_6H_4CH_3$			$-C_6H_4F$		
R'=	$-CF_3$			$-CF_3$			$-CF_3$		
ION	%RA	m/z	%TIC	%RA	m/z	%TIC	%RA	m/z	%TIC
$[GaL_3]^+$ (a)	6.4	(714)	3.3	5.9	(756)	3.1	3.7	(768)	1.8
$[GaL_2(L-F)]^+$	1.8	(695)	0.9	1.4	(737)	0.7	1.6	(749)	0.8
$[GaL_2]^+$ (b)	[a]100.0	(499)	52.2	100.0	(527)	52.5	[a]100.0	(535)	48.5
$[GaL(L-F)]^+$	3.3	(480)	1.7	-	(508)	-	[b]1.9	(516)	0.9
$[GaFL(L-R')]^+$	-	(449)	-	-	(477)	-	[b]1.1	(485)	0.5
$[GaRL]^+$	5.3	(361)	2.8	[b]6.0	(389)	3.1	[b]5.7	(397)	2.8
$[GaFL]^+$ (c)	2.3	(303)	1.2	1.5	(317)	0.8	[b]3.0	(321)	1.5
$[GaF_2(L-R')]^+$	1.6	(253)	0.8	1.0	(267)	0.5	[c]1.7	(271)	0.8
$[Ga]^+$	5.4	(68.9)	2.8	4.3	(68.9)	2.3	10.5	(68.9)	5.1
$[HL]^+$	3.2	(216)	1.7	3.7	(230)	1.9	1.9	(234)	0.9
$[L]^+$	1.2	(215)	0.6	0.9	(229)	0.5	0.9	(233)	0.4
$[HL-R']^+$	4.4	(147)	2.3	5.3	(161)	2.8	3.7	(165)	1.8
$[RCO]^+$	40.9	(105)	21.4	40.3	(119)	21.2	[c]55.4	(123)	26.9
$[R]^+$	11.5	(77)	6.0	10.2	(91)	5.4	12.6	(95)	6.1
$[R']^+$	4.2	(69)	2.2	7.2	(69)	3.8	2.4	(69)	1.2

[a] Identified metastable transitions are indicated by superscripts which relate the daughter ion to its precursor as labelled in column 1.

Table 13. 70 eV-EI mass spectra of compounds **Ga-8a** and **Ga-12a**.

	Ga-8a	**Ga-12a**
R =	$-C_4H_3S$	$-C_{10}H_7$
R'=	$-CF_3$	$-CF_3$

ION	%RA	m/z	%TIC	%RA	m/z	%TIC
$[GaL_3]^+$ (a)	6.6	(732)	2.9	9.5	(864)	4.6
$[GaL_2(L-F)]^+$	1.2	(713)	0.5	1.0	(845)	0.5
$[GaL_2]^+$ (b)	100.0	(511)	44.5	[a]100.0	(599)	48.4
$[GaFL(L-R')]^+$	-	(461)	-	2.1	(549)	1.0
$[GaRL]^+$	13.8	(373)	6.1	[b]6.4	(461)	3.1
$[GaFL]^+$	4.6	(309)	2.0	1.6	(353)	0.8
$[GaF_2(L-R')]^+$	3.2	(259)	1.4	0.8	(303)	0.4
$[GaR_2]^+$	5.3	(235)	2.4	-	(279)	-
$[Ga]^+$	10.1	(68.9)	4.5	5.6	(68.9)	2.7
$[HL]^+$	10.2	(222)	4.5	5.7	(266)	2.8
$[L]^+$	2.3	(221)	1.0	1.4	(265)	0.7
$[HL-R']^+$	9.7	(153)	4.3	4.0	(197)	1.9
$[RCO]^+$ (c)	45.3	(111)	20.2	40.4	(155)	19.5
$[R]^+$	4.1	(83)	1.8	[c]19.6	(127)	9.5
$[R']^+$	8.4	(69)	3.7	7.5	(69)	3.6

[a] Identified metastable transitions are indicated by superscripts which relate the daughter ion to its precursor as labelled in column 1.

Figure 36.

Normalized 70 eV-EI mass spectrum of

tris[1,1,-difluoro-4-phenyl-2,4-butanedionato]Ga(III)

{Ga-1a}.

m/z $[M]^{+\cdot}$ = 660, $[L]^{+}$ = 197

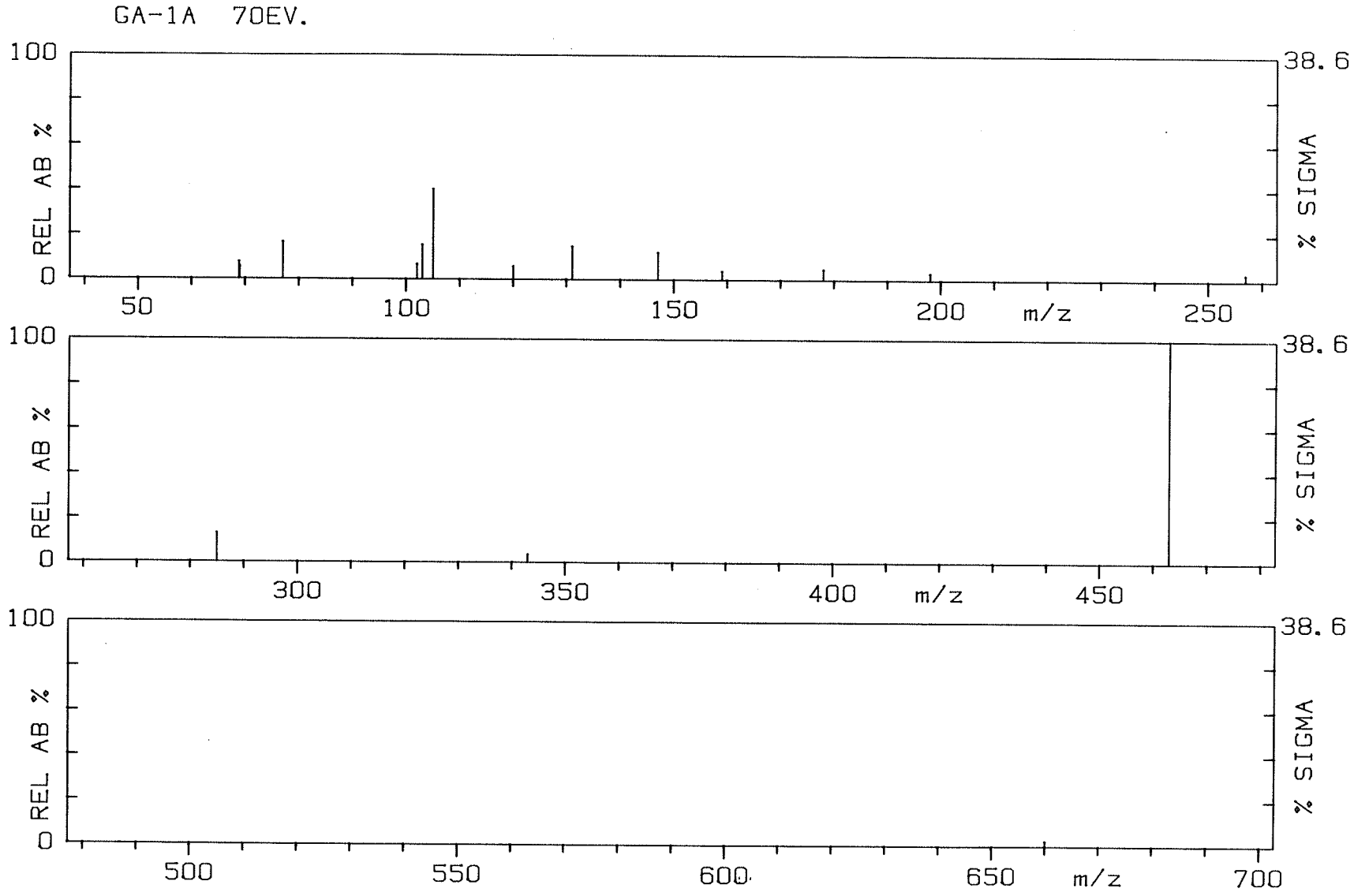
GA-1A 70EV.
100
0 REL AB %
38.6
% SIGMA
50
100
150
200
m/z
250
100
0 REL AB %
38.6
% SIGMA
300
350
400
m/z
450
100
0 REL AB %
38.6
% SIGMA
500
550
600
650
m/z
700

Figure 37.

Normalized 70 eV-EI mass spectrum of

tris[1,1,-difluoro-4-(2'-thienyl)-2,4-butanedionato]Ga(III)

{**Ga-2a**}.

m/z $[M]^{+\cdot}$ = 678, $[L]^{+}$ = 203

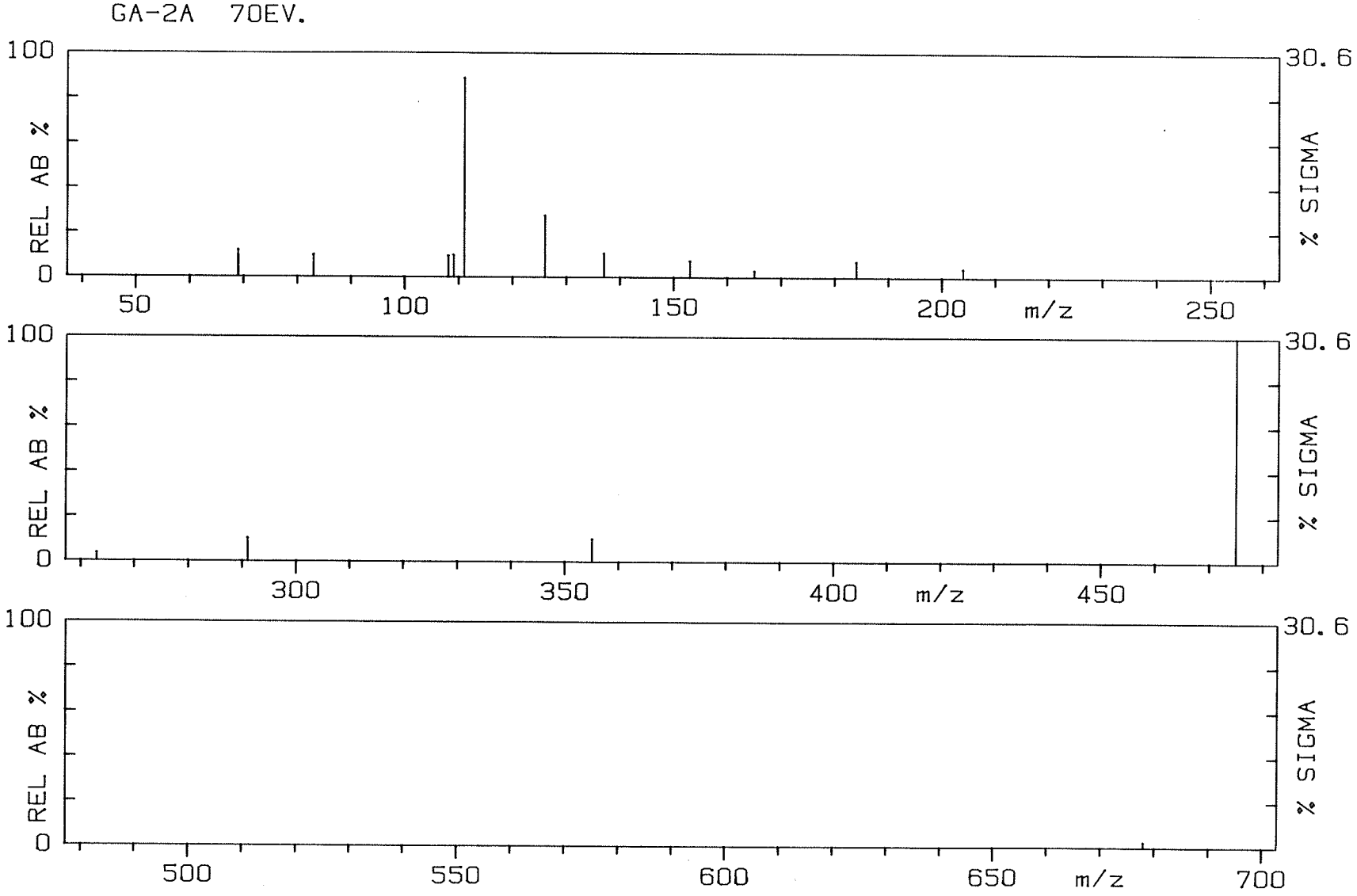
GA-2A 70EV.
100
REL AB %
0
30.6
% SIGMA
50
100
150
200
m/z
250
300
350
400
450
500
550
600
650
700

Figure 38.

Normalized 70 eV-EI mass spectrum of

tris[1,1,1-trifluoro-4-phenyl-2,4-butanedionato]Ga(III)

{**Ga-3a**}.

m/z $[M]^{+\cdot}$ = 714, $[L]^{+}$ = 215

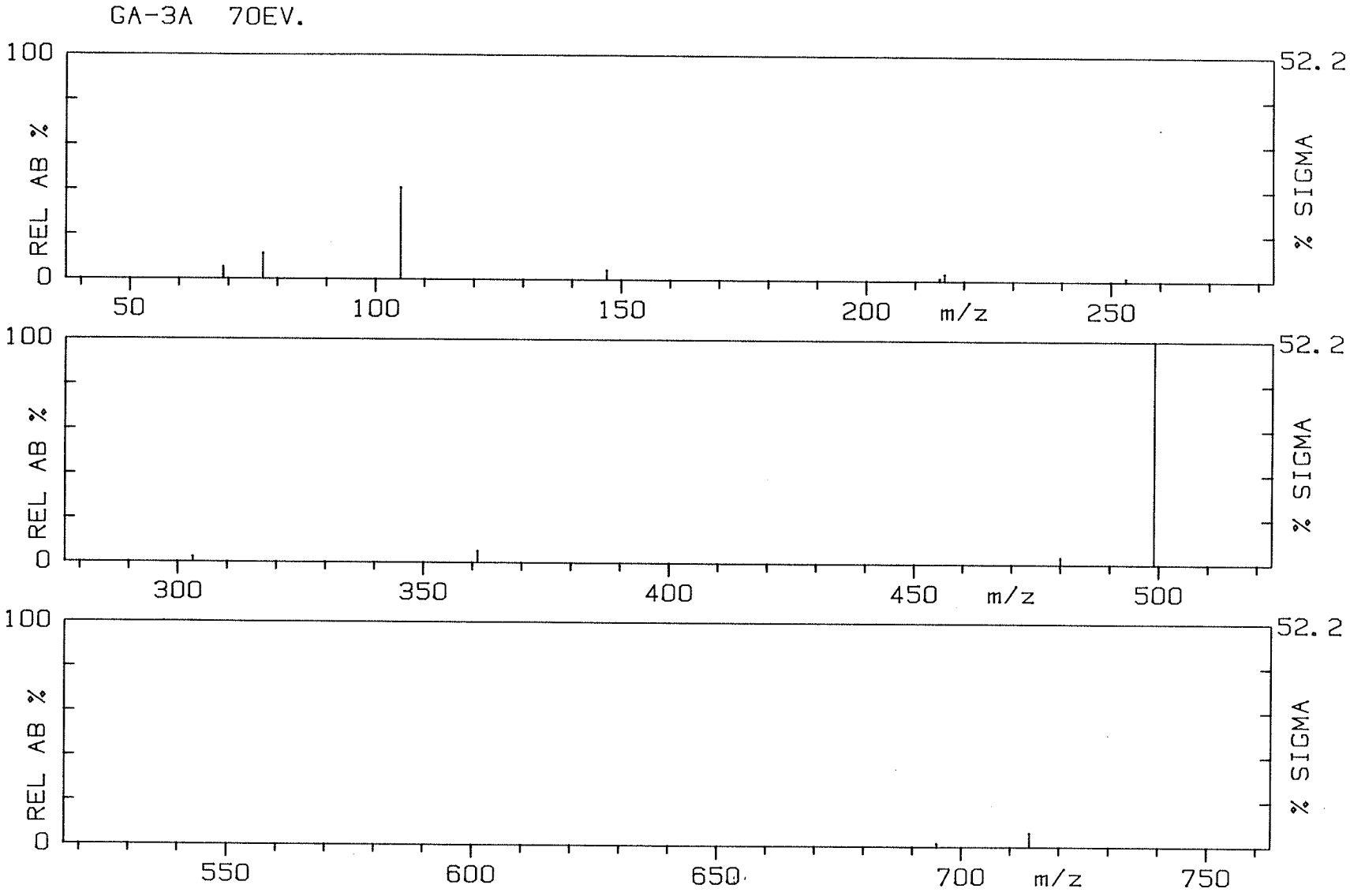
GA-3A 70EV.
100
0
REL AB %
52.2
% SIGMA
50
100
150
200
m/z
250
300
350
400
450
500
550
600
650
700
750

Figure 39.

Normalized 70 eV-EI mass spectrum of

tris[1,1,1-trifluoro-4-(4'-methylphenyl)-2,4-butanedionato]Ga(III)

{**Ga-4a**}.

m/z $[M]^{+\cdot}$ = 756, $[L]^{+}$ = 229

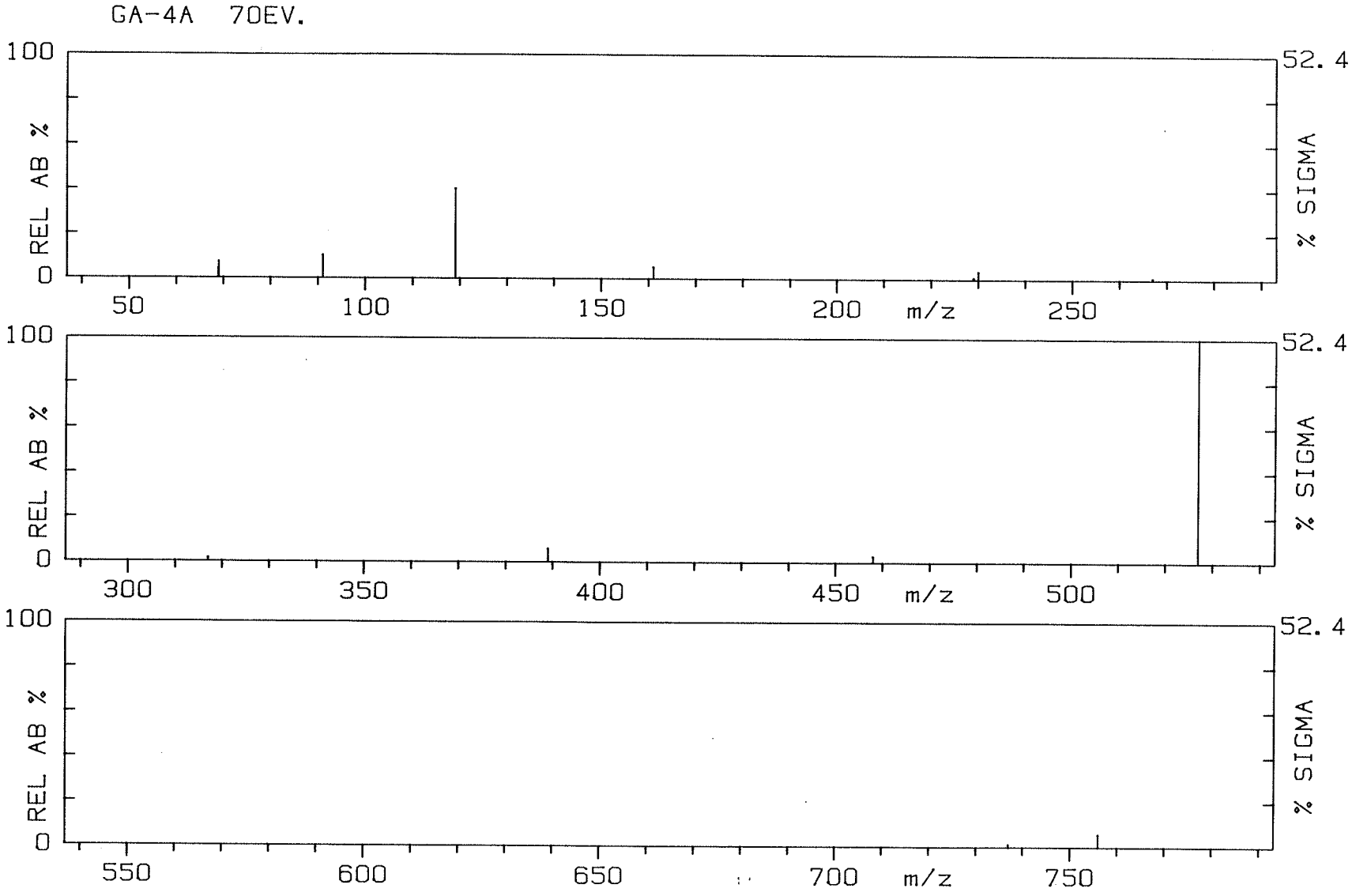
GA-4A 70EV.
100
0 REL AB %
52.4
% SIGMA
50
100
150
200
m/z
250
100
0 REL AB %
52.4
% SIGMA
300
350
400
450
m/z
500
100
0 REL AB %
52.4
% SIGMA
550
600
650
700
m/z
750

Figure 40.

Normalized 70 eV-EI mass spectrum of

tris[1,1,1-trifluoro-4-(4'-fluorophenyl)-2,4-butanedionato]Ga(III)

{Ga-5a}.

m/z $[M]^{+\cdot}$ = 768, $[L]^{+}$ = 233

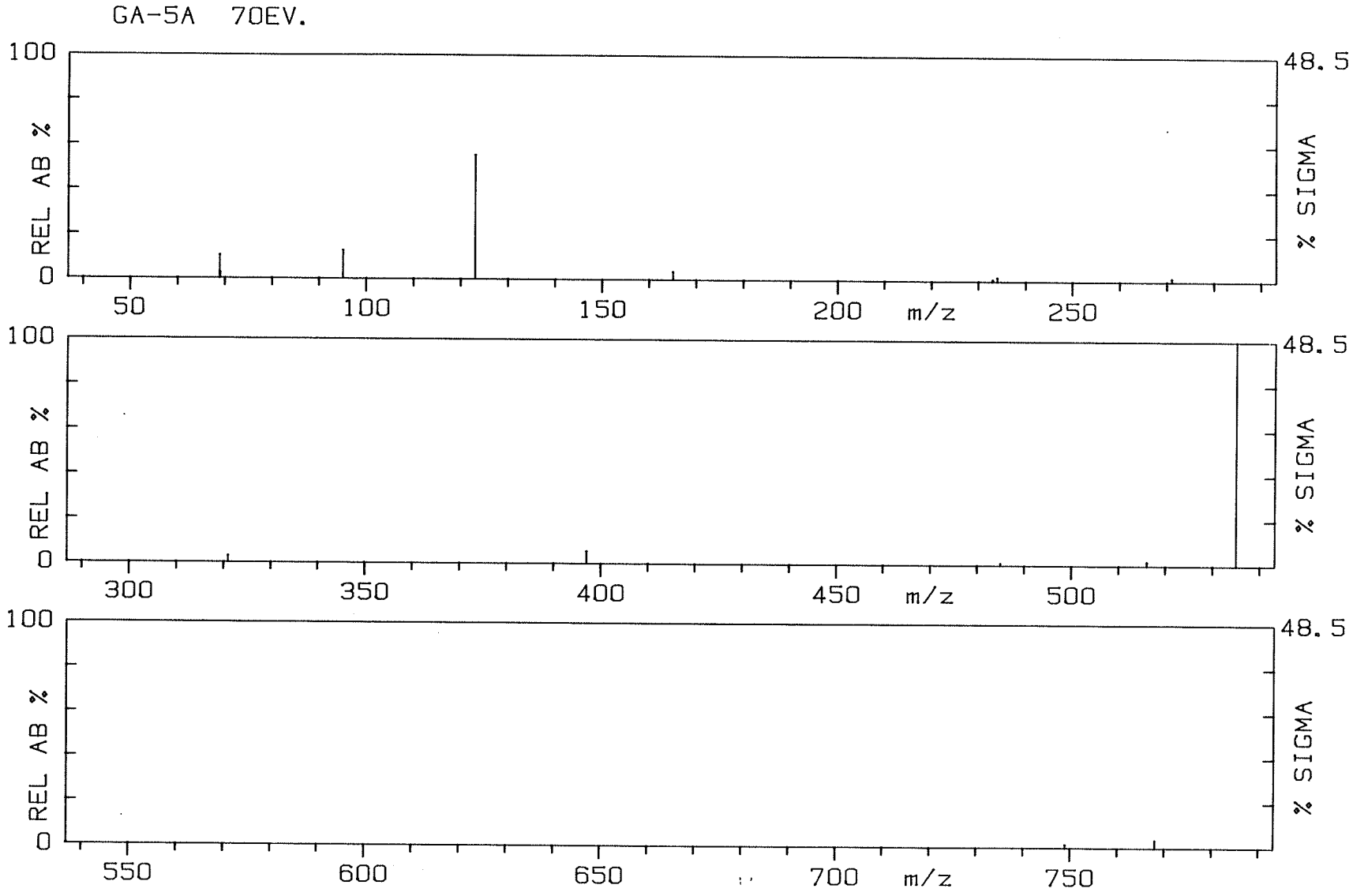
GA-5A 70EV.
100
REL AB %
0
50
100
150
200
m/z
250
48.5
% SIGMA
100
REL AB %
0
300
350
400
450
m/z
500
48.5
% SIGMA
100
REL AB %
0
550
600
650
700
m/z
750
48.5
% SIGMA

Figure 41.

Normalized 70 eV-EI mass spectrum of

tris[1,1,1-trifluoro-4-(2'-thienyl)-2,4-butanedionato]Ga(III)

{Ga-8a}.

m/z $[M]^{+\cdot}$ = 732, $[L]^{+}$ = 221

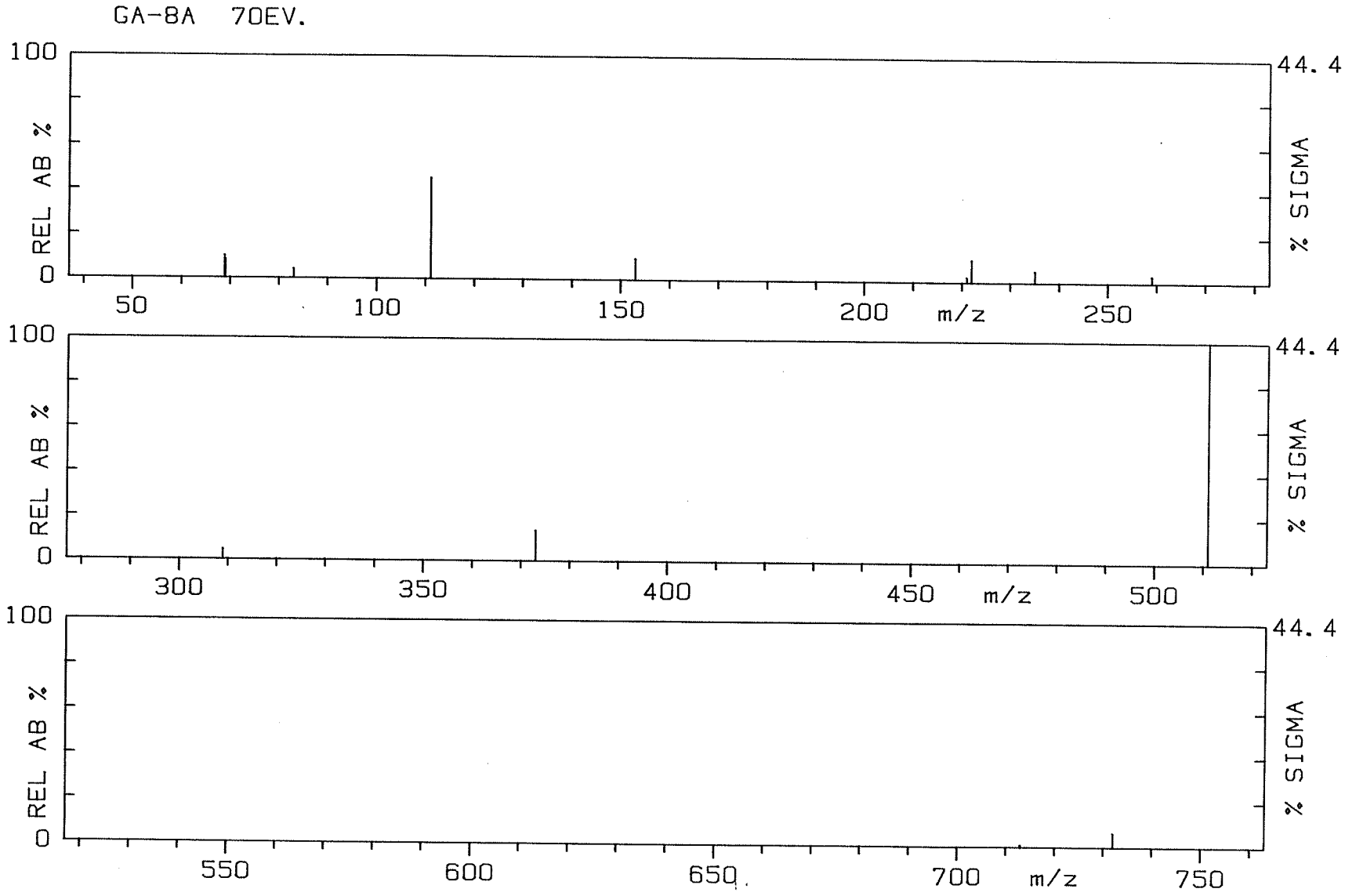
GA-8A 70EV.
100
REL AB %
0
50
100
150
200
m/z
250
44.4
% SIGMA
100
REL AB %
0
300
350
400
450
m/z
500
44.4
% SIGMA
100
REL AB %
0
550
600
650
700
m/z
750
44.4
% SIGMA

Figure 42.

Normalized 70 eV-EI mass spectrum of

tris[1,1,1-trifluoro-4-(2'-naphthyl)-2,4-butanedionato]Ga(III)

{Ga-12a}.

m/z $[M]^{+\cdot}$ = 864, $[L]^{+}$ = 265

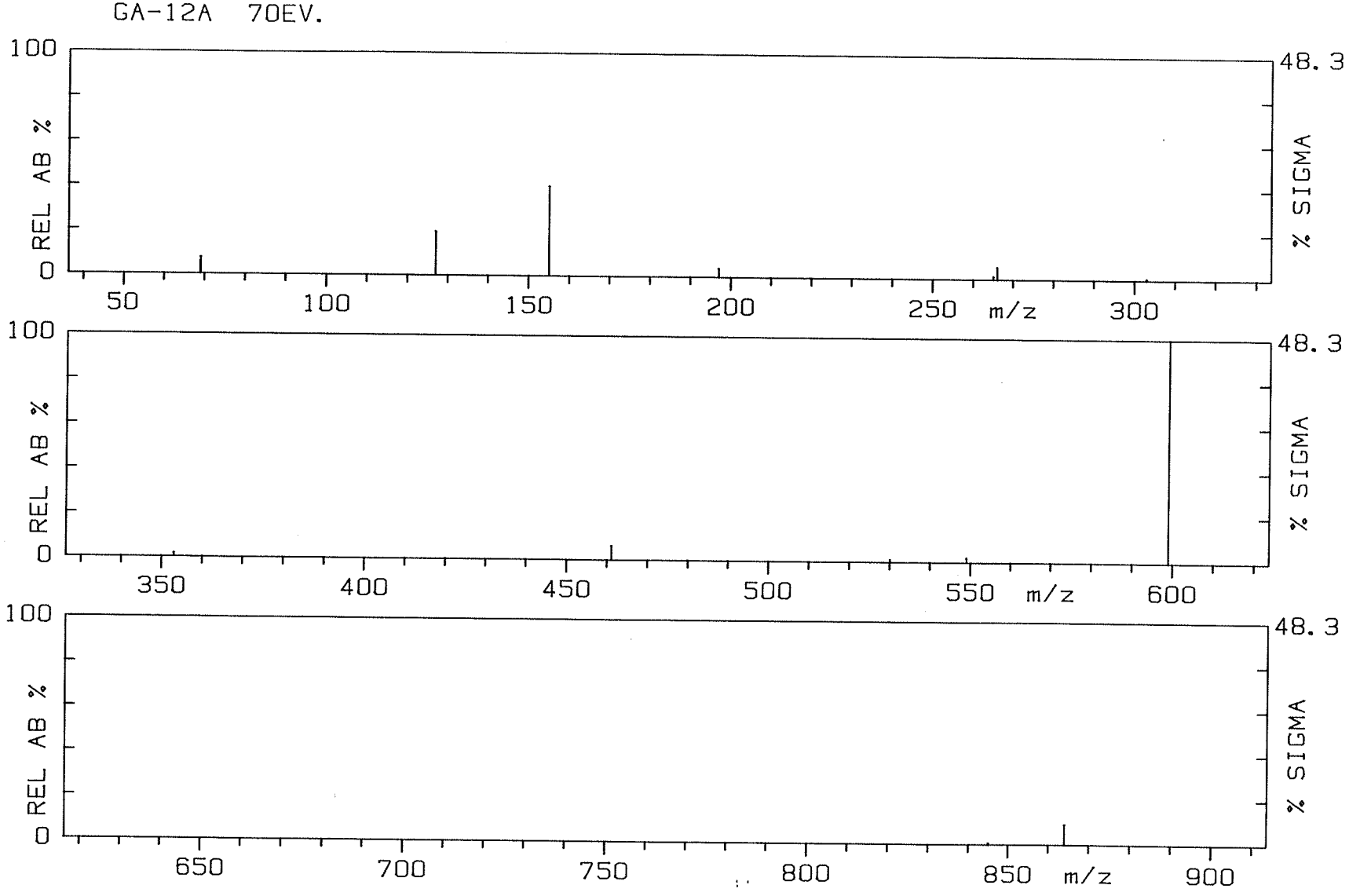
GA-12A 70EV.
100
REL AB %
0
50
100
150
200
250
m/z
300
48.3
% SIGMA
100
REL AB %
0
350
400
450
500
550
m/z
600
48.3
% SIGMA
100
REL AB %
0
650
700
750
800
850
m/z
900
48.3
% SIGMA

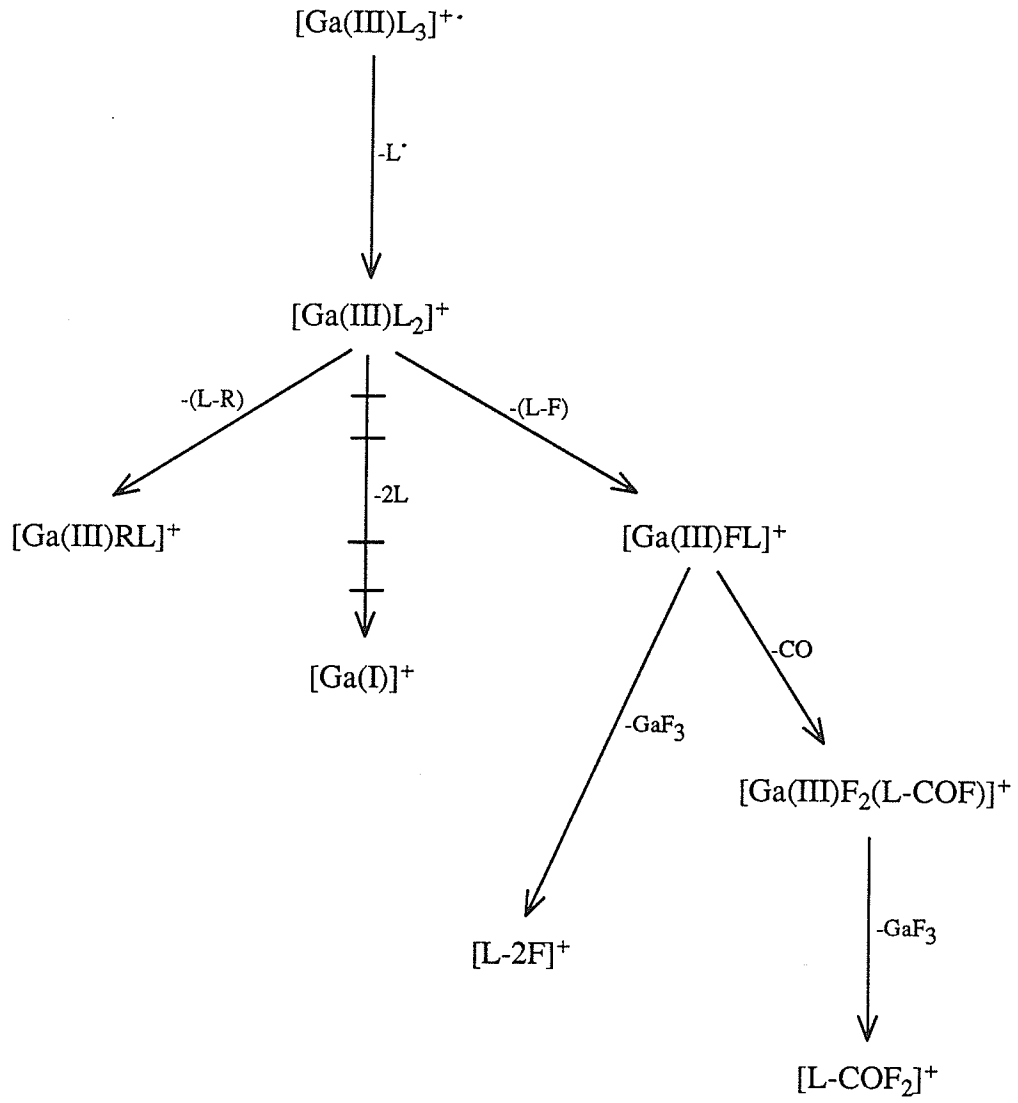

+++> reaction step in which a change in metal oxidation state is proposed.

Scheme 24. Proposed fragmentation pathways for Ga(III) β-diketonates where R' = CHF_2 (Ga-1a and -2a).

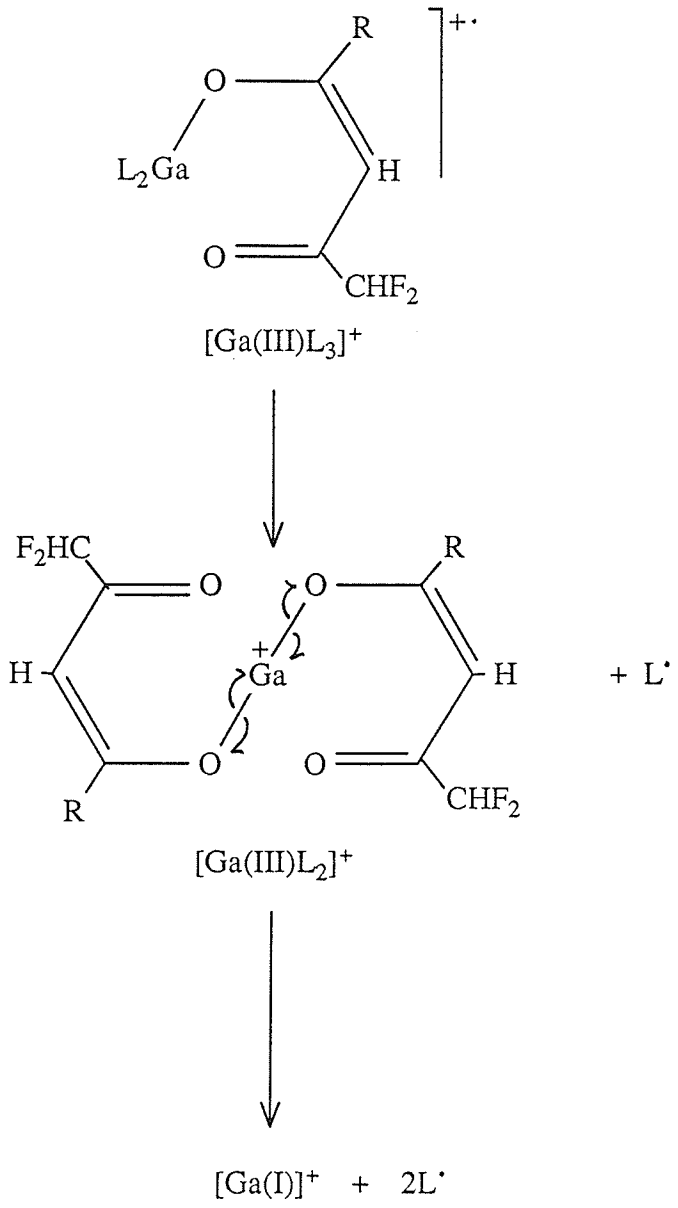

Scheme 25. Suggested mechanism for the formation of $[Ga(III)L_2]^+$ and $[Ga(I)]^+$ in **Ga-1a** and **-2a**.

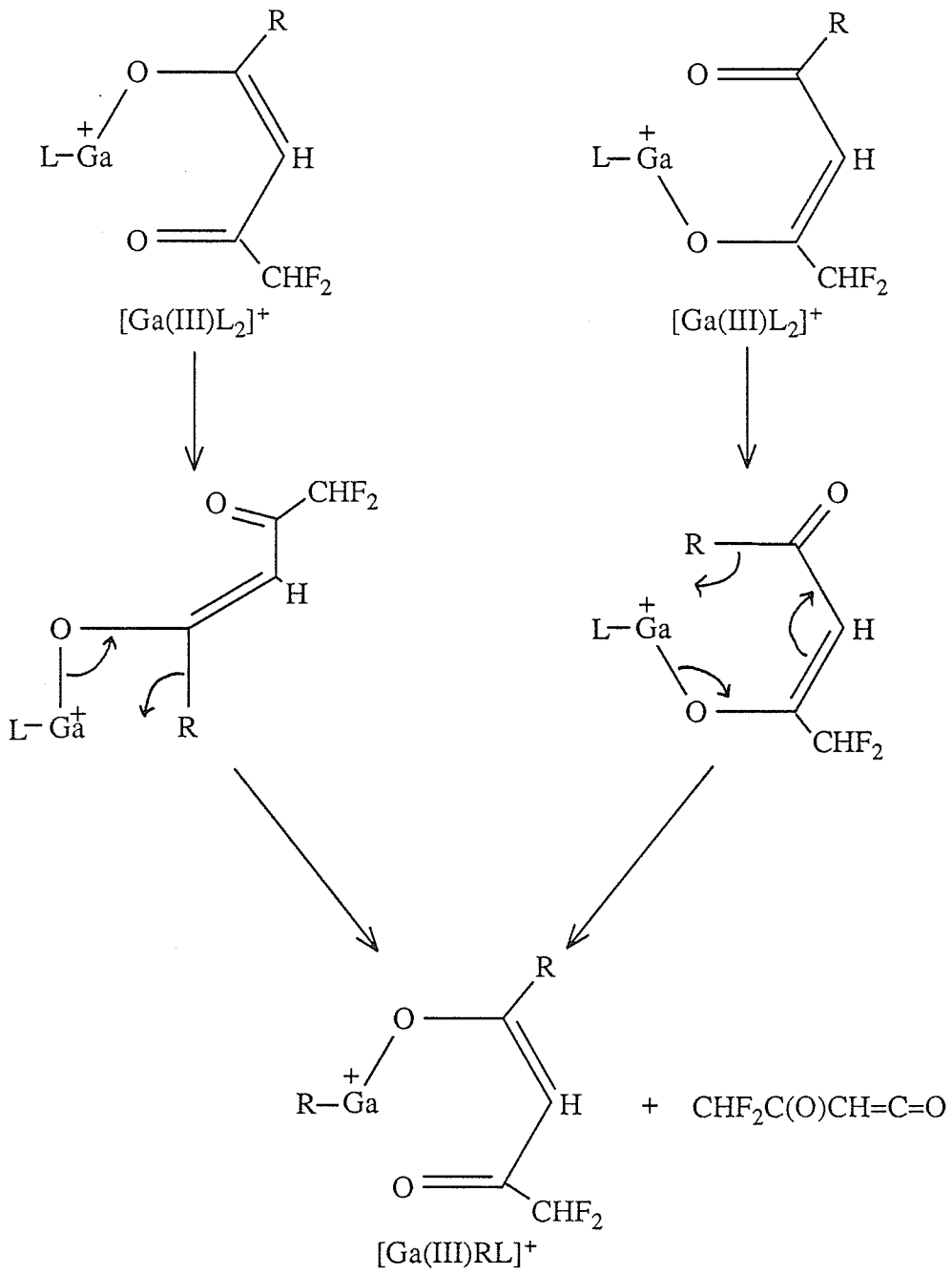

Scheme 26. Suggested mechanism for the formation of $[Ga(III)RL]^+$ in **Ga-1a** and **-2a**.

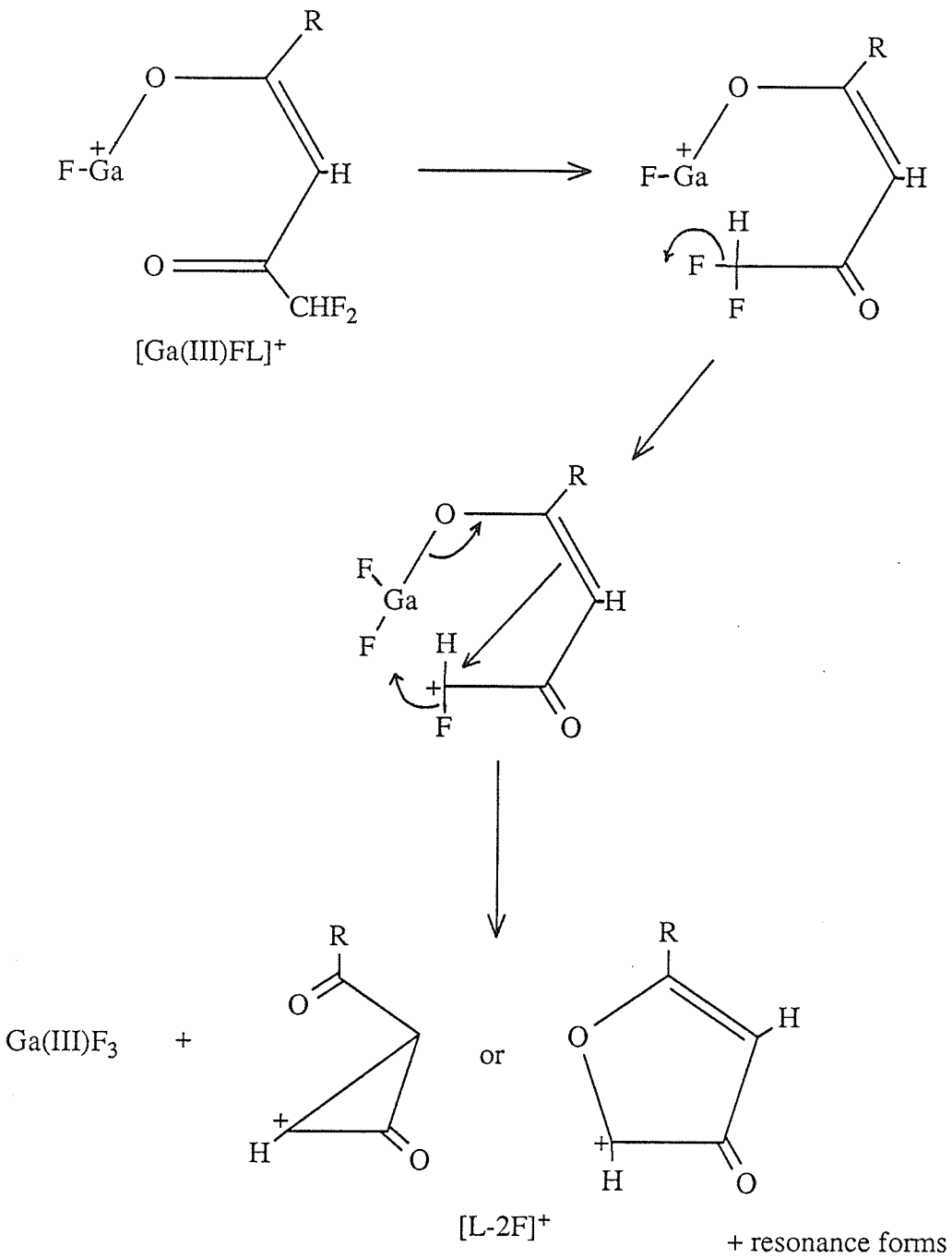

Scheme 27. Suggested mechanism for the elimination of $Ga(III)F_3$ from $[Ga(III)FL]^+$ in **Ga-1a** and **-2a**.

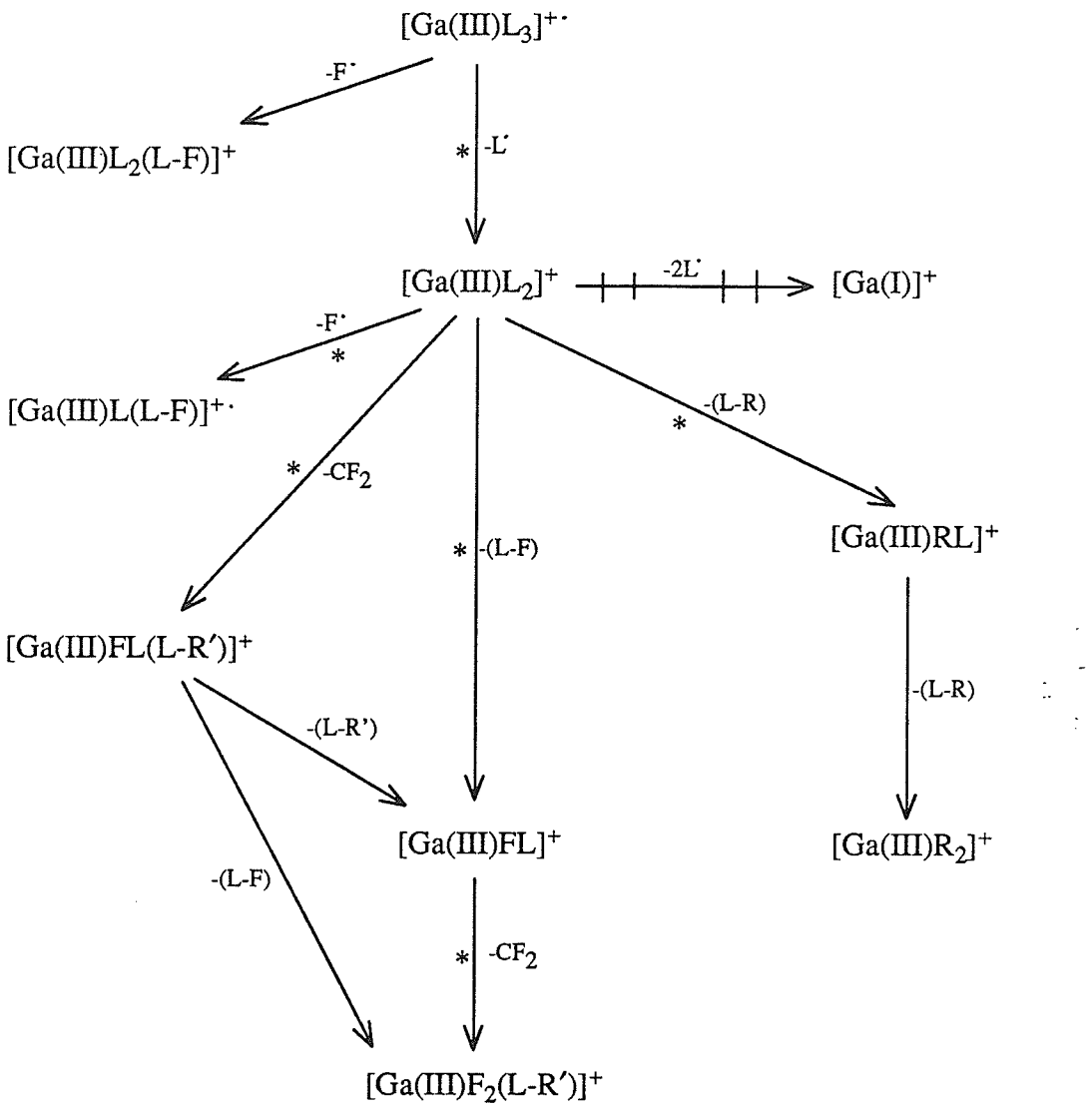

* process confirmed by the observation of a metastable transition in at least one of the complexes.

⟶ reaction step in which a change in metal oxidation state is proposed.

Scheme 28. Proposed fragmentation pathways for Ga(III) β-diketonates where R' = CF_3 (Ga-3a, -4a, -5a, -8a and -12a). Pathways are common to all complexes except where noted.

(c) Co(III) β - diketonates

Relative abundance data for the thirteen Co(III) β-diketonates studied appear in Tables 14-19. Plots of the EI mass spectra are depicted in Figures 43-55. A linked-scanning, metastable analysis of **Co-8a** was carried out. The mass spectrum of one of the chelates (**Co-3a**) has been reported previously (127,128,140).

A general difficulty encountered in the interpretation of the spectra was the consistent appearance of minor peaks at three mass units below the major cobalt-containing ions. From the isotopic pattern and the presence of corresponding fragmentation, these signals were eventually attributed to iron chelates of the ligand under examination. Previous studies (175) have shown that problems can arise with determinations performed on metals that also constitute part of the ion source materials (eg. nickel, cobalt, iron). The result is an exchange between the ligand-bound metal (in this case Co) and a metal of which the ion source is composed (Fe). Fortunately, the mass "separation" between ^{59}Co and ^{56}Fe is large enough to allow for the unambiguous assignment of peak identities and abundances.

Suggested decomposition pathways for the Co(III) β-diketonate complexes possessing a difluoromethyl substituent (R' = CHF_2; Table 14) are shown in Scheme 29. Although molecular ions were observed in the mass spectra of both complexes, no abundance values are formally assigned; the extremely low and variable contributions from the $[M]^{+\cdot}$ signal did not allow for accurate abundance determinations. Loss of a ligand radical from $[Co(III)L_3]^{+\cdot}$ is a dominant process, resulting in the formation of the EE^+ ion $[Co(III)L_2]^+$. The subsequent elimination of a second radical species, either $R'^{\cdot}$ or $L^{\cdot}$, suggests a prior reduction of the complexed metal:

$$[Co(III)L_2]^+ \longrightarrow [Co(II)L_2]^{+\cdot} \longrightarrow [Co(II)L(L\text{-}R')]^+ + R'^{\cdot}$$
$$\longrightarrow [Co(II)L]^+ + L^{\cdot}$$

The stability of the cobalt +2 oxidation state translates into a predominance of EE^o neutral losses ((L-R'), (L-R), CO, CHF), each resulting in a Co(II) fragment ion. Proposed mechanisms for the decomposition sequence

$$[Co(III)L_2]^+ \longrightarrow [Co(II)L_2]^{+\cdot} \longrightarrow [Co(II)L(L\text{-}R')]^+ \longrightarrow$$
$$[Co(II)L]^+ \longrightarrow Co(II)F(L\text{-}COF)]^+ \longrightarrow [L\text{-}COF_2]^+$$

are given in Schemes 30 and 31. A series of intramolecular bond-forming/ bond-breaking processes can be evoked to explain the observed fragmentations. The loss of the neutral species $Co(II)F_2$ in the

fragmentations

$$[Co(II)F(L\text{-}COF)]^+ \longrightarrow [L\text{-}COF_2]^+ + Co(II)F_2 \qquad \text{(Scheme 31)}$$

and

$$[Co(II)L]^+ \longrightarrow [L\text{-}F_2]^+ + Co(II)F_2 \qquad \text{(Scheme 32)}$$

provides confirmatory evidence for fluorine rearrangement to the metal center. Scheme 33 depicts two possible mechanisms for the formation of $[Co(II)F(L\text{-}R')]^+$, one involving the loss of (L-F) from $[Co(II)L(L\text{-}R')]^+$, the other the elimination of the EE^o neutral CHF from $[Co(II)L]^+$. The appearance of the bare metal ion $[Co(I)]^+$ implies a further reduction of cobalt to the +1 oxidation state. Metastable evidence obtained from the linked-scanning experiment conducted on the trifluoromethyl derivative **Co-8a** suggests that $[Co(I)]^+$ arises through the concomitant losses of (L-R') and F$^{\cdot}$ from $[Co(II)F(L\text{-}R')]^+$ as shown in Scheme 33. A metal reduction is entirely in keeping with the well-established nature of the cobalt +1 oxidation state; in fact, with the exception of copper, the +1 state is better known for cobalt than for any other first transition series metal (176). The remaining decompositions:

$$[Co(III)L_2]^+ \longrightarrow [Co(II)FL(L\text{-}R')]^+$$

and

$$[Co(II)L]^+ \longrightarrow [Co(II)R]^+$$

have been described in Schemes 22 and 26 respectively.

The fragmentation pathways for the Co(III) β-diketonate complexes possessing a trifluoromethyl substituent (R' = CF_3; Tables 15-17) are shown in Scheme 34. The molecular ion intensities are very low, while $[Co(III)L_2]^+$ and $[Co(II)L(L\text{-}R')]^+$ are the most abundant of the cobalt-containing fragments. Many of the pathways given in Scheme 34 have been substantiated by metastable evidence and can be rationalized by established mechanisms; these fragmentations and their corresponding schemes are summarized below:

Fragmentation	Scheme
$[Co(III)L_2]^+ \longrightarrow [Co(III)FL(L\text{-}R')]^+$	17
$[Co(II)L]^+ \longrightarrow [Co(II)R]^+$	26
$[Co(II)L_2]^{+\cdot} \longrightarrow [Co(II)L(L\text{-}R')]^+$	30
$[Co(II)L_2]^{+\cdot} \longrightarrow [Co(II)L]^+$	30
$[Co(II)L(L\text{-}R')]^+ \longrightarrow [Co(II)L]^+$	30
$[Co(II)L]^+ \longrightarrow [Co(II)F(L\text{-}COF)]^+$	31
$[Co(II)F(L\text{-}COF)]^+ \longrightarrow [L\text{-}COF_2]^+$	31
$[Co(II)L(L\text{-}R')]^+ \longrightarrow [Co(II)F(L\text{-}R')]^+$	33
$[Co(II)F(L\text{-}R')]^+ \longrightarrow [Co(I)]^+$	33

The elimination of the EE^o neutrals CO_2, RC_2H, CF_2 and CO_2 in the decomposition sequence

$$[Co(II)L(L\text{-}R')]^+ \longrightarrow [Co(II)LCHCR]^+ \longrightarrow [Co(II)L]^+ \longrightarrow$$
$$[Co(II)F(L\text{-}R')]^+ \longrightarrow [Co(II)FCHCR]^+$$

is described in Scheme 35. Assigning carbon dioxide to the 44u neutral fragment was first determined by Clobes, Morris and Koob (140) through

their study of a perdeuterated tris(1,1,1-trifluoro-4-phenyl-2,4-butanedionato)Fe(III) complex that exhibited similar fragmentation behavior. The vinyl carbonium ion character proposed for both $[Co(II)LCHCR]^+$ and $[Co(II)FCHCR]^+$ results from a 1,3 shift of the oxygen to the electron-deficient carbonyl carbon. Resonance stabilization by the adjacent aromatic group promotes formation of the resulting ion:

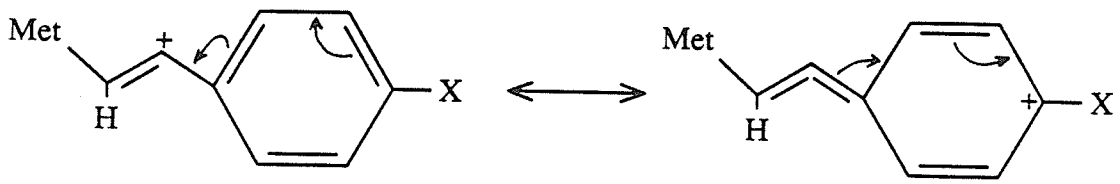

$X = H, CH_3$

Two possible routes leading to the formation of the ion $[Co(II)R]^+$ from $[Co(II)L]^+$ are shown in Scheme 34. One involves the direct migration of the aryl group from the ligand to the metal. A similar rearrangement was observed for the di- and trifluoromethyl-substituted Ga(III) β-diketonates in the decomposition

$$[Ga(III)L_2]^+ \longrightarrow [Ga(III)RL]^+ \quad \text{(Scheme 26)}$$

The second pathway proceeds via the elimination of the EE^o neutrals CF_2, HF and C_3O_2; Scheme 36 shows the sequential loss of HF and C_3O_2 in

$$[Co(II)F(L\text{-}CF_3)]^+ \longrightarrow [Co(II)(L\text{-}CF_2\text{-}HF)]^+ \longrightarrow [Co(II)R]^+$$

Results by Clobes et al. (128) using a deuterated Fe(III) analog established that the hydrogen in HF originates from the bridging

position of the ligand. The loss of HF is followed by the migration of the aryl group to the positive cobalt center and the expulsion of the neutral fragment C_3O_2.

Complex **Co-8a** (R = C_4H_3S) gives a unique fragment at m/z 363; metastable results confirm that its parent is $[CoL_2]^+$. Two structures appear possible: $[Co(II)L_2\text{-}2R']^+$ or $[Co(III)RL]^+$. The loss of two R'· radicals seems unlikely, as it would involve the energetically-unfavorable elimination of an OE· neutral (CF_3·) from an EE^+ ion ($[Co(II)L(L\text{-}R')]^+$). On the other hand, the transition

$$[Co(III)L_2]^+ \longrightarrow [Co(III)RL]^+$$

does have a parallel in the loss of (L-R) in

$$[Ga(III)L_2]^+ \longrightarrow [Ga(III)RL]^+ \quad \text{(Scheme 26)}$$

The loss of CF_3· from $[Co(III)RL]^+$ is suggested to occur in the spectrum of **Co-11a**, producing the ion $[Co(II)R(L\text{-}R')]^+$ (m/z 262). Implied in this process is the prior reduction of Co(III) to Co(II) to give the $OE^{+\cdot}$ ion $[Co(II)RL]^{+\cdot}$. The very low abundance of $[Co(III)RL]^+$ in **Co-8a** and its absence in the mass spectrum of **Co-11a** reflect the greater stability of the cobalt +2 oxidation state as compared to the +3 state.

Once again, a correlation can be drawn between the stabilities of the fluorine-to-metal transfer ions and the electron-withdrawing capabilities of the aryl (R) ring substituents. The correspondence is rather tenuous, however, as only a small selection of fluorine transfer

ions are observed in the cobalt spectra. The fact that Co^{2+} is a borderline acid may account for the reduced numbers of fluorine migrations; HSAB theory predicts only a minimal attraction between a borderline acid and a hard base. Nevertheless, an examination of the ion currents carried by $[Co(II)F(L\text{-}R')]^+$, the only fluorine-transfer fragment common to all seven trifluoromethyl-substituted Co(III) complexes, reveals a familiar pattern (%TIC in parentheses): R = 4-methylphenyl (1.4) < phenyl (2.1) = 2-naphthyl (2.3) < 4-chlorophenyl (3.1) < 5-chloro-2'-thienyl (3.6) < 2-thienyl (4.8) < 2-furyl (9.6).

Suggested fragmentation routes for the Co(III) β-diketonates possessing pentafluoroethyl (R' = C_2F_5; Table 18) and heptafluoropropyl (R' = C_3F_7; Table 19) substituents are shown in Scheme 37. Several of the decompositions have been previously detailed:

Fragmentation	Scheme
$[Co(III)L_2]^+ \longrightarrow [Co(III)FL(L\text{-}CF_3)]^+$	17
$[Co(II)L]^+ \longrightarrow [Co(II)R]^+$	26
$[Co(II)L_2]^{+\cdot} \longrightarrow [Co(II)L(L\text{-}R')]^+$	30
$[Co(II)L_2]^{+\cdot} \longrightarrow [Co(II)L]^+$	30
$[Co(II)L(L\text{-}R')]^+ \longrightarrow [Co(II)L]^+$	30
$[Co(II)L]^+ \longrightarrow [Co(II)F(L\text{-}COF)]^+$	31
$[Co(II)F(L\text{-}COF)]^+ \longrightarrow [L\text{-}COF_2]^+$	31
$[Co(II)L(L\text{-}R')]^+ \longrightarrow [Co(II)F(L\text{-}R')]^+$	33
$[Co(II)F(L\text{-}R')]^+ \longrightarrow [Co(I)]^+$	33
$[Co(II)L(L\text{-}R')]^+ \longrightarrow [Co(II)LCHCR]^+$	35

$$[Co(II)LCHCR]^+ \longrightarrow [Co(II)L]^+ \qquad 35$$

$$[Co(II)L]^+ \longrightarrow [Co(II)F(L\text{-}C_2F_5)]^+ \qquad 35$$

In sharp contrast to the weak molecular ion abundances encountered for the di- and trifluoromethyl-substituted Co(III) complexes, the perfluoroethyl and perfluoropropyl derivatives generally exhibit strong $[M]^{+\cdot}$ abundances. One possible explanation may be that the highly electronegative C_2F_5 and C_3F_7 groups stabilize the metal in its +3 oxidation state. Besides $[Co(III)L_3]^{+\cdot}$, the ions $[Co(III)L_2]^+$, $[Co(III)L(L\text{-}32)]^+$, $[Co(II)L(L\text{-}R')]^+$ and $[Co(II)L]^+$ dominate the metal-containing peaks.

Fluorine transfer processes appear to decline in both number and significance as the extent of ligand fluorination increases. Comparing the %TIC carried by the fluorine migration ions when R = C_6H_5 and C_4H_3S (the only R groups common to all R' classifications) for each of the four fluorinated R' groups reveals a striking dependence between ion abundance and the nature of the R' group (%TIC in parentheses): CF_3 (8.0) > CHF_2 (6.8) > C_2F_5 (3.8) > C_3F_7 (0.6). It is apparent that in the competition for fluorine, the more highly-fluorinated (harder) the R' group, the less likely fluorine migration to the soft, borderline acid Co(II) center will be. The ordering CF_3 > CHF_2 can be attributed to the factors discussed earlier: the greater resonance stability of CF_2 versus CHF, and the enhanced statistical probability of fluorine transfer occurring from a CF_3 group as compared to a CHF_2 moiety.

Table 14. 70 eV-EI mass spectra of compounds **Co-1a** and **Co-2a.**

	Co-1a	**Co-2a**
R =	$-C_6H_5$	$-C_4H_3S$
R'=	$-CHF_2$	$-CHF_2$

ION	%RA	m/z	%TIC	%RA	m/z	%TIC
$[CoL_3]^+$	-	(650)	-	-	(668)	-
$[CoL_2]^+$	45.0	(453)	11.5	26.5	(465)	7.7
$[CoFL(L-R')]^+$	2.8	(421)	0.7	-	(433)	-
$[CoL(L-R')]^+$	50.6	(402)	12.9	27.3	(414)	7.9
$[CoL]^+$	5.6	(256)	1.4	5.0	(262)	1.5
$[CoF(L-COF)]^+$	8.0	(228)	2.0	5.4	(234)	1.6
$[CoF(L-R')]^+$	6.3	(224)	1.6	3.2	(230)	0.9
$[CoR]^+$	2.5	(136)	0.6	3.0	(142)	0.9
$[Co]^+$	3.5	(59)	0.9	-	(59)	-
$[HL]^+$	3.4	(198)	0.9	25.5	(204)	7.4
$[L-F]^+$	10.5	(178)	2.7	1.6	(184)	0.5
$[L-2F]^+$	3.8	(159)	1.0	2.6	(165)	0.8
$[HL-R']^+$	23.6	(147)	6.0	60.7	(153)	17.7
$[L-COF_2]^+$	4.0	(131)	1.0	3.6	(137)	1.0
$[RCO]^+$	100.0	(105)	25.5	100.0	(111)	29.1
$[RCCH]^+$	30.0	(102)	7.7	4.7	(108)	1.4
$[R]^+$	50.7	(77)	12.9	13.5	(83)	3.9
[CF3]$^+$	25.9	(69)	6.6	60.8	(69)	17.7
$[R']^+$	15.4	(51)	3.9	-	(51)	-

Table 15. 70 eV-EI mass spectra of compounds **Co–3a**, **Co–4a** and **Co–6a**.

	Co–3a			**Co–4a**			**Co–6a**		
R =	$-C_6H_5$			$-C_6H_4CH_3$			$-C_6H_4Cl$		
R'=	$-CF_3$			$-CF_3$			$-CF_3$		
ION	%RA	m/z	%TIC	%RA	m/z	%TIC	%RA	m/z	%TIC
$[CoL_3]^+$	0.2	(704)	0.1	-	(746)	-	-	(806)	-
$[CoL_2]^+$	45.2	(489)	12.1	29.8	(517)	9.4	34.9	(557)	11.0
$[CoL(L-R')]^+$	34.4	(420)	9.2	20.1	(448)	6.3	23.2	(488)	7.3
$[CoLCHCR]^+$	1.7	(376)	0.5	1.8	(404)	0.6	-	(444)	-
$[CoL]^+$	6.9	(274)	1.8	2.9	(288)	0.9	9.0	(308)	2.8
$[CoF(L-R')]^+$	8.0	(224)	2.1	4.3	(238)	1.4	9.8	(258)	3.1
$[CoR]^+$	1.9	(136)	0.5	-	(150)	-	1.4	(170)	0.4
$[Co]^+$	2.1	(59)	0.6	-	(59)	-	2.6	(59)	0.8
$[HL]^+$	26.1	(216)	7.0	22.3	(230)	7.0	17.8	(250)	5.6
$[L]^+$	3.0	(215)	0.8	1.6	(229)	0.5	-	(249)	-
$[HL-CH_3]^+$	-	(201)	-	3.4	(215)	1.1	-	(235)	-
$[HL-R']^+$	31.7	(147)	8.5	30.1	(161)	9.5	35.2	(181)	11.1
$[RC_3O]^+$	2.3	(129)	0.6	-	(143)	-	-	(163)	-
$[RCO]^+$	100.0	(105)	26.7	100.0	(119)	31.4	100.0	(139)	31.4
$[RCCH]^+$	2.1	(102)	0.6	-	(116)	-	1.5	(136)	0.5
$[R]^+$	51.5	(77)	13.8	40.8	(91)	12.8	29.6	(111)	9.3
$[HL-R']^{2+}$	-	(73.5)	-	2.6	(80.5)	0.8	3.5	(90.5)	1.1
$[R-HCl]^+$	-	(41)	-	-	(55)	-	10.8	(75)	3.4
$[R']^+$	57.1	(69)	15.3	58.3	(69)	18.3	39.1	(69)	12.3

Table 16. 70 eV-EI mass spectra of compounds **Co-8a** and **Co-10a**.

	Co-8a	**Co-10a**
R =	$-C_4H_3S$	$-C_4H_2SCl$
R'=	$-CF_3$	$-CF_3$

ION	%RA	m/z	%TIC	%RA	m/z	%TIC
$[CoL_3]^+$	-	(722)	-	-	(824)	-
$[CoL_2]^+$ (a)	57.3	(501)	17.1	30.0	(569)	7.4
$[CoFL(L-R')]^+$	-	(451)	-	2.0	(519)	0.5
$[CoL(L-R')]^+$ (b)	[a]42.3	(432)	12.6	11.1	(500)	2.8
$[CoLCHCR]^+$	[b]3.3	(388)	1.0	-	(456)	-
$[CoRL]^+$	[a]1.1	(363)	0.3	-	(431)	-
$[CoL]^+$ (c)	[a,b]19.7	(280)	5.9	15.4	(314)	3.8
$[CoF(L-COF)]^+$	[c]1.6	(252)	0.5	1.7	(286)	0.4
$[CoF(L-R')]^+$ (d)	[b,c]16.1	(230)	4.8	14.4	(264)	3.6
$[Co(L-CF_2-HF)]^+$	[d]2.7	(210)	0.8	-	(244)	-
$[CoFCHCR]^+$	[d]2.0	(186)	0.6	-	(220)	-
$[CoR]^+$	[c]7.6	(142)	2.3	4.0	(176)	1.0
$[Co]^+$	[d]2.1	(59)	0.6	1.4	(59)	0.3
$[HL]^+$	16.5	(222)	4.9	33.9	(256)	8.4
$[L-S]^+$	[a]4.7	(189)	1.4	-	(223)	-
$[L-Cl]^+$	-	(186)	-	68.1	(220)	16.9
$[L-COF_2]^+$	1.3	(155)	0.4	1.6	(189)	0.4
$[HL-R']^+$	16.8	(153)	5.0	37.2	(187)	9.2
$[RC_3O]^+$	1.4	(135)	0.4	1.3	(169)	0.3

Table 16. (continued).

$[RCO]^+$	[b,d]100.0 (111) 29.8	100.0 (145) 24.8
$[RCCH]^+$	1.8 (108) 0.5	2.1 (142) 0.5
$[R]^+$	6.1 (83) 1.8	5.2 (117) 1.3
$[HL-R']^{2+}$	1.8 (76.5) 0.5	4.0 (93.5) 1.0
$[R']^+$	32.5 (69) 9.7	69.7 (69) 17.3

[a] Identified metastable transitions are indicated by superscripts which relate the daughter ion to its precursor as labelled in column 1.

Table 17. 70 eV-EI mass spectra of compounds **Co-11a** and **Co-12a.**

	Co-11a			**Co-12a**		
R =	$-C_4H_3O$			$-C_{10}H_7$		
R'=	$-CF_3$			$-CF_3$		
ION	%RA	m/z	%TIC	%RA	m/z	%TIC
$[CoL_3]^+$	2.0	(674)	0.4	-	(854)	-
$[CoL_2]^+$	66.2	(469)	14.2	46.3	(589)	12.2
$[CoFL(L-COF)]^+$	1.7	(441)	0.4	-	(561)	-
$[CoL(L-R')]^+$	73.0	(400)	15.7	23.7	(520)	6.2
$[CoL]^+$	14.1	(264)	3.0	2.7	(324)	0.7
$[CoR(L-R')]^+$	8.0	(262)	1.7	-	(322)	-
$[CoF(L-COF)]^+$	2.8	(236)	0.6	-	(296)	-
$[CoF(L-R')]^+$	44.5	(214)	9.6	8.9	(274)	2.3
$[Co(L-CF_2-HF)]^+$	8.5	(194)	1.8	-	(254)	-
$[CoFCHCR]^+$	3.0	(170)	0.6	-	(230)	-
$[CoR]^+$	7.8	(126)	1.7	2.5	(186)	0.7
$[Co]^+$	4.7	(59)	1.0	2.0	(59)	0.5
$[HL]^+$	19.0	(206)	4.1	20.4	(266)	5.4
$[L]^+$	-	(205)	-	3.9	(265)	1.0
$[L-COF_2]^+$	2.7	(139)	0.5	1.2	(199)	0.3
$[HL-R']^+$	39.1	(137)	8.4	19.9	(197)	5.2
$[RC_3O]^+$	2.0	(119)	0.4	-	(179)	-
$[HL-95]^+$	4.6	(111)	1.0	-	(171)	-
$[RCO]^+$	100.0	(95)	21.5	100.0	(155)	26.3

Table 17. (continued).

$[RCCH]^+$	2.3 (92) 0.5	6.6 (152) 1.7
$[R]^+$	3.3 (67) 0.7	75.1 (127) 19.7
$[HL\text{-}R']^{2+}$	2.1 (68.5) 0.5	2.7 (98.5) 0.7
$[R']^+$	57.6 (69) 12.4	61.5 (69) 16.2

Table 18. 70 eV-EI mass spectra of compounds **Co-13a** and **Co-14a**.

	Co-13a			**Co-14a**		
R =	$-C_6H_5$			$-C_4H_3S$		
R'=	$-C_2F_5$			$-C_2F_5$		
ION	%RA	m/z	%TIC	%RA	m/z	%TIC
$[CoL_3]^+$	9.3	(854)	4.6	1.9	(872)	0.7
$[CoL_2]^+$	19.7	(589)	9.8	37.1	(601)	13.0
$[CoL(L-32)]^+$	-	(557)	-	11.6	(569)	4.1
$[CoFL(L-CF_3)]^+$	1.5	(539)	0.7	-	(551)	-
$[CoL(L-R')]^+$	19.3	(470)	9.6	36.4	(482)	12.7
$[CoLCHCR]^+$	-	(426)	-	1.3	(438)	0.5
$[CoL]^+$	4.1	(324)	2.0	13.9	(330)	4.9
$[CoF(L-COF)]^+$	-	(296)	-	2.3	(302)	0.8
$[CoF(L-R')]^+$	2.2	(224)	1.1	3.4	(230)	1.2
$[CoR]^+$	2.1	(136)	1.0	11.1	(142)	3.9
$[Co]^+$	0.8	(59)	0.4	1.7	(59)	0.6
$[HL]^+$	0.4	(266)	0.2	7.4	(272)	2.6
$[L]^+$	0.2	(265)	0.1	-	(271)	-
$[L-S]^+$	-	(233)	-	1.8	(239)	0.6
$[L-COF_2]^+$	1.3	(199)	0.6	2.6	(205)	0.9
$[HL-95]^+$	1.1	(171)	0.5	3.1	(177)	1.1
$[HL-R']^+$	4.6	(147)	2.3	15.4	(153)	5.4
$[RC_3O]^+$	-	(129)	-	1.3	(135)	0.5

Table 18. (continued).

$[RCO]^+$	100.0 (105) 50.0	100.0 (111) 35.0
$[RCCH]^+$	0.3 (102) 0.1	2.0 (108) 0.7
$[R]^+$	25.4 (77) 12.7	7.4 (83) 2.6
$[CF_3]^+$	8.7 (69) 4.3	26.9 (69) 9.4

Table 19. 70 eV-EI mass spectra of compounds **Co-16a** and **Co-17a**.

	Co-16a	**Co-17a**
R =	$-C_6H_5$	$-C_4H_3S$
R'=	$-C_3F_7$	$-C_3F_7$

ION	%RA	m/z	%TIC	%RA	m/z	%TIC
$[CoL_3]^+$	5.3	(1004)	2.0	0.1	(1022)	-
$[CoL_2(L-32)]^+$	-	(972)	-	3.3	(990)	0.9
$[CoL_2]^+$	15.1	(689)	5.8	33.8	(701)	9.6
$[CoL(L-F)]^+$	-	(670)	-	2.1	(682)	0.6
$[CoL(L-32)]^+$	19.6	(657)	7.5	41.2	(669)	11.7
$[CoL(L-R')]^+$	14.3	(520)	5.5	35.4	(532)	10.1
[CoLCHCR]+	-	(476)	-	1.9	(488)	0.5
$[CoL]^+$	2.6	(374)	1.0	14.3	(380)	4.1
$[CoF(L-COF)]^+$	-	(346)	-	2.1	(352)	0.6
$[CoR]^+$	0.8	(136)	0.3	7.7	(142)	2.2
$[HL]^+$	5.8	(316)	2.2	16.0	(322)	4.5
$[L-S]^+$	-	(283)	-	1.1	(289)	0.3
$[L-COF_2]^+$	-	(249)	-	2.1	(255)	0.6
$[HL-95]^+$	1.3	(221)	0.5	3.9	(227)	1.1
$[HL-R']^+$	33.9	(147)	13.0	32.6	(153)	9.3
$[RCO]^+$	100.0	(105)	38.4	100.0	(111)	28.4
$[RCCH]^+$	1.8	(102)	0.7	2.7	(108)	0.8
$[R]^+$	26.7	(77)	10.3	8.4	(83)	2.4
$[HL-R']^{2+}$	-	(73.5)	-	3.1	(76.5)	0.9
$[CF_3]^+$	33.2	(69)	12.7	42.0	(69)	11.9

Figure 43.

Normalized 70 eV-EI mass spectrum of

tris[1,1-difluoro-4-phenyl-2,4-butanedionato]Co(III)

{**Co-1a**}.

m/z $[M]^{+\cdot}$ = 650, $[L]^{+}$ = 197

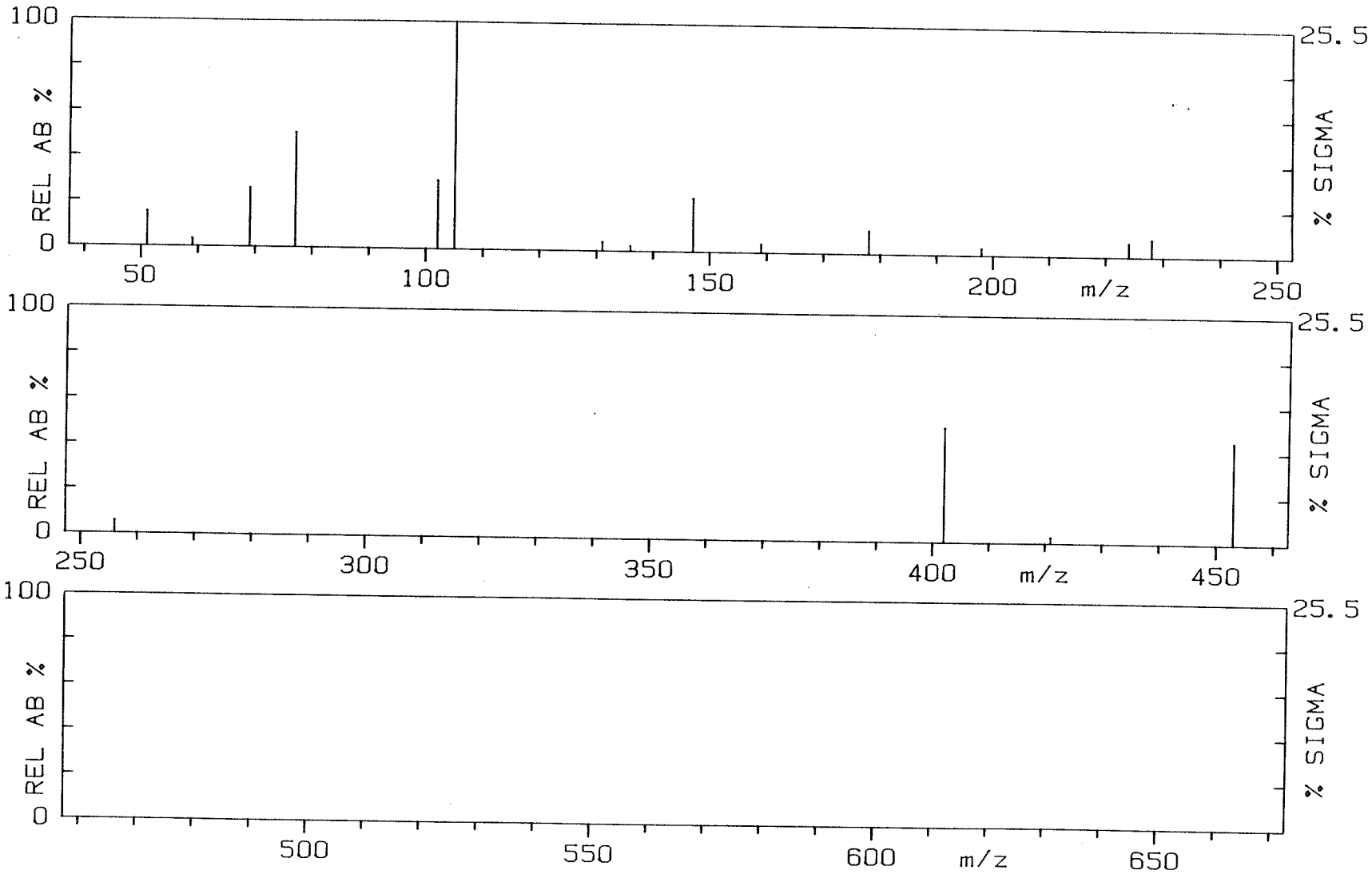
CO-1A 70EV.
100
0 REL AB %
25.5
% SIGMA
50
100
150
200
m/z
250
250
300
350
400
450
500
550
600
650

Figure 44.

Normalized 70 eV-EI mass spectrum of

tris[1,1,-difluoro-4-(2'-thienyl)-2,4-butanedionato]Co(III)

{**Co-2a**}.

m/z $[M]^{+\cdot}$ = 668, $[L]^{+}$ = 203

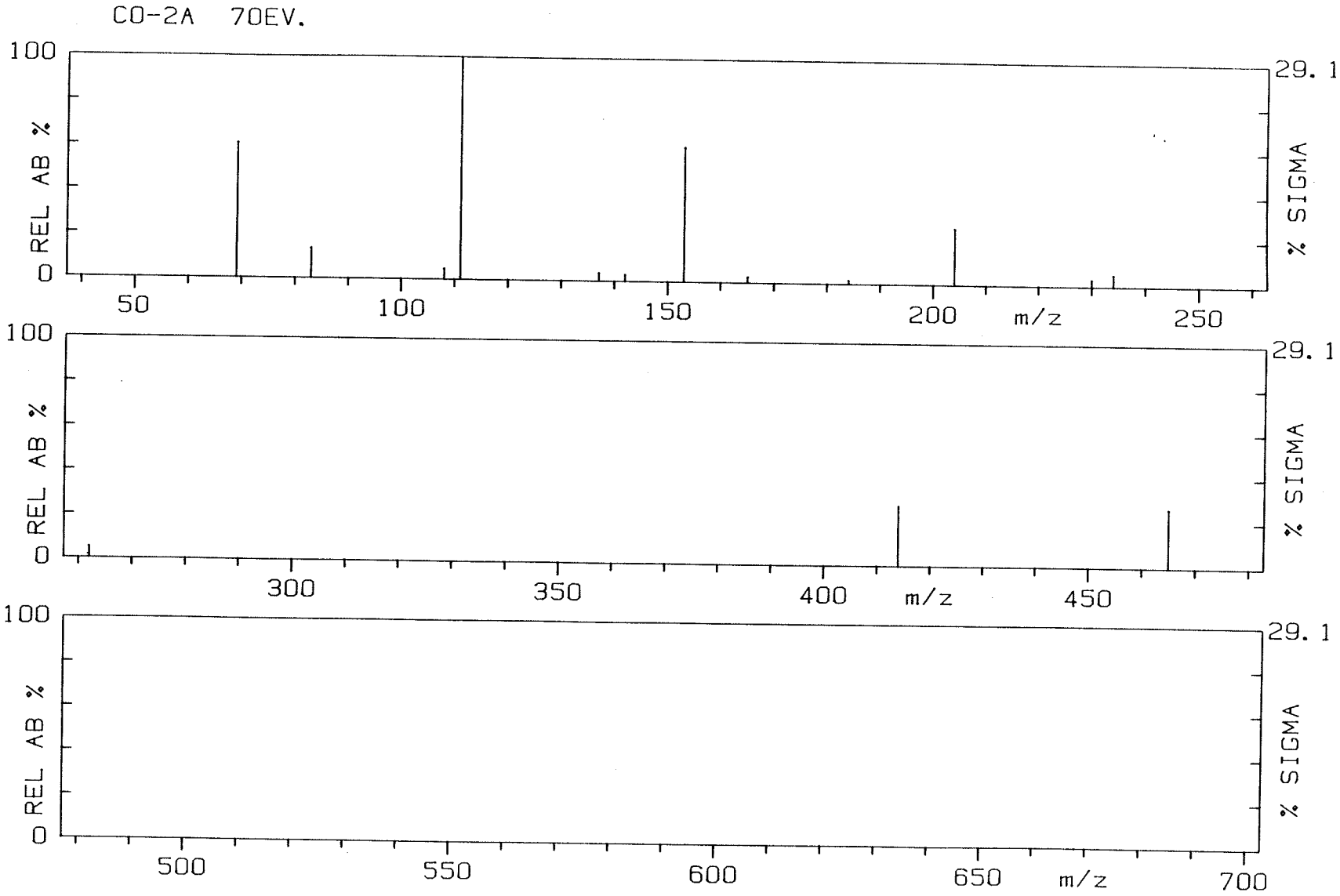
CO-2A 70EV.
100
0
REL AB %
50
100
150
200
m/z
250
29. 1
% SIGMA
100
0
REL AB %
300
350
400
m/z
450
29. 1
% SIGMA
100
0
REL AB %
500
550
600
650
m/z
700
29. 1
% SIGMA

Figure 45.

Normalized 70 eV-EI mass spectrum of

tris[1,1,1-trifluoro-4-phenyl-2,4-butanedionato]Co(III)

{Co-3a}.

m/z $[M]^{+\cdot}$ = 704, $[L]^{+}$ = 215

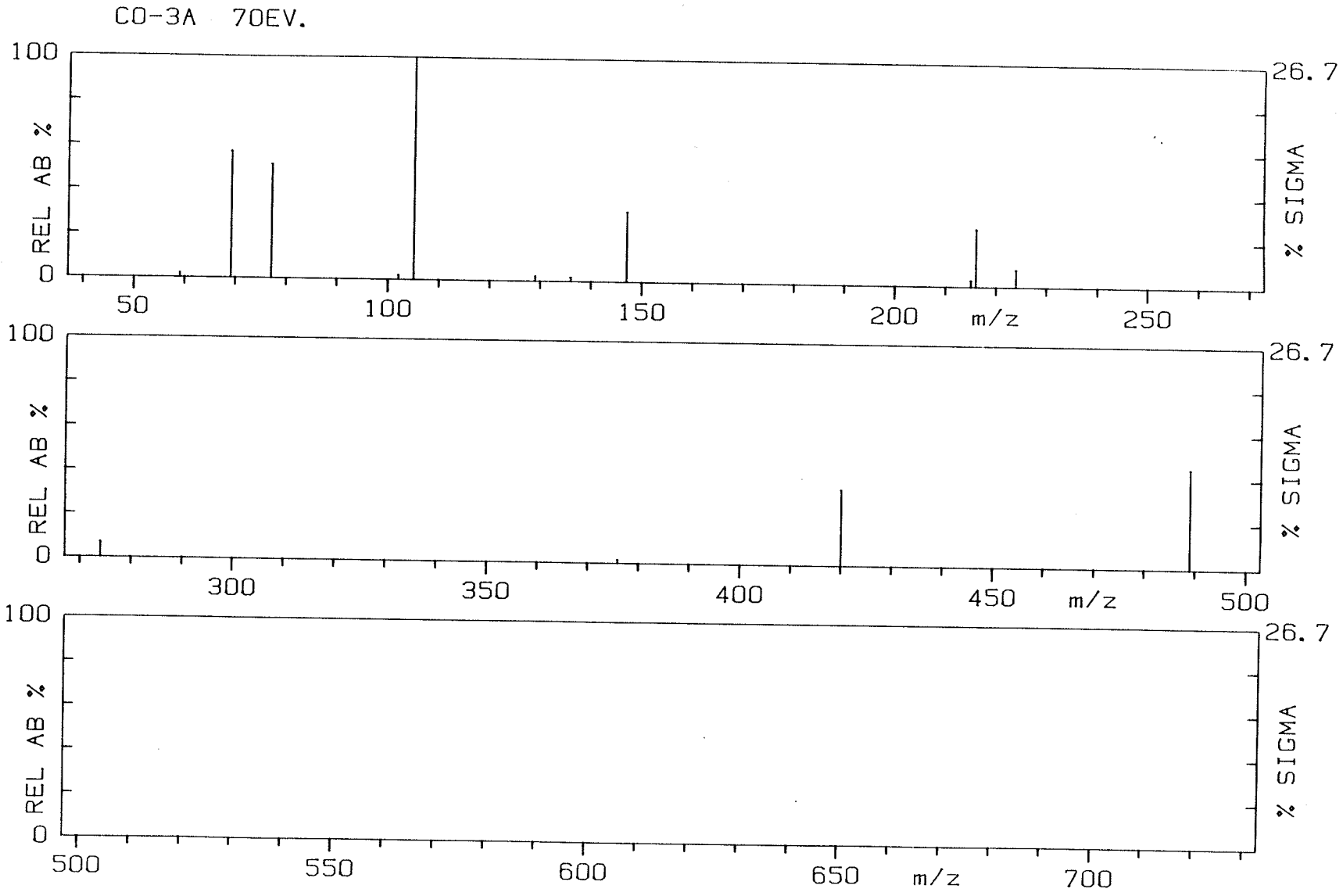
CO-3A 70EV.
100
REL AB %
0
50
100
150
200
m/z
250
26.7
% SIGMA
100
REL AB %
0
300
350
400
450
m/z
500
26.7
% SIGMA
100
REL AB %
0
500
550
600
650
m/z
700
26.7
% SIGMA

Figure 46.

Normalized 70 eV-EI mass spectrum of

tris[1,1,1-trifluoro-4-(4'-methylphenyl)-2,4-butanedionato]Co(III)

{**Co-4a**}.

m/z $[M]^{+\cdot}$ = 746, $[L]^{+}$ = 229

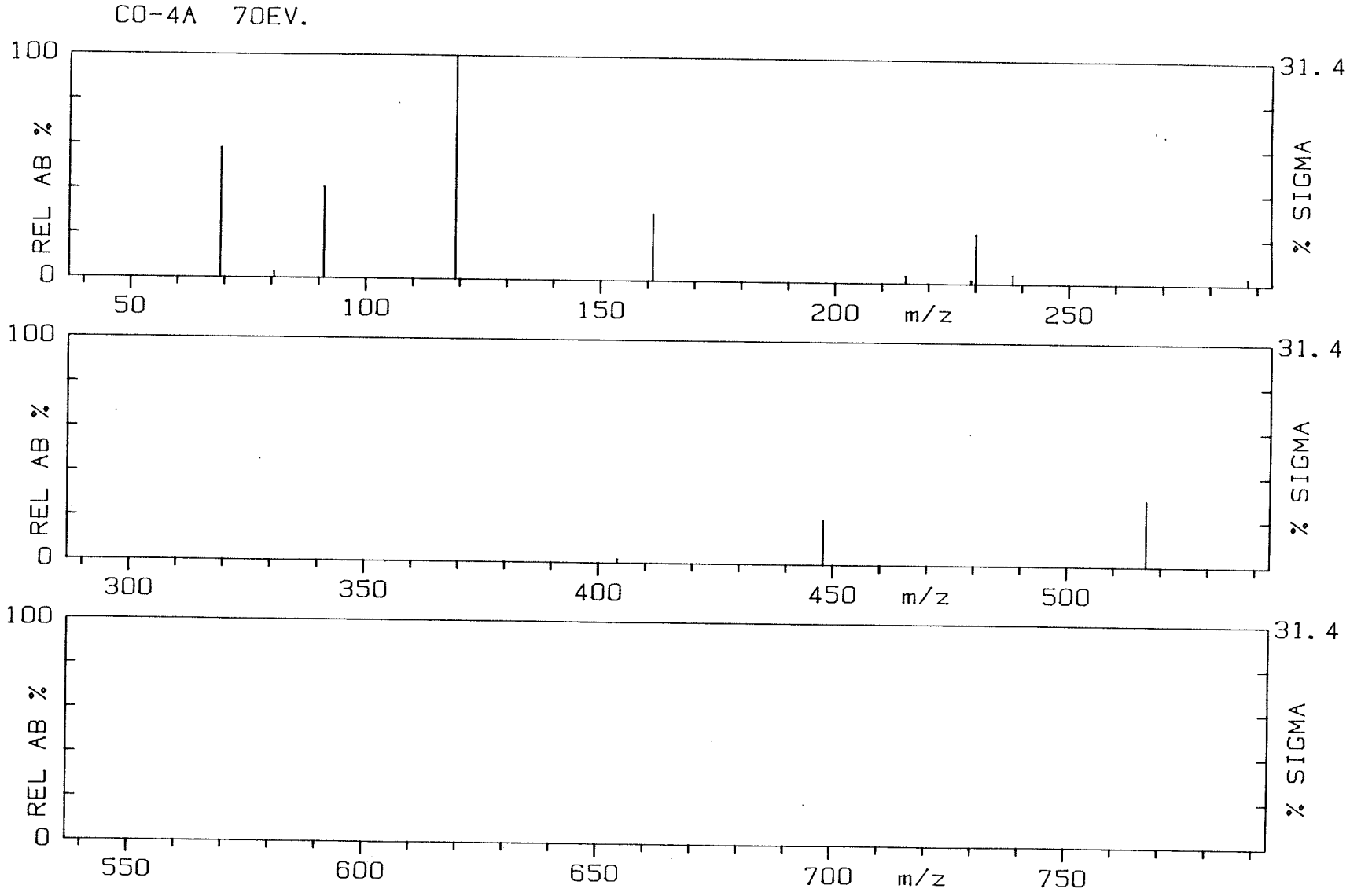
CO-4A 70EV.
100
0
REL AB %
50
100
150
200
m/z
250
31.4
% SIGMA
100
0
REL AB %
300
350
400
450
m/z
500
31.4
% SIGMA
100
0
REL AB %
550
600
650
700
m/z
750
31.4
% SIGMA

Figure 47.

Normalized 70 eV-EI mass spectrum of

tris[1,1,1-trifluoro-4-(4'-chlorophenyl)-2,4-butanedionato]Co(III)

{**Co-6a**}.

m/z $[M]^{+\cdot}$ = 806, $[L]^{+}$ = 249

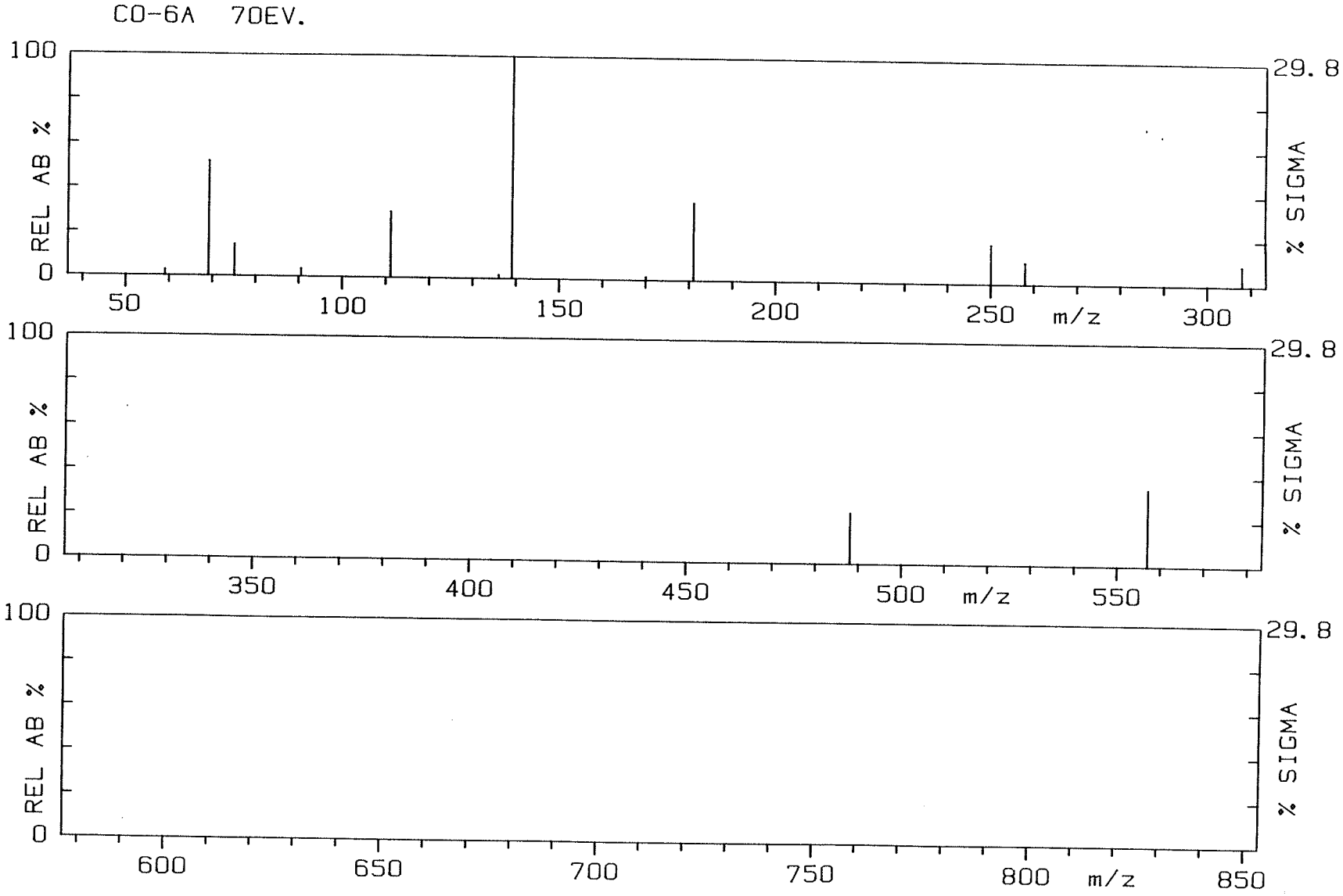
CO-6A 70EV.
100
REL AB %
0
50
100
150
200
250
m/z
300
29.8
% SIGMA
100
REL AB %
0
350
400
450
500
m/z
550
29.8
% SIGMA
100
REL AB %
0
600
650
700
750
800
m/z
850
29.8
% SIGMA

Figure 48.

Normalized 70 eV-EI mass spectrum of

tris[1,1,1-trifluoro-4-(2'-thienyl)-2,4-butanedionato]Co(III)

{**Co-8a**}.

m/z $[M]^{+\cdot}$ = 722, $[L]^{+}$ = 221

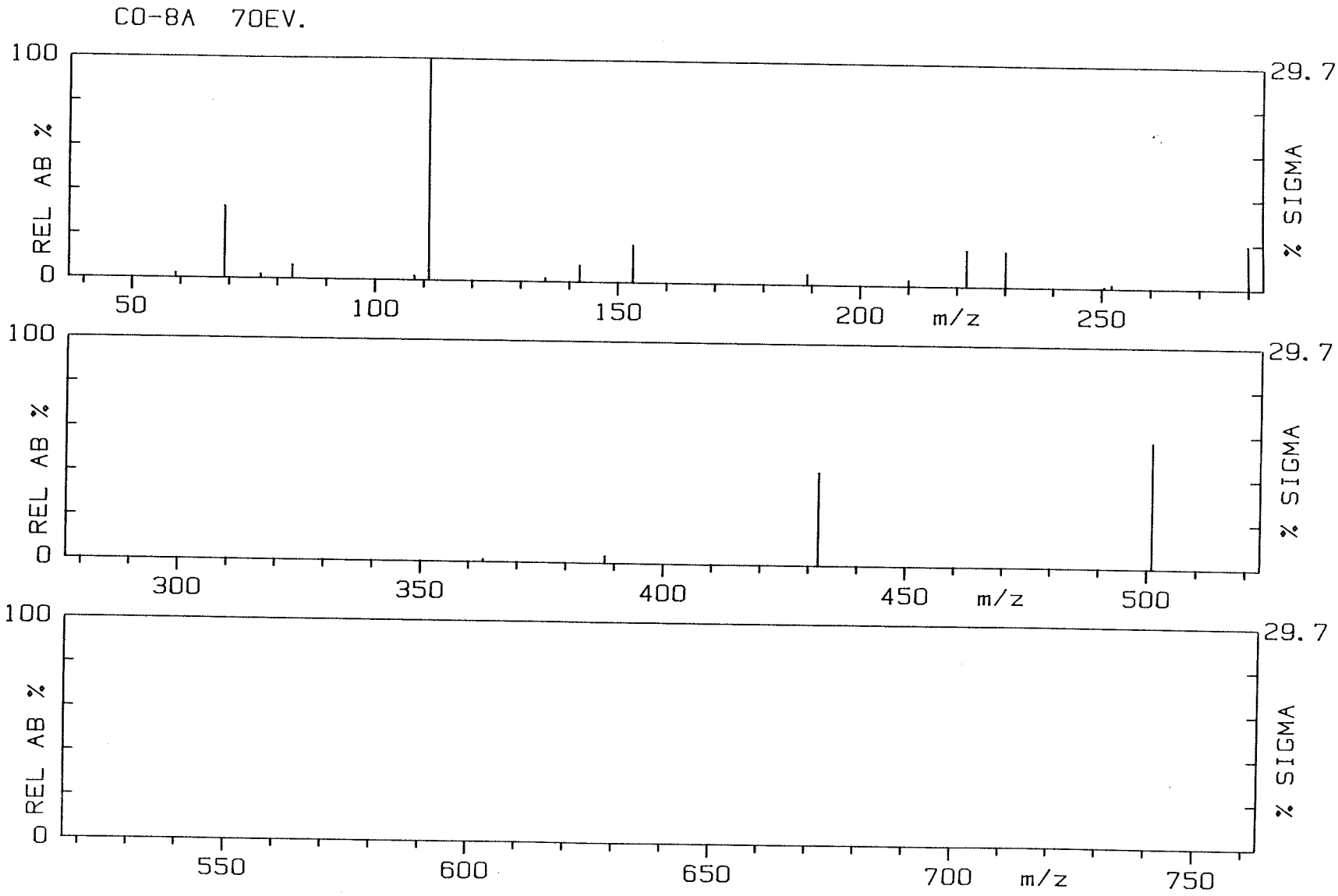
CO-8A 70EV.
100
REL AB %
0
50
100
150
200
m/z
250
29.7
% SIGMA
100
REL AB %
0
300
350
400
450
m/z
500
29.7
% SIGMA
100
REL AB %
0
550
600
650
700
m/z
750
29.7
% SIGMA

Figure 49.

Normalized 70 eV-EI mass spectrum of

tris[1,1,1-trifluoro-4-(5'-chloro-2'-thienyl)-2,4-butanedionato]Co(III)

{**Co-10a**}.

m/z $[M]^{+\cdot}$ = 824, $[L]^{+}$ = 255

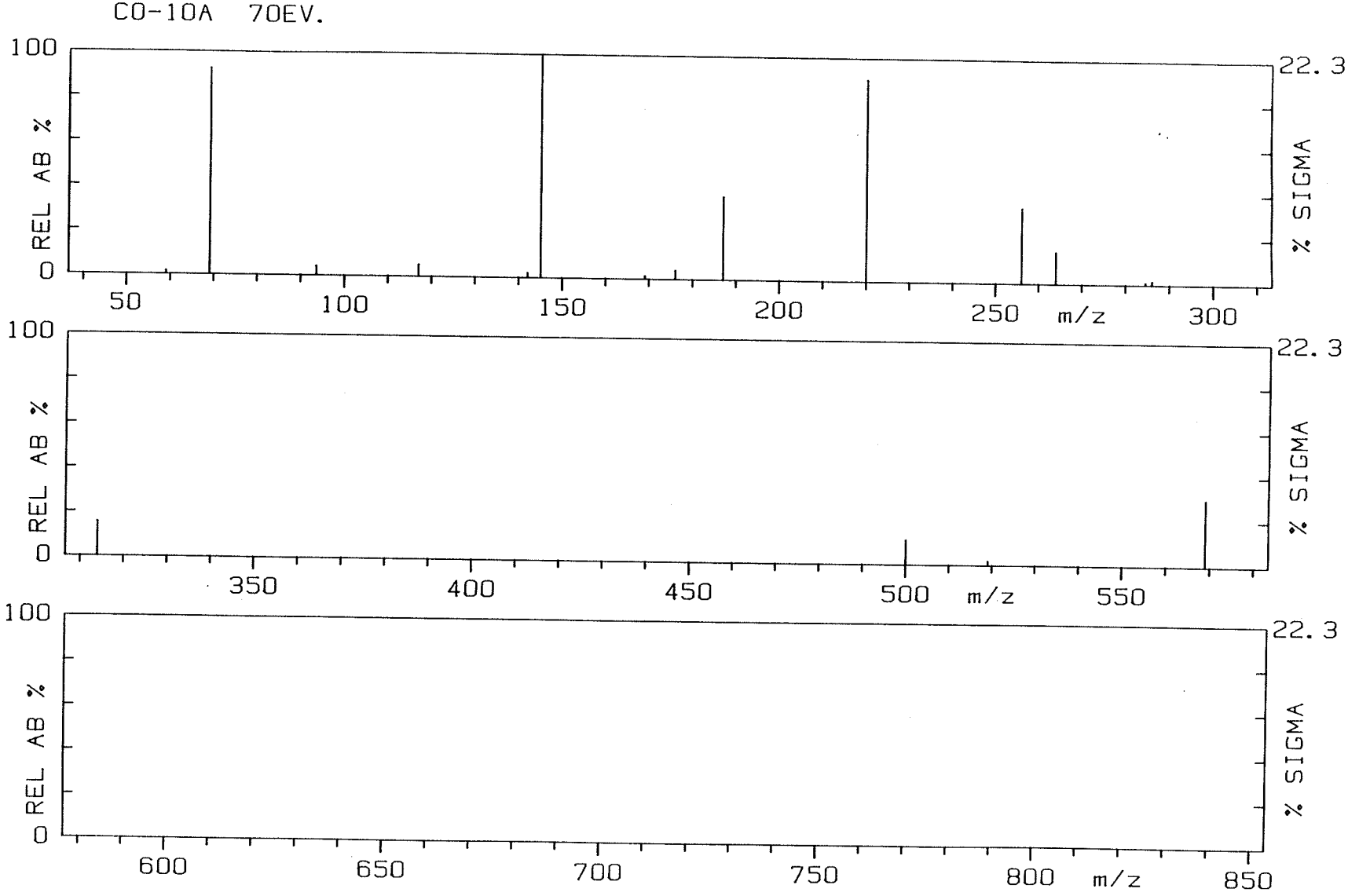
CO-10A 70EV.
100
0
REL AB %
22.3
% SIGMA
50
100
150
200
250
m/z
300
350
400
450
500
550
600
650
700
750
800
850

Figure 50.

Normalized 70 eV-EI mass spectrum of

tris[1,1,1-trifluoro-4-(2'-furyl)-2,4-butanedionato]Co(III)

{**Co-11a**}.

m/z $[M]^{+\cdot}$ = 674, $[L]^{+}$ = 205

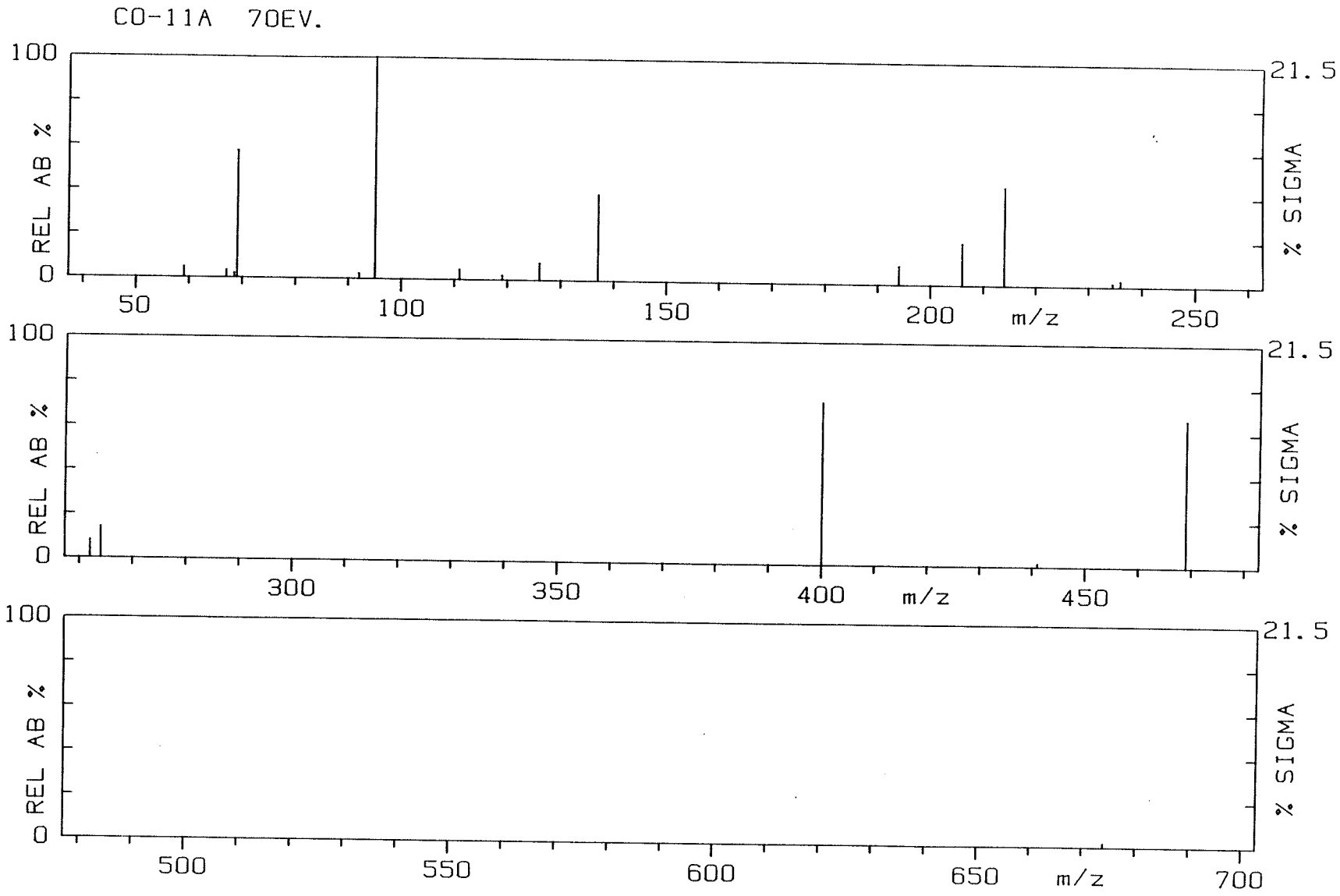
CO-11A 70EV.
100
REL AB %
0
21.5
% SIGMA
50
100
150
200
m/z
250
300
350
400
450
500
550
600
650
700

Figure 51.

Normalized 70 eV-EI mass spectrum of

tris[1,1,1-trifluoro-4-(2'-naphthyl)-2,4-butanedionato]Co(III)

{**Co-12a**}.

m/z $[M]^{+\cdot}$ = 854, $[L]^{+}$ = 265

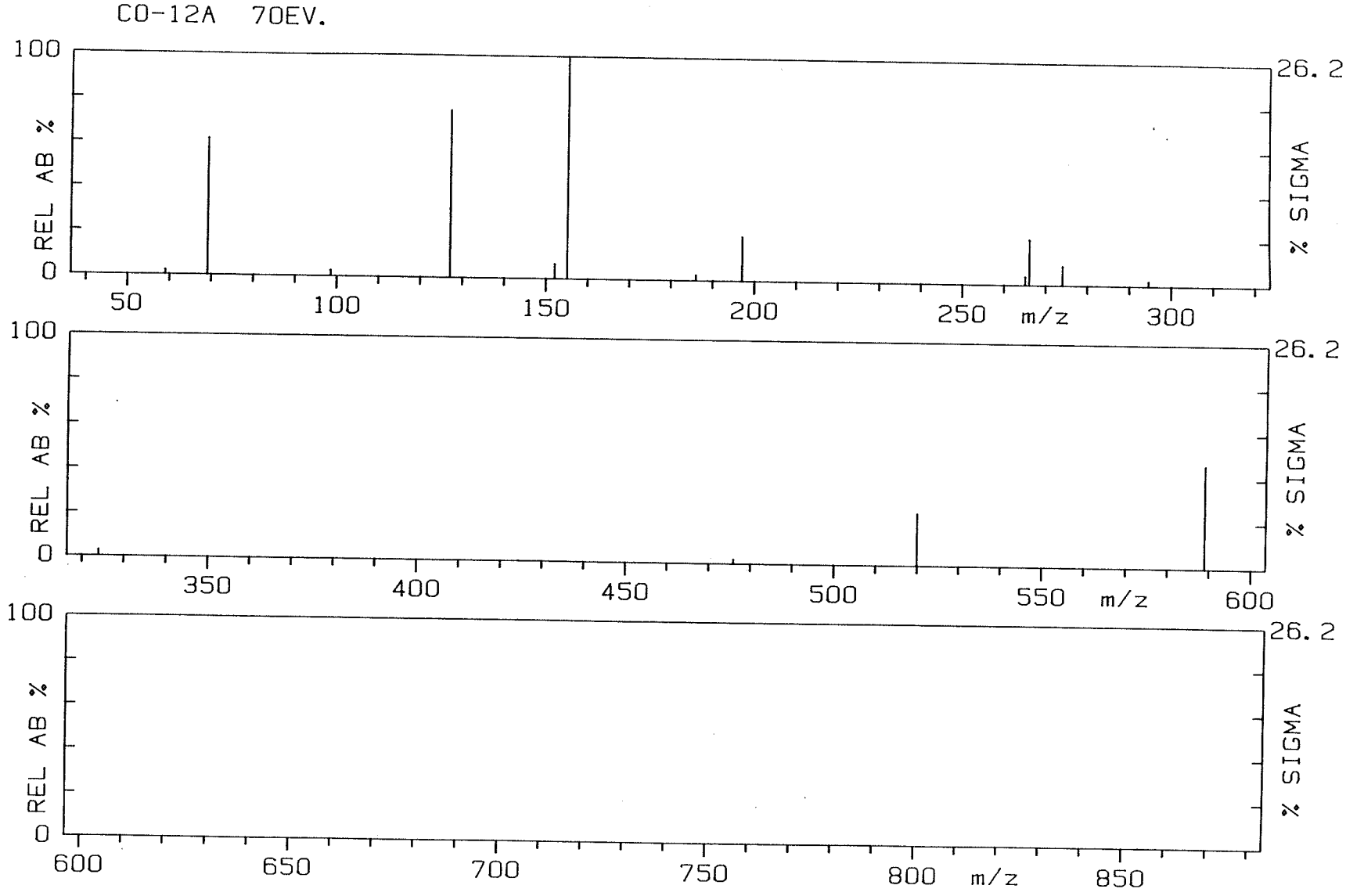
CO-12A 70EV.
100
REL AB %
0
50
100
150
200
250
m/z
300
26.2
% SIGMA
100
REL AB %
0
350
400
450
500
550
m/z
600
26.2
% SIGMA
100
REL AB %
0
600
650
700
750
800
m/z
850
26.2
% SIGMA

Figure 52.

Normalized 70 eV-EI mass spectrum of

tris[1,1,1,2,2-pentafluoro-5-phenyl-3,5-pentanedionato]Co(III)

{**Co-13a**}.

m/z $[M]^{+\cdot}$ = 854, $[L]^{+}$ = 265

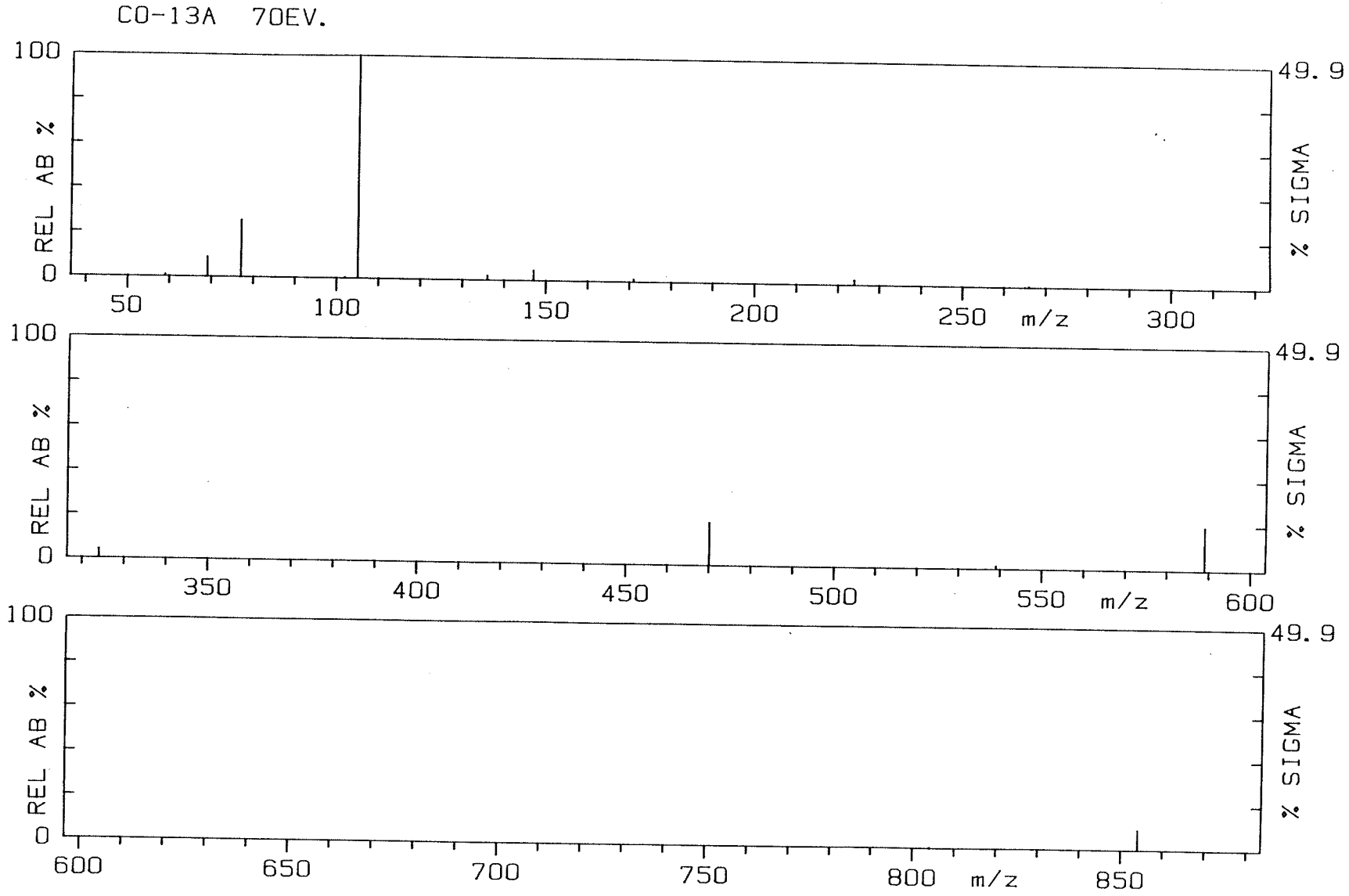
CO-13A 70EV.
100
REL AB %
0
50
100
150
200
250
m/z
300
49.9
% SIGMA
100
REL AB %
0
350
400
450
500
550
m/z
600
49.9
% SIGMA
100
REL AB %
0
600
650
700
750
800
m/z
850
49.9
% SIGMA

Figure 53.

Normalized 70 eV-EI mass spectrum of

tris[1,1,1,2,2-pentafluoro-5-(2'-thienyl)-3,5-pentanedionato]Co(III)

{**Co-14a**}.

m/z $[M]^{+\cdot}$ = 872, $[L]^{+}$ = 271

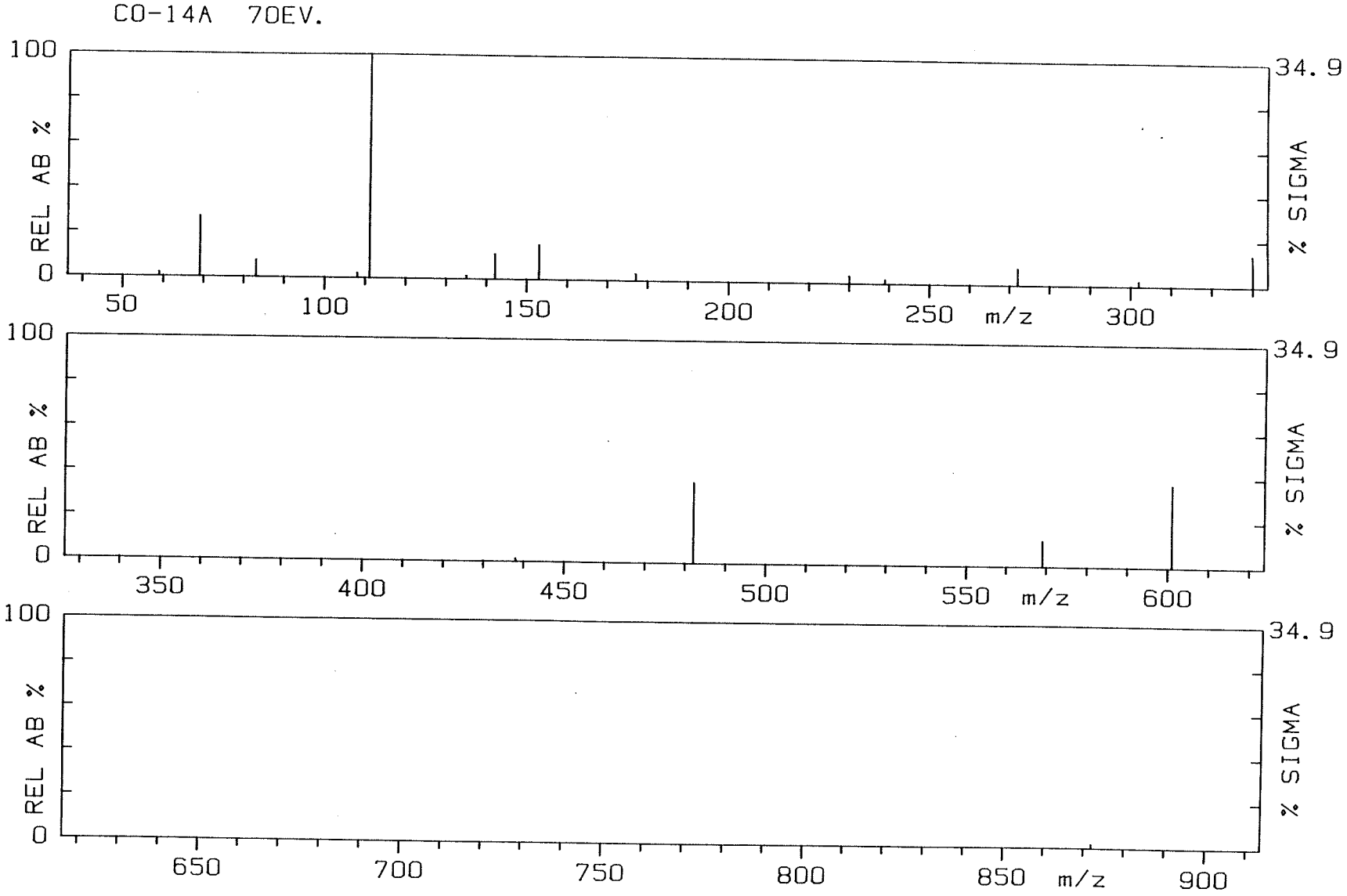
CO-14A 70EV.
100
0
REL AB %
34.9
% SIGMA
50
100
150
200
250
m/z
300
350
400
450
500
550
600
650
700
750
800
850
900

Figure 54.

Normalized 70 eV-EI mass spectrum of

tris[1,1,1,2,2,3,3-heptafluoro-6-phenyl-4,6-hexanedionato]Co(III)

{**Co-16a**}.

m/z $[M]^{+\cdot}$ = 1004, $[L]^{+}$ = 315

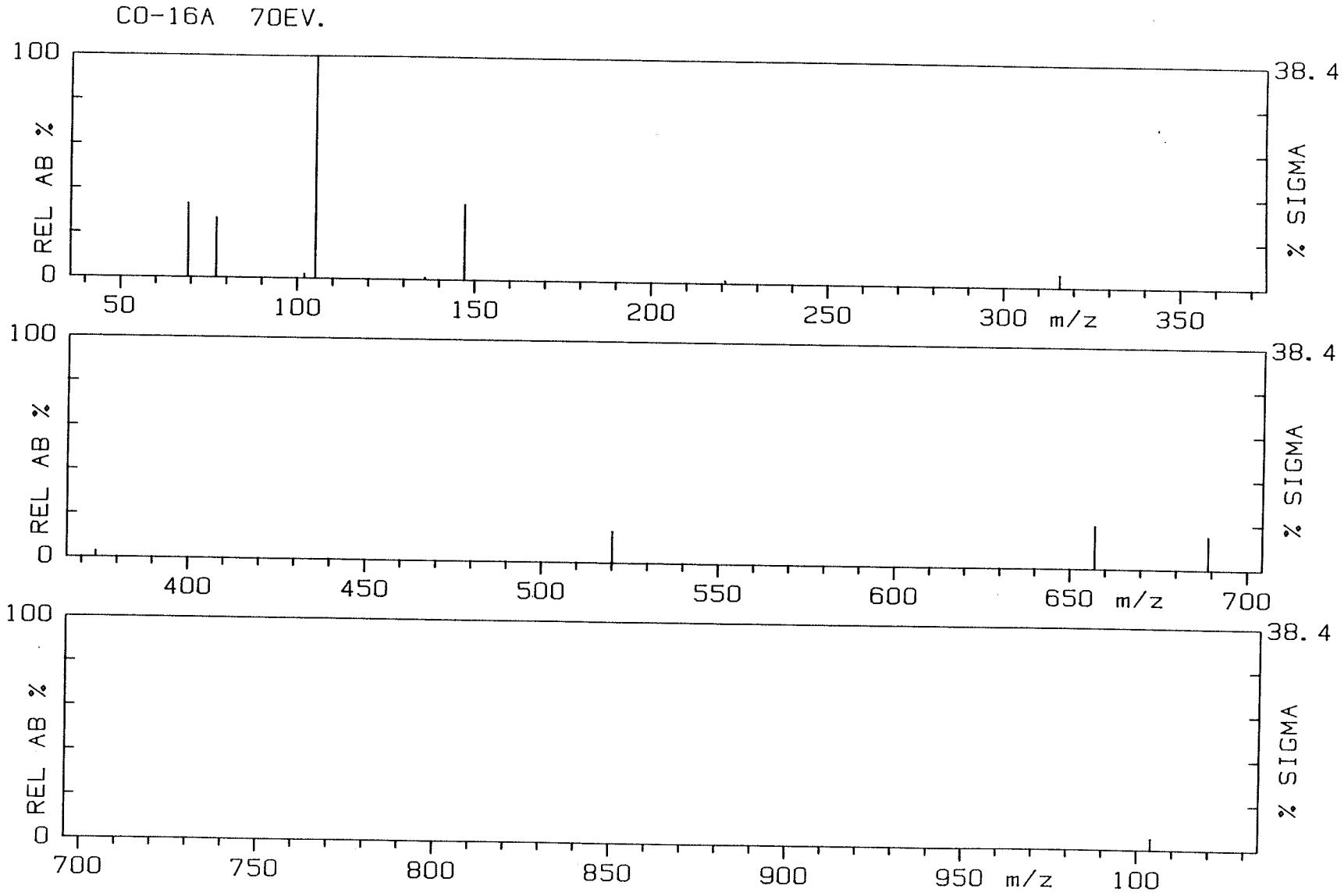
CO-16A 70EV.
100
REL AB %
0
38.4
% SIGMA
50
100
150
200
250
300
m/z
350
400
450
500
550
600
650
700
700
750
800
850
900
950
100

Figure 55.

Normalized 70 eV-EI masss spectrum of

tris[1,1,1,2,2,3,3-heptafluoro-6-(2'-thienyl)-4,6-hexanedionato]Co(III)

{**Co-17a**}.

m/z $[M]^{+\cdot}$ = 1022, $[L]^{+}$ = 321

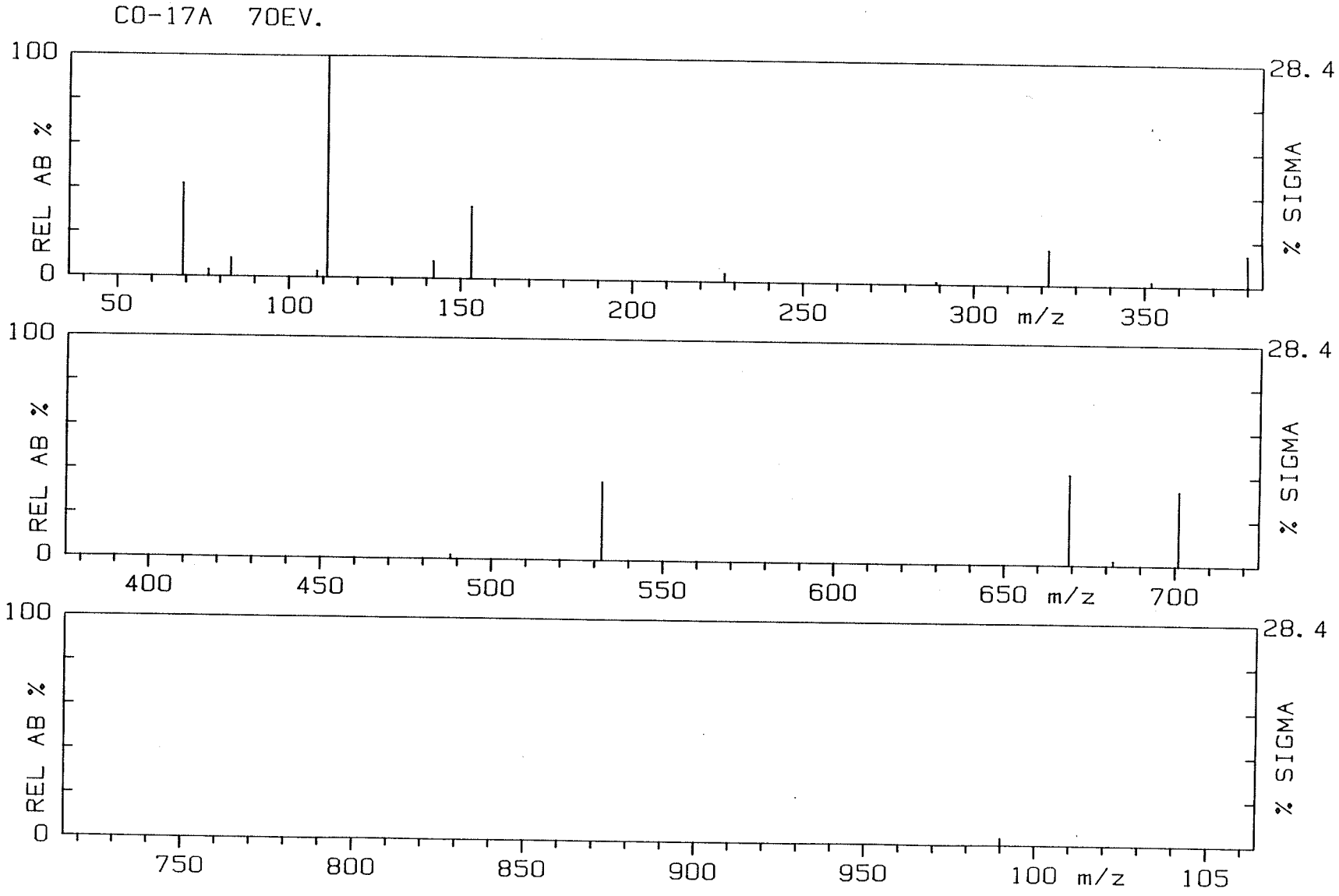
CO-17A 70EV.
100
0
REL AB %
28.4
% SIGMA
50
100
150
200
250
300
m/z
350
400
450
500
550
600
650
700
750
800
850
900
950
100
105

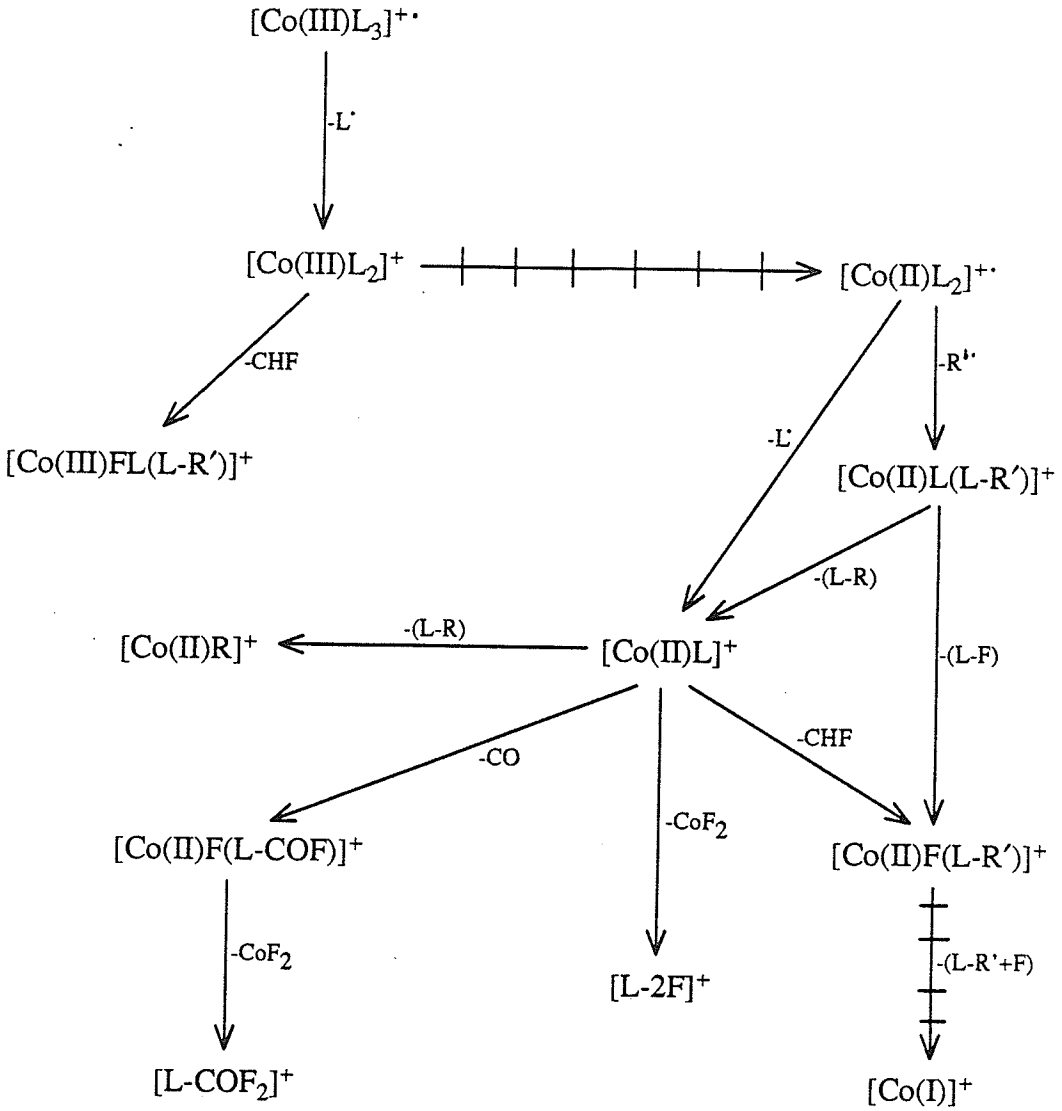

⟶ reaction step in which a change in metal oxidation state is proposed.

Scheme 29. Proposed fragmentation pathways for Co(III) β-diketonates where R' = CHF_2 (**Co–1a** and **–2a**). Pathways are common to all complexes except where noted.

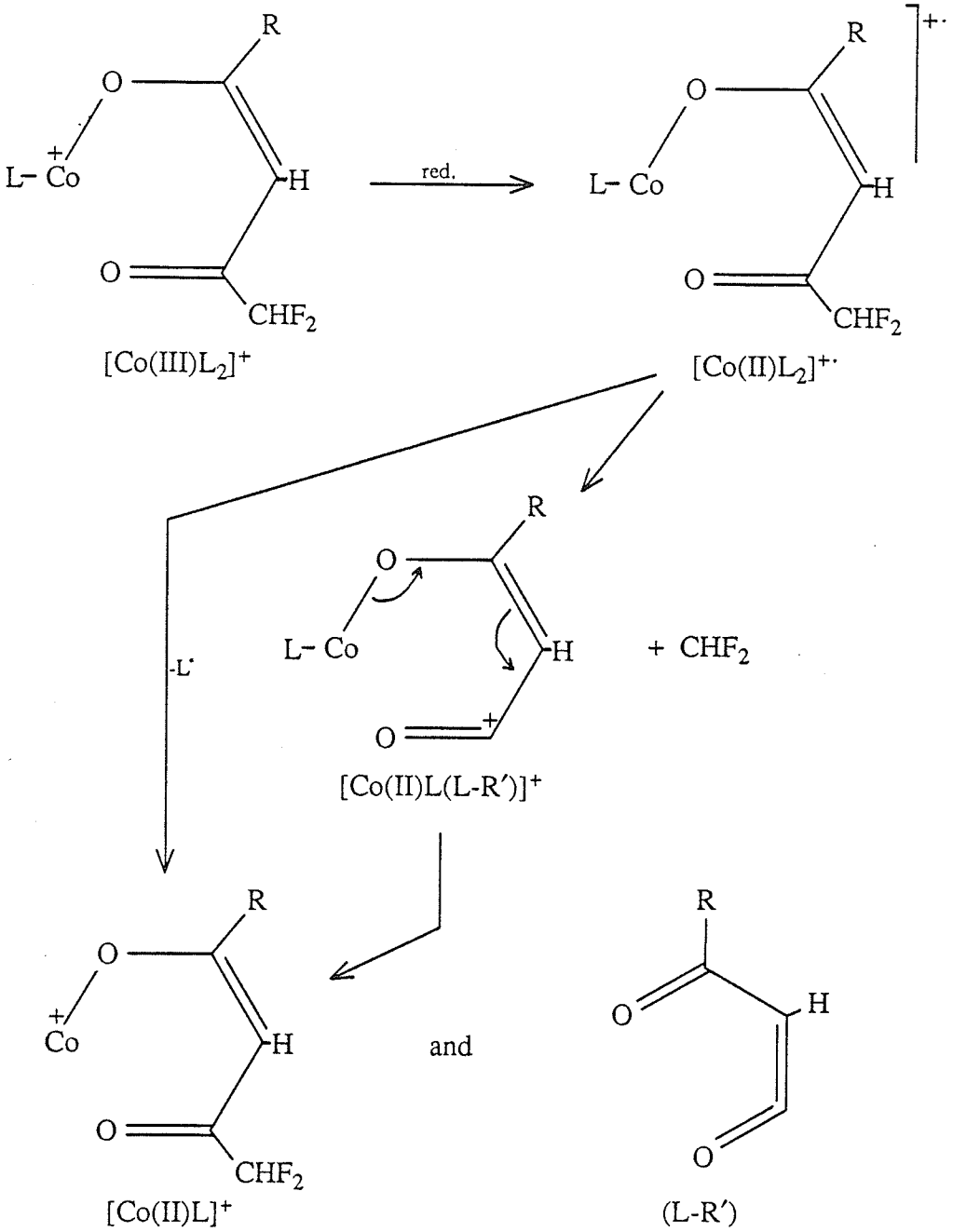

Scheme 30. Suggested mechanism for the formation of $[Co(II)L(L\text{-}R')]^+$ and $[Co(II)L]^+$ in **Co-1a** and **-2a.**

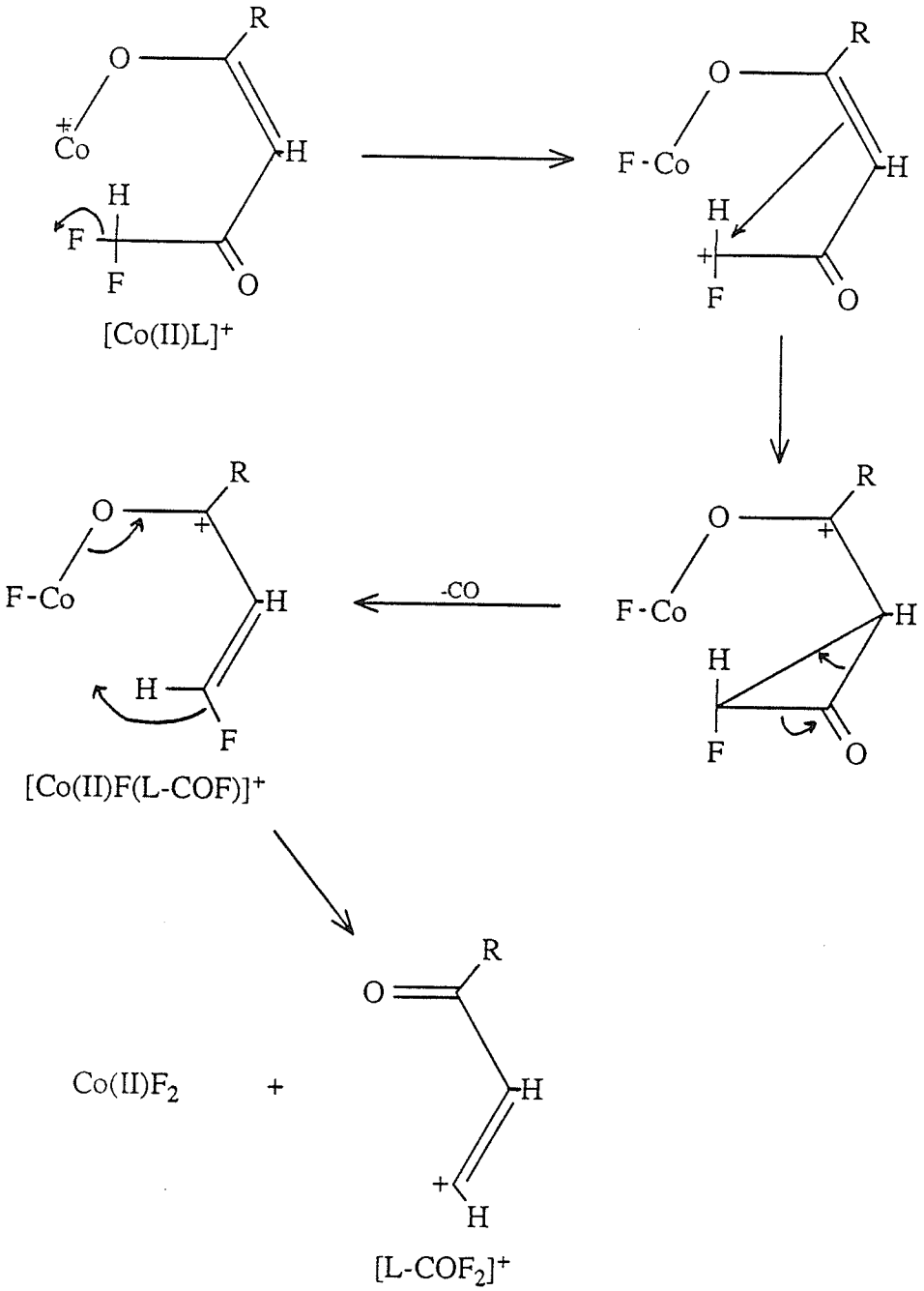

Scheme 31. Suggested mechanism for the formation of $[Co(II)F(L\text{-}COF)]^+$ and $[L\text{-}COF_2]^+$ in **Co-1a** and **-2a.**

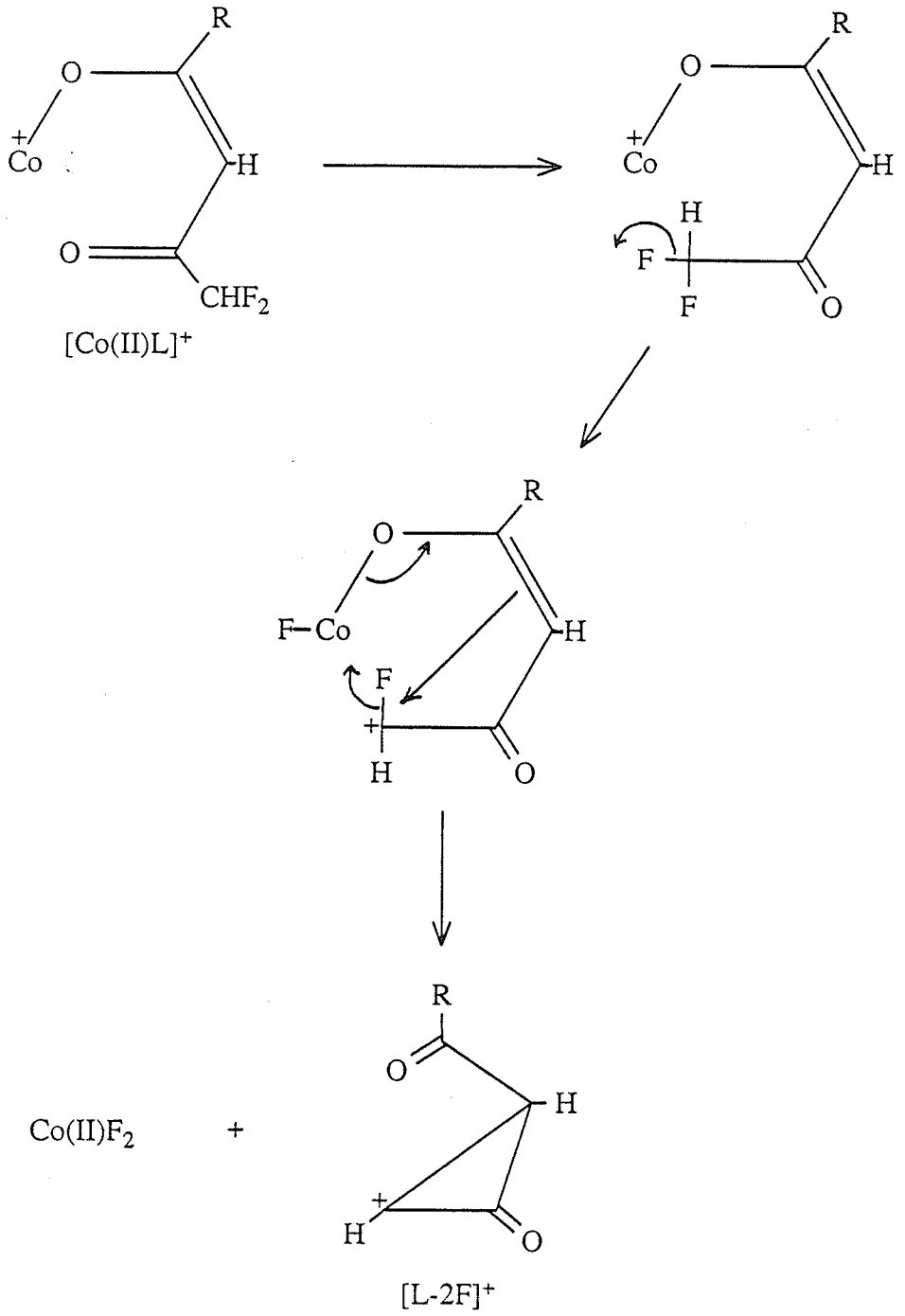

Scheme 32. Suggested mechanism for the elimination of $Co(II)F_2$ from $[Co(II)L]^+$ in **Co-1a** and **-2a.**

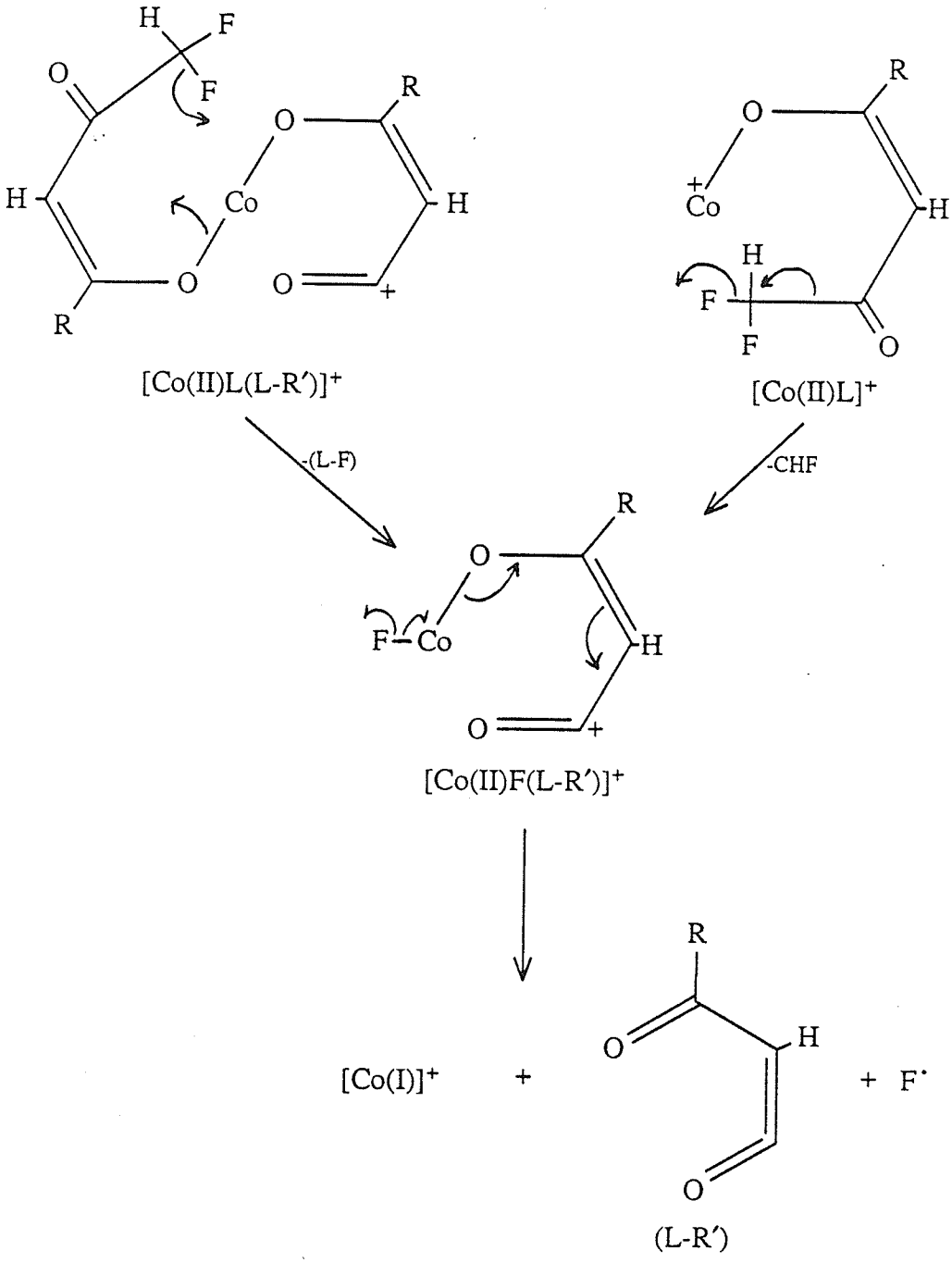

Scheme 33. Suggested mechanism for the formation of $[Co(II)F(L\text{-}R')]^+$ and $[Co(I)]^+$ in **Co-1a** and **-2a.**

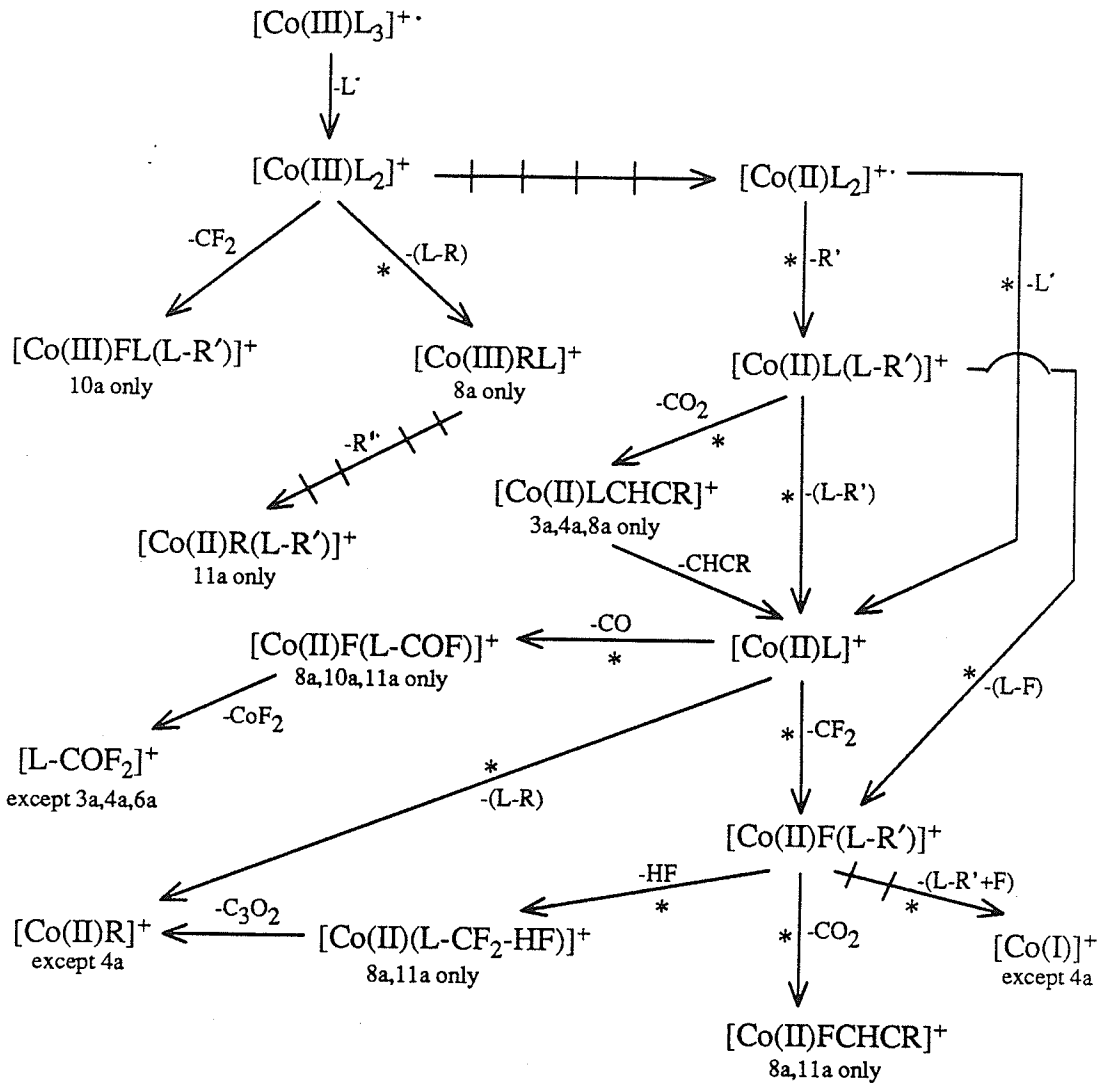

* process confirmed by the observation of a metastable transition in at least one of the complexes.

⟶ reaction step in which a change in metal oxidation state is proposed.

Scheme 34. Proposed fragmentation pathways for Co(III) β-diketonates where R' = CF_3 (**Co–3a, –4a, –6a, –8a, –10a, –11a** and **–12a**). Pathways are common to all complexes except where noted.

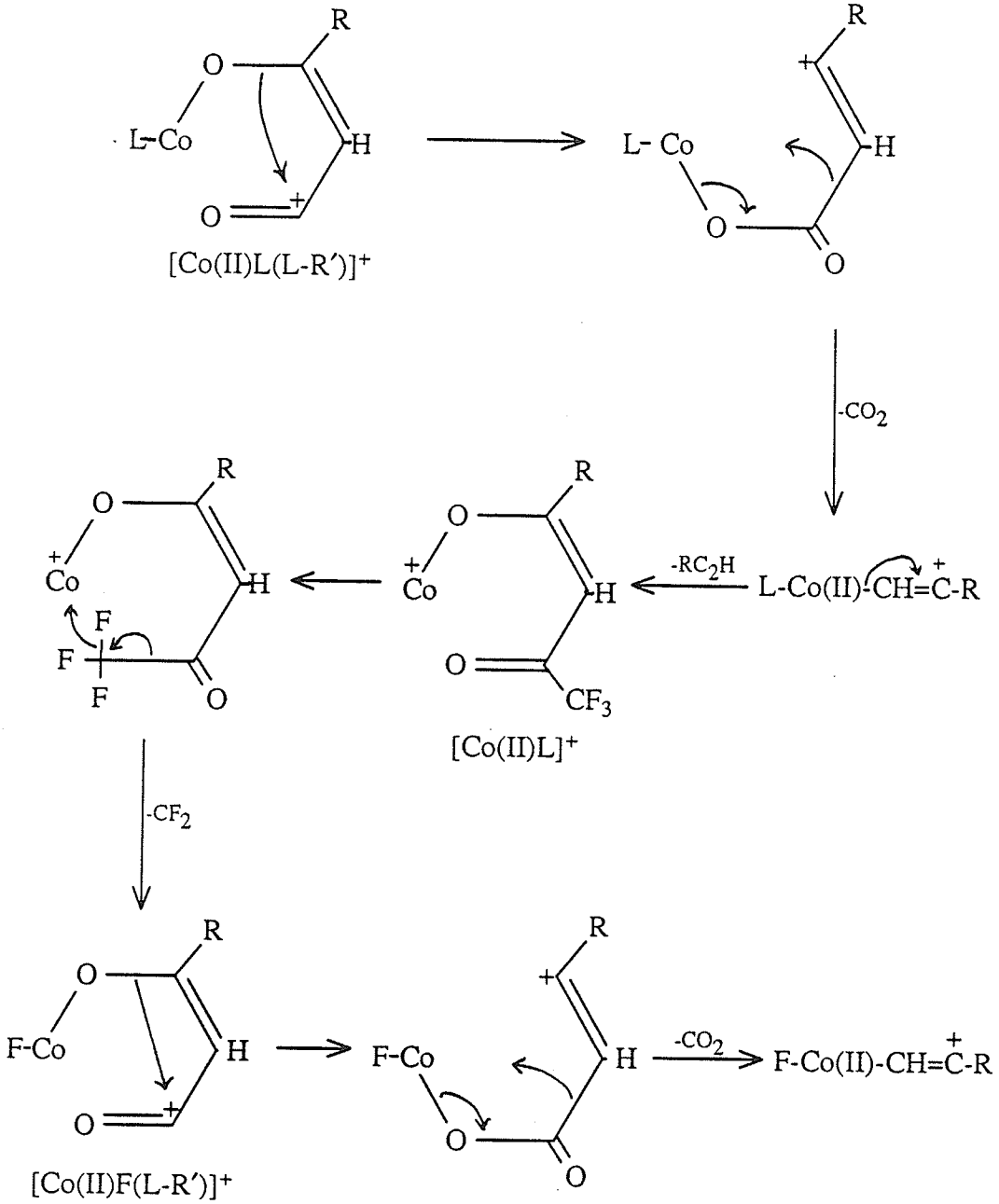

Scheme 35. Suggested mechanism for the formation of $[Co(II)LCHCR]^+$, $[Co(II)L]^+$, $[Co(II)F(L\text{-}R')]^+$ and $[Co(II)FCHCR]^+$ in **Co-3a, -4a, -6a, -8a, -10a, -11a** and **-12a.**

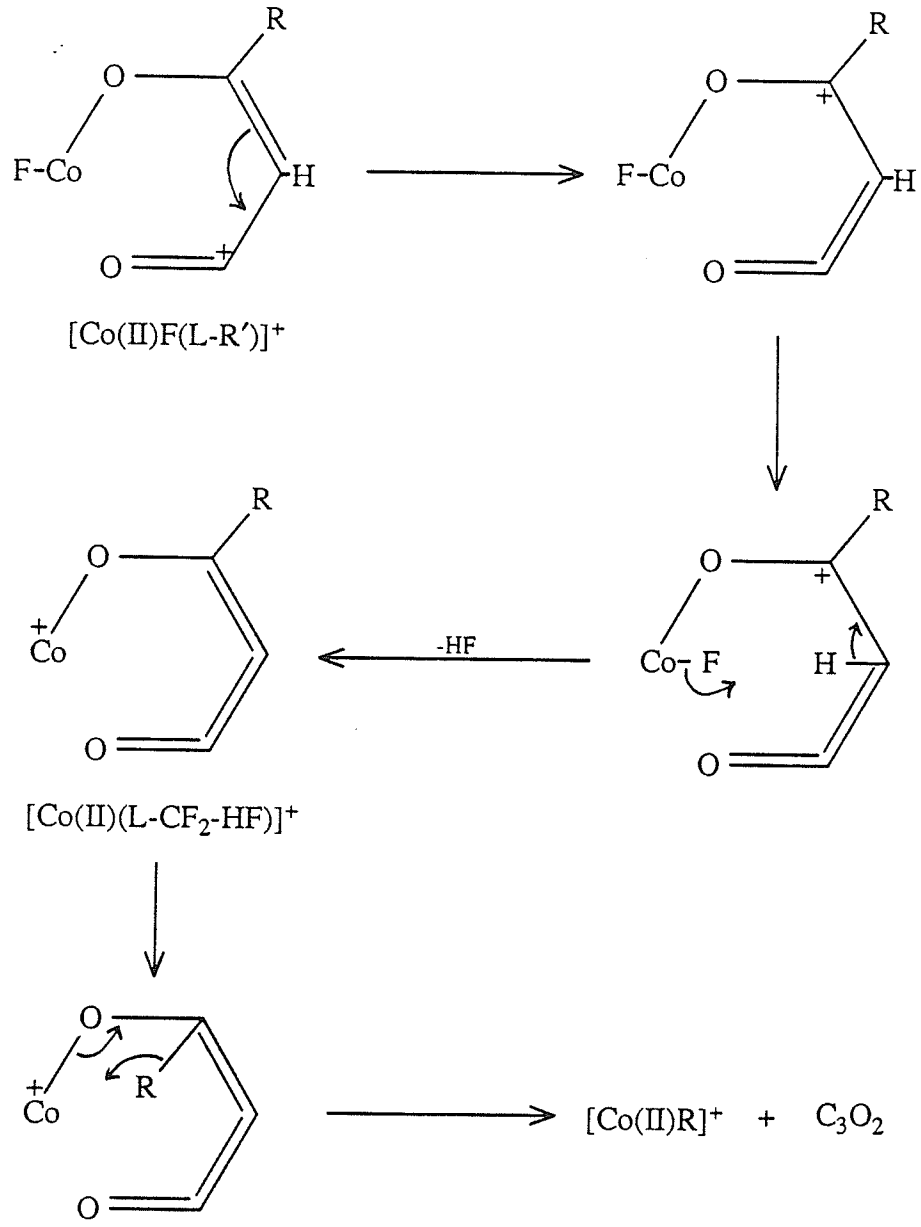

Scheme 36. Suggested mechanism for the formation of $[Co(II)(L\text{-}CF_2\text{-}HF)]^+$ and $[Co(II)R]^+$ in **Co-8a** and **-11a.**

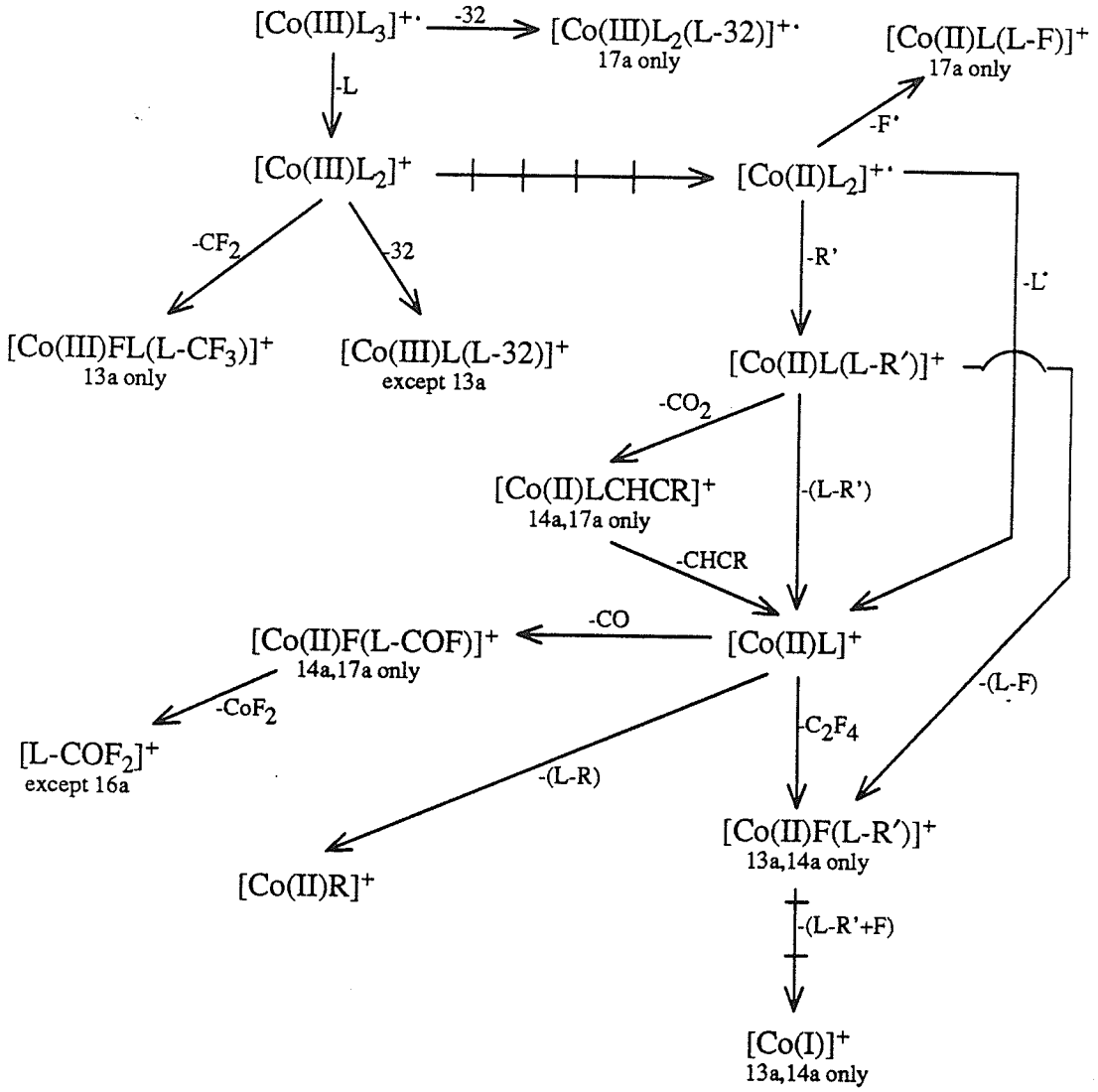

⟶⟶ reaction step in which a change in metal oxidation state is proposed.

Scheme 37. Proposed fragmentation pathways for Co(III) β-diketonates where R' = C_2F_5 (**Co–13a** and **–14a**) or C_3F_7 (**Co–16a** and **–17a**). Pathways are common to all complexes except where noted.

(d) Ni(II) β-diketonates

Relative abundance data for the nine Ni(II) β-diketonates studied appear in Tables 20-23. Plots of the EI mass spectra are presented in Figures 56-64. A linked-scanning, metastable study was conducted on **Ni-2a**. A reference to the mass spectrum of **Ni-8a** has been made by Terlouw and Heerma (175).

In nickel chelates, as for cobalt, gas-phase, metal-ligand exchange reactions within the ion source are widespread. For instance, the persistent appearance of peaks at two mass units below the major ^{58}Ni-containing ions can be attributed to minor ^{56}Fe contamination. Similar signals at $[M-6]^{+\cdot}$ in some of the spectra may arise from ^{52}Cr-containing ions and if so, represent hitherto undocumented chromium exchange processes.

Suggested decomposition pathways for the Ni(II) β-diketonate complexes possessing a difluoromethyl substituent (R' = CHF_2; Table 20) are shown in Scheme 38. The two most abundant nickel-containing ions are $[Ni(II)L_2]^{+\cdot}$ and $[Ni(II)L(L-R')]^{+}$, the latter arising from the former through the loss of R'$\cdot$ (supported by metastable transition). Many of the pathways outlined in Scheme 38 can be rationalized by established mechanisms; these fragmentations and their corresponding schemes are summarized below:

Fragmentation	Scheme
$[Ni(II)L]^+ \longrightarrow [Ni(II)R]^+$	26
$[Ni(II)L_2]^{+\cdot} \longrightarrow [Ni(II)L(L\text{-}R')]^+$	30
$[Ni(II)L(L\text{-}R')]^+ \longrightarrow [Ni(II)L]^+$	30
$[Ni(II)L]^+ \longrightarrow [Ni(II)F(L\text{-}COF)]^+$	31
$[Ni(II)F(L\text{-}COF)]^+ \longrightarrow [L\text{-}COF_2]^+$	31
$[Ni(II)L]^+ \longrightarrow [L\text{-}2F]^+$	32
$[Ni(II)L]^+ \longrightarrow [Ni(II)F(L\text{-}R')]^+$	33
$[Ni(II)L(L\text{-}R')]^+ \longrightarrow [Ni(II)F(L\text{-}R')]^+$	33
$[Ni(II)F(L\text{-}R')]^+ \longrightarrow [Ni(I)]^+$	33
$[Ni(II)F(L\text{-}R')]^+ \longrightarrow [Ni(II)(L\text{-}CHF\text{-}HF)]^+$	36
$[Ni(II)(L\text{-}CHF\text{-}HF)]^+ \longrightarrow [Ni(II)R]^+$	36

The reaction sequence leading to the formation of the bare metal ion $[Ni(I)]^+$ must necessarily involve the reduction of Ni(II) to Ni(I). The +1 oxidation state of nickel is known to be moderately stable and $[Ni(I)]^+$ ions have been reported in the spectra of Ni(II) acetylacetonates (105,115).

Fluorine migration to the metal is observed or inferred in the following fragmentations:

$$[Ni(II)L]^+ \longrightarrow [Ni(II)F(L\text{-}R')]^+$$

$$[Ni(II)L]^+ \longrightarrow [Ni(II)F(L\text{-}COF)]^+$$

$$[Ni(II)L]^+ \longrightarrow [L\text{-}2F]^+ + Ni(II)F_2$$

$$[Ni(II)F(L\text{-}COF)]^+ \longrightarrow [L\text{-}COF_2]^+ + Ni(II)F_2$$

The borderline acid character of Ni(II) is likely responsible for the limited number and low abundances of the fluorine transfer products.

Proposed fragmentation routes for the Ni(II) β-diketonates possessing a trifluoromethyl substituent (R' = CF_3; Table 21) are given in Scheme 39. The major metal-containing ions are once again $[Ni(II)L_2]^{+\cdot}$ and $[Ni(II)L(L\text{-}R')]^+$. Several of the decompositions have been previously detailed:

Fragmentation	Scheme
$[Ni(II)L_2]^{+\cdot} \longrightarrow [Ni(II)RL]^+$	26
$[Ni(II)L]^+ \longrightarrow [Ni(II)R]^{+\cdot}$	26
$[Ni(II)L_2]^+ \longrightarrow [Ni(II)L(L\text{-}R')]^+$	30
$[Ni(II)L(L\text{-}R')]^+ \longrightarrow [Ni(II)L]^+$	30
$[Ni(II)L]^+ \longrightarrow [Ni(II)F(L\text{-}R')]^+$	33
$[Ni(II)L(L\text{-}R')]^+ \longrightarrow [Ni(II)F(L\text{-}R')]^+$	33
$[Ni(II)F(L\text{-}R')]^+ \longrightarrow [Ni(I)]^+$	33
$[Ni(II)L(L\text{-}R')]^+ \longrightarrow [Ni(II)LCHCR]^+$	35
$[Ni(II)LCHCR]^+ \longrightarrow [Ni(II)L]^+$	35
$[Ni(II)F(L\text{-}R')]^+ \longrightarrow [Ni(II)(L\text{-}CF_2\text{-}HF)]^+$	36
$[Ni(II)(L\text{-}CF_2\text{-}HF)]^+ \longrightarrow [Ni(II)R]^+$	36

The only ion resulting from a fluorine transfer reaction is $[Ni(II)F(L\text{-}R')]^+$, while there are no indications of neutral nickel fluoride elimination. Other major nickel-containing species include $[Ni(I)]^+$, $[Ni(II)R]^+$ and $[Ni(II)L]^+$.

Suggested decomposition pathways for the Ni(II) β-diketonate complexes possessing pentafluoroethyl (R' = C_2F_5; Table 22) or heptafluoropropyl (R' = C_3F_7; Table 23) substituents are shown in Scheme 40. The mechanisms behind several of the fragmentations are known:

Fragmentation	Scheme
$[Ni(II)L]^+ \longrightarrow [Ni(II)R]^+$	26
$[Ni(II)L_2]^{+\cdot} \longrightarrow [Ni(II)L(L\text{-}R')]^+$	30
$[Ni(II)L(L\text{-}R')]^+ \longrightarrow [Ni(II)L]^+$	30
$[Ni(II)L(L\text{-}R')]^+ \longrightarrow [Ni(II)LCHCR]^+$	35
$[Ni(II)LCHCR]^+ \longrightarrow [Ni(II)L]^+$	35

In principle, the ion at $[Ni(II)L(L\text{-}47)]^+$ (nominal m/z 541 in **Ni-13a**, m/z 533 in **Ni-14a** and m/z 641 in **Ni-16a**) can be assigned one or more of the following structures: $[Ni(II)L(L\text{-}COF)]^+$, $[Ni(II)L(L\text{-}CH_3S)]^+$, $[Ni(II)L(L\text{-}CH_3O_2)]^+$, $[Ni(II)L(L\text{-}C_2H_7O)]^+$ or $[Ni(II)L(L\text{-}C_2H_4F)]^+$. However, the only fragment listed above that does not appear to violate elemental composition constraints or structural limitations is $[Ni(II)L(L\text{-}COF)]^+$. A proposed mechanism for complexes **Ni-13a** and **Ni-14a** based on the step-wise losses of F and CO is illustrated in Scheme 41. The transfer of a fluorine to the terminal CF_2 group in the final step is facilitated by the electron-deficient nature of the CF_2 moiety. An analogous mechanism can be proposed for the C_3F_7 derivative.

Scheme 42 depicts a suggested mechanism for the formation of $[Ni(III)FL(L\text{-}CF_3)]^+$ from $[Ni(II)L_2]^{+\cdot}$ in complexes **Ni-13a** and **Ni-14a.** An increase in the oxidation state of nickel is proposed, followed by fluorine-to-metal migration and the elimination of CF_2. Although +2 is the most common and stable oxidation state of nickel, expansion to Ni(III) may be aided in this instance by the electron-withdrawing capabilities of the perfluoroethyl substituent.

Many of the chelates studied in this section exhibit weakly-abundant ions attributable to $[Ni(L\text{-}H)]^+$. Metastable evidence indicates that this species is formed by the loss of the EE^o neutral HL from the molecular ion $[Ni(II)L_2]^{+\cdot}$. A plausible mechanism involving intramolecular ligand-to-ligand hydrogen transfer is given in Scheme 43. Two canonical forms of the final product are shown, based on the possibility of a Ni(II) or a Ni(I) oxidation state.

Another novel decomposition product found in the spectra of the Ni(II) β-diketonates is the ion $[NiHL]^{+\cdot}$, also formed as a result of hydrogen migration. The origin of the transferred hydrogen in complexes of this type has been the subject of considerable discussion (120,125,177). Two possible mechanisms, shown in Schemes 44 and 45, involve the migration of a bridging hydrogen from one of the ligands of the molecular ion to either the metal (Scheme 44) or one of the oxygen atoms of the other ligand (Scheme 45). Hydrogen transfer to the metal is considered by some (115) to be the more viable explanation; if hydrogen migration to other sites did occur, then $[MetHL]^+$ ions should be observed for β-diketonate complexes of other metals as well. Scheme 46 outlines an alternative mechanism for the formation of

$[NiHL]^{+\cdot}$ in complexes where R = phenyl (**Ni-1a,-3a,-13a** and **-16a**). Here the migrating hydrogen atom originates from the ortho position of the phenyl group and transfers to the metal by way of a six-membered ring, McLafferty-like intermediate. Lacey and co-workers (120) first suggested this type of rearrangement in their study of the mass spectra of Co(II) and Ni(II) complexes of 1,3-diphenyl-1,3-propanedione.

The issue of whether one, two or all three of the above mechanisms are at work in hydrogen transfers of this type has not been adequately resolved. While deuterium-labelling studies (120,177) indicate that the main reaction in bis(1,3-diphenyl-1,3-propanedionato)Ni(II) is hydrogen rearrangement from the ortho position of the phenyl ring (with a minor contribution from the bridging position), the results are also consistent with extensive scrambling of the ortho- and bridging-hydrogens prior to fragmentation. The $[NiHL]^{+\cdot}$ abundances given in Tables 20-23 however, seem to provide a clearer indication of the prevailing mechanism. Comparing the average %TIC for the four $[NiHL]^{+\cdot}$ ions formed when R = phenyl (**Ni-1a,-3a,-13a** and **-16a**; ave. %TIC = 0.8) with the four $[NiHL]^{+\cdot}$ ions generated when R = 2'-thienyl (**Ni-2a,-8a, -14a** and **-17a**; ave. %TIC = 0.1) reveals a decided preference for hydrogen transfer in the phenyl-substituted complexes, suggesting that hydrogen rearrangement in these Ni(II) chelates is strongly influenced by the nature of the aryl substituent and thus more closely aligned with the mechanism given in Scheme 46 (the only mechanism in which the R group is directly involved in the hydrogen rearrangement). If hydrogen migration from the bridging ligand position was the dominant mechanism, then approximately equal $[NiHL]^{+}$ abundances should be expected, regardless of the nature of the R group.

Table 20. 70 eV-EI mass spectra of compounds **Ni-1a** and **Ni-2a.**

	Ni-1a	**Ni-2a**
R =	$-C_6H_5$	$-C_4H_3S$
R'=	$-CHF_2$	$-CHF_2$

ION	%RA	m/z	%TIC	%RA	m/z	%TIC
$[NiL_2]^+$ (a)	41.9	(452)	14.4	86.4	(464)	20.0
$[NiL(L-R')]^+$ (b)	50.8	(401)	17.4	[a]84.7	(413)	19.6
$[NiHL]^+$	0.7	(256)	0.2	[a]0.5	(262)	0.1
$[NiL]^+$ (c)	4.8	(255)	1.6	[b]11.6	(261)	2.7
$[NiL-H]^+$	-	(254)	-	[a]0.1	(260)	-
$[NiF(L-COF)]^+$	4.9	(227)	1.7	[c]9.1	(233)	2.1
$[NiF(L-R')]+$	2.0	(223)	0.7	3.6	(229)	0.9
$[Ni(L-CHF-HF)]^+$	1.5	(203)	0.5	4.4	(209)	1.0
$[NiR]^+$	5.3	(135)	1.8	[c]11.2	(141)	2.6
$[Ni]^+$	5.2	(58)	1.8	6.8	(58)	1.6
$[HL]^+$	-	(198)	-	16.4	(204)	3.8
$[L-F]^+$	3.1	(178)	1.1	2.5	(184)	0.6
	1.3	(175)	0.4	3.8	(181)	0.9
$[L-2F]^+$	2.9	(159)	1.0	3.7	(165)	0.9
$[HL-R']^+$	5.1	(147)	1.7	34.2	(153)	7.9
$[L-COF_2]^+$	5.7	(131)	2.0	4.3	(137)	1.0

Table 20. (continued).

$[RCO]^+$	100.0 (105) 34.3	[b]100.0 (111) 23.2
$[RCCH]^+$	12.0 (102) 4.1	5.4 (108) 1.3
$[R]^+$	38.6 (77) 13.2	6.7 (83) 1.6
$[HL\text{-}R']^{2+}$	- (73.5) -	2.2 (76.5) 0.5
$[C_3HO_2]^+$	5.8 (69) 2.0	33.9 (69) 7.9

[a] Identified metastable transitions are indicated by superscripts which relate the daughter ion to its precursor as labelled in column 1.

Table 21. 70 eV-EI mass spectra of compounds **Ni-3a**, **Ni-8a** and **Ni-9a**.

	Ni-3a	**Ni-8a**	**Ni-9a**
R =	$-C_6H_5$	$-C_4H_3S$	$-C_4H_2SCH_3$
R'=	$-CF_3$	$-CF_3$	$-CF_3$

ION	%RA	m/z	%TIC	%RA	m/z	%TIC	%RA	m/z	%TIC
$[NiL_2]^+$	35.5	(488)	10.7	20.1	(500)	5.7	29.2	(528)	8.2
$[NiL(L-R')]^+$	27.5	(419)	8.3	13.5	(431)	3.8	18.5	(459)	5.2
$[NiLCHCR]^+$	0.7	(375)	0.2	0.3	(387)	0.1	1.2	(415)	0.3
$[NiRL]^+$	0.4	(350)	0.1	0.3	(362)	0.1	1.9	(390)	0.5
$[NiHL]^+$	4.0	(274)	1.2	0.5	(280)	0.1	1.3	(294)	0.4
$[NiL]^+$	5.8	(273)	1.7	5.8	(279)	1.6	7.0	(293)	2.0
$[NiL-H]^+$	0.6	(272)	0.2	-	(278)	-	1.0	(292)	0.3
$[NiF(L-R')]^+$	4.6	(223)	1.4	-	(229)	-	3.9	(243)	1.1
$[Ni(L-CF_2-HF)]^+$	1.5	(203)	0.5	1.9	(209)	0.5	1.6	(223)	0.5
$[NiR]^+$	5.9	(135)	1.8	5.2	(141)	1.5	6.8	(155)	1.9
$[Ni]^+$	3.8	(58)	1.1	-	(58)	-	8.4	(58)	2.4
$[HL]^+$	19.6	(216)	5.9	50.1	(222)	14.2	37.0	(236)	10.4
$[L]^+$	2.8	(215)	0.8	0.9	(221)	0.3	0.9	(235)	0.3
$[L-S]^+$	-	(183)	-	4.2	(189)	1.2	9.6	(203)	2.7
$[HL-R']^+$	26.3	(147)	7.9	54.9	(153)	15.5	35.7	(167)	10.1
$[RCO]^+$	100.0	(105)	30.1	100.0	(111)	28.3	100.0	(125)	28.2
$[RCH_2]^+$	1.9	(91)	0.6	2.7	(97)	0.8	-	(111)	-
$[R]^+$	42.1	(77)	12.7	9.8	(83)	2.8	13.9	(97)	3.9
$[HL-R']^{2+}$	3.5	(73.5)	1.1	5.7	(76.5)	1.6	2.3	(83.5)	0.6
$[R']^+$	42.9	(69)	12.9	79.7	(69)	22.5	59.9	(69)	16.9
	4.9	(57)	1.5	-	(57)	-	14.8	(57)	4.2

Table 22. 70 eV-EI mass spectra of compounds **Ni-13a** and **Ni-14a**.

	Ni-13a	**Ni-14a**
R =	$-C_6H_5$	$-C_4H_3S$
R'=	$-C_2F_5$	$-C_2F_5$

ION	%RA	m/z	%TIC	%RA	m/z	%TIC
$[NiL_2]^+$	57.6	(588)	16.7	18.4	(600)	5.1
$[NiL(L-F)]^+$	2.5	(569)	0.7	0.6	(581)	0.2
$[NiL(L-COF)]^+$	1.5	(541)	0.5	0.4	(553)	0.1
$[NiFL(L-CF_3]^+$	1.6	(538)	0.5	1.0	(550)	0.3
$[NiL(L-R')]^+$	55.8	(469)	16.2	19.4	(481)	5.3
$[NiLCHCR]^+$	1.5	(425)	0.5	0.6	(437)	0.2
$[NiHL]+$	3.8	(324)	1.1	0.5	(330)	0.1
$[NiL]^+$	8.1	(323)	2.4	7.2	(329)	2.0
$[NiL-H]^+$	0.4	(322)	0.1	0.4	(328)	0.1
$[NiR]^+$	7.4	(135)	2.1	7.5	(141)	2.1
$[HL]^+$	7.6	(266)	2.2	34.1	(272)	9.4
$[L]^+$	1.3	(265)	0.4	0.4	(271)	0.1
$[HL-R']^+$	24.1	(147)	7.0	66.3	(153)	18.3
$[R']^+$	2.2	(119)	0.6	3.5	(119)	1.0
$[RCO]^+$	100.0	(105)	29.0	100.0	(111)	27.5
$[RCCH]^+$	2.1	(102)	0.6	2.7	(108)	0.7
$[R]^+$	34.9	(77)	10.1	8.9	(83)	2.5
$[HL-R']^{2+}$	1.8	(73.5)	0.5	5.7	(76.5)	1.6
$[CF_3]^+$	33.9	(69)	9.8	86.4	(69)	23.8

Table 23. 70 eV-EI mass spectra of compounds **Ni-16a** and **Ni-17a.**

	Ni-16a	**Ni-17a**
R =	$-C_6H_5$	$-C_4H_3S$
R'=	$-C_3F_7$	$-C_3F_7$

ION	%RA	m/z	%TIC	%RA	m/z	%TIC
$[NiL_2]^+$	21.3	(688)	7.5	4.9	(700)	1.6
$[NiL(L-F)]^+$	1.6	(669)	0.6	-	(681)	-
$[NiL(L-COF)]^+$	0.9	(641)	0.3	-	(653)	-
$[NiL(L-R')]^+$	28.4	(519)	10.0	5.0	(531)	1.6
$[NiLCHCR]^+$	0.9	(475)	0.3	-	(487)	-
$[NiHL]^+$	1.4	(374)	0.5	0.2	(380)	0.1
$[NiL]^+$	4.1	(373)	1.4	2.1	(379)	0.7
$[NiL-H]^+$	-	(372)	-	-	(378)	-
$[NiR]^+$	5.0	(135)	1.8	2.1	(141)	0.7
$[HL]^+$	5.0	(316)	1.8	31.4	(322)	10.3
$[L]^+$	0.9	(315)	0.3	0.3	(321)	0.1
$[HL-R']^+$	32.4	(147)	11.4	100.0	(153)	32.9
$[RCO]^+$	100.0	(105)	35.2	93.6	(111)	30.8
$[RCCH]^+$	2.8	(102)	1.0	3.6	(108)	1.2
	2.1	(91)	0.7	3.0	(97)	1.0
	-	(79)	-	3.7	(85)	1.2
$[R]^+$	34.6	(77)	12.2	5.6	(83)	1.8
$[HL-R']^{2+}$	2.5	(73.5)	0.9	3.4	(76.5)	1.1
$[CF_3]^+$	40.3	(69)	14.2	44.7	(69)	14.7

Figure 56.

Normalized 70 eV-EI mass spectrum of

bis[1,1-difluoro-4-phenyl-2,4-butanedionato]Ni(II)

(**Ni-1a**).

m/z $[M]^{+\cdot}$ = 452, $[L]^{+}$ = 197

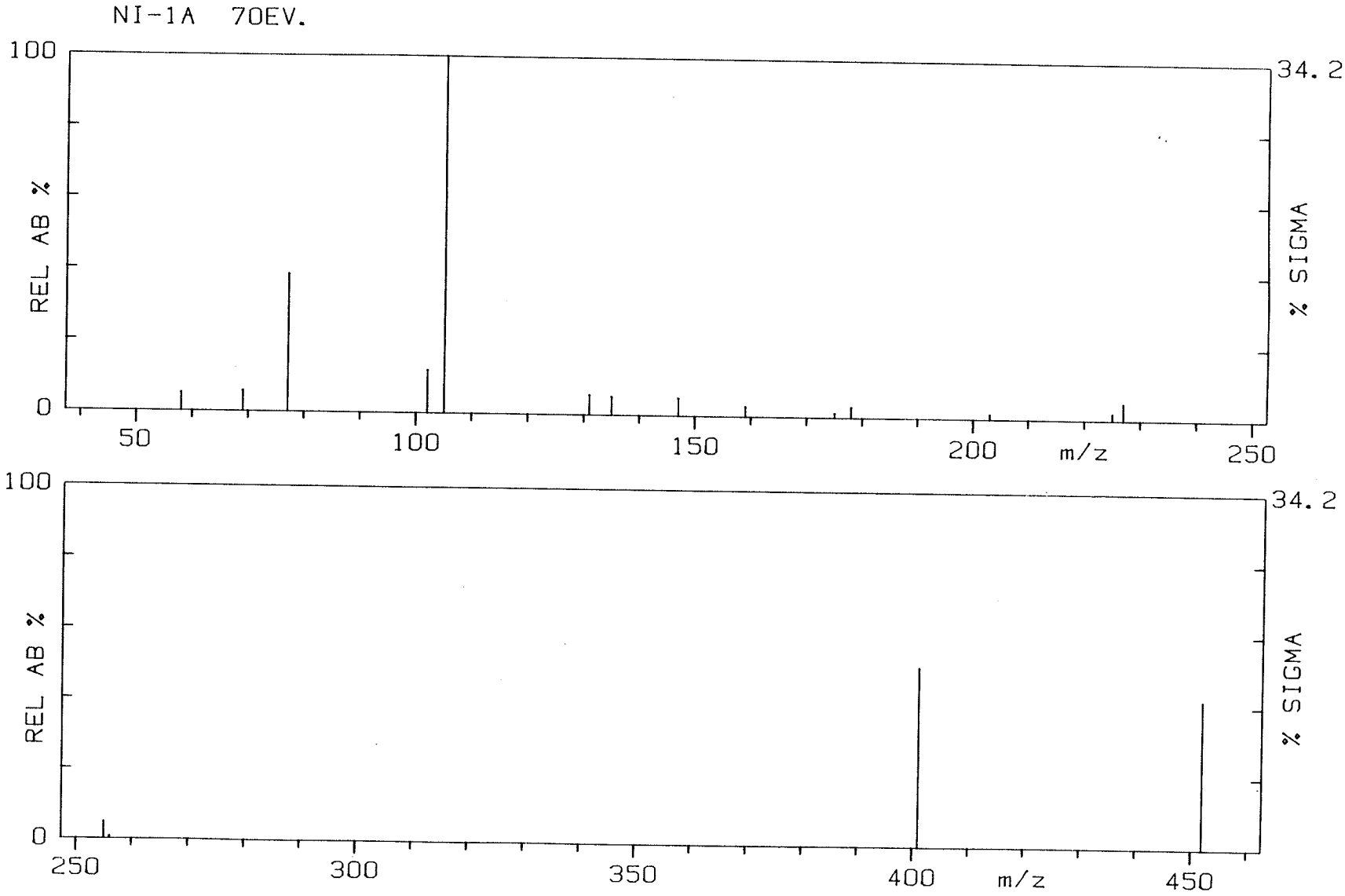
NI-1A 70EV.
100
REL AB %
0
50
100
150
200
m/z
250
34.2
% SIGMA
100
REL AB %
0
250
300
350
400
m/z
450
34.2
% SIGMA

Figure 57.

Normalized 70 eV-EI mass spectrum of

bis[1,1-difluoro-4-(2'-thienyl)-2,4-butanedionato]Ni(II)

{**Ni-2a**}.

m/z $[M]^{+\cdot}$ = 464, $[L]^{+}$ = 203

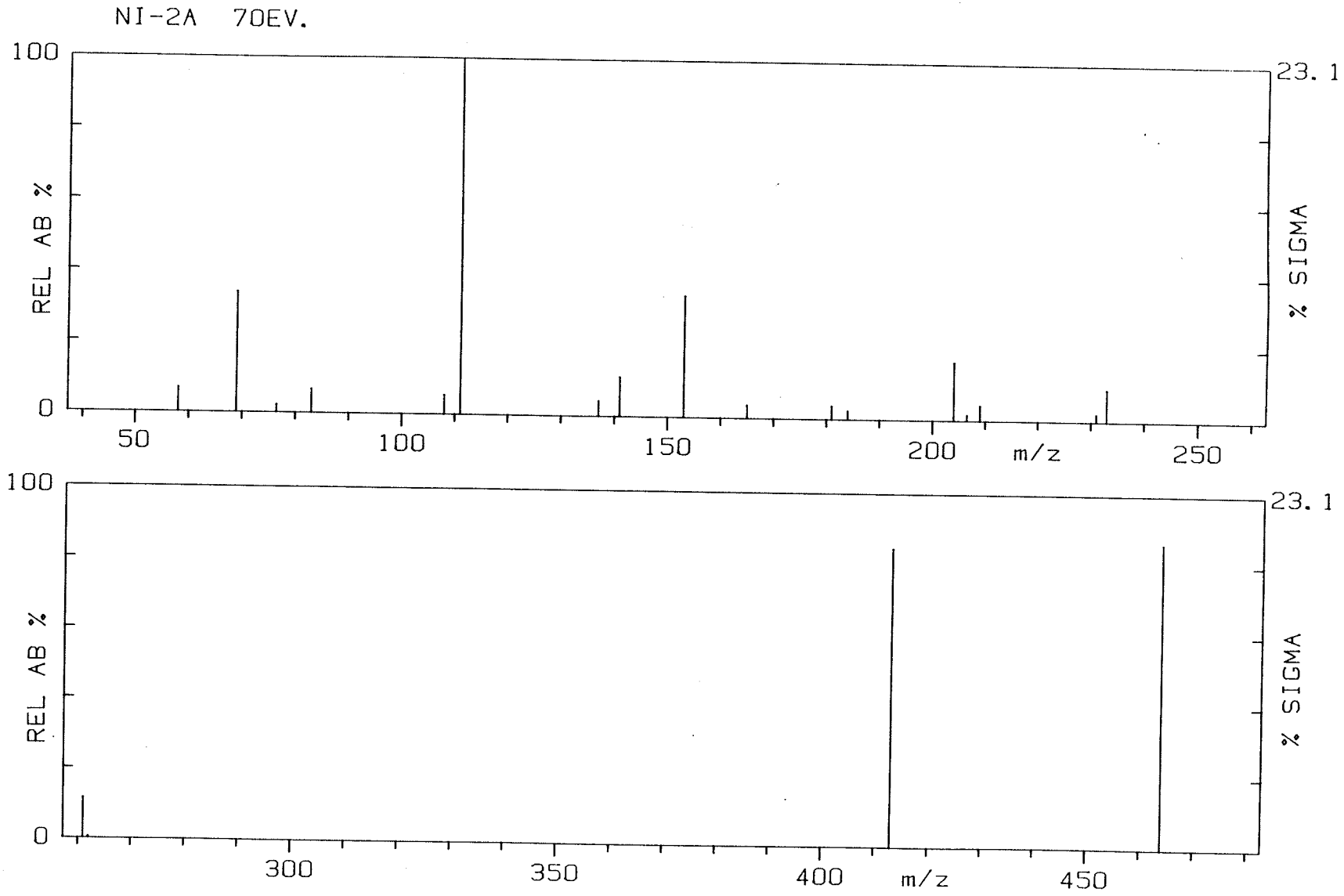
NI-2A 70EV.
100
REL AB %
0
50
100
150
200
m/z
250
23.1
% SIGMA
100
REL AB %
0
300
350
400
m/z
450
23.1
% SIGMA

Figure 58.

Normalized 70 eV-EI mass spectrum of

bis[1,1,1-trifluoro-4-phenyl-2,4-butanedionato]Ni(II)

{Ni-3a}.

m/z $[M]^{+\cdot}$ = 488, $[L]^{+}$ = 215

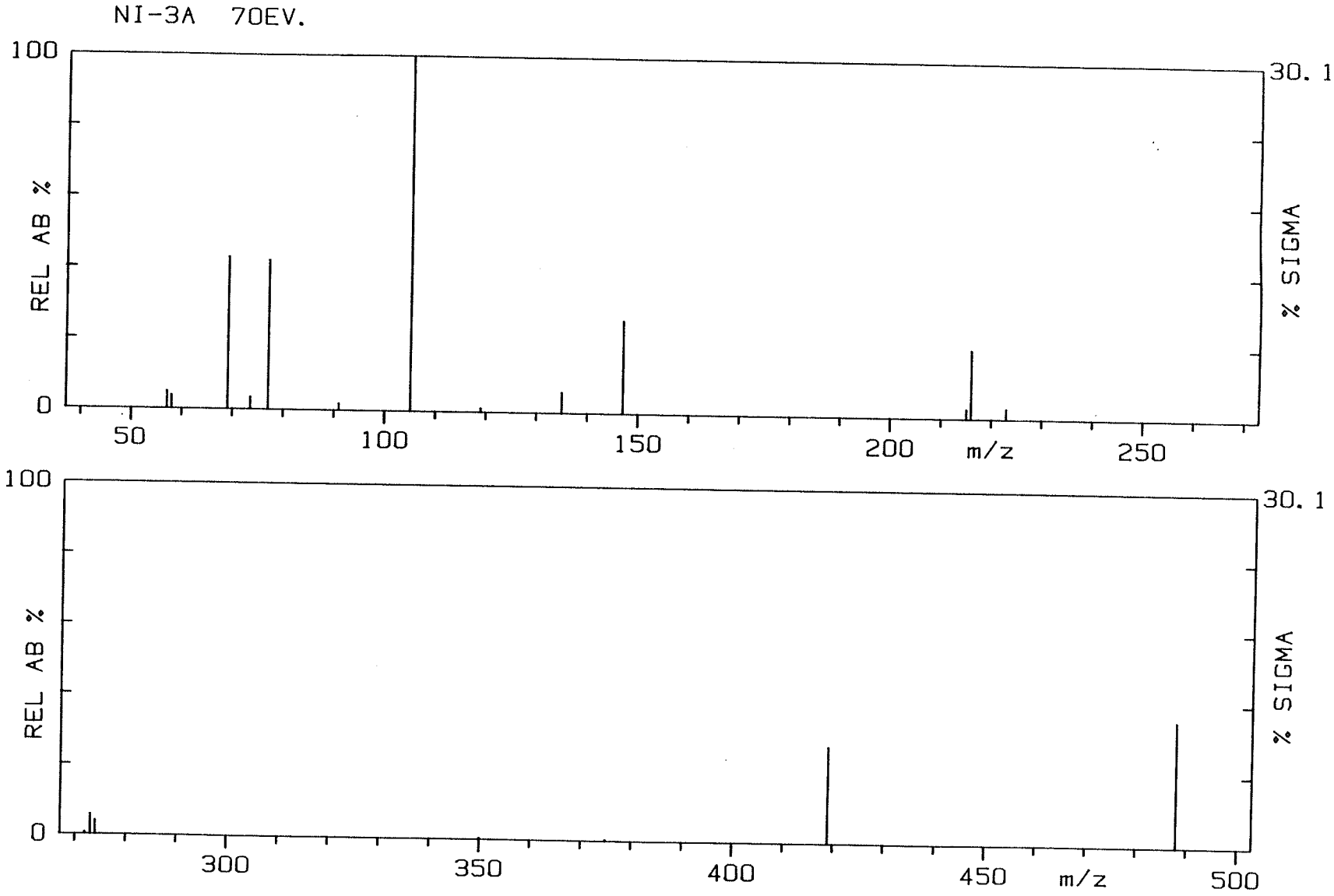
NI-3A 70EV.
100
REL AB %
0
50
100
150
200
m/z
250
30.1
% SIGMA
100
REL AB %
0
300
350
400
450
m/z
500
30.1
% SIGMA

Figure 59.

Normalized 70 eV-EI mass spectrum of

bis[1,1,1-trifluoro-4-(2'-thienyl)-2,4-butanedionato]Ni(II)

{**Ni-8a**}.

m/z $[M]^{+\cdot}$ = 500, $[L]^{+}$ = 221

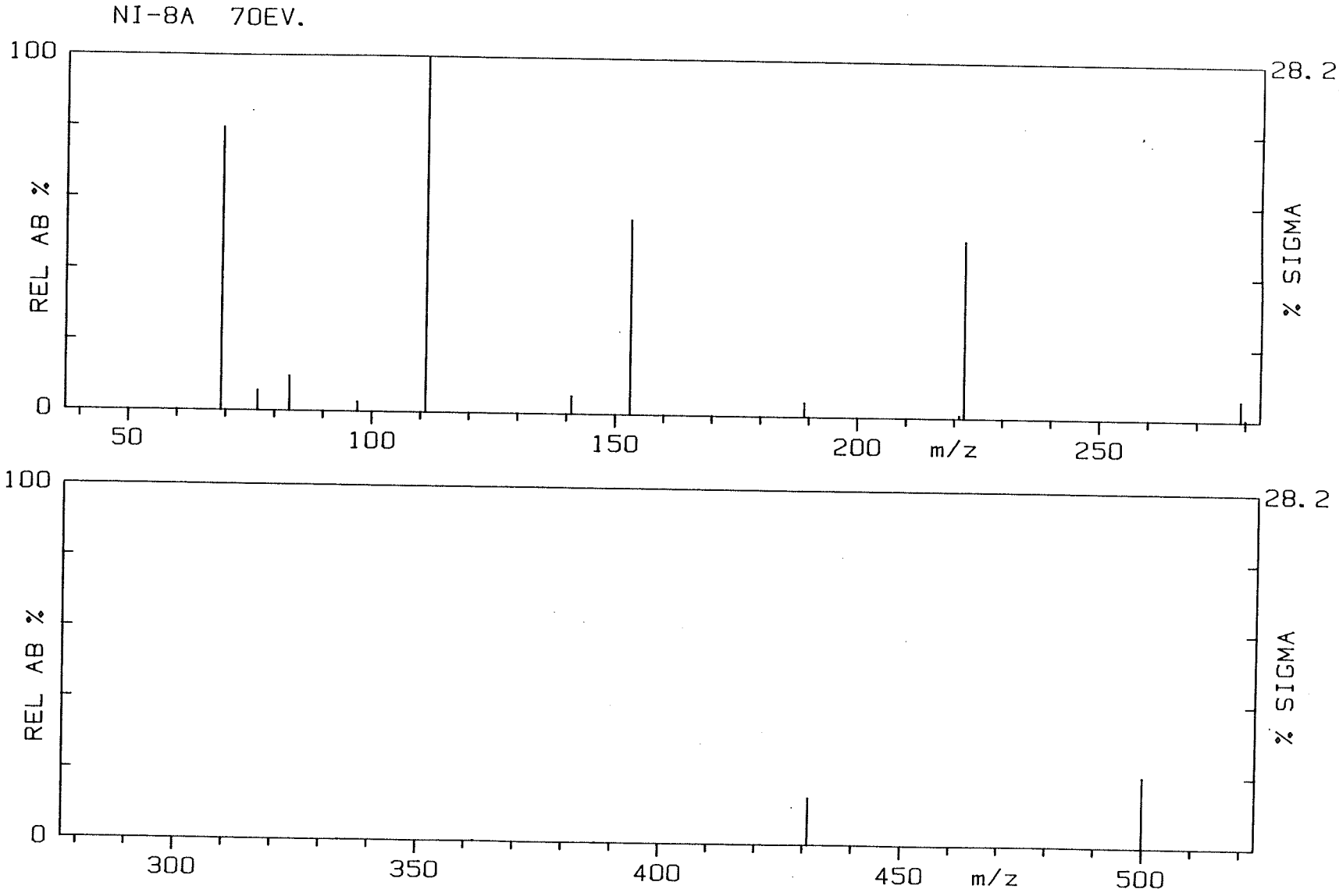
NI-8A 70EV.
100
REL AB %
0
50
100
150
200
m/z
250
28.2
% SIGMA
100
REL AB %
0
300
350
400
450
m/z
500
28.2
% SIGMA

Figure 60.

Normalized 70 eV-EI mass spectrum of

bis[1,1,1-trifluoro-4-(5'-methyl-2'-thienyl)-2,4-butanedionato]Ni(II)

(**Ni-9a**).

m/z $[M]^{+\cdot}$ = 528, $[L]^{+}$ = 235

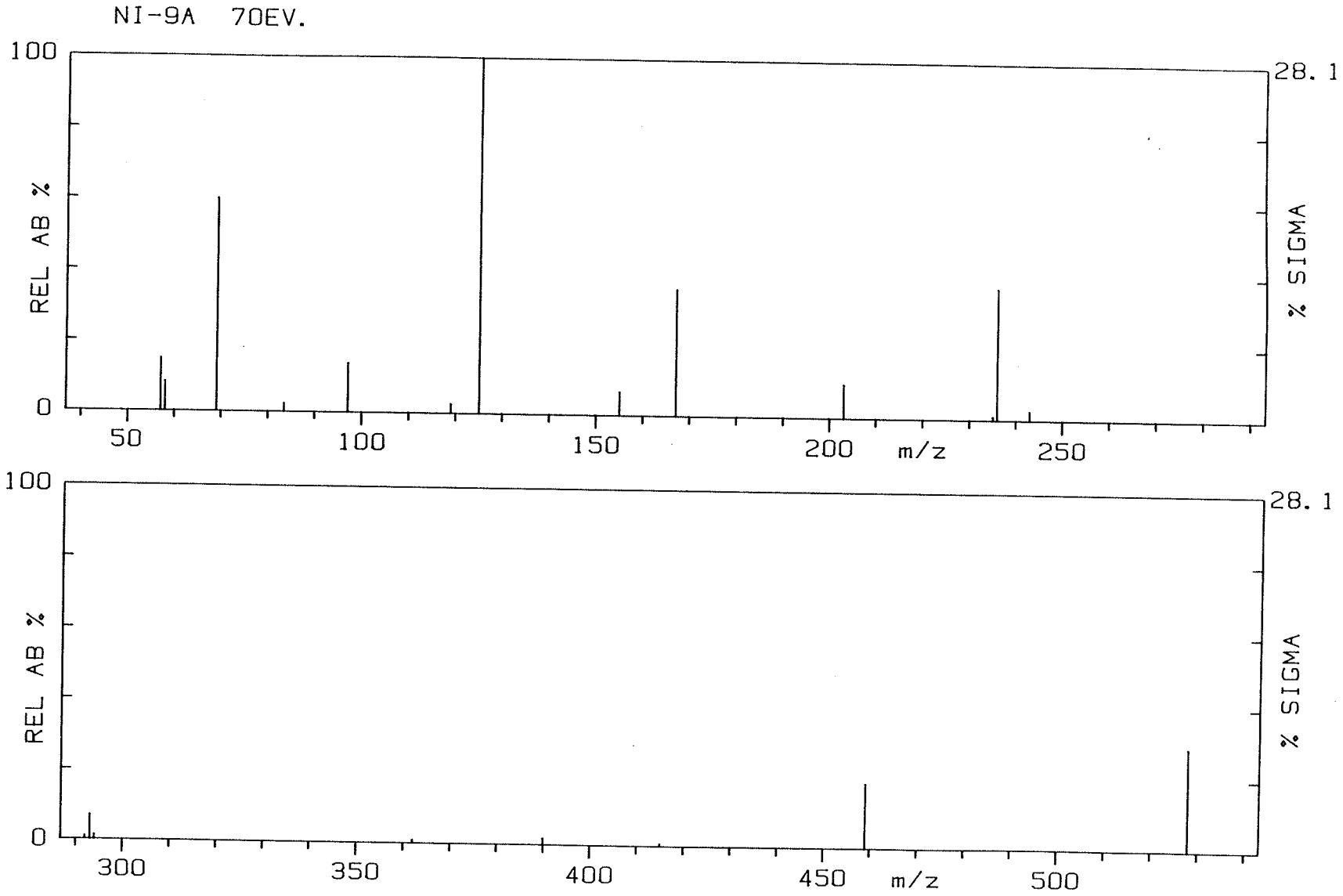
NI-9A 70EV.
100
REL AB %
0
50
100
150
200
m/z
250
28.1
% SIGMA
100
REL AB %
0
300
350
400
450
m/z
500
28.1
% SIGMA

Figure 61.

Normalized 70 eV-EI mass spectrum of

bis[1,1,1,2,2-pentafluoro-5-phenyl-3,5-pentanedionato]Ni(II)

{**Ni-13a**}.

m/z $[M]^{+\cdot}$ = 588, $[L]^{+}$ = 265

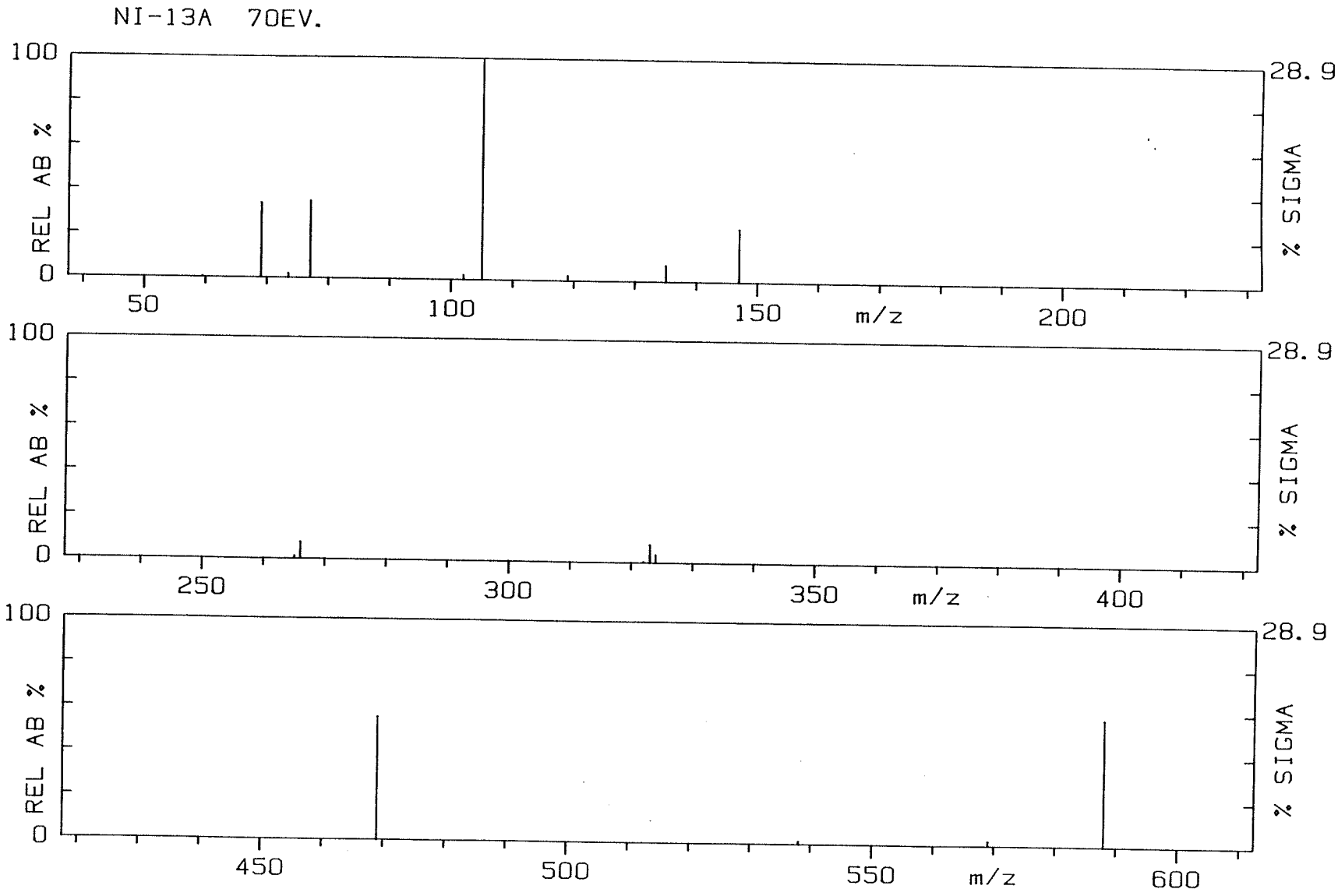
NI-13A 70EV.
100
0
REL AB %
28.9
% SIGMA
50
100
150
m/z
200
250
300
350
400
450
500
550
600

Figure 62.

Normalized 70 eV-EI mass spectrum of

bis[1,1,1,2,2-pentafluoro-5-(2'-thienyl)-3,5-pentanedionato]Ni(II)

{**Ni-14a**}.

m/z $[M]^{+\cdot}$ = 600, $[L]^{+}$ = 271

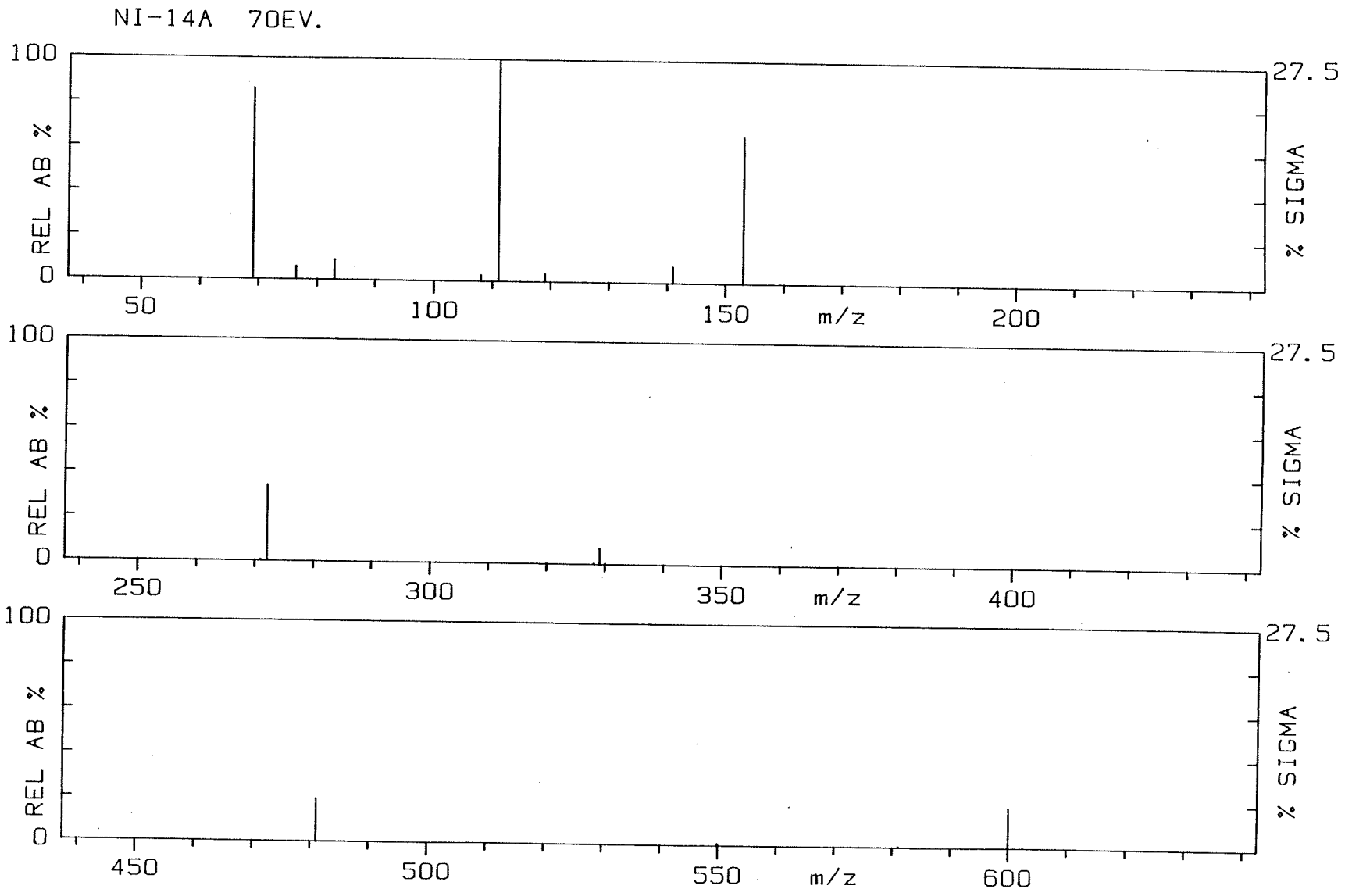
NI-14A 70EV.
100
0
REL AB %
50
100
150
m/z
200
27.5
% SIGMA
100
0
REL AB %
250
300
350
m/z
400
27.5
% SIGMA
100
0
REL AB %
450
500
550
m/z
600
27.5
% SIGMA

Figure 63.

Normalized 70 eV-EI mass spectrum of

bis[1,1,1,2,2,3,3-heptafluoro-6-phenyl-4,6-hexanedionato]Ni(II)

{**Ni-16a**}.

m/z $[M]^{+\cdot}$ = 688, $[L]^{+}$ = 315

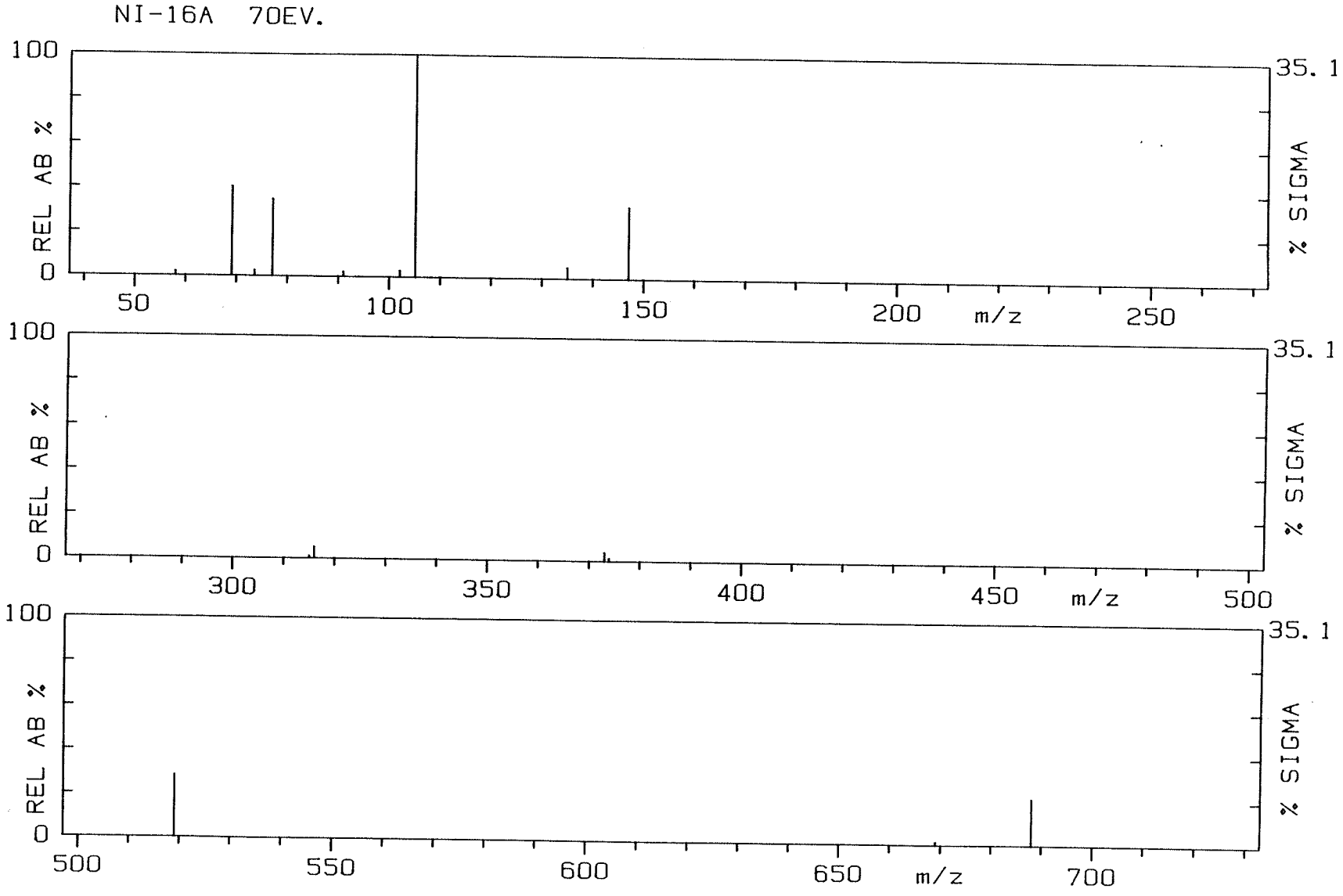
NI-16A 70EV.
100
0
REL AB %
35. 1
% SIGMA
50
100
150
200
m/z
250
300
350
400
450
500
550
600
650
700

Figure 64.

Normalized 70 eV-EI mass spectrum of

bis[1,1,1,2,2,3,3-heptafluoro-6-(2'-thienyl)-4,6-hexanedionato]Ni(II)

{**Ni-17a**}.

m/z $[M]^{+\cdot}$ = 700, $[L]^{+}$ = 321

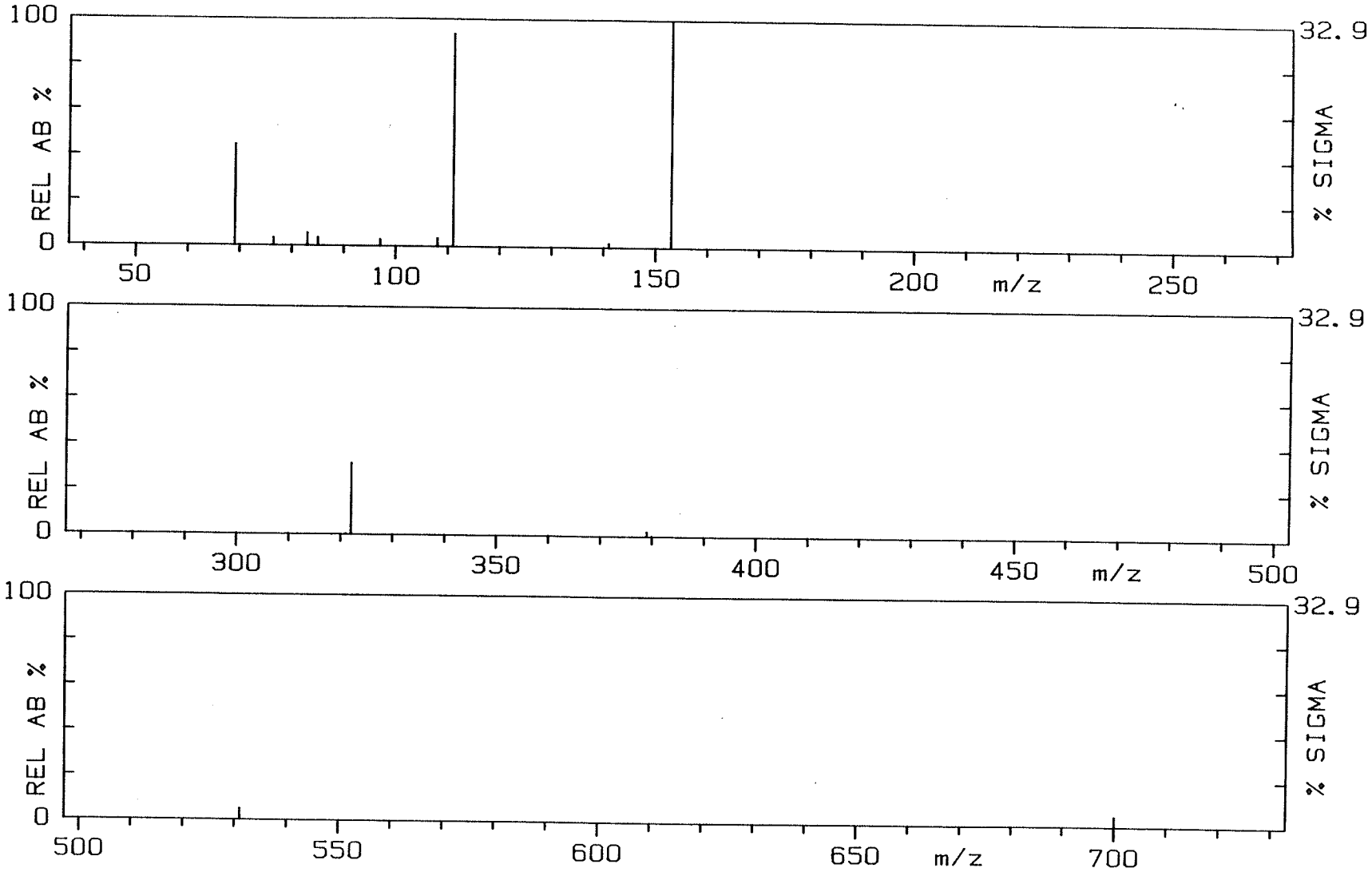
NI-17A 70EV.
100
REL AB %
0
50
100
150
200
m/z
250
32.9
% SIGMA
100
REL AB %
0
300
350
400
450
m/z
500
32.9
% SIGMA
100
REL AB %
0
500
550
600
650
m/z
700
32.9
% SIGMA

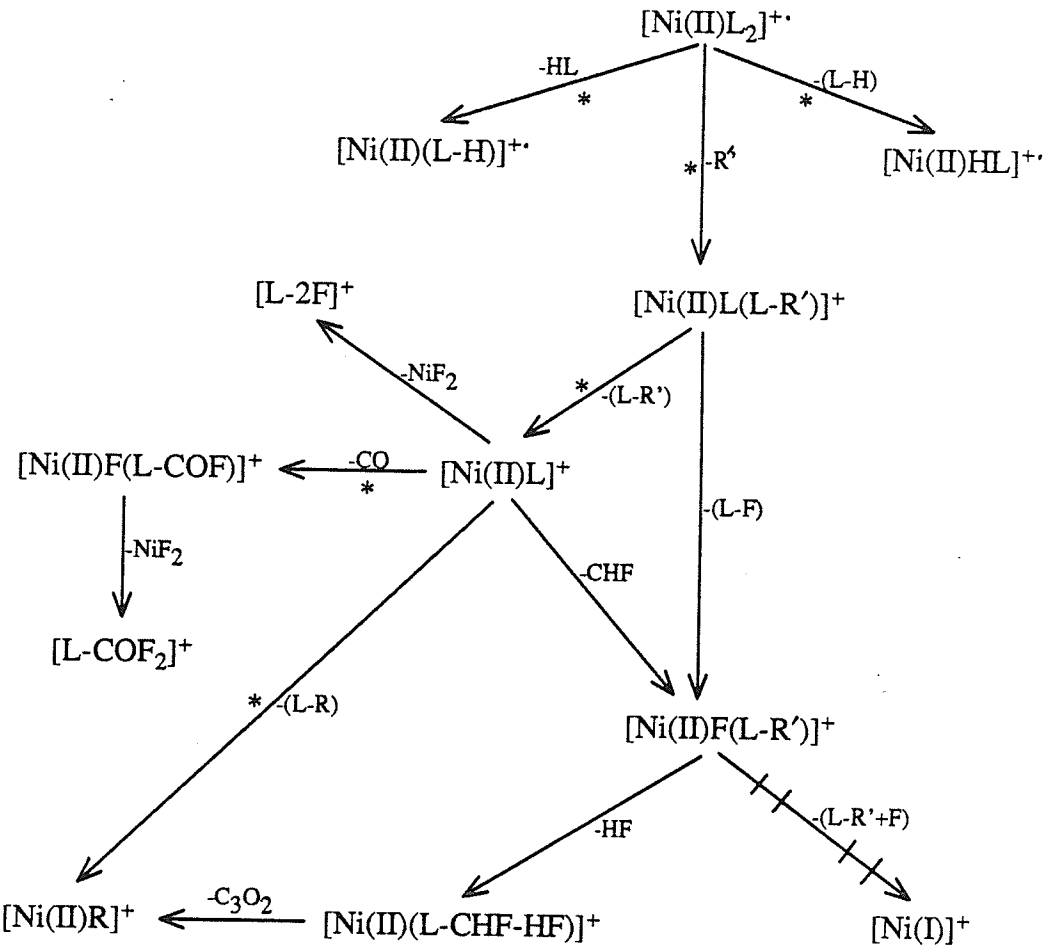

* process confirmed by the observation of a metastable transition in at least one of the complexes.

⟶ reaction step in which a change in oxidation state is proposed.

Scheme 38. Proposed fragmentation pathways for Ni(II) β-diketonates where R' = CHF_2 (**Ni-1a** and **-2a**).

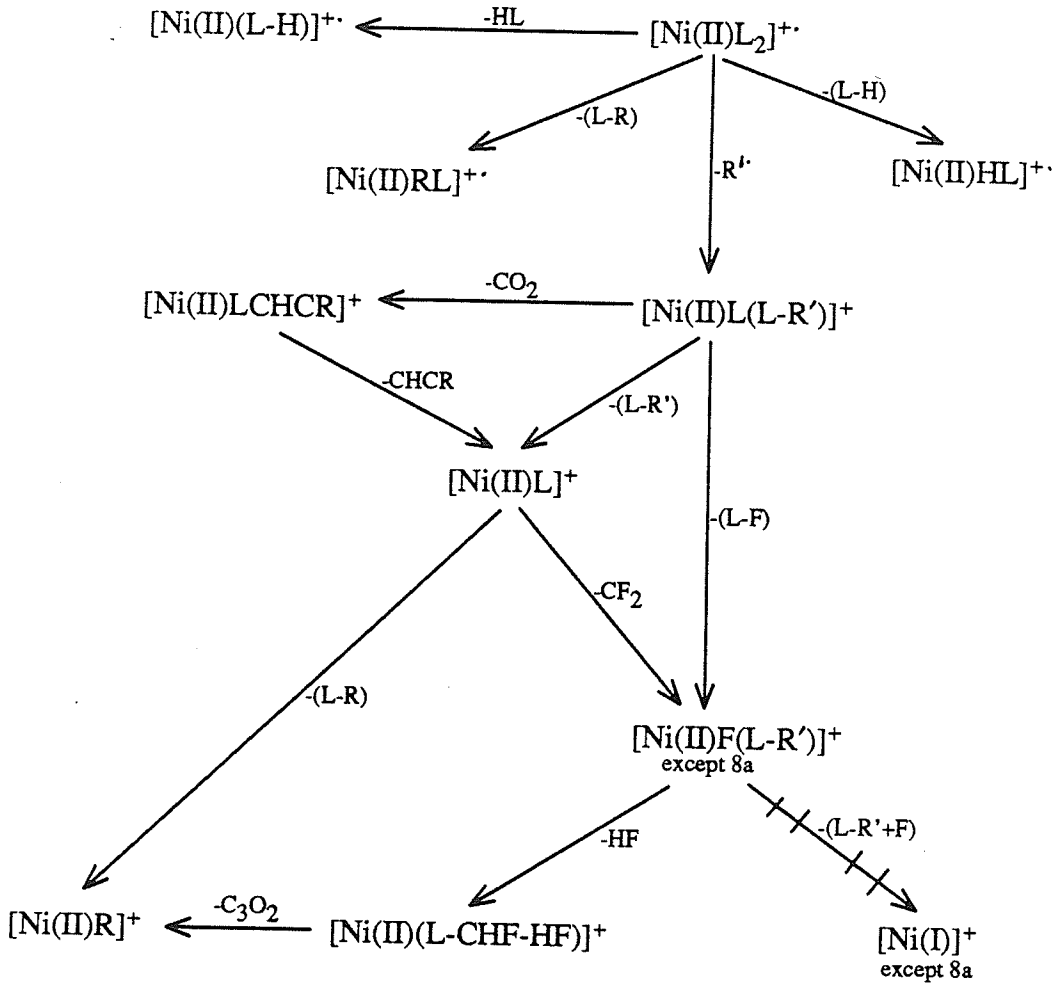

⟶⟶ reaction step in which a change in oxidation state is proposed.

Scheme 39. Proposed fragmentation pathways for Ni(II) β-diketonates where R' = CF_3 (**Ni-3a, -8a** and **-9a**). Pathways are common to all complexes except where noted.

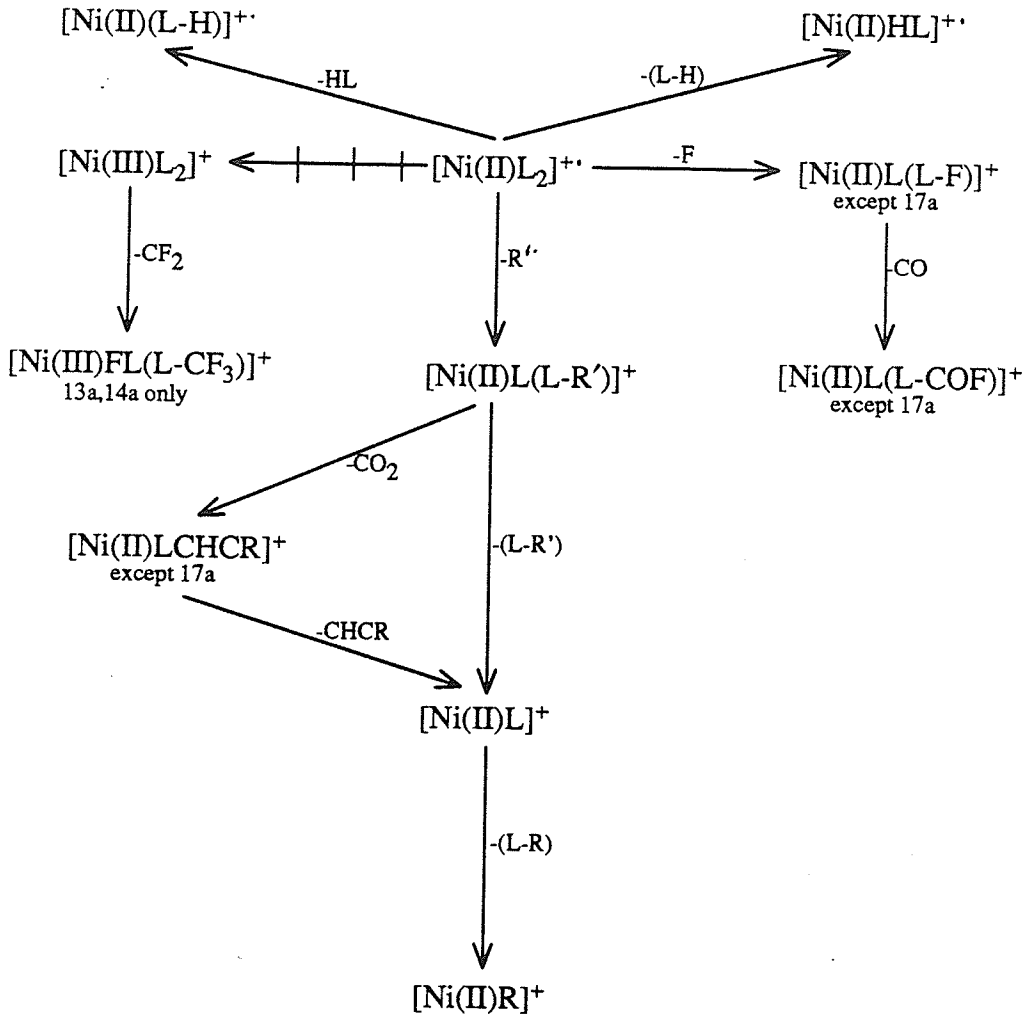

⟶⟶ reaction step in which a change in oxidation state is proposed.

Scheme 40. Proposed fragmentation pathways for Ni(II) β-diketonates where R' = C_2F_5 (**Ni-13a** and **-14a**) or C_3F_7 (**Ni-16a** and **-17a**). Pathways are common to all complexes except where noted.

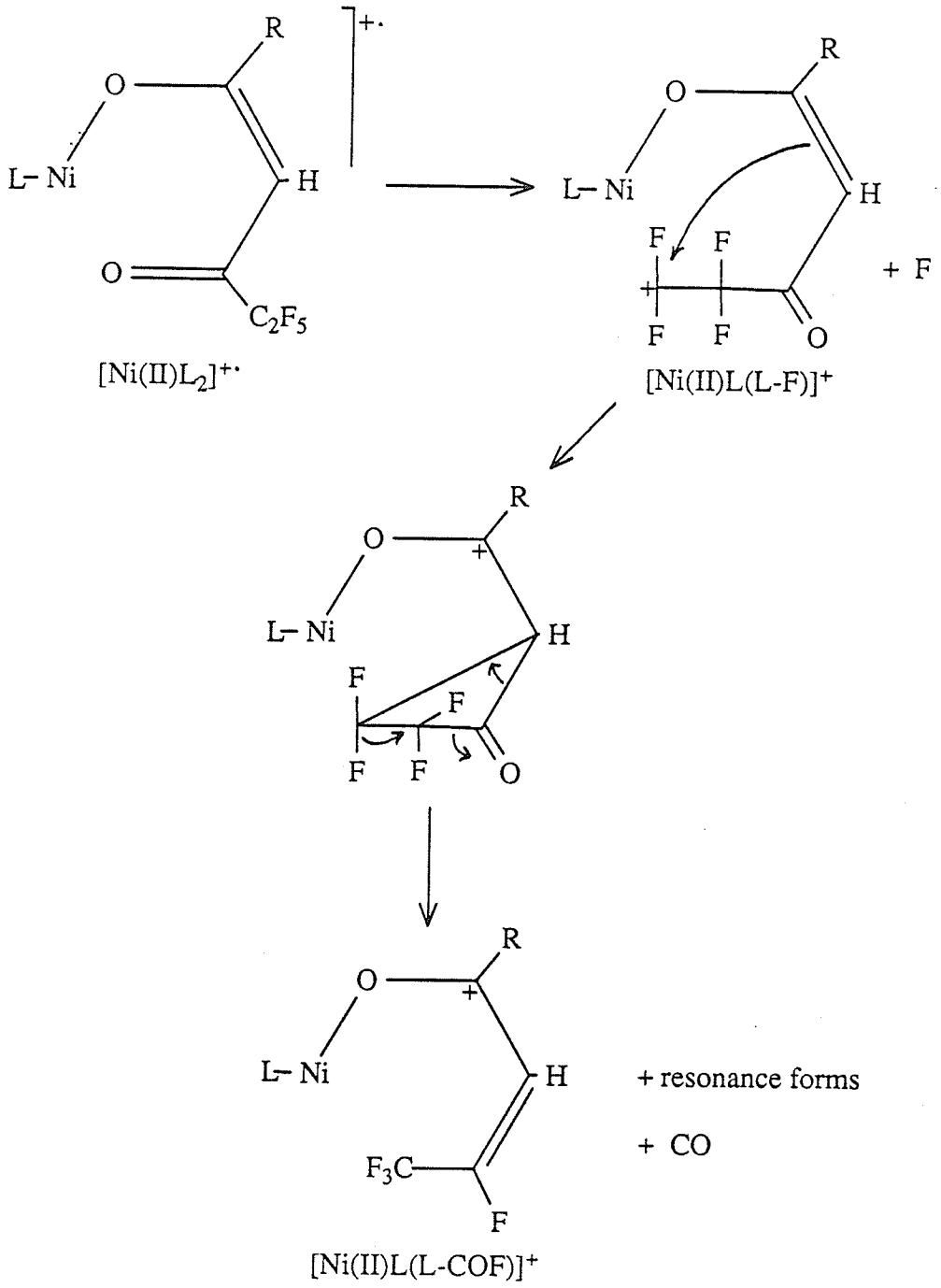

Scheme 41. Suggested mechanism for the formation of [Ni(II)L(L–COF)]+ in **Ni–13a** and **–14a.**

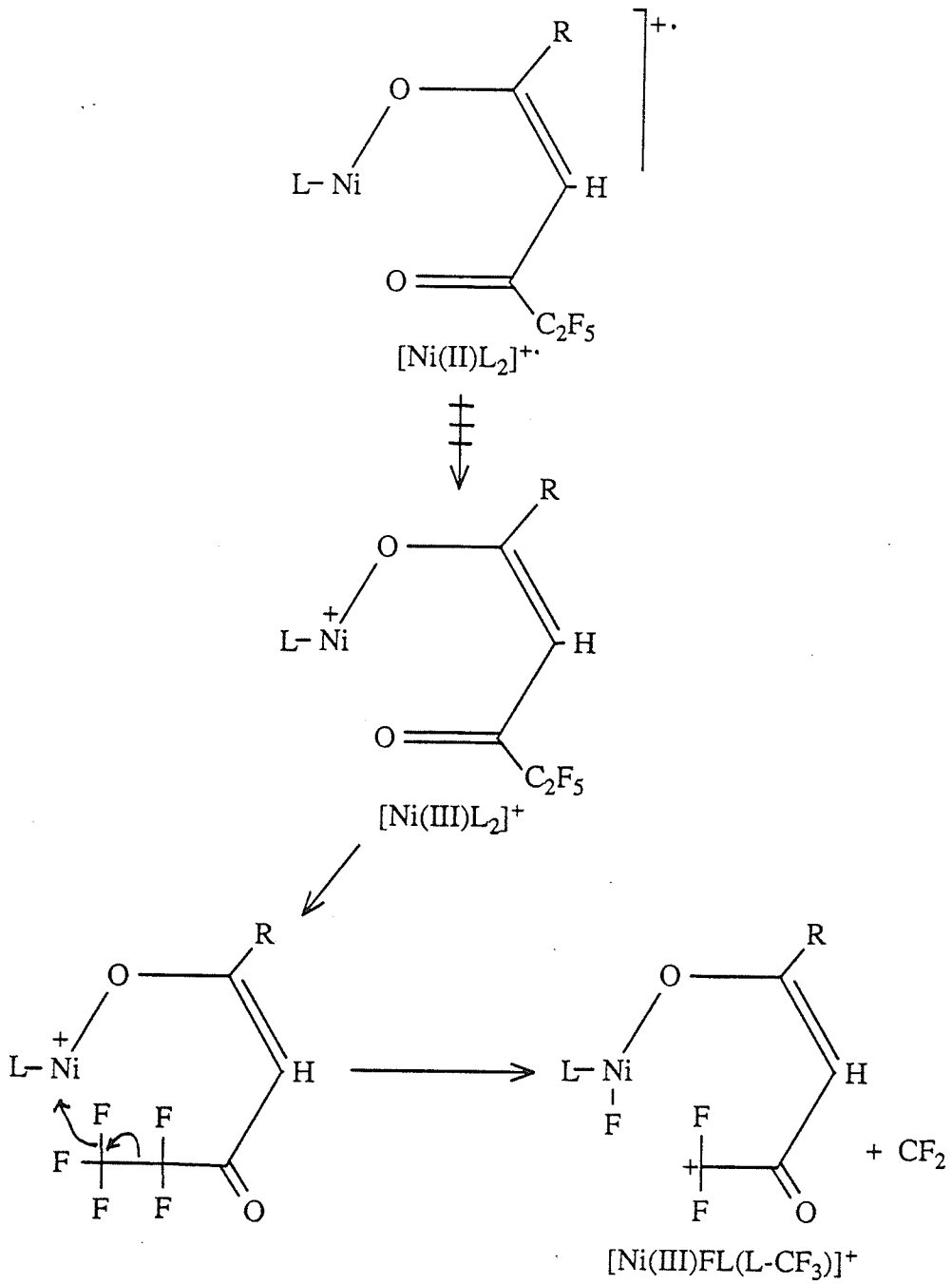

Scheme 42. Suggested mechanism for the formation of $[Ni(III)FL(L\text{-}CF_3)]^+$ in **Ni-13a** and **-14a.**

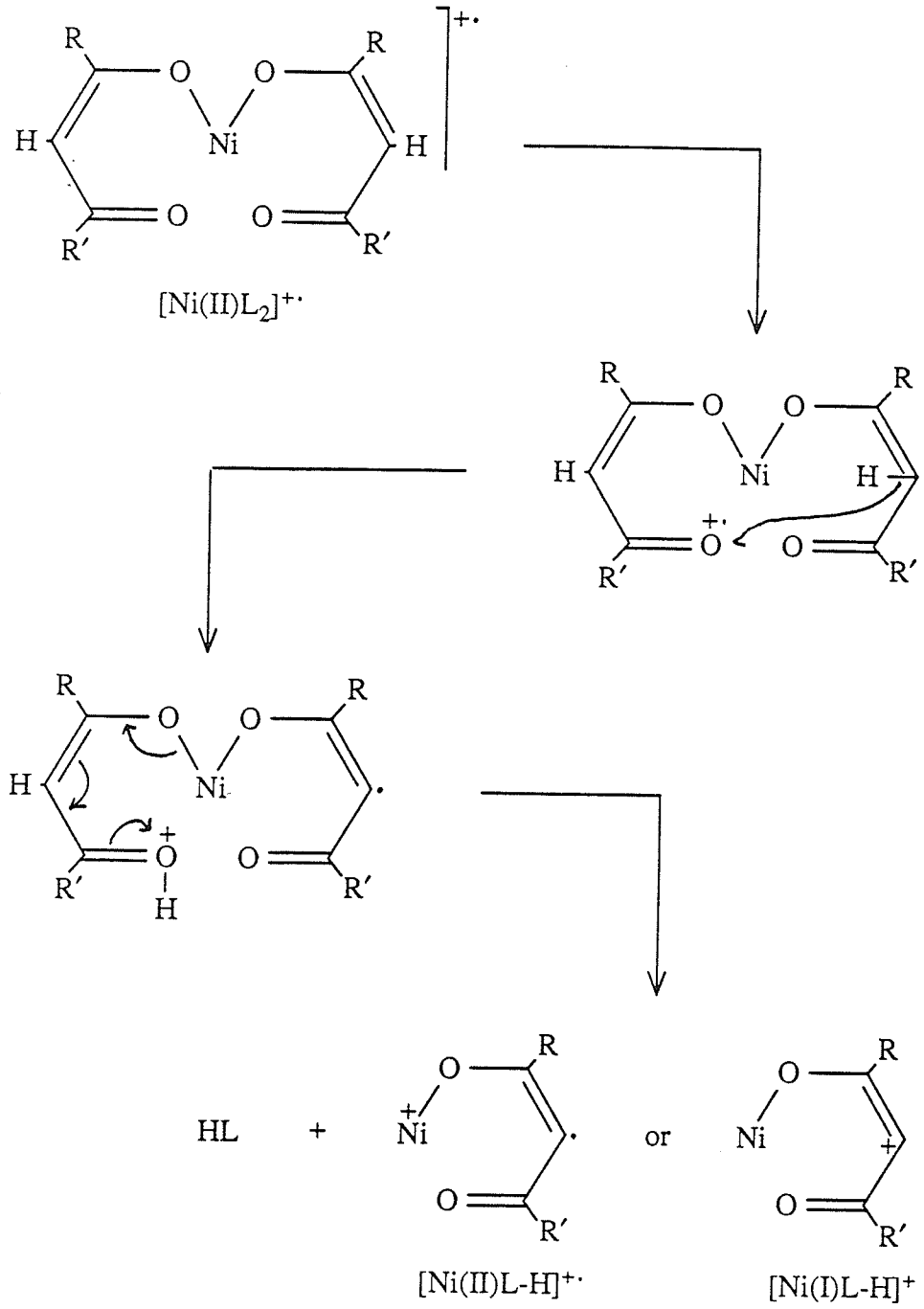

Scheme 43. Suggested mechanism for the formation of $[Ni(L-H)]^+$ in **Ni-3a, -9a, 13a** and **-14a.**

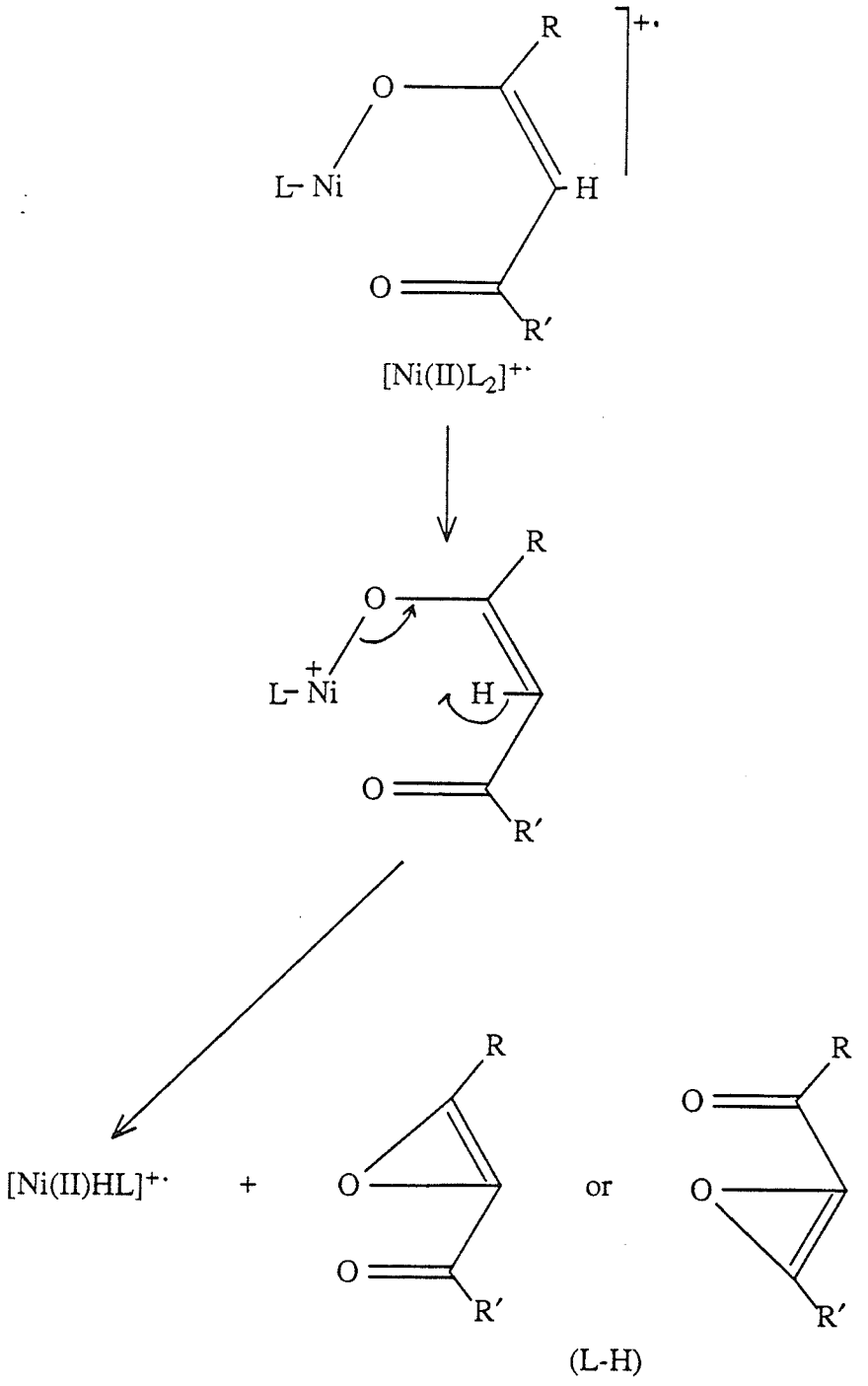

Scheme 44. Suggested mechanism for the formation of $[Ni(II)HL]^{+\cdot}$ (involving hydrogen transfer from the bridging carbon to the metal) in **Ni-1a, -2a, -3a, -8a, -9a, -13a, -14a, -16a, -17a.**

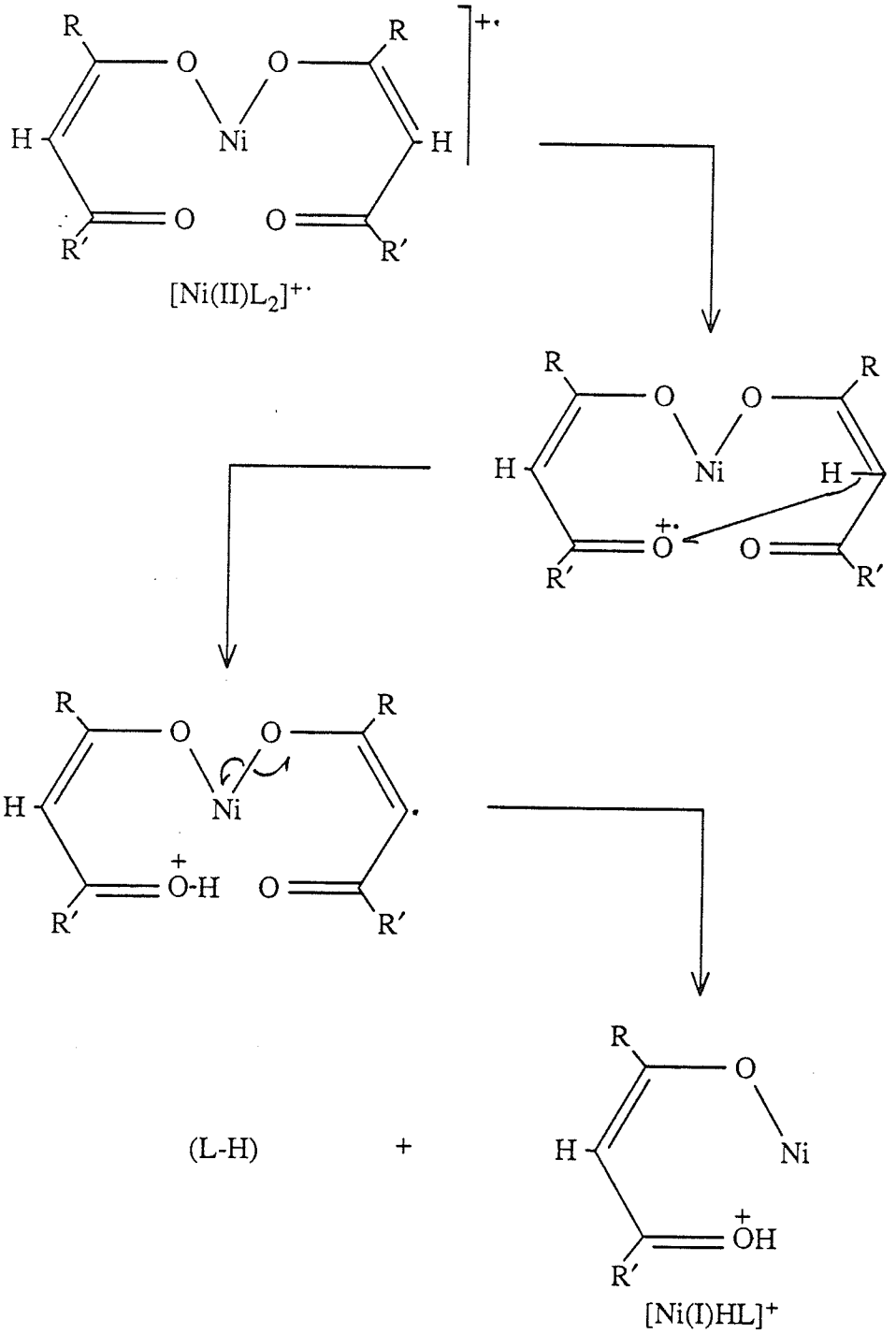

Scheme 45. Suggested mechanism for the formation of $[Ni(I)HL]^+$ (involving hydrogen transfer to oxygen atom of other ligand) in **Ni-1a, -2a, -3a, -8a, -9a, -13a, -14a, -16a** and **-17a.**

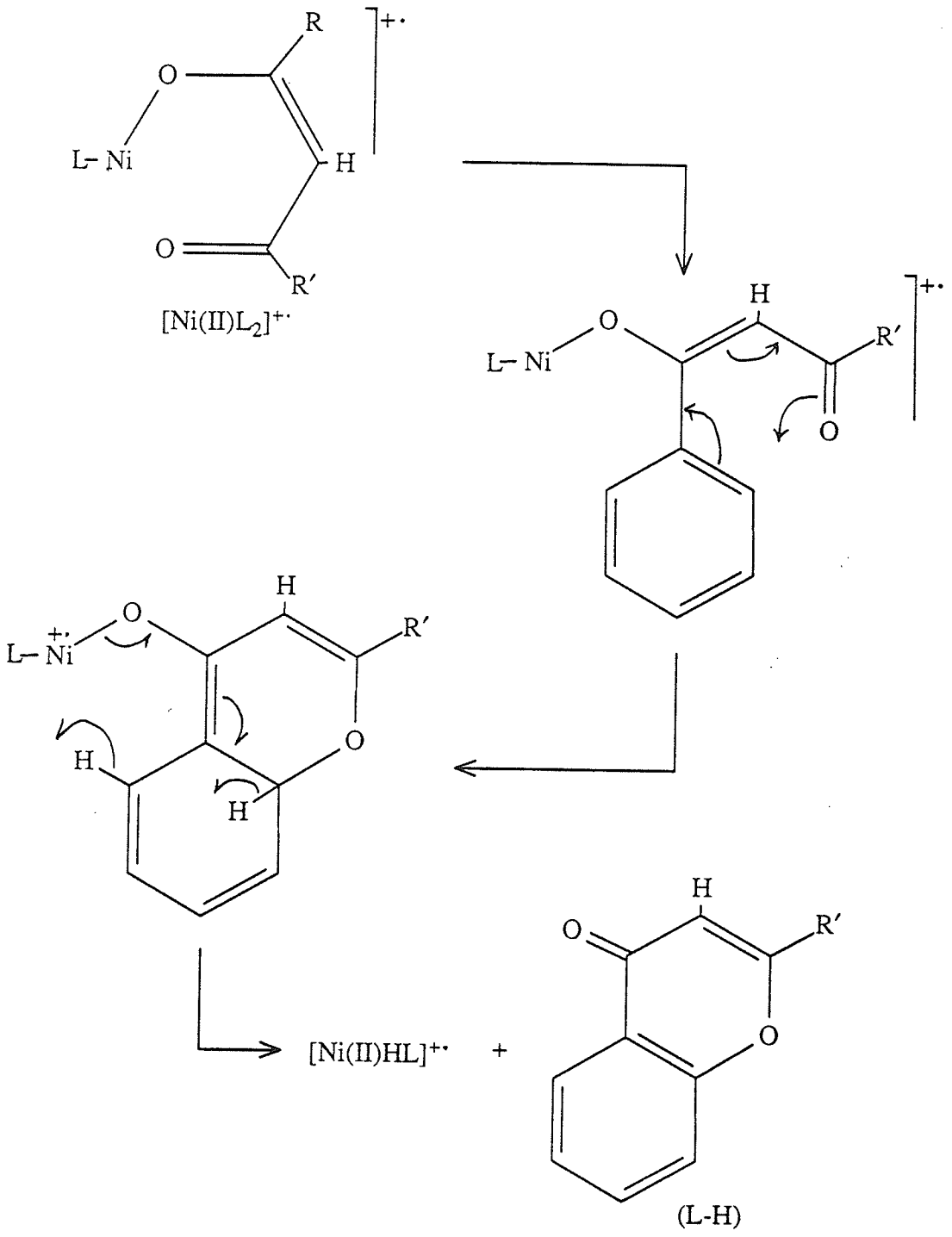

Scheme 46. Suggested mechanism for the formation of $[Ni(II)HL]^{+\cdot}$ in **Ni-1a, -3a, -13a** and **-16a.**

(e) Pd(II) β-diketonates

Relative abundance data for the six Pd(II) β-diketonates studied appear in Tables 24-26 while plots of the corresponding EI mass spectra are featured in Figures 65-70. Complex **Pd-8a** was the focus of a linked-scanning, metastable study. Das (142) has previously published the mass spectra of these compounds.

All of the spectra in this section are characterized by a large number of metal-containing ions. With the aid of metastable results, fragmentation routes and mechanisms have been proposed for the majority of these fragments. In some instances however, no reaction pathways could be elucidated; many products appear to be the result of extensive gas-phase rearrangements.

Suggested decomposition pathways for the trifluoromethyl-substituted chelates (R' = CF_3; Table 24) are shown in Scheme 47. The major ions common to both spectra include $[Pd(II)L_2]^+$, $[Pd(II)RL]^{+\cdot}$, $[Pd(II)RCHR]^+$ and $[Pd(II)R]^+$, among others. Some of the fragmentations have already been discussed:

Fragmentation	Scheme
$[Pd(II)L_2]^{+\cdot} \longrightarrow [Pd(II)RL]^{+\cdot}$	26
$[Pd(II)RL]^{+\cdot} \longrightarrow [Pd(II)R_2]^{+\cdot}$	26
$[Pd(II)L(L\text{-}R')]^{+} \longrightarrow [Pd(II)L]^{+}$	30
$[Pd(II)L]^{+} \longrightarrow [Pd(II)F(L\text{-}COF)]^{+}$	31

A mechanism for the formation of $[Pd(II)L\text{-}H]^{+\cdot}$ and $[Pd(II)(L\text{-}H\text{-}R')]^{+}$ is proposed in Scheme 48. The intramolecular transfer of a bridging hydrogen from $[M]^{+\cdot}$ into the neutral product HL (thereby yielding $[Pd(II)L\text{-}H]^{+\cdot}$) is not unlike the suggested mechanism for $[Ni(II)L\text{-}H]^{+\cdot}$ formation (see Scheme 43). The subsequent loss of the OE· neutral R'· can then give $[Pd(II)(L\text{-}H\text{-}R')]^{+}$, although metastable evidence indicates that $[Pd(II)(L\text{-}H\text{-}R')]^{+}$ also arises directly from $[Pd(II)L_2]^{+\cdot}$. Both routes are illustrated in Scheme 48.

The elimination of CO from $[Pd(II)RL]^{+\cdot}$ can be seen to proceed through a formal Pd(III) oxidation state as depicted in Scheme 49. Fluorine migration to the metal is then possible, followed by a rearrangement of the ligand to allow for the release of carbon monoxide. Charge delocalization into the aromatic substituent situated alpha to the proposed positive-charge site can aid in the stability of such a structure.

Suggested reaction pathways for the Pd(II) β-diketonates possessing pentafluoroethyl (R' = C_2F_5; Table 25) or heptafluoropropyl (R' = C_3F_7; Table 26) substituents are shown in Scheme 50. As seen in the CF_3-substituted analogs, many of the decompositions are known:

Fragmentation	Scheme
$[Pd(II)L_2]^{+\cdot}$ ---> $[Pd(II)RL]^{+\cdot}$	26
$[Pd(II)RL]^{+\cdot}$ ---> $[Pd(II)R_2]^{+\cdot}$	26
$[Pd(II)L(L\text{-}R')]^{+}$ ---> $[Pd(II)L]^{+}$	30
$[Pd(II)L]^{+}$ ---> $[Pd(II)F(L\text{-}COF)]^{+}$	31
$[Pd(II)L_2]^{+\cdot}$ ---> $[Pd(II)L\text{-}H]^{+\cdot}$	48
$[Pd(II)L\text{-}H]^{+\cdot}$ ---> $[Pd(II)(L\text{-}H\text{-}R')]^{+}$	48
$[Pd(II)RL]^{+\cdot}$ ---> $[Pd(III)FR(L\text{-}COF)]^{+}$	49

Three metal-containing ions appear in Tables 25 and 26 which were not evident in the spectra of compounds **Pd-3a** and **Pd-8a**: $[Pd(III)FL(L\text{-}CF_3)]^{+}$, $[Pd(II)R(L\text{-}R'CO)]^{+}$ and $[Pd(II)R'CHCR]^{+}$. The loss of CF_2 from the molecular ion (to give $[Pd(III)FL(L\text{-}CF_3)]^{+}$) has been described in Scheme 42. Scheme 51 outlines the formation of $[Pd(II)R(L\text{-}R'CO)]^{+}$ from $[Pd(II)RL]^{+\cdot}$. A mechanism describing the elimination of CO_2 from $[Pd(II)L]^{+}$ (to yield $[Pd(II)R'CHCR]^{+}$) is given in Scheme 52; it is not clear whether the perfluoroalkyl group or the aromatic R group migrates to the metal, although charge delocalization by an adjacent aromatic group partially stabilizes the vinyl carbonium ion formed in Scheme 52.

The Pd(II) β-diketonates possessing a 2-thienyl substituent ($R = C_4H_3S$; **Pd-8a,-14a** and **-17a**) each exhibit a strongly-abundant signal corresponding to the loss of 16 mass units from $[Pd(II)L]^{+}$ (m/z 311, 361 and 411, respectively). The structure $[Pd(II)(L\text{-}O)]^{+}$ has been assigned, based on the observed masses and isotopic distribution. Intense metastable transitions in the linked-scanning spectra of **Pd-8a** indicate that both $[Pd(II)RL]^{+\cdot}$ and $[Pd(II)L_2]^{+\cdot}$ are parents; on this

basis, suggested mechanisms for the formation of $[Pd(II)(L-O)]^+$ are presented in Scheme 53. The rationale behind the extraordinary abundance of this species when R = 2-thienyl may lie in the resonance stability of the final product, a stability afforded by the intramolecular donation of the sulfur lone pair (see Scheme 53). Das's report (142) of an abundant "$[PdL-16]^+$" ion in the mass spectrum of bis(1,1,1-trifluoro-4-(2'-furyl)-2,4-butanedionato)Pd(II) lends additional support to this argument and reiterates the importance of a substituent-based, heteroatom lone pair in the formation of $[Pd(II)(L-O)]^+$.

Table 24. 70 eV-EI mass spectra of compounds **Pd-3a** and **Pd-8a.**

	Pd-3a			**Pd-8a**		
R =	$-C_6H_5$			$-C_4H_3S$		
R'=	$-CF_3$			$-CF_3$		
ION	%RA	m/z	%TIC	%RA	m/z	%TIC
$[PdL_2]^+$ (a)	100.0	(536)	18.5	100.0	(548)	15.9
$[PdL(L-F)]^+$	1.8	(517)	0.3	-	(529)	-
$[PdL(L-R')]^+$	6.4	(467)	1.2	[a]6.3	(479)	1.0
$[PdRL]^+$ (b)	14.6	(398)	2.7	[a]23.5	(410)	3.7
$[PdFR(L-COF)]^+$	29.5	(370)	5.5	[b]3.4	(382)	0.5
$[PdR(L-R')]^+$	4.3	(329)	0.8	[a]6.2	(341)	1.0
$[PdL]^+$	4.0	(321)	0.7	[a]3.4	(327)	0.5
$[PdL-H]^+$	4.1	(320)	0.8	[a]5.6	(326)	0.9
$[PdL-O]^+$	4.7	(305)	0.9	[a,b]80.9	(311)	12.9
$[PdF(L-COF)]^+$	7.8	(293)	1.4	[c]4.6	(299)	0.7
$[PdRCHR]^+$	49.2	(273)	9.1	[b]28.6	(285)	4.6
$[PdL_2]^{2+}$	4.1	(268)	0.8	7.9	(274)	1.3
$[PdR_2]^+$	-	(260)	-	[b]13.1	(272)	2.1
$[PdL-H-R']^+$	14.2	(251)	2.6	[a]4.0	(257)	0.6
$[PdRC_2O]^+$	4.9	(223)	0.9	-	(229)	-
$[PdRCO]^+$	4.6	(211)	0.9	-	(217)	-
$[PdRCH]^+$	9.9	(196)	1.8	9.7	(202)	1.5
$[PdRC]^+$	15.8	(195)	2.9	14.6	(201)	2.3
$[PdR]^+$	95.5	(183)	17.7	[b]66.1	(189)	10.5

Table 24. (continued).

$[PdCOCH]^+$	-	(147)	-	9.8 (147)	1.6
$[Pd]^+$	10.6	(106)	2.0	9.7 (106)	1.5
$[HL]^+$	12.7	(216)	2.4	32.6 (222)	5.2
$[L]^+$	4.1	(215)	0.8	1.3 (221)	0.2
$[RCHR]^+$	10.0	(167)	1.9	[a,b]17.6 (179)	2.8
$[R_2]^+$	-	(154)	-	[a,b]9.9 (166)	1.6
$[HL-R']^+$	15.1	(147)	2.8	29.4 (153)	4.7
$[RC_3O]^+$	-	(129)	-	1.9 (135)	0.3
$[RCO]_+$	40.4	(105)	7.5	[a,b]65.1 (111)	10.4
$[RCH]^+$	3.6	(90)	0.7	2.9 (96)	0.5
$[RC]^+$	6.3	(89)	1.2	1.6 (95)	0.3
$[R]^+$	36.4	(77)	6.7	15.5 (83)	2.5
$[HL-R']^{2+}$	1.4	(73.5)	0.3	3.2 (76.5)	0.5
$[R']^+$	24.0	(69)	4.4	49.8 (69)	7.9

[a] Identified metastable transitions are indicated by superscripts which relate the daughter ion to its precursor as labelled in column 1.

Table 25. 70 eV-EI mass spectra of compounds **Pd-13a** and **Pd-14a.**

	Pd-13a	**Pd-14a**
R =	$-C_6H_5$	$-C_4H_3S$
R'=	$-C_2F_5$	$-C_2F_5$

ION	%RA	m/z	%TIC	%RA	m/z	%TIC
$[PdL_2]^+$	92.5	(636)	15.4	100.0	(648)	15.5
$[PdFL(L-CF_3)]^+$	7.2	(586)	1.2	3.1	(598)	0.5
$[PdL(L-R')]^+$	13.9	(517)	2.3	11.3	(529)	1.7
$[PdRL]^+$	13.3	(448)	2.2	18.9	(460)	2.9
$[PdFR(L-COF)]^+$	21.0	(420)	3.5	3.3	(432)	0.5
$[PdL]^+$	4.6	(371)	0.8	5.1	(377)	0.8
$[PdL-H]^+$	4.6	(370)	0.8	7.1	(376)	1.1
$[PdL-O]^+$	3.5	(355)	0.6	81.0	(361)	12.5
$[PdF(L-COF)]^+$	7.9	(343)	1.3	5.0	(349)	0.8
$[PdR(L-R')]^+$	13.4	(329)	2.2	15.2	(341)	2.4
$[PdR'CHCR]^+$	-	(327)	-	11.7	(333)	1.8
$[PdL_2]^{2+}$	8.5	(318)	1.4	7.0	(324)	1.1
$[PdR(L-R'CO)]^+$	5.5	(301)	0.9	7.1	(313)	1.1
$[PdRCHR]^+$	45.0	(273)	7.5	16.6	(285)	2.6
$[PdR_2]^+$	-	(260)	-	17.2	(272)	2.7
$[PdL-H-R']^+$	30.6	(251)	5.1	7.4	(257)	1.1
$[PdRCO]^+$	4.0	(211)	0.7	-	(217)	-
$[PdRCH]^+$	14.6	(196)	2.4	16.0	(202)	2.5
$[PdRC]^+$	22.9	(195)	3.8	21.1	(201)	3.3

Table 25. (continued).

$[PdCOCH]^+$	-	(147)	-	12.6 (147)	1.9
$[PdR]^+$	100.0	(183)	16.6	78.6 (189)	12.2
$[Pd]^+$	9.1	(106)	1.5	9.8 (106)	1.5
$[HL]^+$	9.4	(266)	1.6	12.0 (272)	1.9
$[L]^+$	3.4	(265)	0.6	0.7 (271)	0.1
$[L-S]^+$	-	(233)	-	5.9 (239)	0.9
$[R_2CH]^+$	9.7	(167)	1.6	19.2 (179)	3.0
$[R_2]^+$	-	(154)	-	9.5 (166)	1.5
$[HL-R']^+$	24.0	(147)	4.0	23.3 (153)	3.6
$[RC_3O]^+$	-	(129)	-	2.5 (135)	0.4
$[RCO]^+$	50.0	(105)	8.3	62.8 (111)	9.7
$[RCH]^+$	4.4	(90)	0.7	4.3 (96)	0.7
$[RC]^+$	7.0	(89)	1.2	1.7 (95)	0.3
$[R]^+$	39.6	(77)	6.6	12.5 (83)	1.9
$[HL-R']^{2+}$	1.8	(73.5)	0.3	2.2 (76.5)	0.3
$[CF_3]^+$	33.3	(69)	5.5	34.9 (69)	5.4

Table 26. 70 eV-EI mass spectra of compounds **Pd-16a** and **Pd-17a.**

	Pd-16a			**Pd-17a**		
R =	$-C_6H_5$			$-C_4H_3S$		
R'=	$-C_3F_7$			$-C_3F_7$		
ION	%RA	m/z	%TIC	%RA	m/z	%TIC
$[PdL_2]^+$	77.3	(736)	14.1	100.0	(748)	12.8
$[PdFL(L-CF_3)]^+$	2.8	(686)	0.5	2.6	(698)	0.3
$[PdL(L-R')]^+$	12.3	(567)	2.2	18.1	(579)	2.3
$[PdRL]^+$	9.8	(498)	1.8	16.4	(510)	2.1
$[PdFR(L-COF)]^+$	13.0	(470)	2.4	3.5	(482)	0.4
$[PdL]^+$	3.3	(421)	0.6	6.3	(427)	0.8
$[PdL-H]^+$	3.1	(420)	0.6	8.2	(426)	1.0
$[PdL-O]^+$	2.3	(405)	0.4	83.8	(411)	10.7
$[PdF(L-COF)]^+$	6.6	(393)	1.2	6.0	(399)	0.8
$[PdR'CHCR]^+$	-	(377)	-	12.5	(383)	1.6
$[PdL_2]^{2+}$	3.6	(368)	0.7	7.4	(374)	0.9
$[PdR(L-R')]^+$	12.1	(329)	2.2	22.2	(341)	2.8
$[PdR(L-R'CO)]^+$	5.4	(301)	1.0	7.6	(313)	1.0
$[PdRCHR]^+$	35.3	(273)	6.4	17.1	(285)	2.2
$[PdR_2]^+$	-	(260)	-	21.7	(272)	2.8
$[PdL-H-R']^+$	32.4	(251)	5.9	10.9	(257)	1.4
$[PdRC_2O]^+$	9.9	(223)	1.8	5.9	(229)	0.8
$[PdRCO]^+$	3.5	(211)	0.6	-	(217)	-
$[PdRCH]^+$	17.0	(196)	3.1	20.9	(202)	2.7

Table 26. (continued).

$[PdRC]^+$	24.5	(195)	4.5	26.3 (201)	3.4
$[PdR]^+$	100.0	(183)	18.2	94.2 (189)	12.1
$[PdCOCH]^+$	-	(147)	-	13.6 (147)	1.7
$[Pd]^+$	7.9	(106)	1.4	9.8 (106)	1.3
$[HL]^+$	4.6	(316)	0.8	18.5 (322)	2.4
$[L]^+$	2.6	(315)	0.5	1.4 (321)	0.2
$[L-S]^+$	-	(283)	-	6.9 (289)	0.9
$[R_2CH]^+$	7.6	(167)	1.4	21.5 (179)	2.8
$[R_2]^+$	-	(154)	-	9.5 (166)	1.2
$[HL-R']^+$	22.4	(147)	4.1	41.4 (153)	5.3
$[RC_3O]^+$	-	(129)	-	2.8 (135)	0.4
$[RCOCH]^+$	3.7	(118)	0.7	4.5 (124)	0.6
$[RCO]^+$	50.1	(105)	9.1	81.8 (111)	10.5
$[RCH]^+$	5.2	(90)	0.9	6.1 (96)	0.8
$[RC]^+$	6.7	(89)	1.2	1.9 (95)	0.2
$[R]^+$	35.0	(77)	6.4	13.5 (83)	1.7
$[HL-R']^{2+}$	1.4	(73.5)	0.3	3.4 (76.5)	0.4
$[CF_3]^+$	28.6	(69)	5.2	53.2 (69)	6.8

Figure 65.

Normalized 70 eV-EI mass spectrum of

bis[1,1,1-trifluoro-4-phenyl-2,4-butanedionato]Pd(II)

{Pd-3a}.

m/z $[M]^{+\cdot}$ = 536, $[L]^{+}$ = 215

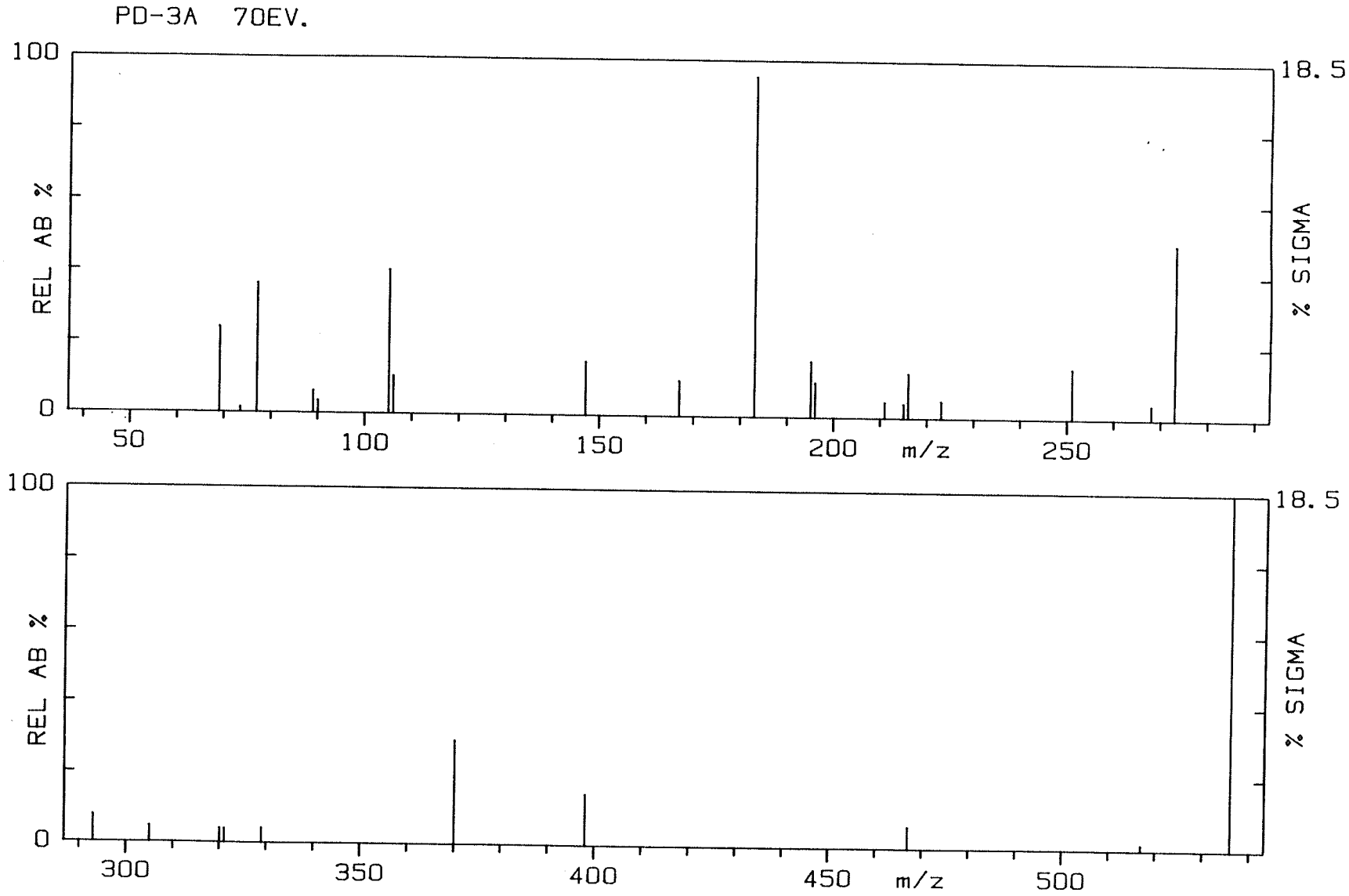
PD-3A 70EV.
100
REL AB %
0
50
100
150
200
m/z
250
18.5
% SIGMA
100
REL AB %
0
300
350
400
450
m/z
500
18.5
% SIGMA

Figure 66.

Normalized 70 eV-EI mass spectrum of

bis[1,1,1-trifluoro-4-(2'-thienyl)-2,4-butanedionato]Pd(II)

{**Pd-8a**}.

m/z $[M]^{+\cdot}$ = 548, $[L]^{+}$ = 221

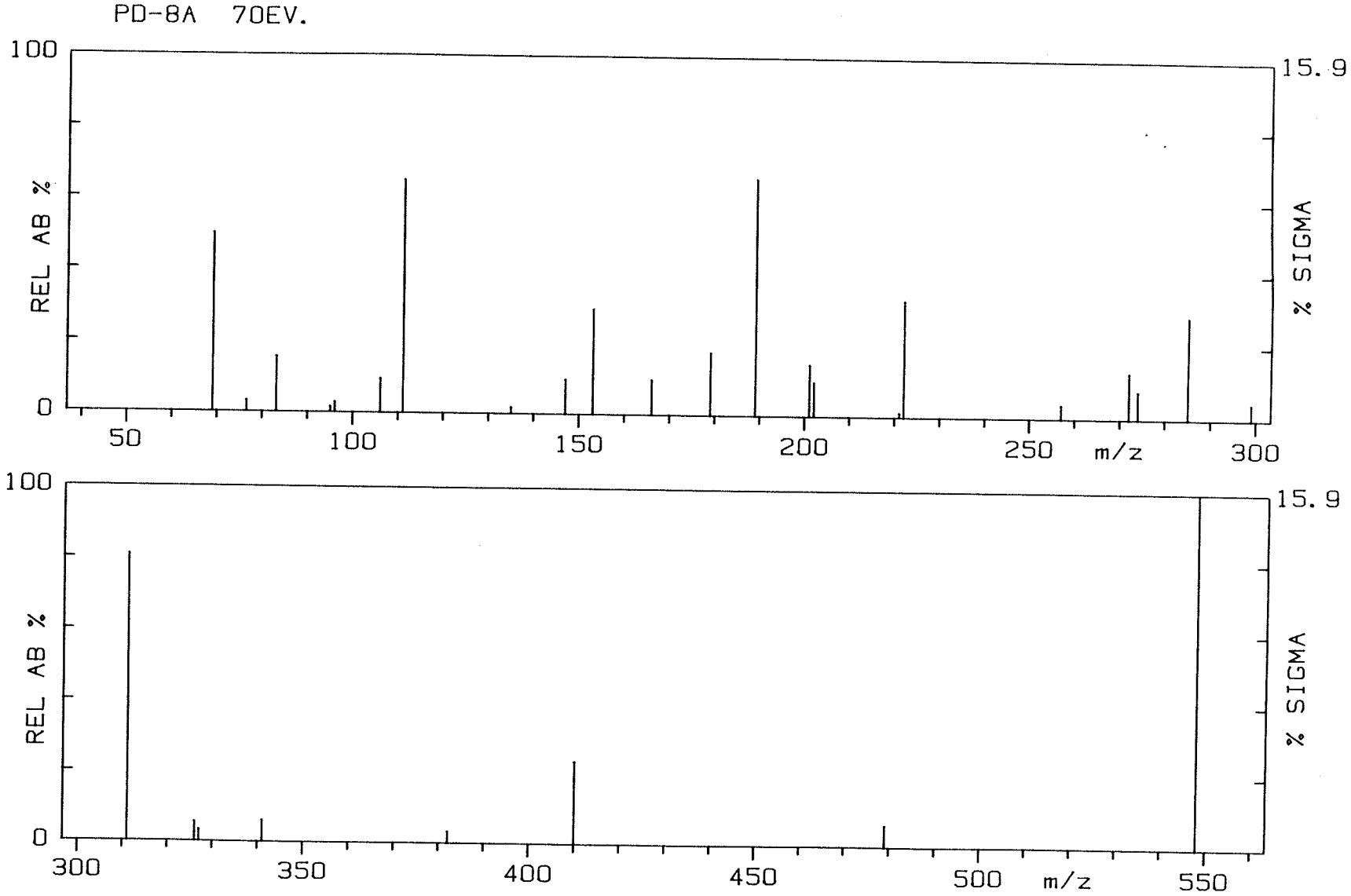
PD-8A 70EV.
100
REL AB %
0
50
100
150
200
250
m/z
300
15.9
% SIGMA
100
REL AB %
0
300
350
400
450
500
m/z
550
15.9
% SIGMA

Figure 67.

Normalized 70 eV-EI mass spectrum of

bis[1,1,1,2,2-pentafluoro-5-phenyl-3,5-pentanedionato]Pd(II)

(**Pd-13a**).

m/z $[M]^{+\cdot}$ = 636, $[L]^{+}$ = 265

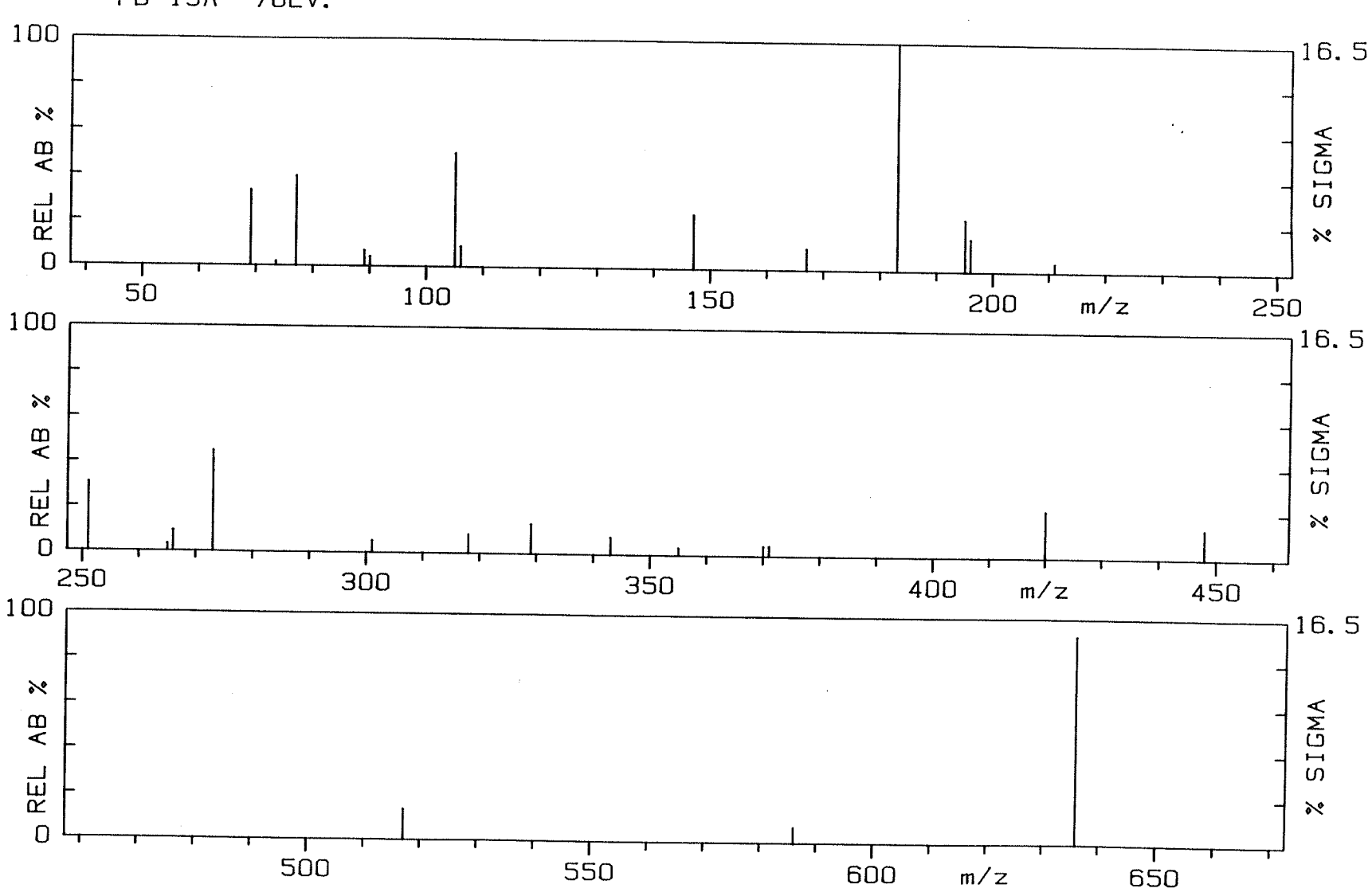
PD-13A 70EV.
100
REL AB %
0
50
100
150
200
m/z
250
16.5
% SIGMA
100
REL AB %
0
250
300
350
400
m/z
450
16.5
% SIGMA
100
REL AB %
0
500
550
600
m/z
650
16.5
% SIGMA

Figure 68.

Normalized 70 eV-EI mass spectrum of

bis[1,1,1,2,2-pentafluoro-5-(2'-thienyl)-3,5-pentanedionato]Pd(II)

{**Pd-14a**}.

m/z $[M]^{+\cdot}$ = 648, $[L]^{+}$ = 271

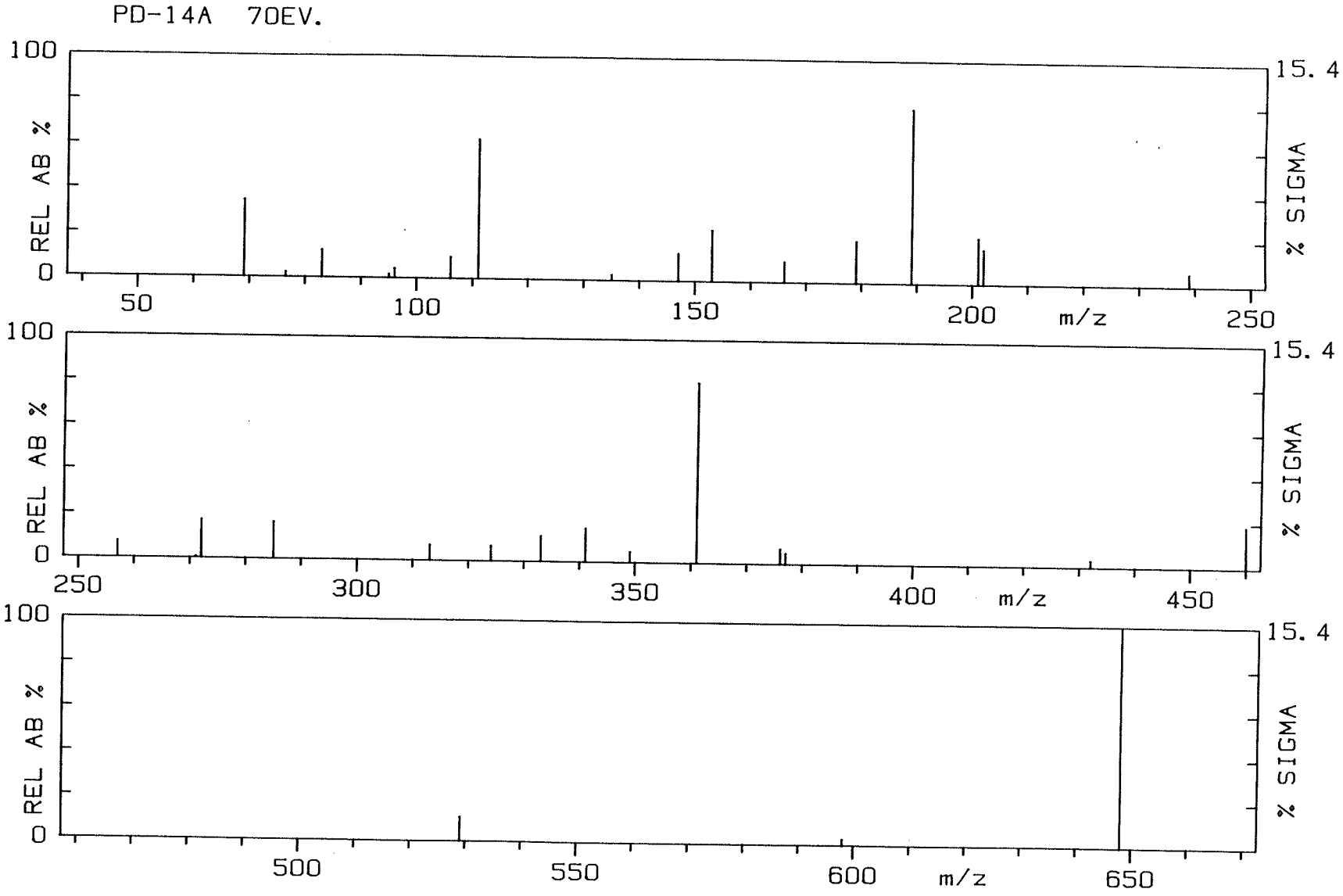
PD-14A 70EV.
100
0
REL AB %
50
100
150
200
m/z
250
15.4
% SIGMA
100
0
REL AB %
250
300
350
400
m/z
450
15.4
% SIGMA
100
0
REL AB %
500
550
600
m/z
650
15.4
% SIGMA

Figure 69.

Normalized 70 eV-EI mass spectrum of

bis[1,1,1,2,2,3,3-heptafluoro-6-phenyl-4,6-hexanedionato]Pd(II)

{Pd-16a}.

m/z $[M]^{+\cdot}$ = 736, $[L]^{+}$ = 315

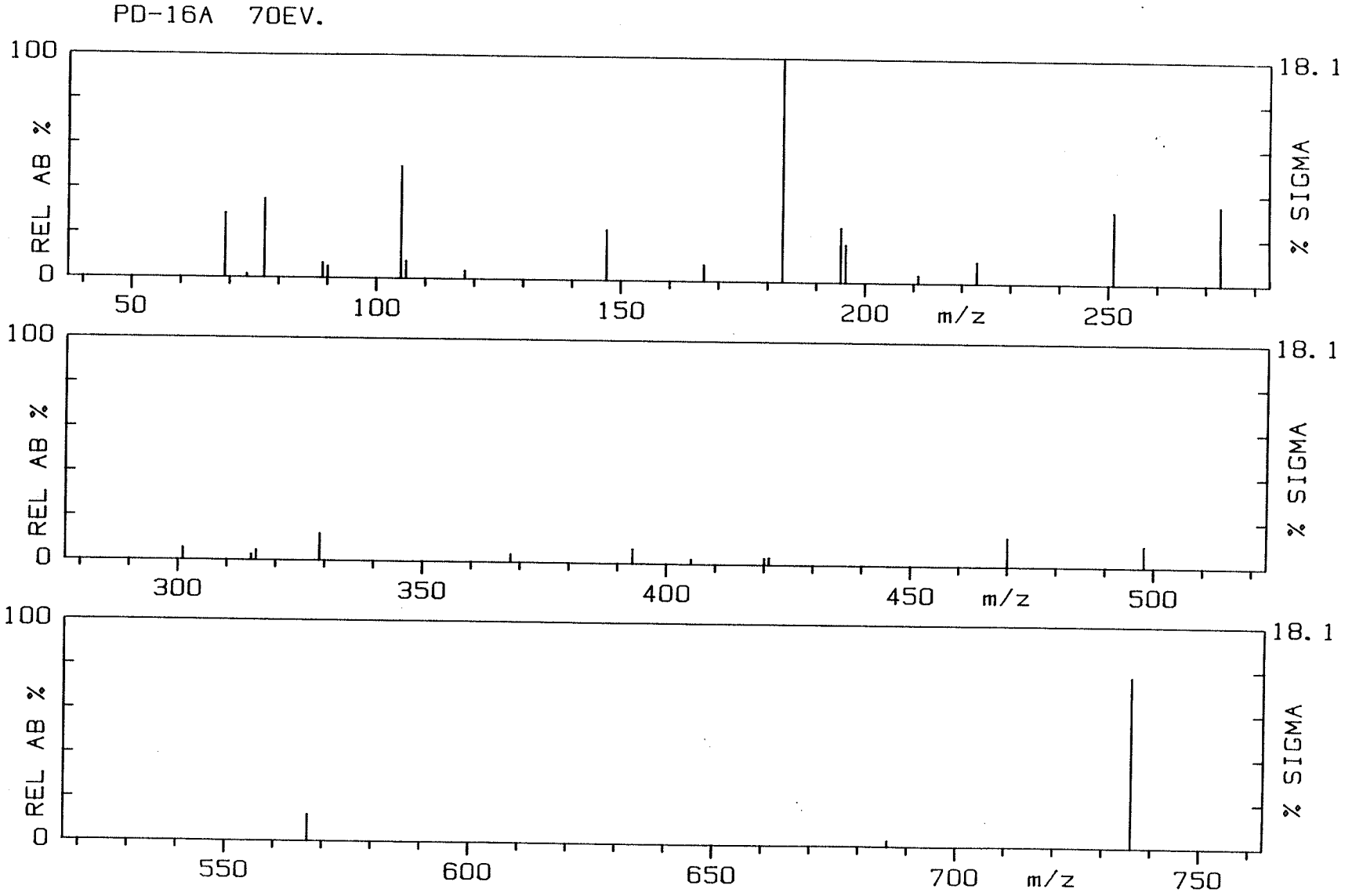
PD-16A 70EV.
100
REL AB %
0
50
100
150
200
m/z
250
18.1
% SIGMA
100
REL AB %
0
300
350
400
450
m/z
500
18.1
% SIGMA
100
REL AB %
0
550
600
650
700
m/z
750
18.1
% SIGMA

Figure 70.

Normalized 70 eV-EI mass spectrum of

bis[1,1,1,2,2,3,3-heptafluoro-6-(2'-thienyl)-4,6-hexanedionato]Pd(II)

{**Pd-17a**}.

m/z $[M]^{+\cdot}$ = 748, $[L]^{+}$ = 321

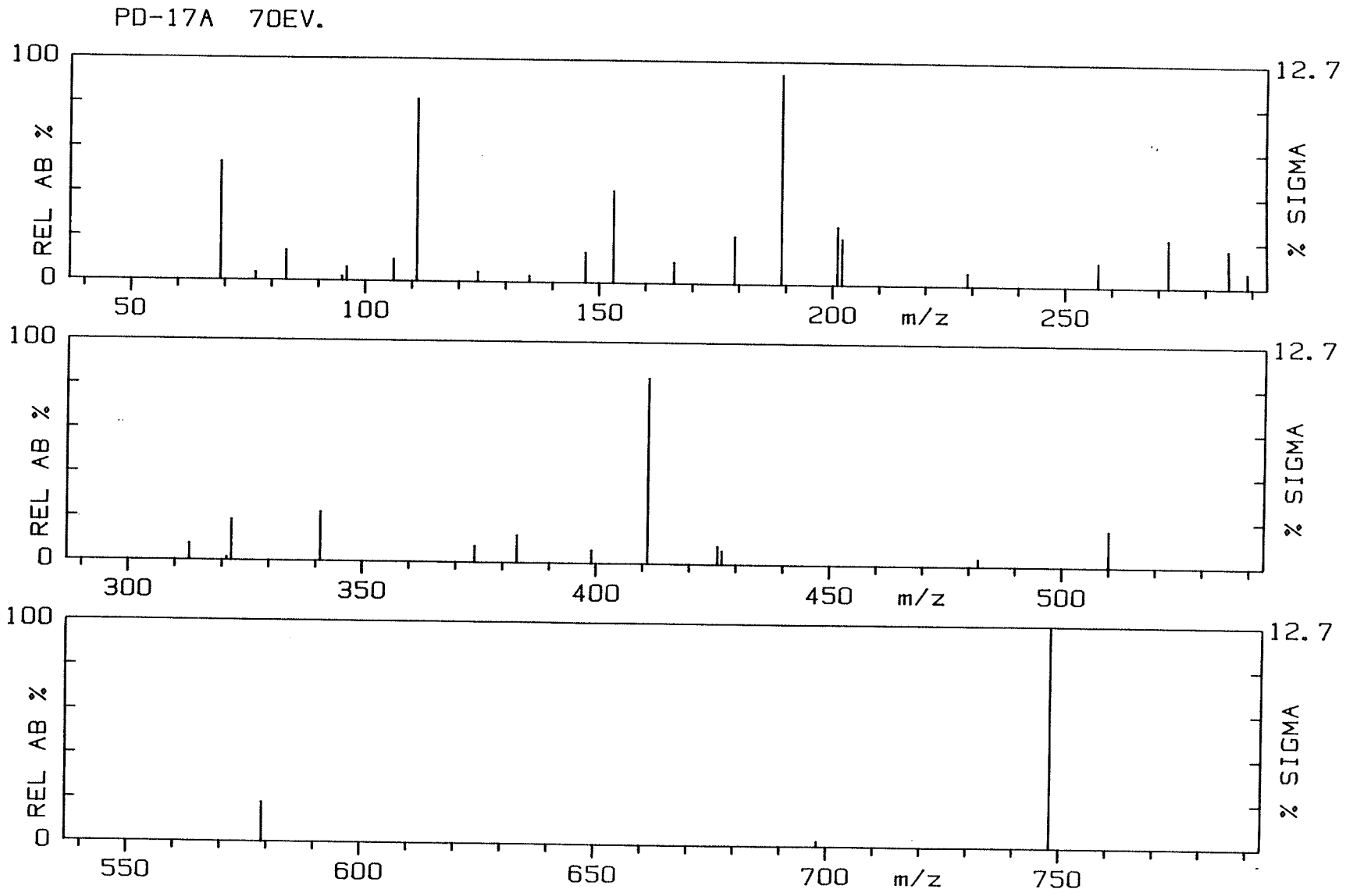
PD-17A 70EV.
100
REL AB %
0
50
100
150
200
m/z
250
12.7
% SIGMA
100
REL AB %
0
300
350
400
450
m/z
500
12.7
% SIGMA
100
REL AB %
0
550
600
650
700
m/z
750
12.7
% SIGMA

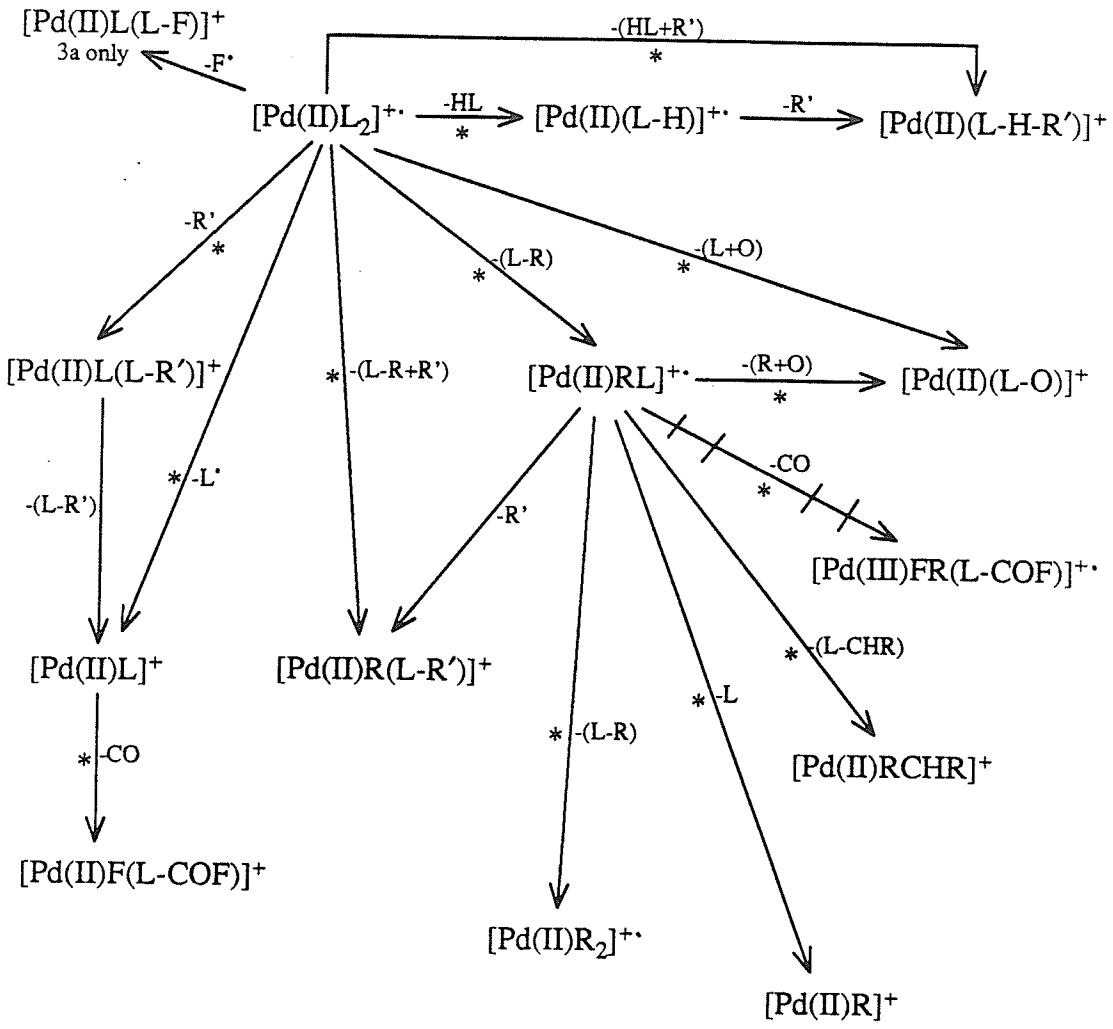

* process confirmed by the observation of a metastable transition in at least one of the complexes.

⟶⟶ reaction step in which a change in metal oxidation state is proposed.

Scheme 47. Proposed fragmentation pathways for Pd(II) β-diketonates where R' = CF_3 (**Pd–3a** and **–8a**). Pathways are common to both complexes except where noted.

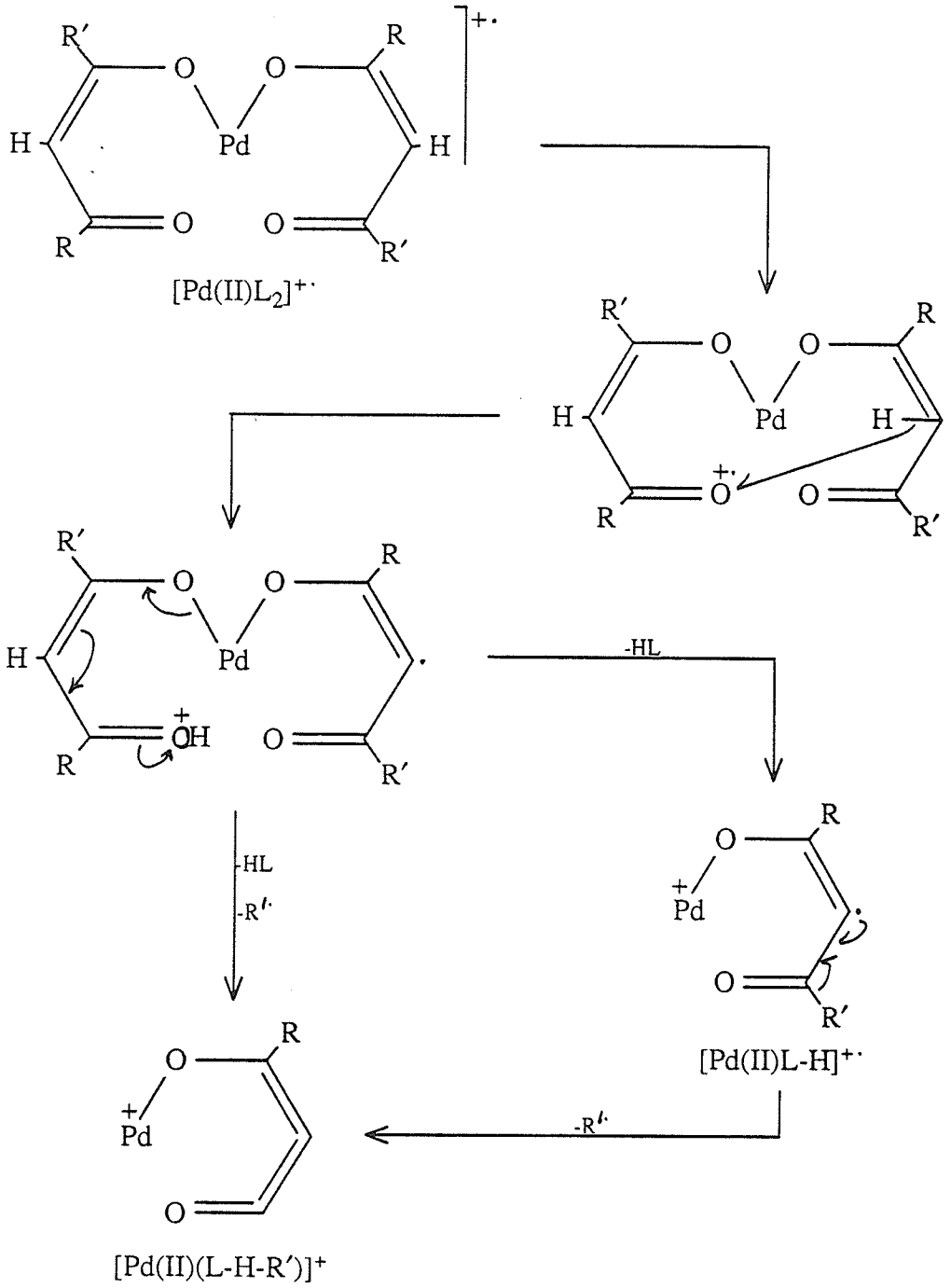

Scheme 48. Suggested mechanism for the formation of $[Pd(II)(L-H)]^{+\cdot}$ and $[Pd(II)(L-H-R')]^{+}$ in **Pd-3a** and **-8a**.

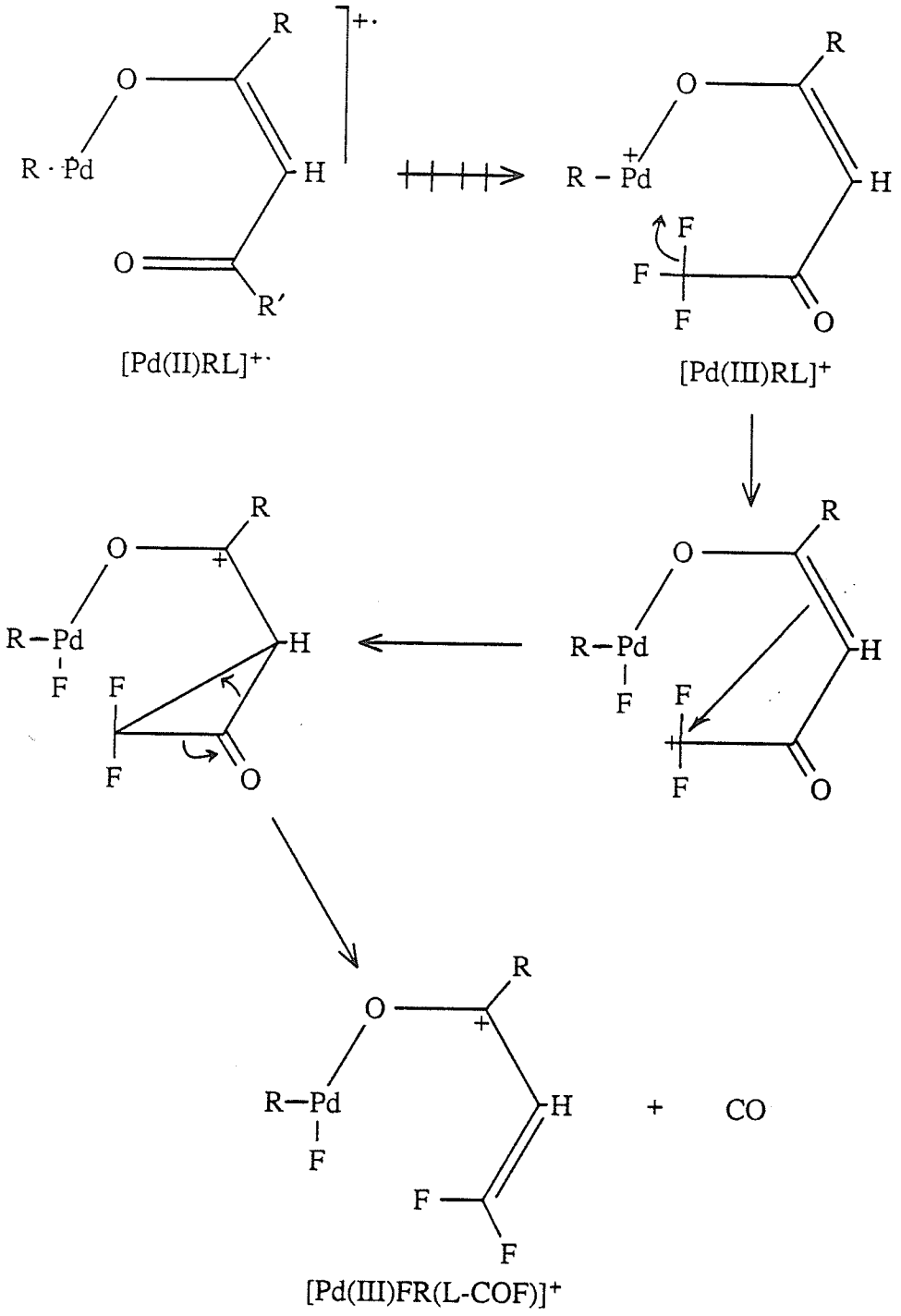

Scheme 49. Suggested mechanism for the formation of [Pd(III)FR(L-COF)]+ in **Pd-3a** and **-8a**.

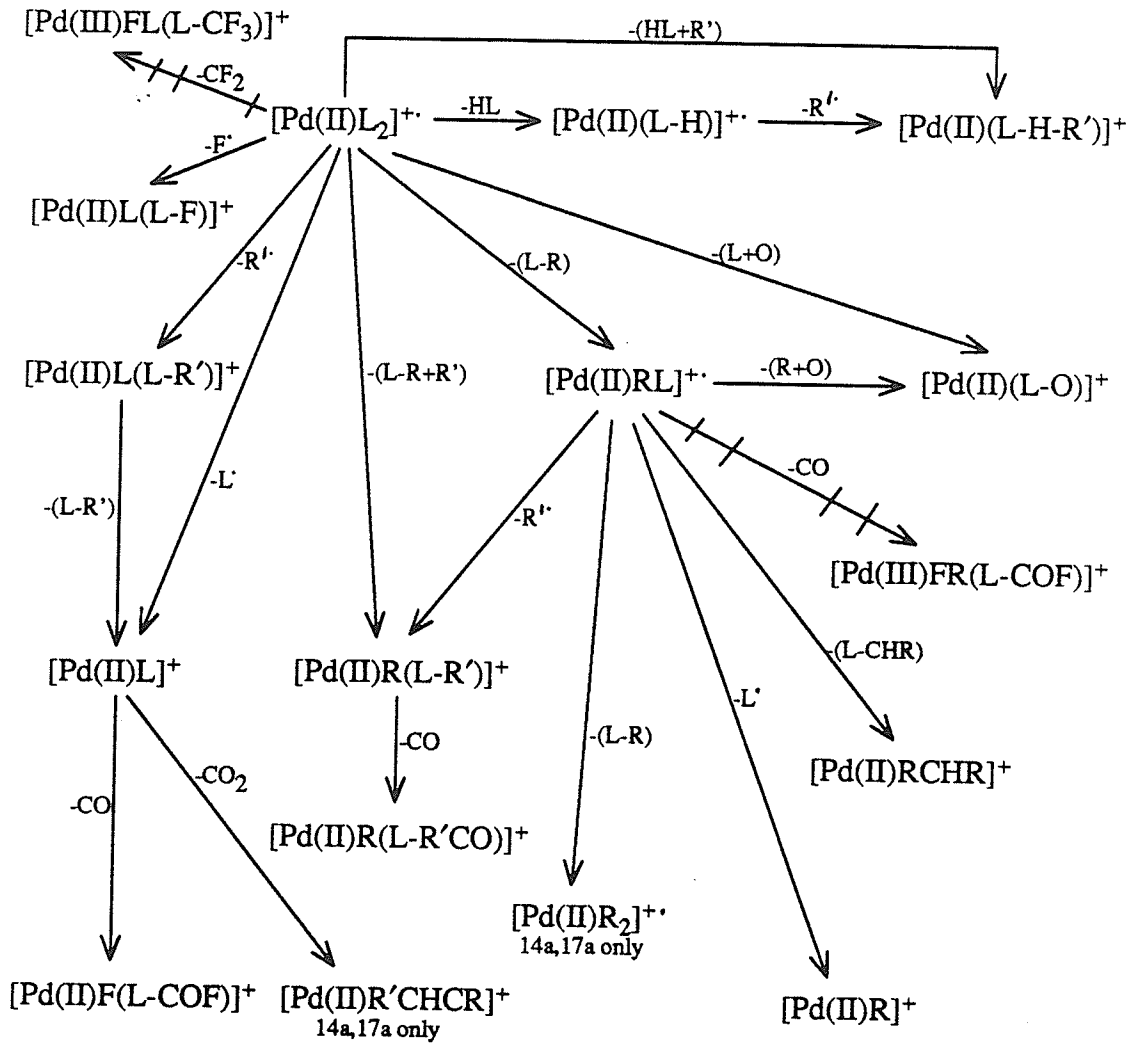

⟶ reaction step in which a change in metal oxidation state is proposed.

Scheme 50. Proposed fragmentation pathways for Pd(II) β-diketonates where R' = C_2F_5 (**Pd–13a** and **–14a**) or C_3F_7 (**Pd–16a** and **–17a**). Pathways are common to all complexes except where noted.

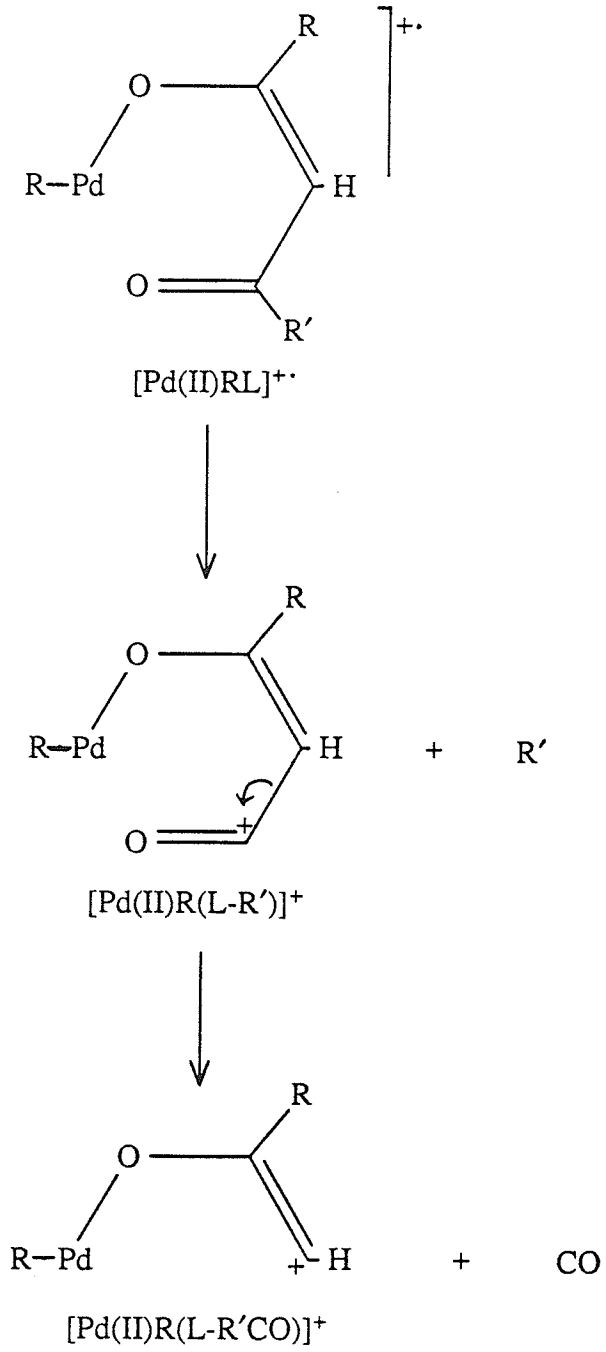

Scheme 51. Suggested mechanism for the formation of $[Pd(II)R(L\text{-}R'CO)]^+$ in **Pd-13a, -14a, -16a** and **-17a.**

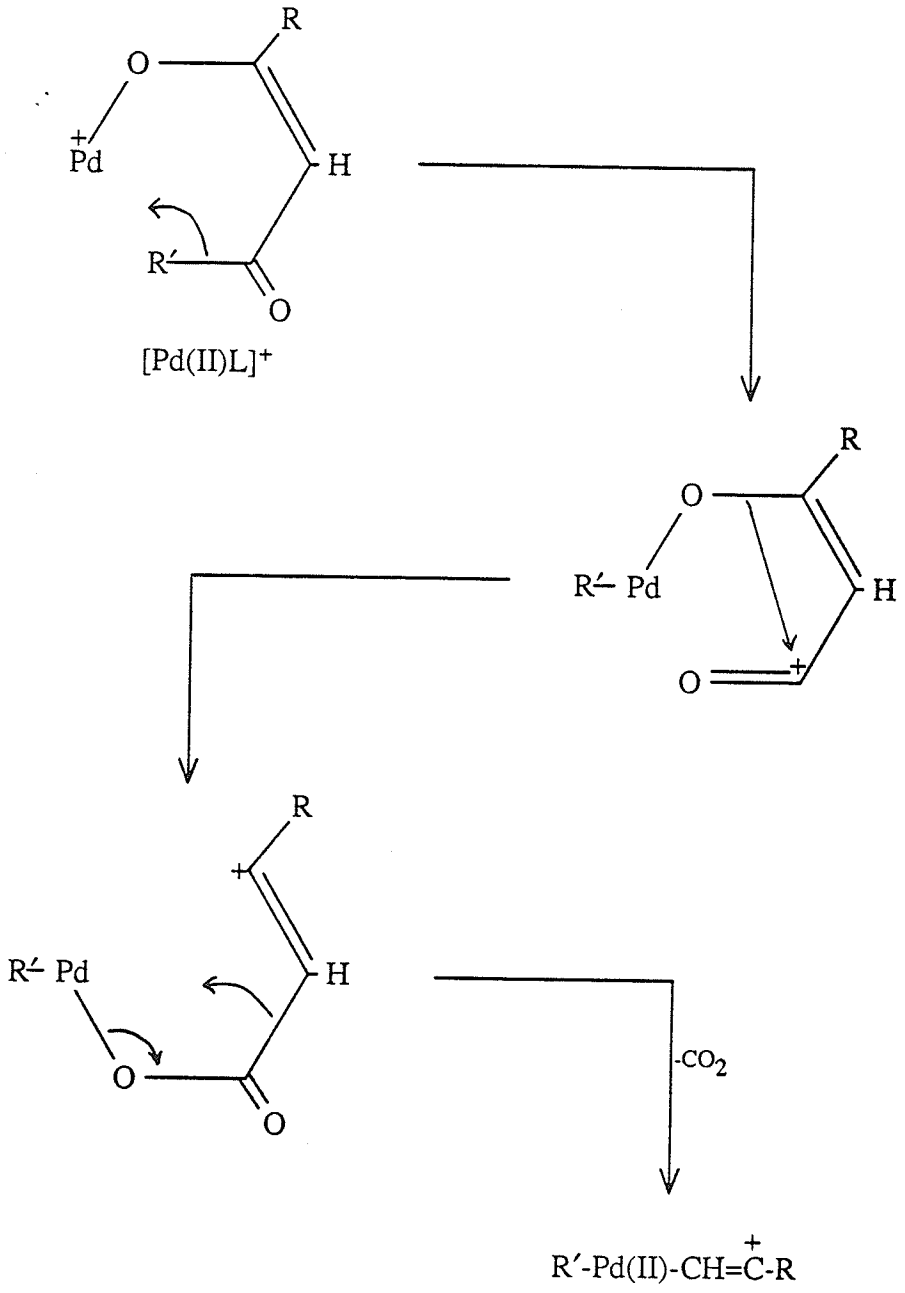

Scheme 52. Suggested mechanism for the formation of $[Pd(II)R'CHCR]^+$ in **Pd-13a, -14a, -16a** and **-17a.**

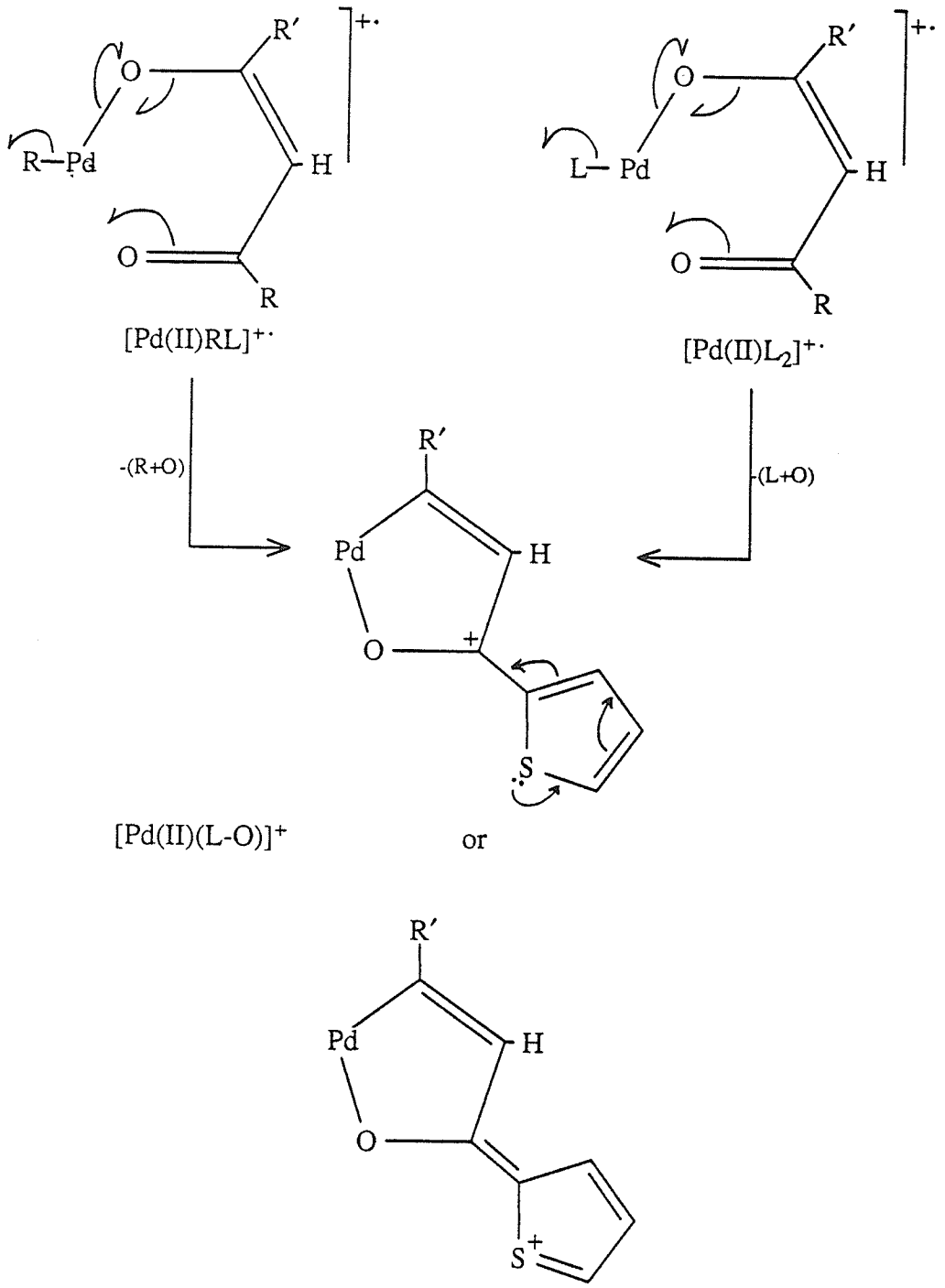

Scheme 53. Suggested mechanisms for the formation of $[Pd(II)(L\text{-}O)]^+$ in **Pd-8a, -14a** and **-17a** (R = 2-thienyl).

(f) Cu(II) β-diketonates

Relative abundance data for the eleven Cu(II) β-diketonates studied appear in Tables 27-37. Plots of the 70 eV EI mass spectra are given in Figures 71-81. A linked-scanning, metastable analysis of **Cu-13a** was used in delineating fragmentation pathways. Reichert and Westmore (125) have published the electron ionization mass spectra of **Cu-3a**, **Cu-8a**, **Cu-11a** and **Cu-12a**.

In addition to recording spectra at the usual 70 eV ionizing energy, scans at 20 and 12 eV (nominal) were also acquired, thereby presenting an opportunity to evaluate the influence of electron energy upon the nature of the mass spectra. Spectral comparisons based on ionization energy will be reserved for the latter part of this discussion. Unless otherwise stated, references to ion abundances and fragmentation routes refer to 70 eV data.

As the mass spectra of all of the Cu(II) β-diketonates studied are quite similar, their decomposition pathways will be considered together. Scheme 54 depicts the suggested fragmentation pathways for the CHF_2- (Tables 27 and 28), CF_3- (Tables 29-33), C_2F_5- (Tables 34 and 35) and C_3F_7- (Tables 36 and 37) substituted Cu(II) β-diketonates. The most abundant metal containing species include $[Cu(II)L_2]^{+\cdot}$, $[Cu(II)L(L\text{-}R')]^+$, $[Cu(I)L_2\text{-}2R']^+$ and $[Cu(I)(L\text{-}R')]^+$. Metastable evidence confirms many of the pathways shown in Scheme 54, of which several have received prior mention:

Fragmentation	Scheme
$[Cu(II)L_2]^{+\cdot} \longrightarrow [Cu(II)RL]^{+\cdot}$	26
$[Cu(II)L]^+ \longrightarrow [Cu(II)R]^+$	26
$[Cu(II)L(L\text{-}R')]^+ \longrightarrow [Cu(II)L]^+$	30
$[Cu(I)(L\text{-}R')]^+ \longrightarrow [Cu(I)]^+$	30
$[Cu(I)(L\text{-}R')]^+ \longrightarrow [Cu(I)CHCR]^+$	35
$[Cu(I)CHCR]^+ \longrightarrow [Cu(I)]^+$	35
$[Cu(II)L_2]^{+\cdot} \longrightarrow [Cu(II)L(L\text{-}F)]^+$	41
$[Cu(II)L(L\text{-}F)]^+ \longrightarrow [Cu(II)L(L\text{-}COF)]^+$	41
$[Cu(II)L_2]^{+\cdot} \longrightarrow [Cu(III)FL(L\text{-}CF_3)]^+$	42
$[Cu(II)L_2]^{+\cdot} \longrightarrow [Cu(II)(L\text{-}H)]^{+\cdot}$	43
$[Cu(II)L_2]^{+\cdot} \longrightarrow [Cu(II)HL]^{+\cdot}$	44-46

The importance of the Cu(I) oxidation state is exemplified in several of the above mechanisms, as well as in the formation of $[L]^+$ as shown in Scheme 55(a). A cyclic, resonance-stabilized ligand ion (Scheme 55(b)) may indirectly aid in the elimination of Cu(I)L.

Scheme 56 outlines a proposed mechanism for the consecutive losses of two R'· radicals from the molecular ion. The process is considered to involve a reduction in the Cu(II) valence state to give the unique species $[Cu(I)L_2\text{-}2R']^+$. A similar mechanism has been proposed by Lacey and Shannon (109) for the elimination of two methyl radicals from the molecular ion of bis(2,4-pentanedionato)copper(II). For the complexes possessing a CF_3 substituent (see Tables 29-33), $[Cu(I)L_2\text{-}2R']^+$ is isobaric with $[Cu(II)RL]^{+\cdot}$. Even under high resolution conditions, these two species are virtually indistinguishable; in **Cu-3a** for example, the mass difference between $[Cu(I)L_2\text{-}2R']^+$ (355.00316 u) and $[Cu(II)RL]^{+\cdot}$ (355.00071 u) is only 2.45 mmu. Reichert and Westmore (125) attempted to resolve this problem by using ligands deuterated at the bridging carbon atom of the chelate ring and monitoring the mass changes in the resulting fragment ions (expected mass change of +2 for $[Cu(II)L_2\text{-}2R']^+$ and +1 for $[Cu(II)RL]^{+\cdot}$ as compared to their non-deuterated analogs). They concluded that when R = aliphatic group (eg. methyl), both $[Cu(I)L_2\text{-}2R']^+$ and $[Cu(II)RL]^{+\cdot}$ occur with equal regularity, but that $[Cu(II)RL]^{+\cdot}$ is favored when R = aryl group (eg. phenyl, 2-thienyl, 2-furyl and 2-naphthyl). However, the present findings appear to refute the generality of these conclusions. For example, in the six complexes for which R' = CHF_2, C_2F_5 and C_3F_7, the two ions of interest no longer appear at the same mass, so their relative abundances can be easily compared. The results of such a comparison indicate an overwhelming preference for the formation of $[Cu(I)L_2\text{-}2R']^+$ (average %TIC = 7.5) versus $[Cu(II)RL]^{+\cdot}$ (average %TIC = 0.2). Despite minor differences in C-R' bond strengths and electronic

properties, extrapolation of these findings to the CF_3-substituted Cu(II) complexes appears reasonable, at least on the basis of available evidence.

The linked-scanning data support three possible precursors for the ion $[Cu(I)(L-R')]^+$; two of the proposed mechanisms, one starting from $[Cu(I)L(L-R')]^{+\cdot}$ and the other from $[Cu(I)L_2-2R']^+$, are shown in Schemes 57(a) and (b), respectively. The third route, illustrated in Scheme 58, involves reduction of $[Cu(II)L]^+$ to $[Cu(I)L]^{+\cdot}$, followed by the alpha-cleavage of the R' group to yield $[Cu(I)(L-R')]^+$.

The suggested mechanisms for the formation of $[Cu(II)HL]^+$ and $[Cu(II)(L-H)]^{+\cdot}$ are similar to those presented for the Ni(II) β-diketonates (see Schemes 43-46). The stability of the Cu(I) oxidation state may in fact favor the univalent forms of these ions, $[Cu(I)HL]^+$ and $[Cu(I)(L-H)]^+$. Again, the marked influence of the R group on the $[CuHL]^+$ abundances is in evidence (ave. %TIC in parentheses): 2-thienyl (0.8) < 5-methyl-2-thienyl (1.0) < 2-furyl (1.5) < phenyl (1.6) << 2-naphthyl (6.9).

Varying the ionization energy appears to bring about some subtle changes in the appearance of the mass spectra. Although comparatively few differences are detected between the 70 and 20 eV scans, reduction of the ionizing electron beam to 12 eV results in significantly lower

fragmentation (it should be noted that 12 eV lies just above the ionization threshold of most of these complexes). The ions least affected by a drop in the electron energy appear to be those arising from single-step fragmentations, that is, fragmentations proceeding directly from the molecular ion; examples include $[Cu(II)L(L-R')]^+$, $[Cu(II)(L-H)]^{+\cdot}$, $[Cu(II)HL]^{+\cdot}$, $[L]^+$ and $[Cu(III)FL(L-CF_3)]^+$. By contrast, ions such as $[Cu(I)L_2-2R']^+$, $[Cu(II)L]^+$, $[Cu(I)(L-R')]^+$, $[Cu(I)CHCR]^+$ and $[Cu(I)]^+$, which depend upon two or more decomposition steps for their formation, are noticeably suppressed in the 12 eV mass spectra. The decrease in $[Cu(II)L]^+$ abundance affirms the results of the metastable study which showed $[Cu(II)L(L-R')]^+$, but not $[Cu(II)L_2]^{+\cdot}$, to be a precursor of $[Cu(II)L]^+$.

Table 27. 70, 20 and 12 eV-EI mass spectra of compound **Cu-1a.**

		Cu-1a				
	R =		$-C_6H_5$			
	R'=		$-CHF_2$			
	EE=	70eV		20eV		12eV	

ION	%RA	m/z	%TIC	%RA	%TIC	%RA	%TIC
$[CuL_2]^+$	43.3	(457)	12.1	100.0	47.4	100.0	78.2
$[CuL_2-R']^+$	31.8	(406)	8.9	43.5	20.6	3.6	2.8
$[CuL_2-2R']^+$	35.2	(355)	9.8	22.6	10.7	-	-
$[CuRL]^+$	0.4	(337)	0.1	0.5	0.2	-	-
$[CuLH]^+$	2.7	(261)	0.8	5.2	2.5	2.6	2.0
$[CuL]^+$	0.7	(260)	0.2	0.4	0.2	-	-
$[CuL-H]^+$	2.7	(259)	0.8	4.4	2.1	-	-
$[CuL-R']^+$	43.6	(209)	12.1	4.7	2.2	-	-
$[CuRCCH]^+$	3.1	(165)	0.9	-	-	-	-
$[CuR]^+$	1.5	(140)	0.4	-	-	-	-
$[Cu]^+$	3.9	(63)	1.1	-	-	-	-
$[HL]^+$	4.8	(198)	1.3	2.2	1.0	-	-
$[L]^+$	5.0	(197)	1.4	6.7	3.2	2.5	2.0
$[HL-R']^+$	35.7	(147)	9.9	12.1	5.7	2.0	1.6
$[RCO]^+$	100.0	(105)	27.8	9.3	4.4	17.1	13.4
$[R]^+$	36.6	(77)	10.2	-	-	-	-
$[R']^+$	10.2	(51)	2.8	-	-	-	-

Table 28. 70, 20 and 12 eV-EI mass spectra of compound **Cu-2a.**

				Cu-2a			
	R =			$-C_4H_3S$			
	R'=			$-CHF_2$			
	EE=	70eV		20eV		12eV	
ION	%RA	m/z	%TIC	%RA	%TIC	%RA	%TIC
$[CuL_2]^+$ (a)	42.3	(469)	12.3	42.2	9.8	100.0	33.1
$[CuL(L-R')]^+$ (b)	[a]34.3	(418)	10.0	33.0	7.7	27.8	9.2
$[CuL_2-2R']^+$	[b]27.9	(367)	8.1	26.9	6.3	3.1	1.0
$[CuRL]^+$	1.5	(349)	0.4	-	-	-	-
$[CuLH]^+$	2.2	(267)	0.6	2.8	0.7	3.5	1.2
$[CuL]^+$	1.4	(266)	0.4	2.1	0.5	0.7	0.2
$[CuL-H]^+$	4.7	(265)	1.4	5.3	1.2	7.6	2.5
$[Cu(L-R')]^+$	39.0	(215)	11.3	40.6	9.5	0.2	0.1
$[CuCHCR]^+$	7.7	(171)	2.2	7.4	1.7	-	-
$[CuR]^+$	3.3	(146)	1.0	-	-	-	-
$[Cu]^+$	6.9	(63)	2.0	1.6	0.4	-	-
$[HL]^+$ (c)	20.8	(204)	6.0	49.0	11.4	55.8	18.5
$[L]^+$	3.1	(203)	0.9	4.1	1.0	2.9	1.0
$[HL-R']^+$	[c]36.7	(153)	10.7	100.0	23.3	74.4	24.6
$[RCO]^+$	100.0	(111)	29.1	75.3	17.5	19.7	6.5
$[R]^+$	11.3	(83)	3.3	37.6	8.8	6.3	2.1
$[R']^+$	5.8	(51)	1.7	1.2	0.3	-	-

[a] Identified metastable transitions are indicated by superscripts which relate the daughter ion to its precursor as labelled in column 1.

Table 29. 70, 20 and 12 eV-EI mass spectra of compound **Cu-3a.**

		Cu-3a	
R =		$-C_6H_5$	
R'=		$-CF_3$	
EE=	70eV	20eV	12eV

ION	%RA	m/z	%TIC	%RA	%TIC	%RA	%TIC
$[CuL_2]^+$	30.6	(493)	8.6	82.7	17.6	100.0	46.6
$[CuL(L-COF)]^+$	2.4	(446)	0.7	3.8	0.8	2.2	1.0
$[CuL_2-R']^+$	11.0	(424)	3.1	22.0	4.7	4.4	2.0
$[CuL_2-2R']^+/[CuRL]^+$	8.7	(355)	2.5	17.1	3.6	-	-
$[CuLH]^+$	4.3	(279)	1.2	10.6	2.3	6.0	2.8
$[CuL]^+$	2.2	(278)	0.6	3.9	0.8	1.8	0.8
$[CuL-H]^+$	4.4	(277)	1.2	10.0	2.1	3.5	1.6
$[CuL-R']^+$	23.2	(209)	6.5	29.4	6.3	-	-
$[CuCHCR]^+$	3.6	(165)	1.0	6.9	1.5	-	-
$[CuR]^+$	4.6	(140)	1.3	-	-	-	-
$[Cu]^+$	9.1	(63)	2.6	-	-	-	-
$[HL]^+$	28.9	(216)	8.1	58.0	12.4	52.2	24.3
$[L]^+$	10.9	(215)	3.1	22.9	4.9	6.7	3.1
$[HL-R']^+$	31.0	(147)	8.7	54.0	11.5	24.6	11.5
$[RCO]^+$	100.0	(105)	28.2	100.0	21.3	15.5	7.2
$[R]^+$	34.5	(77)	9.7	9.1	1.9	-	-
$[R']^+$	45.7	(69)	12.9	38.4	8.2	-	-

Table 30. 70, 20 and 12 eV-EI mass spectra of compound **Cu-8a.**

				Cu-8a			
R =				$-C_4H_3S$			
R'=				$-CF_3$			
EE=	70eV			20eV		12eV	
ION	%RA	m/z	%TIC	%RA	%TIC	%RA	%TIC
$[CuL_2]^+$	36.0	(505)	11.1	100.0	28.6	100.0	58.6
$[CuL(L-COF)]^+$	2.1	(458)	0.6	2.0	0.6	-	-
$[CuL_2-R']^+$	15.9	(436)	4.9	30.9	8.9	8.2	4.8
$[CuL_2-2R']^+/[CuRL]^+$	9.8	(367)	3.0	14.1	4.0	-	-
$[CuLH]^+$	3.5	(285)	1.1	6.1	1.7	2.0	1.2
$[CuL]^+$	4.1	(284)	1.3	4.3	1.2	-	-
$[CuL-H]^+$	8.8	(283)	2.7	14.5	4.2	7.1	4.2
$[CuL-R']^+$	38.5	(215)	11.9	39.0	11.2	-	-
$[CuCHCR]^+$	6.3	(171)	1.9	2.3	0.7	-	-
$[CuR]^+$	5.9	(146)	1.8	-	-	-	-
$[Cu]^+$	9.4	(63)	2.9	-	-	-	-
$[HL]^+$	20.8	(222)	6.4	25.1	7.2	26.1	15.3
$[L]^+$	6.9	(221)	2.1	10.3	3.0	2.5	1.5
$[HL-R']^+$	20.1	(153)	6.2	21.3	6.1	12.2	7.2
$[RCO]^+$	100.0	(111)	30.8	62.8	18.0	12.5	7.3
$[R]^+$	7.6	(83)	2.3	4.8	1.4	-	-
$[R']^+$	28.9	(69)	8.9	15.9	4.6	-	-

Table 31. 70, 20 and 12 eV-EI mass spectra of compound **Cu-9a.**

		Cu-9a				
R =		$-C_4H_2SCH_3$				
R'=		$-CF_3$				
EE=	70eV		20eV		12eV	
ION	%RA	m/z	%TIC	%RA	%TIC	%RA	%TIC
$[CuL_2]^+$	66.5	(533)	15.0	100.0	25.7	100.0	51.3
$[CuL(L-COF)]^+$	4.4	(486)	1.0	1.6	0.4	-	-
$[CuL_2-R']^+$	14.9	(464)	3.4	12.4	3.2	2.2	1.1
$[CuL_2-2R']^+/[CuRL]^+$	13.7	(395)	3.1	9.3	2.4	-	-
$[CuLH]^+$	4.5	(299)	1.0	3.7	1.0	1.4	0.7
$[CuL]^+$	5.0	(298)	1.1	3.1	0.8	0.2	0.1
$[CuL-H]^+$	85.1	(297)	19.1	83.3	21.4	38.7	19.9
$[CuL-R']^+$	31.7	(229)	7.1	22.1	5.7	-	-
$[CuCHCR]^+$	3.9	(185)	0.9	1.2	0.3	-	-
$[CuR]^+$	5.5	(160)	1.2	-	-	-	-
$[Cu]^+$	4.6	(63)	1.0	-	-	-	-
$[HL]^+$	25.4	(236)	5.7	23.7	6.1	27.8	14.3
$[L]^+$	14.3	(235)	3.2	13.7	3.5	2.3	1.2
$[L-S]^+$	11.4	(203)	2.6	9.3	2.4	2.5	1.3
$[HL-R']^+$	22.2	(167)	5.0	20.9	5.4	11.9	6.1
$[RCO]^+$	100.0	(125)	22.5	70.4	18.1	7.8	4.0
$[R]^+$	8.7	(97)	2.0	4.2	1.1	-	-
$[R']^+$	22.6	(69)	5.1	12.8	3.3	-	-

Table 32. 70, 20 and 12 eV-EI mass spectra of compound **Cu-11a.**

		Cu-11a				
R =		$-C_4H_3O$				
R'=		$-CF_3$				
EE=	70eV		20eV		12eV	
ION	%RA	m/z	%TIC	%RA	%TIC	%RA	%TIC
$[CuL_2]^+$	100.0	(473)	17.4	100.0	27.4	100.0	57.3
$[CuL_2-F]^+$	6.4	(454)	1.1	5.8	1.6	2.5	1.4
$[CuL(L-COF)]^+$	4.9	(426)	0.9	1.7	0.5	-	-
$[CuL_2-R']^+$	57.1	(404)	10.0	38.8	10.6	8.9	5.1
$[CuL_2-2R']^+/[CuRL]^+$	34.3	(335)	6.0	18.7	5.1	-	-
$[CuLH]^+$	8.8	(269)	1.5	7.1	1.9	2.0	1.1
$[CuL]^+$	14.6	(268)	2.5	7.1	1.9	-	-
$[CuL-H]^+$	20.0	(267)	3.5	13.1	3.6	3.7	2.1
$[CuL-R']^+$	40.5	(199)	7.1	46.9	12.8	-	-
$[CuCHCR]^+$	24.3	(155)	4.2	4.4	1.2	-	-
$[CuR]^+$	7.1	(130)	1.2	-	-	-	-
$[Cu]^+$	27.9	(63)	4.9	-	-	-	-
$[HL]^+$	34.5	(206)	6.0	31.4	8.6	33.3	19.1
$[L]^+$	15.4	(205)	2.7	9.6	2.6	2.1	1.2
$[HL-R']^+$	35.0	(137)	6.1	33.9	9.3	18.8	10.8
	18.1	(111)	3.2	5.3	1.5	-	-
$[RCO]^+$	88.3	(95)	15.4	31.5	8.6	3.2	1.8
$[R']^+$	36.0	(69)	6.3	16.0	4.4	-	-

Table 33. 70, 20 and 12 eV-EI mass spectra of compound **Cu-12a.**

				Cu-12a			
	R =			$-C_{10}H_7$			
	R'=			$-CF_3$			
	EE=	70eV		20eV		12eV	
ION		%RA	m/z	%TIC	%RA	%TIC	%RA	%TIC
$[CuL_2]^+$		33.1	(593)	7.5	53.6	10.2	84.2	30.7
$[CuL(L-COF)]^+$		2.0	(546)	0.5	1.0	0.2	-	-
$[CuL_2-R']^+$		3.6	(524)	0.8	3.9	0.7	-	-
$[CuL_2-2R']^+/[CuRL]^+$		3.9	(455)	0.9	4.6	0.9	-	-
$[CuLH]^+$		30.5	(329)	6.9	57.8	11.0	11.6	4.2
$[CuL]^+$		2.3	(328)	0.5	2.8	0.5	0.7	0.3
$[CuL-H]^+$		44.1	(327)	9.9	80.7	15.4	25.4	9.3
$[CuL-R']^+$		16.1	(259)	3.6	16.8	3.2	-	-
$[CuCHCR]^+$		5.0	(215)	1.1	2.9	0.5	-	-
$[CuR]^+$		8.7	(190)	2.0	2.9	0.5	-	-
$[Cu]^+$		5.2	(63)	1.2	-	-	-	-
$[HL]^+$		31.7	(266)	7.1	62.5	11.9	100.0	36.5
$[L]^+$		20.8	(265)	4.7	36.6	7.0	9.0	3.3
$[HL-R']^+$		22.0	(197)	5.0	38.9	7.4	20.8	7.6
$[RCO]^+$		100.0	(155)	22.5	100.0	19.1	11.0	4.0
$[R]^+$		42.5	(127)	9.6	7.9	1.5	-	-
		11.7	(111)	2.6	8.0	1.5	6.3	2.3
		11.8	(105)	2.7	6.9	1.3	-	-
$[R']^+$		49.1	(69)	11.1	42.3	8.1	5.1	1.9

Table 34. 70, 20 and 12 eV-EI mass spectra of compound **Cu-13a.**

		Cu-13a				
R =		$-C_6H_5$				
R'=		$-C_2F_5$				
EE=	70eV		20eV		12eV	
ION	%RA	m/z	%TIC	%RA	%TIC	%RA	%TIC
$[CuL_2]^+$ (a)	65.3	(593)	14.0	100.0	25.9	100.0	58.4
$[CuL_2-F]^+$	3.6	(574)	0.8	1.7	0.4	-	-
$[CuL(L-COF)]^+$	2.2	(546)	0.5	1.5	0.4	-	-
$[CuFL(L-CF_3)]^+$	3.2	(543)	0.7	4.2	1.1	4.3	2.5
$[CuL(L-R')]^+$ (b)	[a]39.8	(474)	8.6	46.3	12.0	9.1	5.3
$[CuRL]^+$	1.6	(405)	0.3	1.7	0.4	-	-
$[CuL_2-2R']^+$ (c)	[b]36.1	(355)	7.8	28.5	7.4	-	-
$[CuLH]^+$	[a]11.5	(329)	2.5	11.3	2.9	4.4	2.6
$[CuL]^+$ (d)	[b]2.4	(328)	0.5	1.4	0.4	-	-
$[CuL-H]^+$	10.7	(327)	2.3	9.2	2.4	3.2	1.9
$[CuL-R']^+$ (e)	*64.6	(209)	13.9	25.8	6.7	-	-
$[CuCHCR]^+$	[e]4.8	(165)	1.0	2.4	0.6	-	-
$[CuR]^+$	4.8	(140)	1.0	-	-	-	-
$[Cu]^+$	[e]10.1	(63)	2.2	-	-	-	-

Table 34. (continued).

$[HL]^+$	11.4 (266)	2.5	29.8	7.7	22.4	13.1
$[L]^+$	[a]18.6 (265)	4.0	17.2	4.5	4.4	2.6
$[HL-R']^+$	18.3 (147)	3.9	42.0	10.9	16.1	9.4
$[RCO]^+$	[#]100.0 (105)	21.5	47.6	12.3	7.2	4.2
$[R]^+$	32.3 (77)	6.9	-	-	-	-
$[CF_3]^+$	18.6 (69)	4.0	20.9	5.4	-	-
	5.4 (51)	1.2	-	-	-	-

[a] Identified metastable transitions are indicated by superscripts which relate the daughter ion to its precursor as labelled in column 1.

* daughter of (a),(b),(c) and (d).

daughter of (a),(b),(c),(d) and (e).

Table 35. 70, 20 and 12 eV-EI mass spectra of compound **Cu-14a.**

				Cu-14a			
	R =			$-C_4H_3S$			
	R'=			$-C_2F_5$			
	EE=	70eV		20eV		12eV	
ION	%RA	m/z	%TIC	%RA	%TIC	%RA	%TIC
$[CuL_2]^+$	42.7	(605)	10.5	100.0	24.3	100.0	66.4
$[CuL(L-F)]^+$	2.8	(586)	0.7	1.7	0.4	-	-
$[CuL(L-R')]^+$	28.6	(486)	7.1	58.6	14.3	11.6	7.7
$[CuL_2-2R']^+$	16.9	(367)	4.2	29.4	7.2	-	-
$[CuLH]^+$	2.4	(335)	0.6	5.2	1.3	2.1	1.4
$[CuL]^+$	1.5	(334)	0.4	2.2	0.5	-	-
$[CuL-H]^+$	8.0	(333)	2.0	16.0	3.9	5.1	3.4
$[CuL-R']^+$	48.3	(215)	11.9	59.4	14.5	-	-
$[CuCHCR]^+$	8.2	(171)	2.0	2.3	0.5	-	-
$[CuR]^+$	5.6	(146)	1.4	-	-	-	-
$[Cu]^+$	8.9	(63)	2.2	-	-	-	-
$[HL]^+$	23.0	(272)	5.7	23.7	5.8	16.7	11.1
$[L]^+$	5.2	(271)	1.3	9.9	2.4	1.3	0.9
$[HL-R']^+$	30.4	(153)	7.5	27.0	6.6	9.7	6.4
$[RCO]^+$	100.0	(111)	24.7	49.2	12.0	4.2	2.8
$[R]^+$	25.9	(83)	6.4	12.6	3.1	-	-
$[CF_3]^+$	46.9	(69)	11.6	16.0	3.9	-	-

Table 36. 70, 20 and 12 eV-EI mass spectra of compound **Cu-16a.**

				Cu-16a			
	R =			$-C_6H_5$			
	R'=			$-C_3F_7$			
	EE=	70eV		20eV		12eV	
ION	%RA	m/z	%TIC	%RA	%TIC	%RA	%TIC
$[CuL_2]^+$	53.8	(693)	13.3	100.0	24.5	100.0	62.5
$[CuL(L-F)]^+$	3.4	(674)	0.8	2.1	0.5	-	-
$[CuL(L-COF)]^+$	6.4	(646)	1.6	9.8	2.4	7.9	4.9
$[CuL(L-R')]^+$	36.0	(524)	8.9	58.6	14.4	6.7	4.2
$[CuRL]^+$	1.0	(455)	0.2	1.3	0.3	-	-
$[CuLH]^+$	5.3	(379)	1.3	13.3	3.3	2.9	1.8
$[CuL]^+$	1.0	(378)	0.2	1.3	0.3	-	-
$[CuL-H]^+$	5.9	(377)	1.5	10.4	2.5	2.3	1.4
$[CuL_2-2R']^+$	23.7	(355)	5.9	39.5	9.7	-	-
$[CuL-R']^+$	54.2	(209)	13.4	30.1	7.4	-	-
$[CuCHCR]^+$	2.4	(165)	0.6	2.3	0.6	-	-
$[CuR]^+$	4.0	(140)	1.0	-	-	-	-
$[Cu]^+$	7.2	(63)	1.8	-	-	-	-
$[HL]^+$	11.4	(316)	2.8	20.8	5.1	18.3	11.4
$[L]^+$	10.3	(315)	2.6	20.5	5.0	2.6	1.6
$[HL-R']^+$	25.4	(147)	6.3	39.5	9.7	14.8	9.3
$[RCO]^+$	100.0	(105)	24.8	47.4	11.6	4.5	2.8
$[R]^+$	26.6	(77)	6.6	-	-	-	-
$[CF_3]^+$	25.7	(69)	6.4	14.8	3.6	-	-

Table 37. 70, 20 and 12 eV-EI mass spectra of compound **Cu-17a.**

		Cu-17a				
R =		$-C_4H_3S$				
R'=		$-C_3F_7$				
EE=	70eV		20eV		12eV	
ION	%RA	m/z	%TIC	%RA	%TIC	%RA	%TIC
$[CuL_2]^+$ (a)	68.3	(705)	13.8	100.0	28.8	100.0	57.7
$[CuL(L-F)]^+$	4.7	(686)	0.9	-	-	-	-
$[CuL(L-COF)]^+$	3.7	(658)	0.7	4.6	1.3	4.2	2.4
$[CuL(L-R)]^+$	4.9	(622)	1.0	-	-	-	-
$[CuL(L-R')]^+$ (b)	[a]52.3	(536)	10.6	36.9	10.6	11.9	6.9
$[CuLH]^+$	[a]4.1	(385)	0.8	3.8	1.1	1.3	0.8
$[CuL]^+$	2.7	(384)	0.5	1.5	0.4	-	-
$[CuL-H]^+$	14.4	(383)	2.9	9.0	2.6	4.0	2.3
$[CuL_2-2R']^+$ (c)	[b]45.8	(367)	9.2	27.5	7.9	-	-
$[CuL-R']^+$	[c]84.1	(215)	17.0	35.4	10.2	-	-
$[CuCHCR]^+$	12.4	(171)	2.5	-	-	-	-
$[CuR]^+$	8.4	(146)	1.7	-	-	-	-
$[Cu]^+$	10.0	(63)	2.0	-	-	-	-
$[HL]^+$	11.7	(322)	2.4	25.8	7.4	0.1	0.1
$[L]^+$	7.9	(321)	1.6	5.8	1.7	27.6	15.9
$[L-S]^+$	8.8	(289)	1.8	6.7	1.9	-	-
$[HL-R']^+$	17.2	(153)	3.5	33.2	9.5	17.0	9.8
$[RCOCH_2]^+$	10.4	(125)	2.1	5.8	1.7	-	-

Table 37. (continued).

$[RCO]^+$	100.0 (111)	20.2	28.8	8.3	6.3	3.6
$[R]^+$	4.8 (83)	1.0	10.3	3.0	-	-
$[CF_3]^+$	18.7 (69)	3.8	17.3	5.0	5.0	2.9

[a] Identified metastable transitions are indicated by superscripts which relate the daughter ion to its precursor as labelled in column 1.

Figure 71.

Normalized 70 eV-EI mass spectrum of

bis[1,1-difluoro-4-phenyl-2,4-butanedionato]Cu(II)

{Cu-1a}.

m/z $[M]^{+\cdot}$ = 457, $[L]^{+}$ = 197

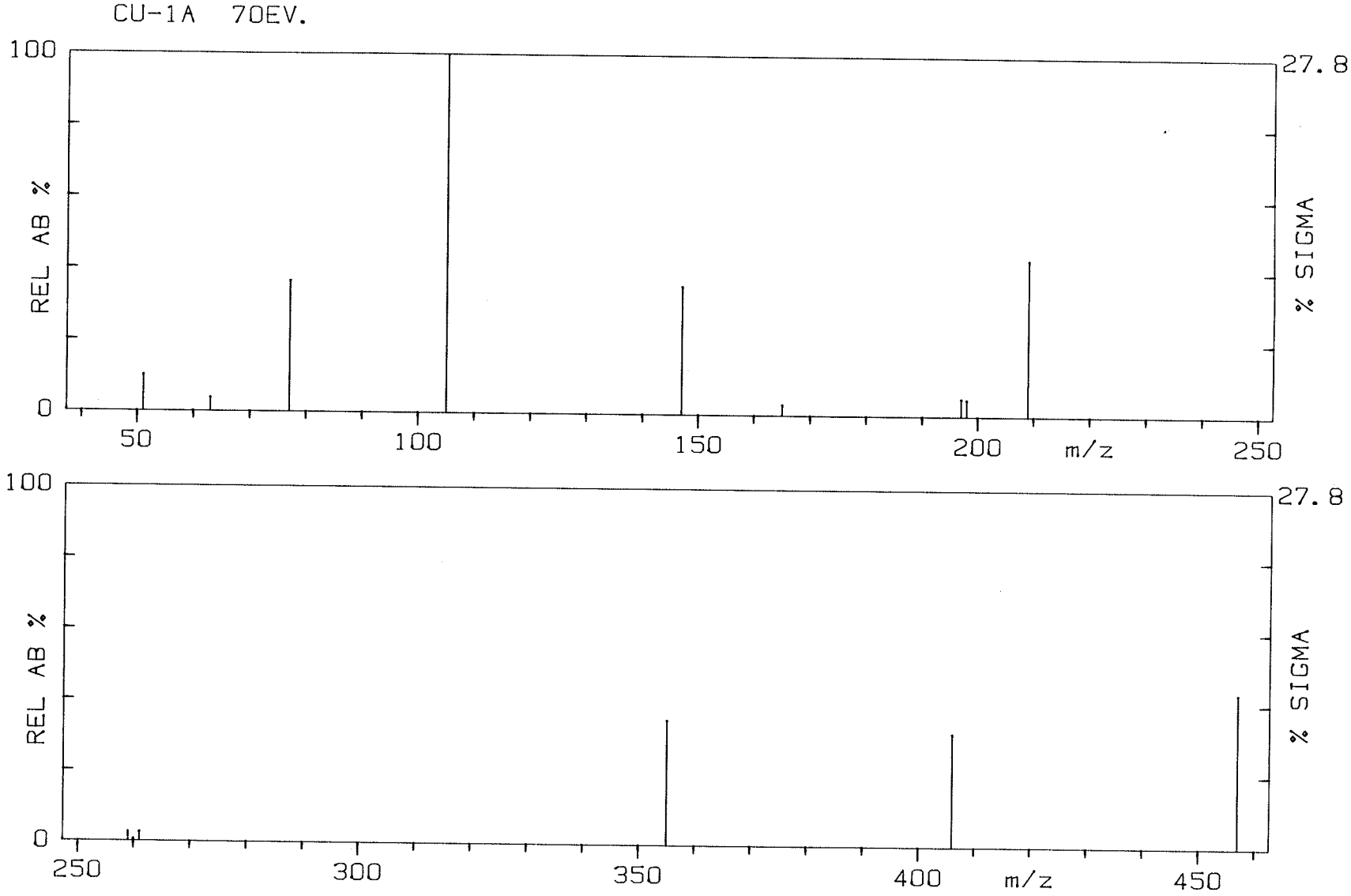
CU-1A 70EV.
100
REL AB %
0
50
100
150
200
m/z
250
27.8
% SIGMA
100
REL AB %
0
250
300
350
400
m/z
450
27.8
% SIGMA

Figure 72.

Normalized 70 eV-EI mass spectrum of

bis[1,1-difluoro-4-(2'-thienyl)-2,4-butanedionato]Cu(II)

{**Cu-2a**}.

m/z $[M]^{+\cdot}$ = 469, $[L]^{+}$ = 203

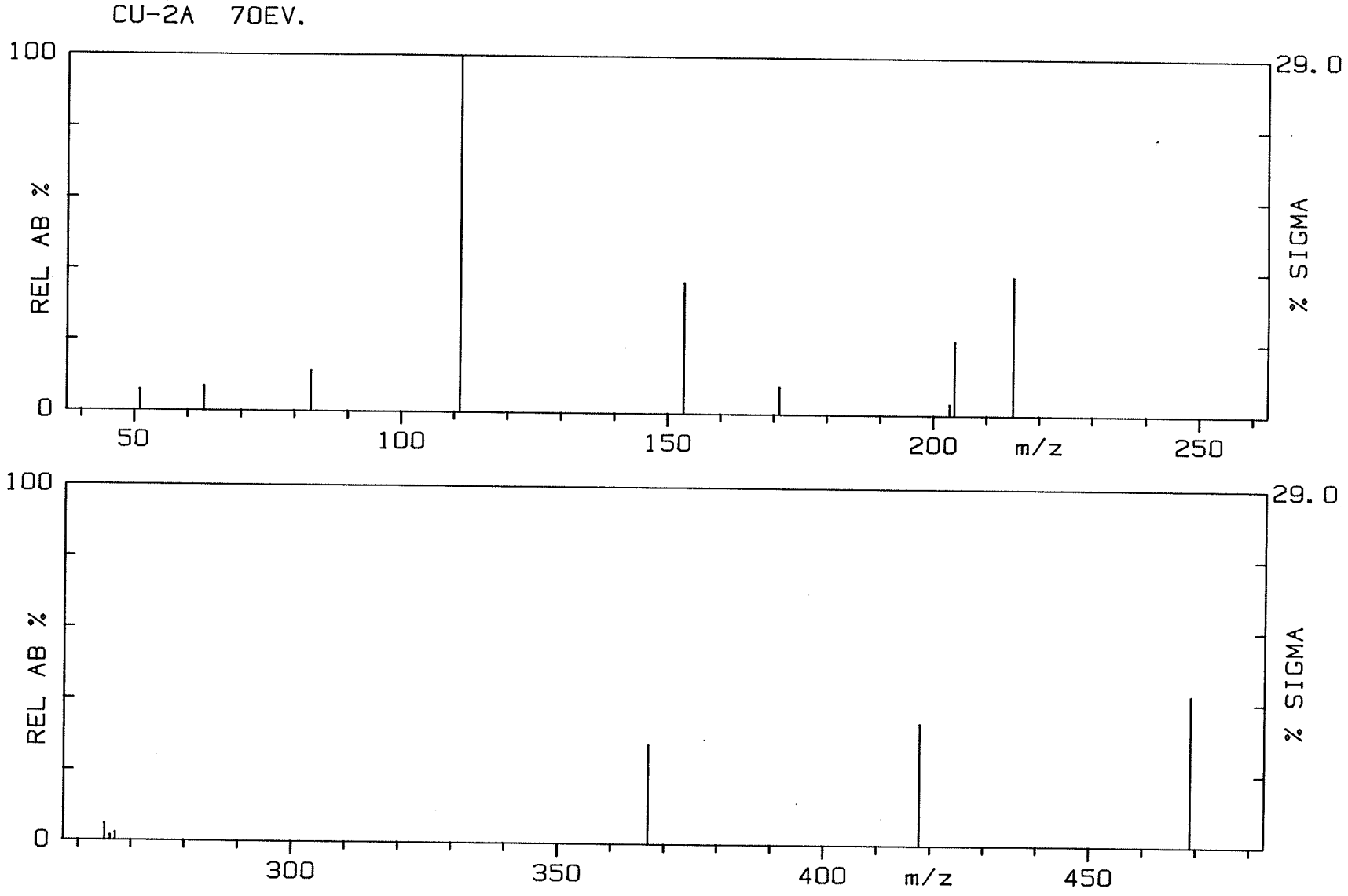
CU-2A 70EV.
100
REL AB %
0
50
100
150
200
m/z
250
29.0
% SIGMA
100
REL AB %
0
300
350
400
m/z
450
29.0
% SIGMA

Figure 73.

Normalized 70 eV-EI mass spectrum of

bis[1,1,1-trifluoro-4-phenyl-2,4-butanedionato]Cu(II)

{Cu-3a}.

m/z $[M]^{+\cdot}$ = 493, $[L]^{+}$ = 215

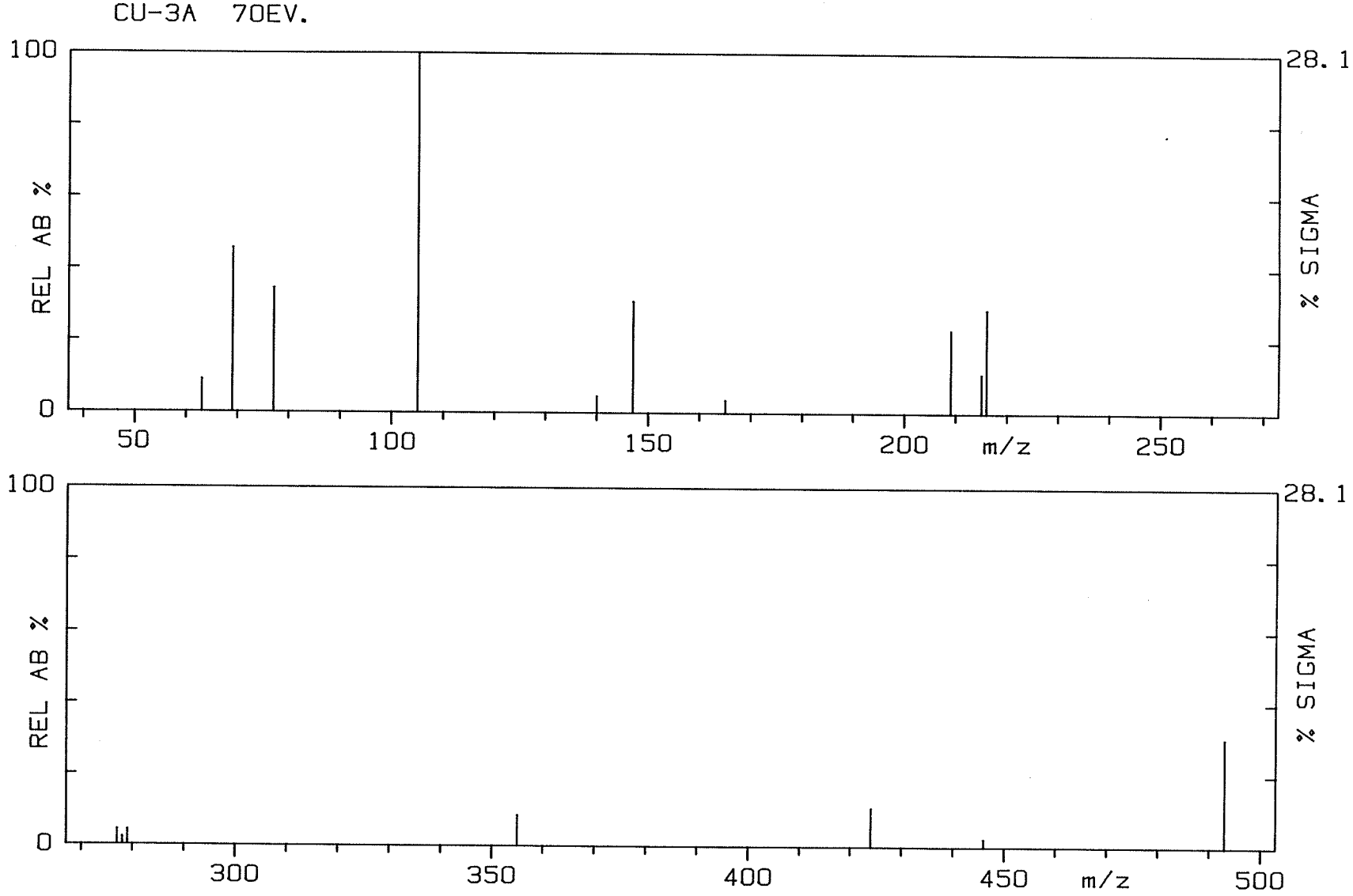
CU-3A 70EV.
100
REL AB %
0
28.1
% SIGMA
50
100
150
200
m/z
250
100
REL AB %
0
28.1
% SIGMA
300
350
400
450
m/z
500

Figure 74.

Normalized 70 eV-EI mass spectrum of

bis[1,1,1-trifluoro-4-(2'-thienyl)-2,4-butanedionato]Cu(II)

{**Cu-8a**}.

m/z $[M]^{+\cdot}$ = 505, $[L]^{+}$ = 221

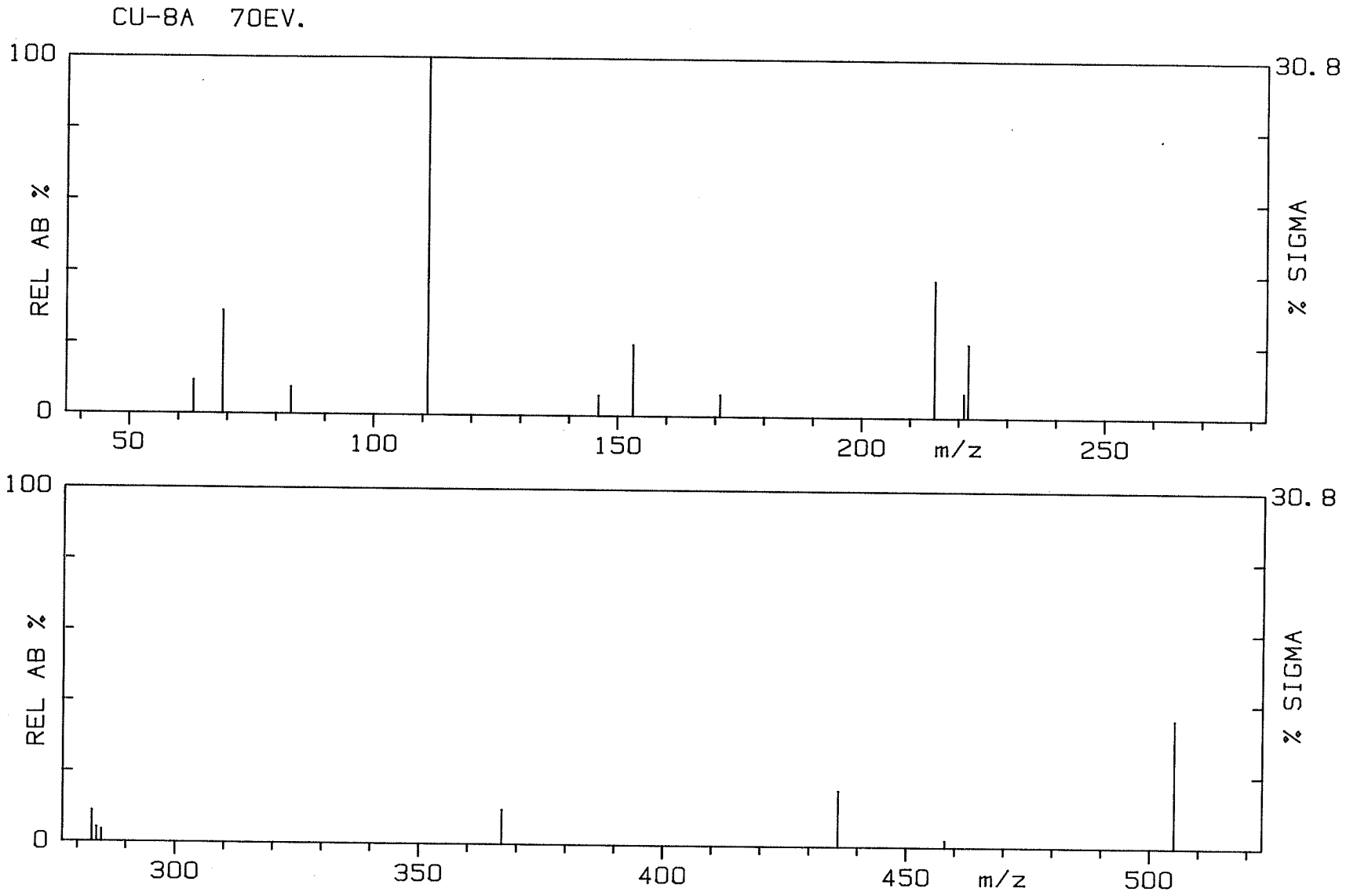
CU-8A 70EV.
100
REL AB %
0
50
100
150
200
m/z
250
30.8
% SIGMA
100
REL AB %
0
300
350
400
450
m/z
500
30.8
% SIGMA

Figure 75.

Normalized 70 eV-EI mass spectrum of

bis[1,1,1-trifluoro-4-(5'-methyl-2'-thienyl)-2,4-butanedionato]Cu(II)

{**Cu-9a**}.

m/z $[M]^{+\cdot}$ = 533, $[L]^{+}$ = 235

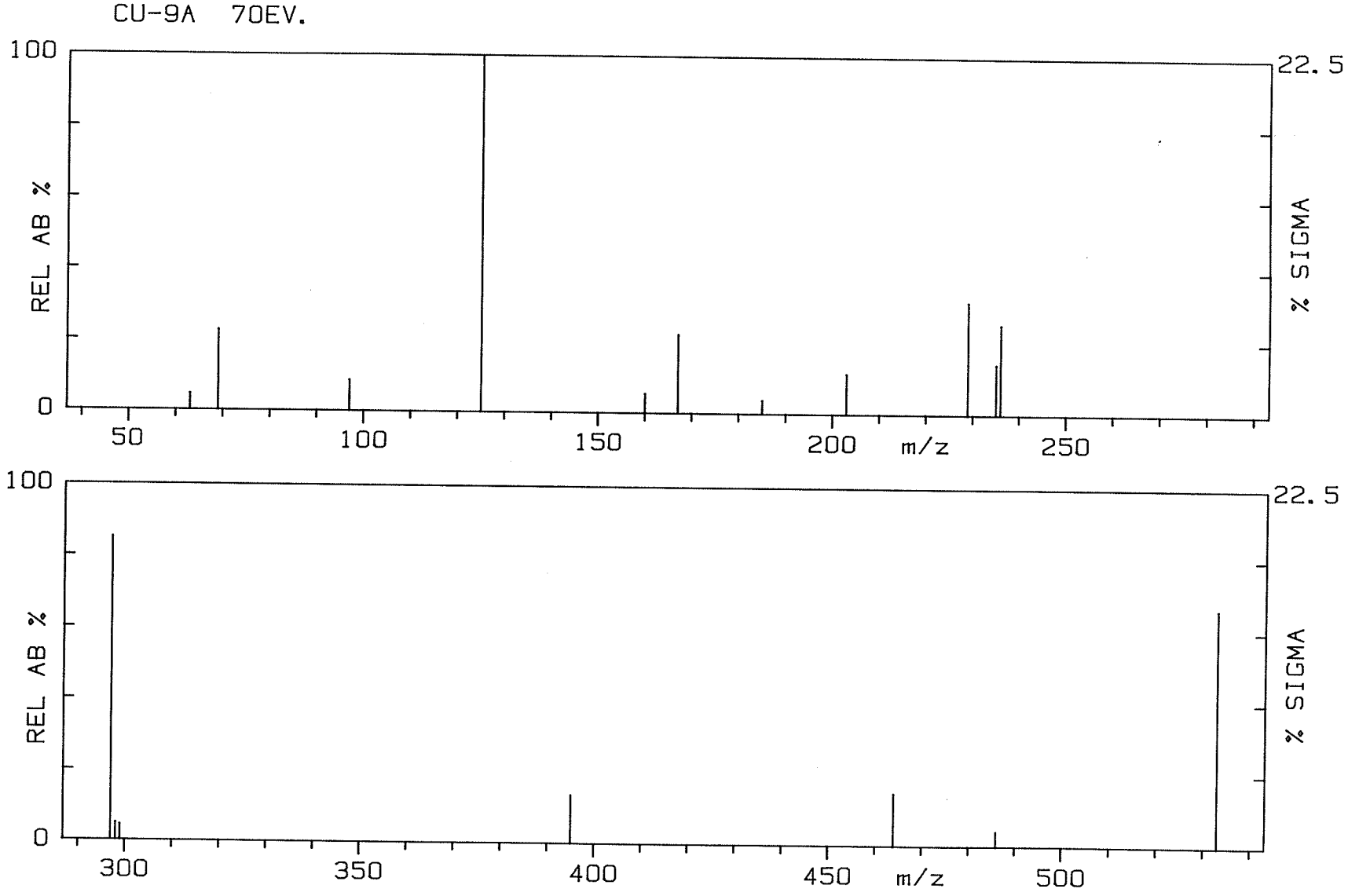
CU-9A 70EV.
100
REL AB %
0
50
100
150
200
m/z
250
22.5
% SIGMA
100
REL AB %
0
300
350
400
450
m/z
500
22.5
% SIGMA

Figure 76.

Normalized 70 eV-EI mass spectrum of

bis[1,1,1-trifluoro-4-(2'-furyl)-2,4-butanedionato]Cu(II)

{**Cu-11a**}.

m/z $[M]^{+\cdot}$ = 473, $[L]^{+}$ = 205

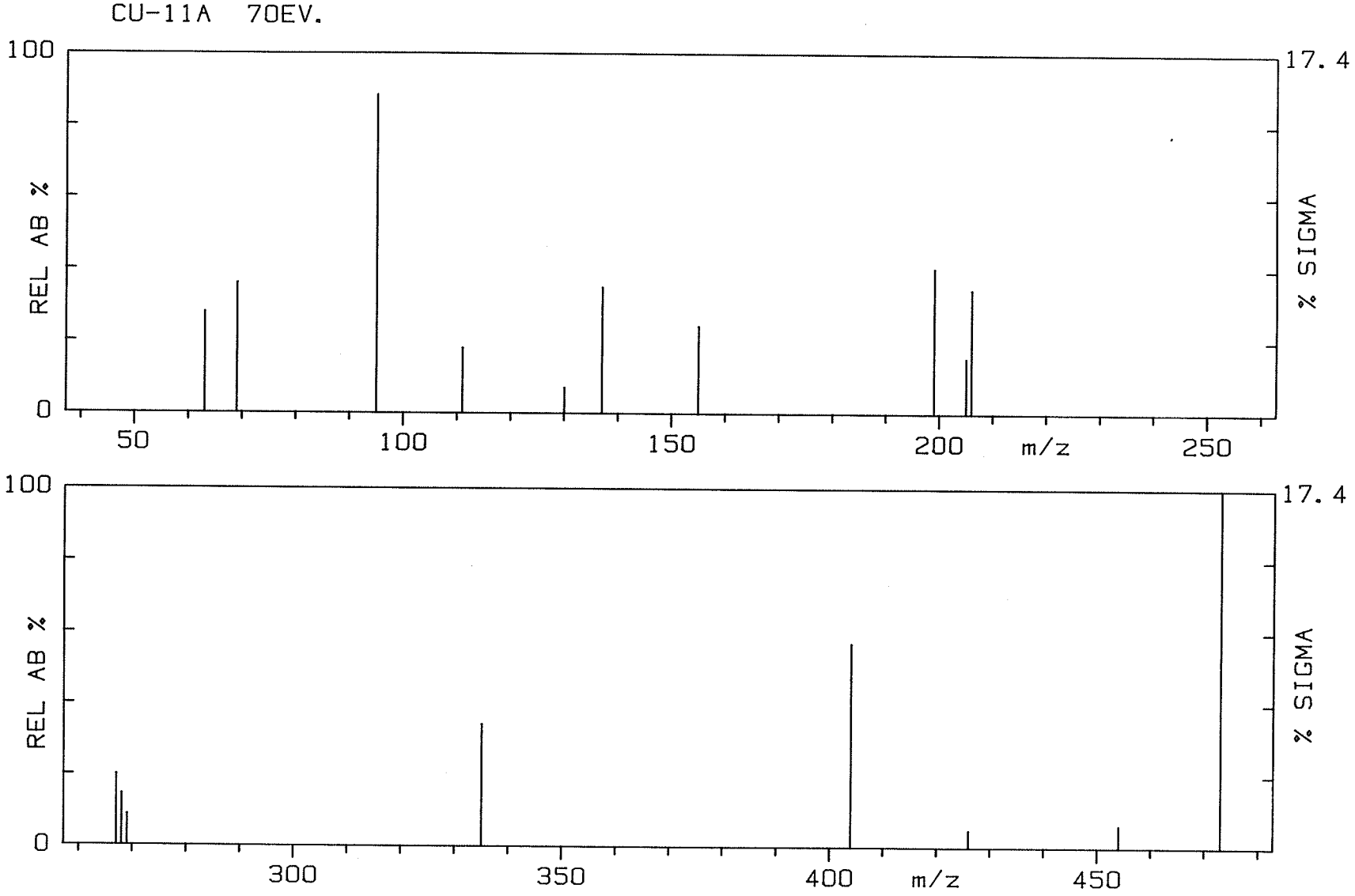
CU-11A 70EV.
100
REL AB %
0
50
100
150
200
m/z
250
17.4
% SIGMA
100
REL AB %
0
300
350
400
m/z
450
17.4
% SIGMA

Figure 77.

Normalized 70 eV-EI mass spectrum of

bis[1,1,1-trifluoro-4-(2'-naphthyl)-2,4-butanedionato]Cu(II)

{Cu-12a}.

m/z $[M]^{+\cdot}$ = 593, $[L]^{+}$ = 265

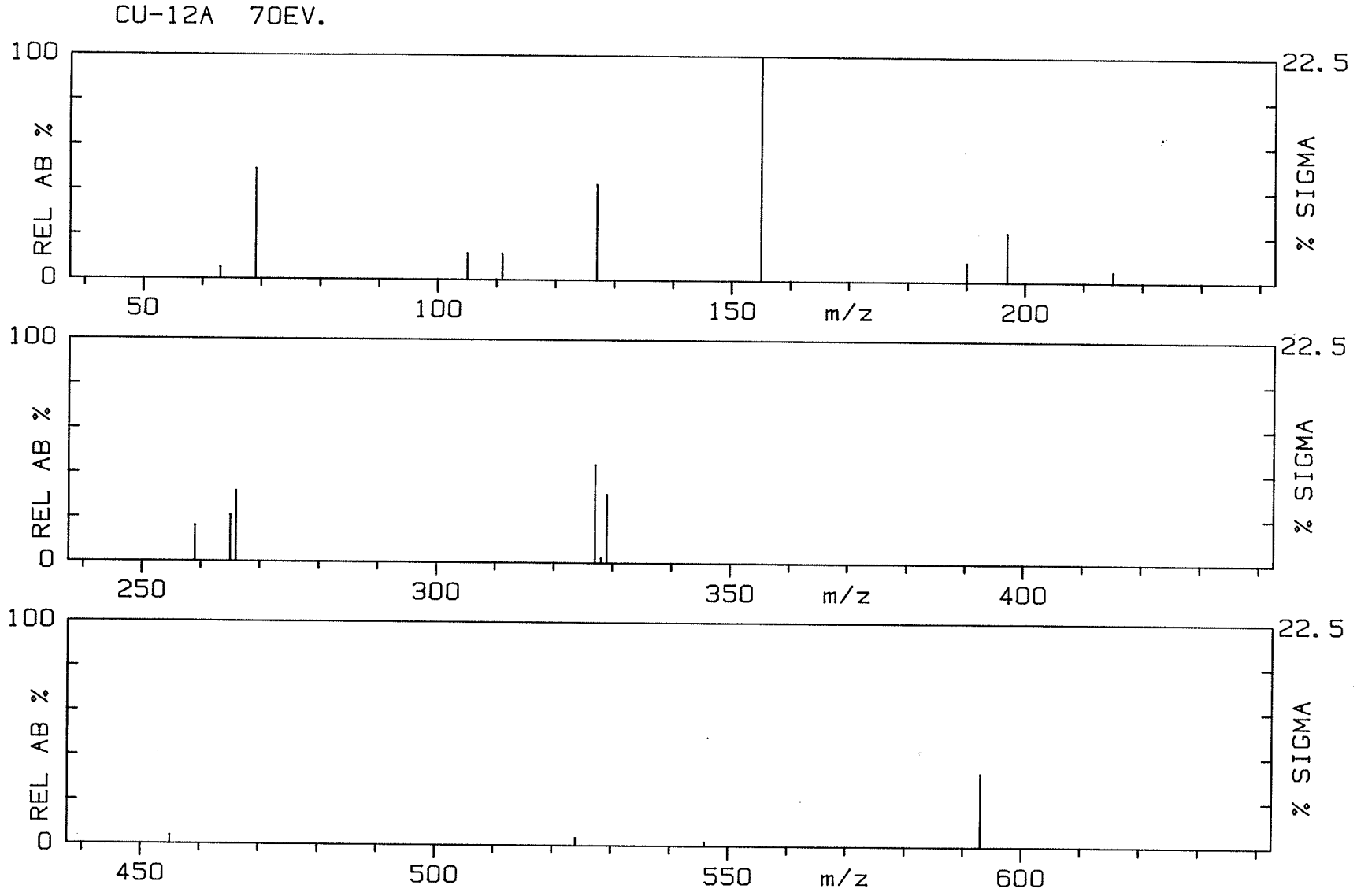
CU-12A 70EV.
100
0
REL AB %
22.5
% SIGMA
50
100
150
m/z
200
250
300
350
400
450
500
550
600

Figure 78.

Normalized 70 eV-EI mass spectrum of

bis[1,1,1,2,2-pentafluoro-5-phenyl-3,5-pentanedionato]Cu(II)

{Cu-13a}.

m/z $[M]^{+\cdot}$ = 593, $[L]^{+}$ = 265

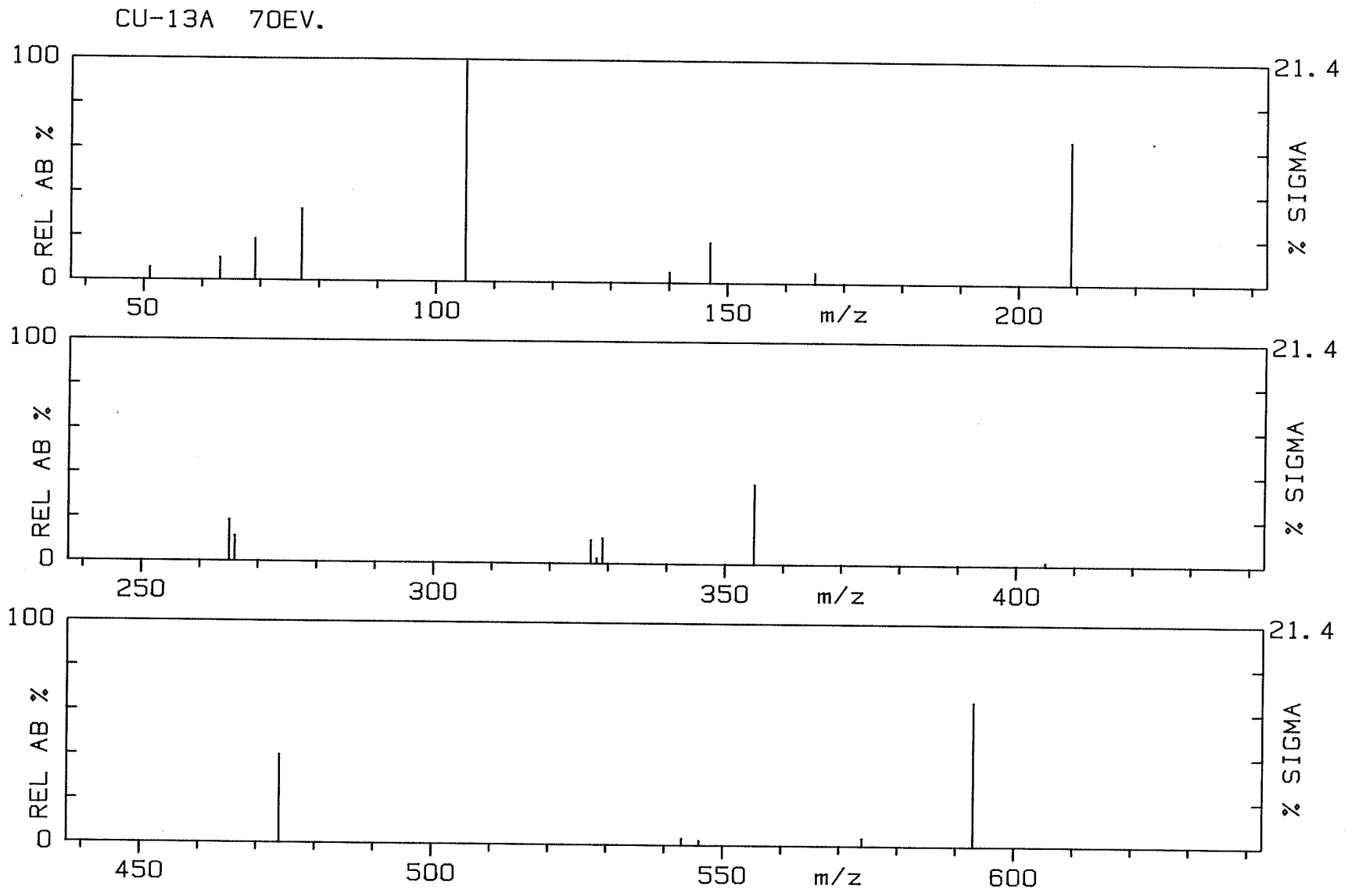
CU-13A 70EV.
100
0
REL AB %
21.4
% SIGMA
50
100
150
m/z
200
250
300
350
400
450
500
550
600

Figure 79.

Normalized 70 eV-EI mass spectrum of

bis[1,1,1,2,2-pentafluoro-5-(2'-thienyl)-3,5-pentanedionato]Cu(II)

{**Cu-14a**}.

m/z $[M]^{+\cdot}$ = 605, $[L]^{+}$ = 271

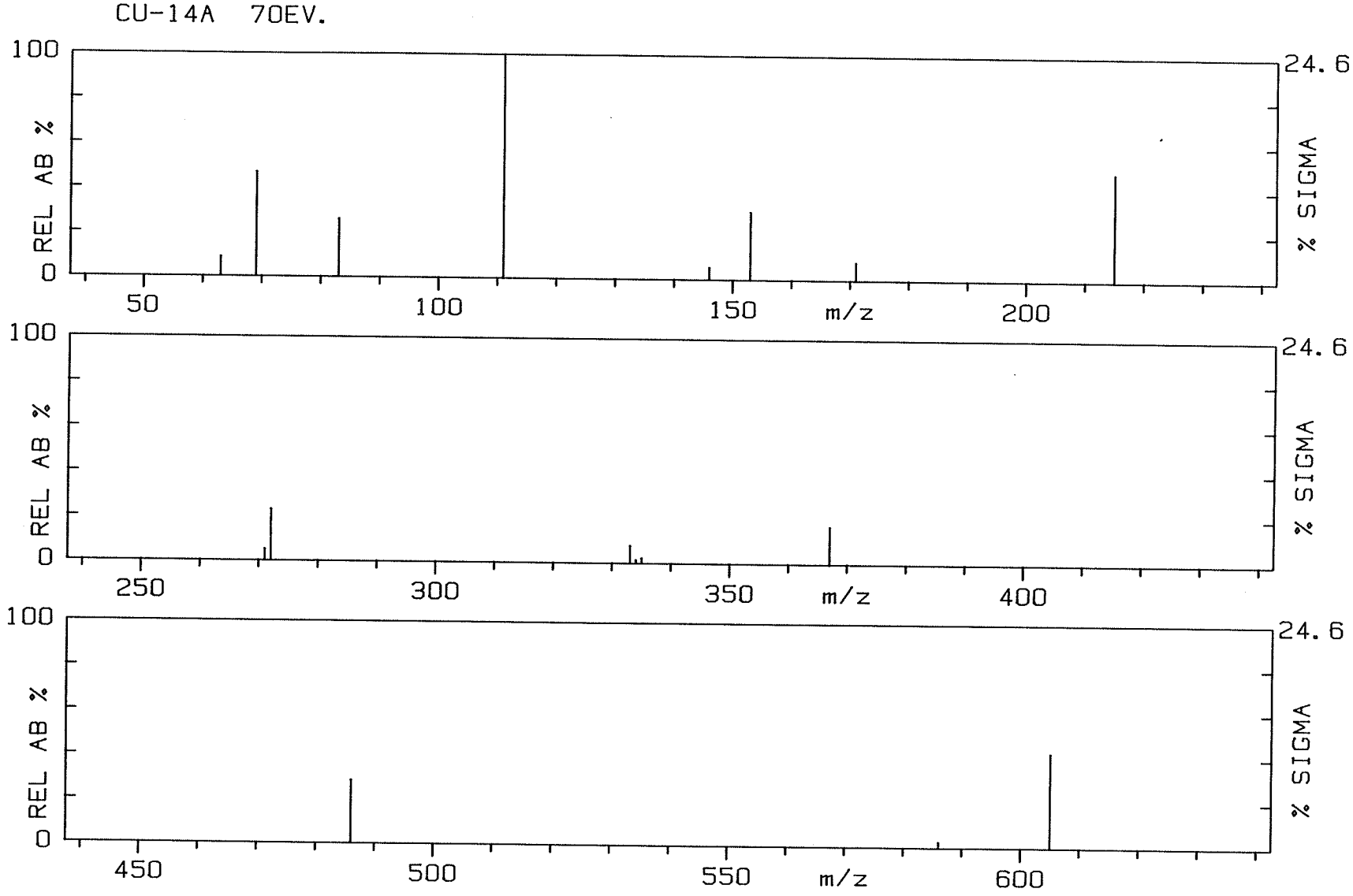
CU-14A 70EV.
100
REL AB %
0
50
100
150
m/z
200
24.6
% SIGMA
100
REL AB %
0
250
300
350
m/z
400
24.6
% SIGMA
100
REL AB %
0
450
500
550
m/z
600
24.6
% SIGMA

Figure 80.

Normalized 70 eV-EI mass spectrum of

bis[1,1,1,2,2,3,3-heptafluoro-6-phenyl-4,6-hexanedionato]Cu(II)

(Cu-16a).

m/z $[M]^{+\cdot}$ = 693, $[L]^{+}$ = 315

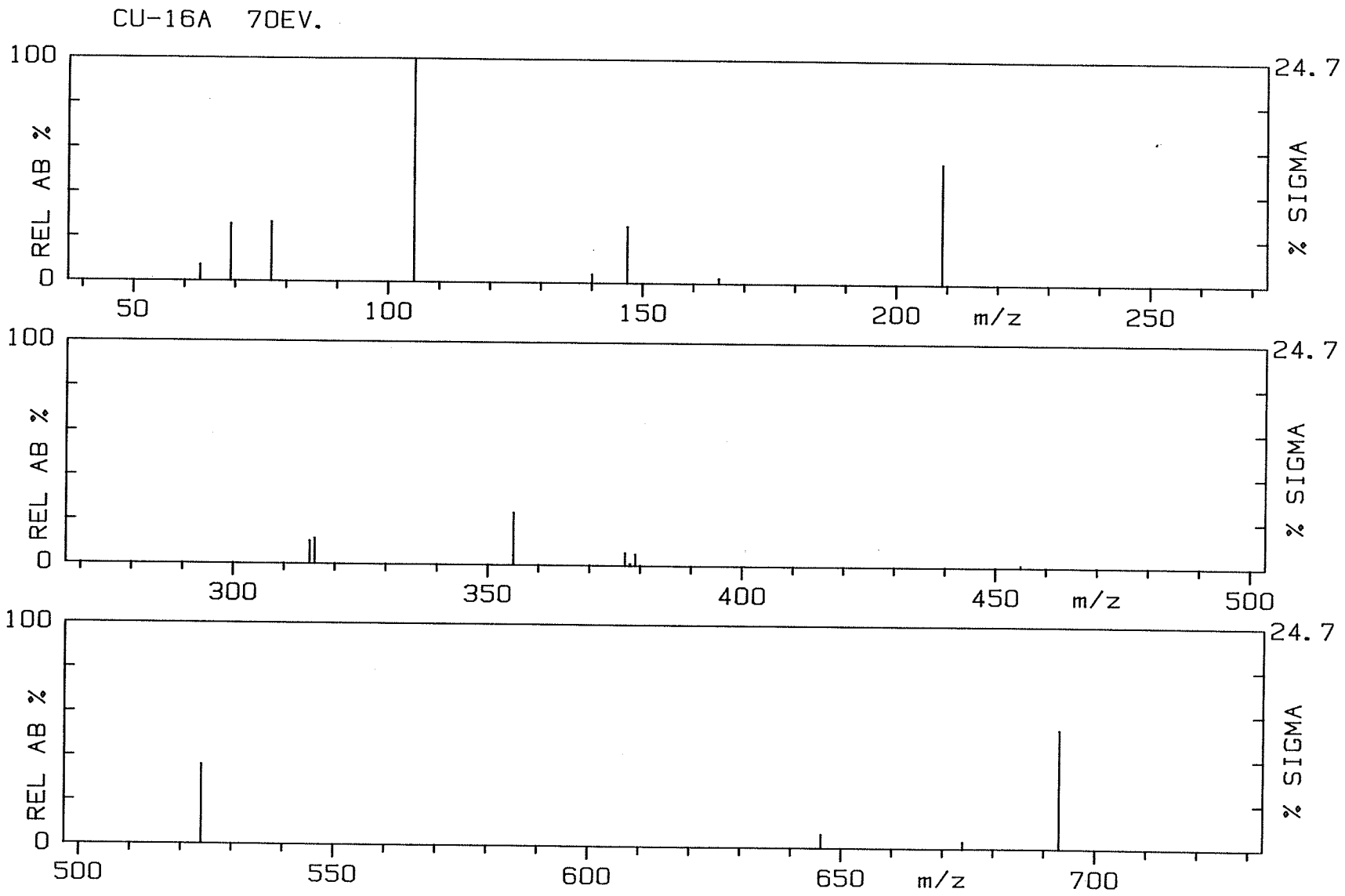
CU-16A 70EV.
100
REL AB %
0
50
100
150
200
m/z
250
24.7
% SIGMA
100
REL AB %
0
300
350
400
450
m/z
500
24.7
% SIGMA
100
REL AB %
0
500
550
600
650
m/z
700
24.7
% SIGMA

Figure 81.

Normalized 70 eV-EI mass spectrum of

bis[1,1,1,2,2,3,3-heptafluoro-6-(2'-thienyl)-4,6-hexanedionato]Cu(II)

{Cu-17a}.

m/z $[M]^{+\cdot}$ = 705, $[L]^{+}$ = 321

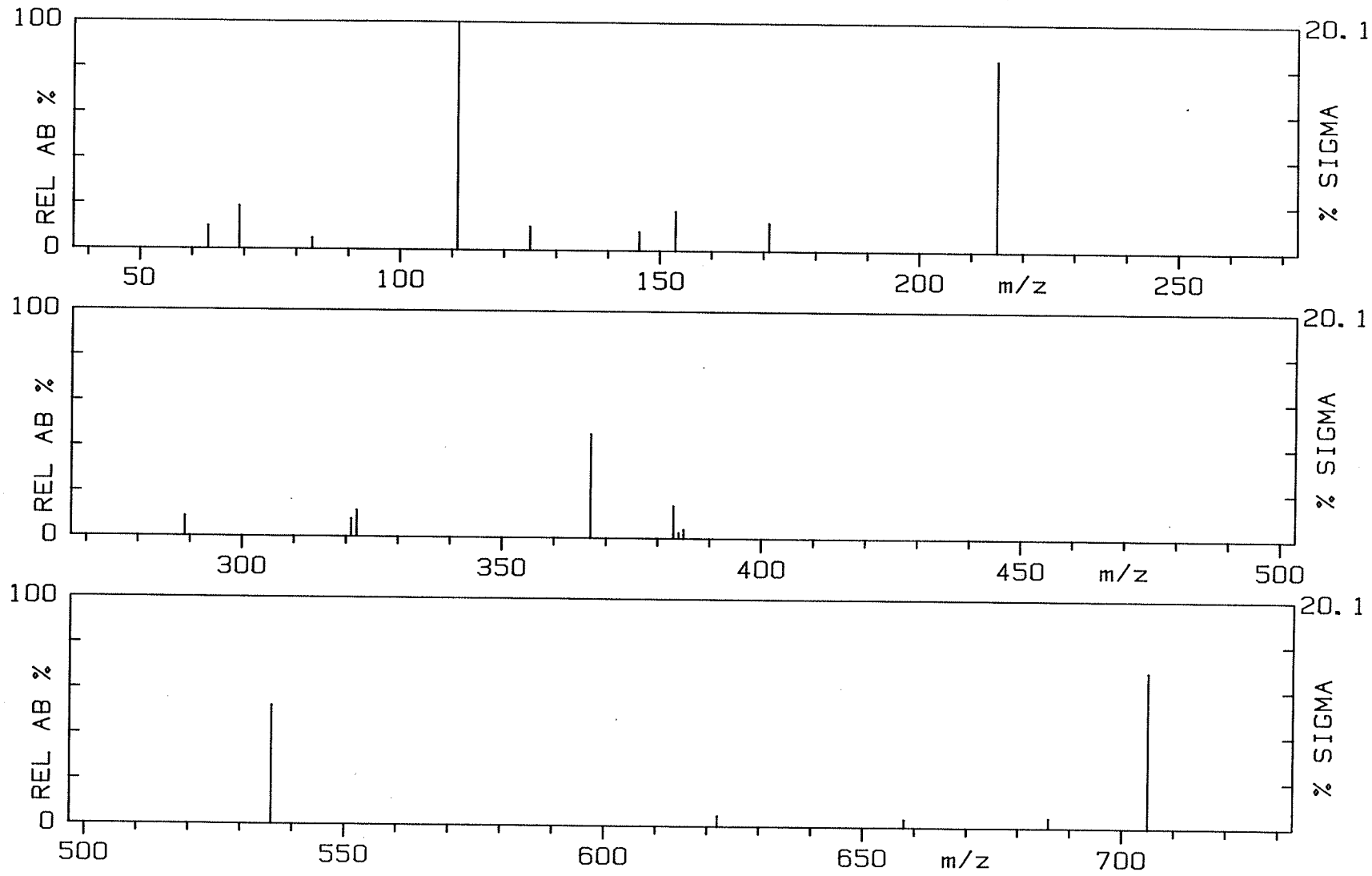
CU-17A 70EV.
100
0
REL AB %
20.1
% SIGMA
50
100
150
200
m/z
250
300
350
400
450
500
550
600
650
700

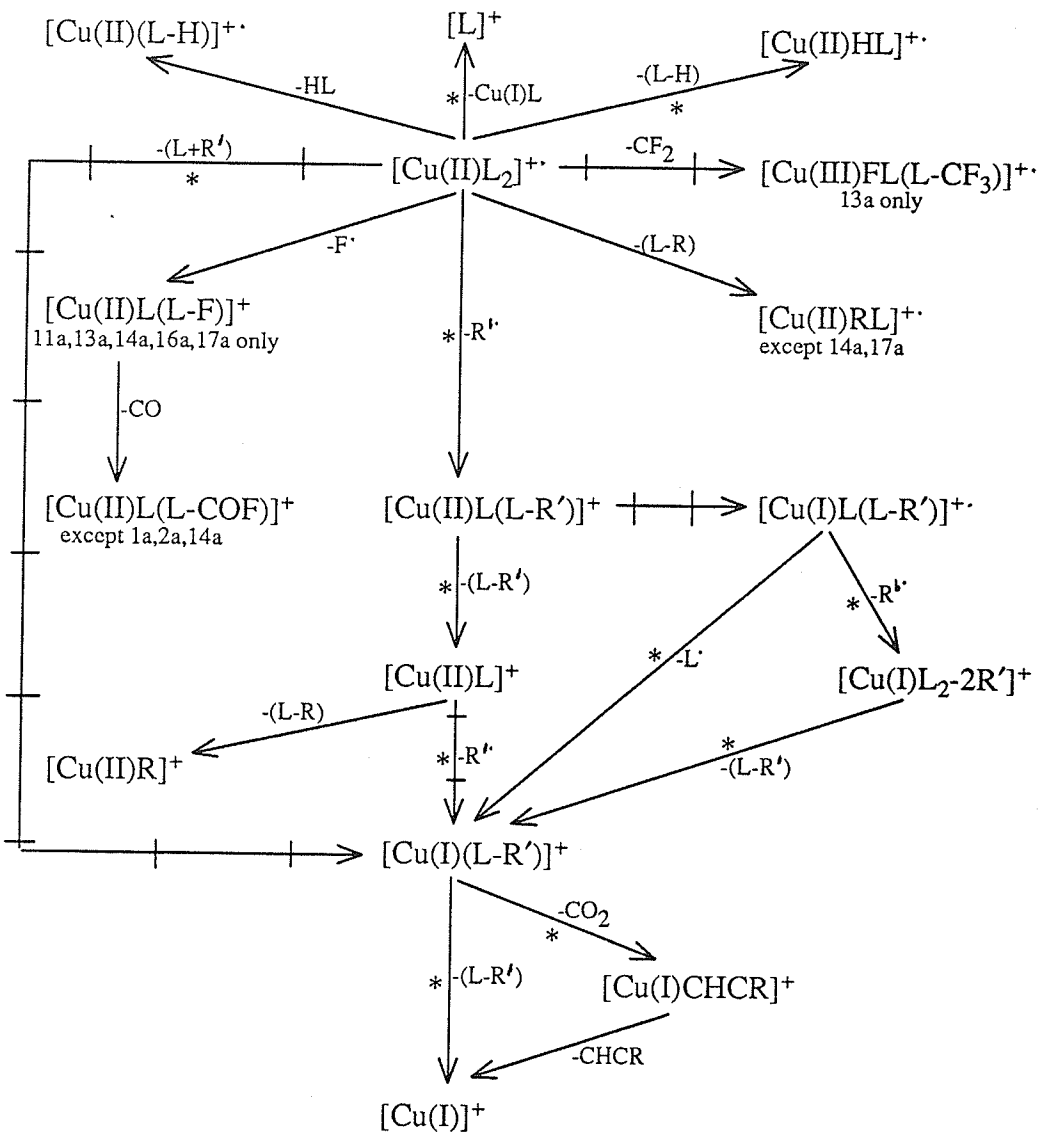

* process confirmed by the observation of a metastable transition in at least one of the complexes.

⟶⟶ reaction step in which a change in metal oxidation state is proposed.

Scheme 54. Proposed fragmentation pathways for Cu(II) β-diketonates where R' = CHF_2 (**Cu-1a** and **-2a**), CF_3 (**Cu-3a, -8a, -9a, -11a** and **-12a**), C_2F_5 (**Cu-13a** and **-14a**) or C_3F_7 (**Cu-16a** and **-17a**). Pathways are common to all complexes except where noted.

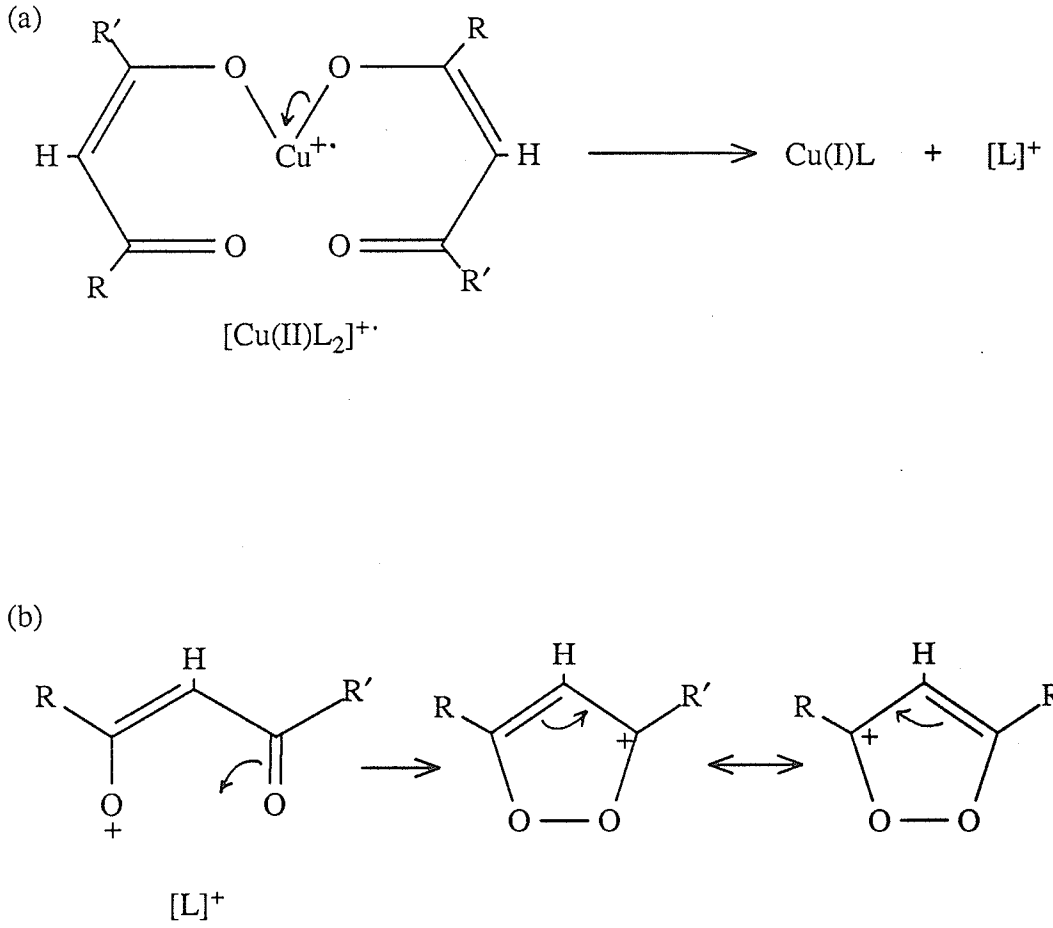

Scheme 55. (a) Suggested mechanism for the formation of $[L]^+$.

(b) Proposed resonance-stabilized forms of $[L]^+$.

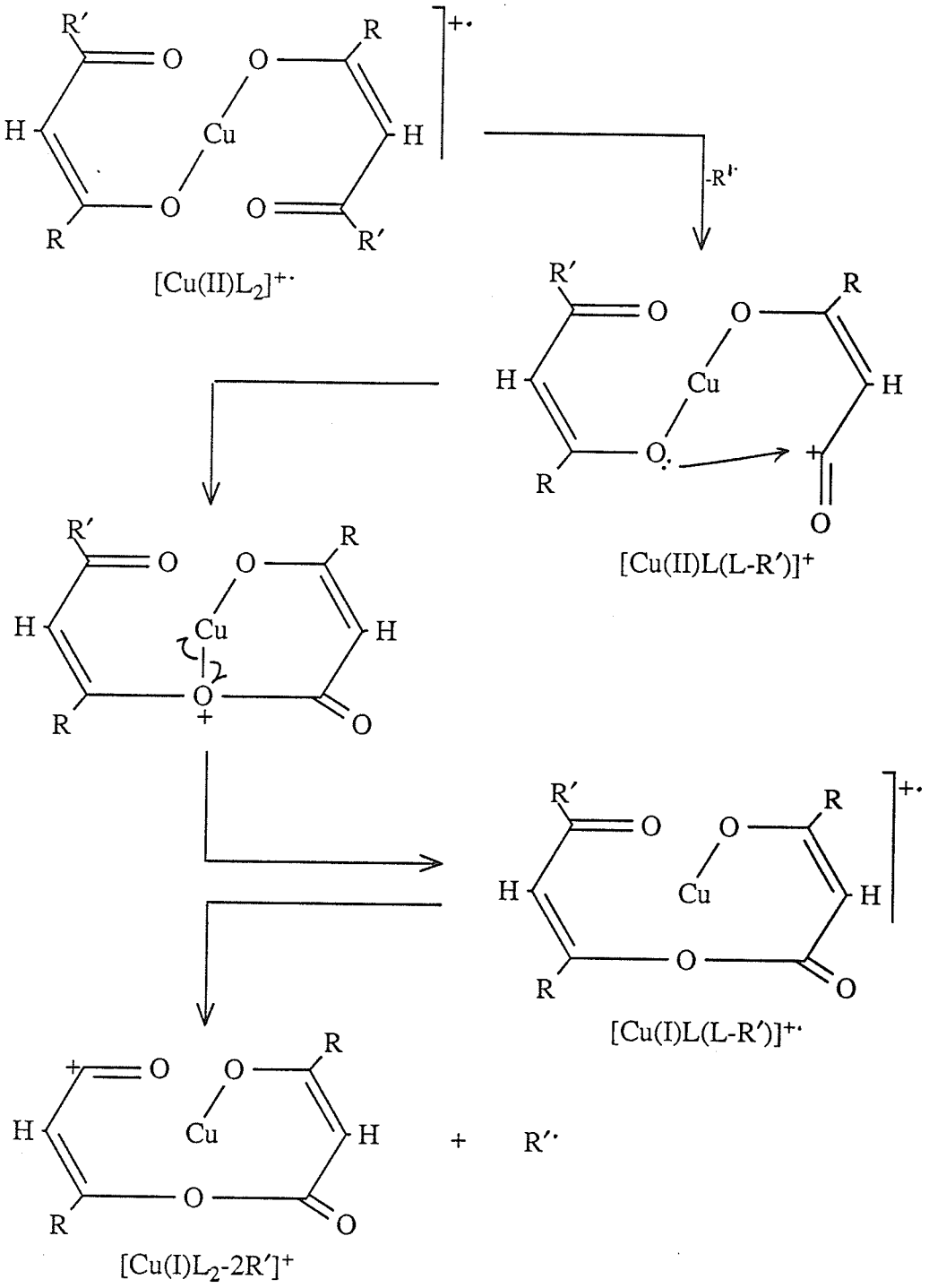

Scheme 56. Suggested mechanism for the formation of $[Cu(I)L_2\text{-}2R']^+$.

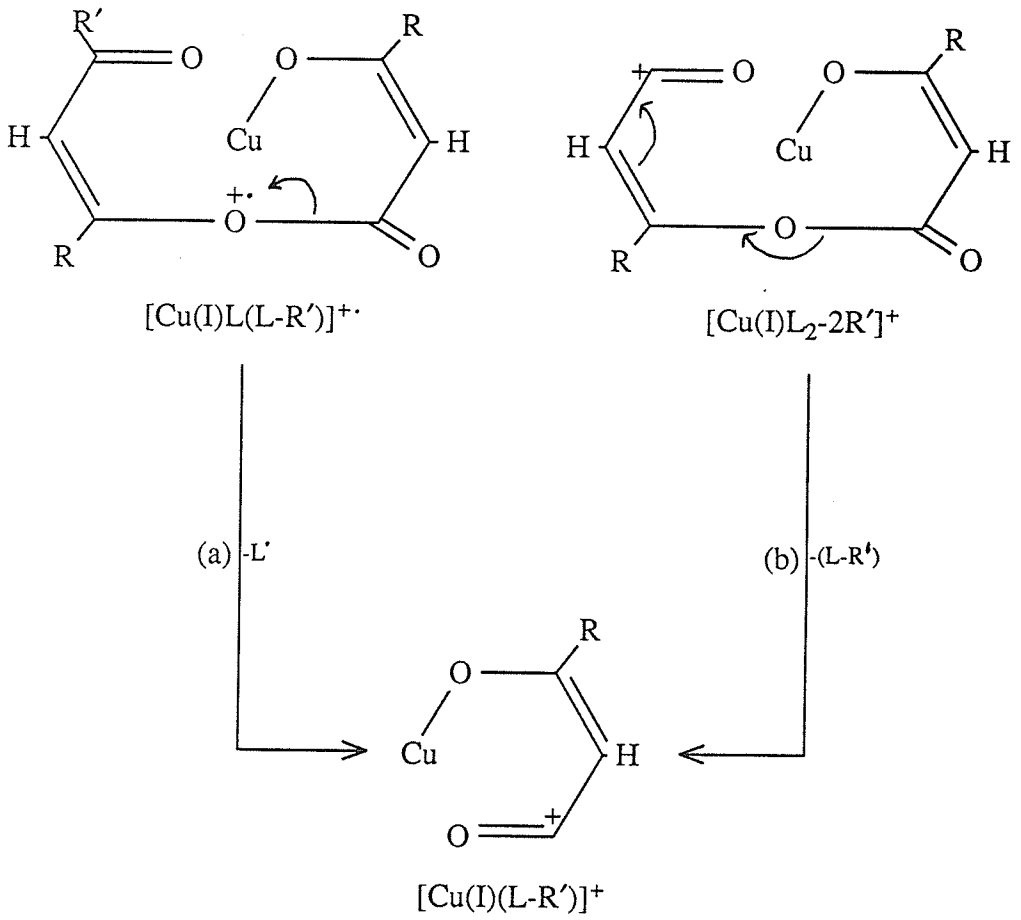

Scheme 57. Suggested mechanism for the formation of $[Cu(I)(L\text{-}R')]^+$ from (a) $[Cu(I)L(L\text{-}R')]^+$ and (b) $[Cu(I)L_2\text{-}2R']^+$.

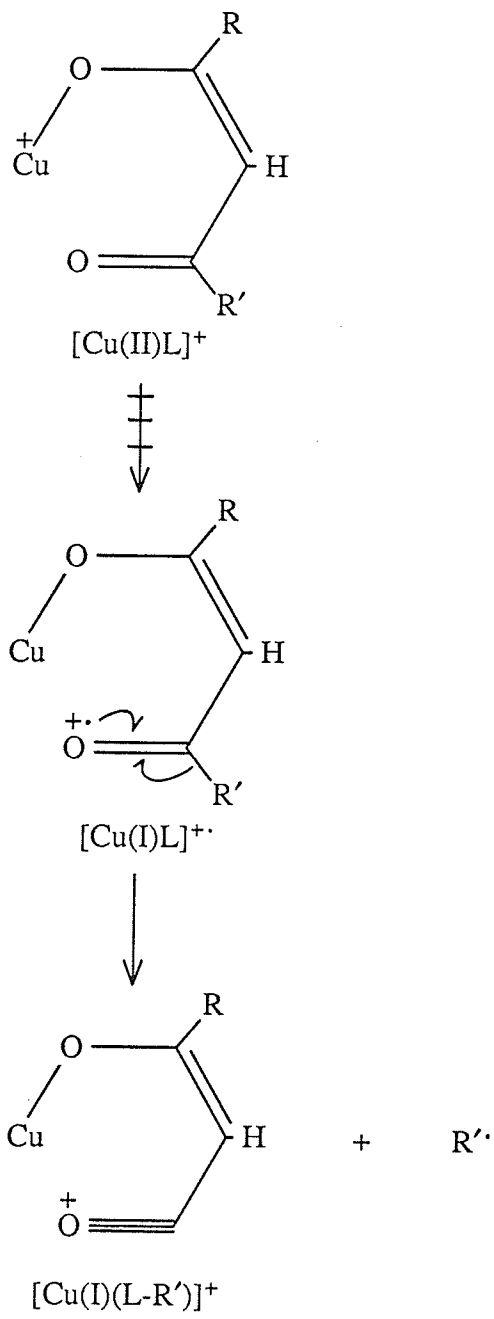

Scheme 58. Suggested mechanism for the formation of $[Cu(I)(L\text{-}R')]^+$ from $[Cu(II)L]^+$.

(g) Zn(II) β-diketonates

Relative abundance data for the nine Zn(II) β-diketonates studied appear in Tables 38–41. Plots of the EI mass spectra are presented in Figures 82–90. Metastable transitions in **Zn–8a** were monitored by linked-scanning techniques. A cursory examination of **Zn–8a** has been reported (175).

Suggested decomposition pathways for the difluoromethyl-substituted Zn(II) chelates (R' = CHF_2; Table 38) are shown in Scheme 59. The ions $[Zn(II)L_2]^{+\cdot}$ and $[Zn(II)L(L\text{–}R')]^{+}$ constitute 90 - 100% of the total ion current carried by the zinc-containing species in these spectra. Many of the observed fragmentations can be rationalized by analogy to mechanisms already presented:

Fragmentation	Scheme
$[Zn(II)L(L\text{-}R')]^+ \longrightarrow [Zn(II)L]^+$	30
$[Zn(II)L]^+ \longrightarrow [Zn(II)F(L\text{-}COF)]^+$	31
$[Zn(II)F(L\text{-}COF)]^+ \longrightarrow [L\text{-}COF_2]^+$	31
$[Zn(II)L]^+ \longrightarrow [L\text{-}2F]^+$	32
$[Zn(II)L(L\text{-}R')]^+ \longrightarrow [Zn(II)LCHCR]^+$	35
$[Zn(II)LCHCR]^+ \longrightarrow [Zn(II)L]^+$	35

Suggested fragmentation routes for the Zn(II) β-diketonate complexes possessing a trifluoromethyl substituent (R' = CF_3; Table 39) are given in Scheme 60. The molecular ion and $[Zn(II)L(L\text{-}R')]^+$ are once again the most dominant metal-containing ions. Metastable evidence confirms several of the pathways shown in Scheme 60; mechanisms for many of these events are well-established:

Fragmentation	Scheme
$[Zn(II)L]^+ \longrightarrow [Zn(II)R]^+$	26
$[Zn(II)L(L\text{-}R')]^+ \longrightarrow [Zn(II)L]^+$	30
$[Zn(II)L(L\text{-}R')]^+ \longrightarrow [Zn(II)LCHCR]^+$	35
$[Zn(II)LCHCR]^+ \longrightarrow [Zn(II)L]^+$	35
$[Zn(II)L]^+ \longrightarrow [Zn(II)F(L\text{-}R')]^+$	35

Although unsubstantiated by metastable evidence, the formation of $[Zn(II)F(L\text{-}R')]^+$ from $[Zn(II)L(L\text{-}R')]^+$ by the loss of the EE^o neutral (L-F) is plausible (see Scheme 33).

Suggested decomposition pathways for the pentafluoroethyl- ($R' = C_2F_5$; Table 40) and heptafluoropropyl- ($R' = C_3F_7$, Table 41) substituted chelates are illustrated in Scheme 61. There are comparatively few differences between the mass spectra of these complexes and those presented in Tables 38 and 39. And as before, many of the fragmentation mechanisms are known:

Fragmentation	Scheme
$[Zn(II)L]^+ \longrightarrow [Zn(II)R]^+$	26
$[Zn(II)L(L\text{-}R')]^+ \longrightarrow [Zn(II)L]^+$	30
$[Zn(II)L(L\text{-}R')]^+ \longrightarrow [Zn(II)LCHCR]^+$	35
$[Zn(II)LCHCR]^+ \longrightarrow [Zn(II)L]^+$	35

While fluorine-to-metal migration was observed to a minor extent in the CHF_2- and CF_3-substituted zinc complexes (eg. $[Zn(II)F(L\text{-}COF)]^+$ and $[Zn(II)F(L\text{-}R')]^+$), there is a total absence of fluorine transfer in the C_2F_5- and C_3F_7-substituted derivatives. The combination of a borderline Zn(II) acceptor and the strong fluorine-retentive nature of the C_2F_5 and C_3F_7 moieties may be responsible for this behavior.

Another distinct trend among the Zn(II) β-diketonates included in this study concerns the relationship between the relative abundance of $[Zn(II)LCHCR]^+$ (a daughter of $[Zn(II)L(L\text{-}R')]^+$ by the elimination of CO_2) and the nature of the R group. When R = phenyl, $[Zn(II)LCHCR]^+$ is not detectable, but when R = 2-thienyl or 5-methyl-2-thienyl, the ion is weakly abundant. An added degree of resonance stabilization may be afforded the ion by the presence of an unshared pair of electrons in the aromatic ring:

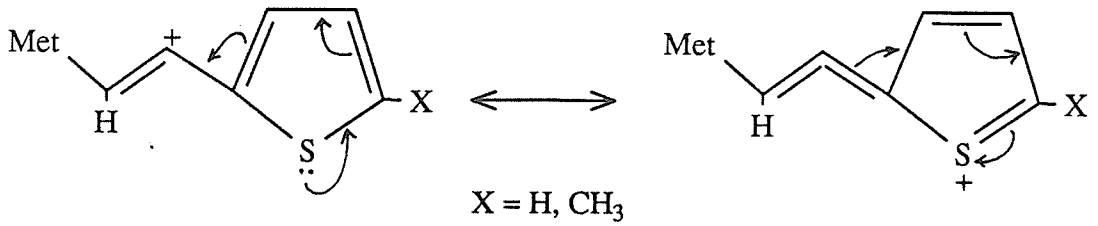

A re-examination of the Co(III) β-diketonate spectra reveals a parallel in the $[Co(II)LCHCR]^+$ abundances, especially when R' = C_2F_5 or C_3F_7 (see Tables 18 and 19). However, the relationship fails to hold for the Ni(II) β-diketonates, where no clear trend is discernable (see Tables 22 and 23).

Table 38. 70 eV-EI mass spectra of compounds **Zn-1a** and **Zn-2a**.

	Zn-1a	**Zn-2a**
R =	$-C_6H_5$	$-C_4H_3S$
R'=	$-CHF_2$	$-CHF_2$

ION	%RA	m/z	%TIC	%RA	m/z	%TIC
$[ZnL_2]^+$	24.2	(458)	10.2	23.5	(470)	12.1
$[ZnL(L-R')]^+$	35.6	(407)	15.0	26.5	(419)	13.7
$[ZnLCHCR]^+$	-	(363)	-	0.5	(375)	0.3
$[ZnL]^+$	-	(261)	-	2.8	(267)	1.4
$[ZnF(L-COF)]^+$	-	(233)	-	0.9	(239)	0.5
$[HL]^+$	2.7	(198)	1.1	2.9	(204)	1.5
$[L]^+$	-	(197)	-	0.5	(203)	0.3
$[L-F]^+$	2.3	(178)	1.0	2.0	(184)	1.0
$[L-2F]^+$	1.5	(159)	0.6	-	(165)	-
$[HL-R']^+$	13.5	(147)	5.7	6.6	(153)	3.4
$[L-COF_2]^+$	2.9	(131)	1.2	2.3	(137)	1.2
$[RCO]^+$	100.0	(105)	42.0	100.0	(111)	51.7
$[RCCH]^+$	5.0	(102)	2.1	6.6	(108)	3.4
$[R]^+$	32.3	(77)	13.6	6.1	(83)	3.2
$[CF_3]^+$	11.7	(69)	4.9	11.2	(69)	5.8
$[R']^+$	6.2	(51)	2.6	2.6	(51)	1.3

Table 39. 70 eV-EI mass spectra of compounds **Zn-3a**, **Zn-8a** and **Zn-9a**.

	Zn-3a	**Zn-8a**	**Zn-9a**
R =	$-C_6H_5$	$-C_4H_3S$	$-C_4H_2SCH_3$
R'=	$-CF_3$	$-CF_3$	$-CF_3$

ION	%RA	m/z	%TIC	%RA	m/z	%TIC	%RA	m/z	%TIC
$[ZnL_2]^+$ (a)	22.6	(494)	11.5	26.5	(506)	13.5	26.8	(534)	12.2
$[ZnL(L-R')]^+$ (b)	22.7	(425)	11.5	[a]22.2	(437)	11.3	18.3	(465)	8.3
$[ZnLCHCR]^+$	-	(381)	-	[b]0.4	(393)	0.2	0.6	(421)	0.3
$[ZnL]^+$ (c)	-	(279)	-	[a,b]3.3	(285)	1.7	-	(299)	-
$[ZnF(L-R')]^+$	0.5	(229)	0.3	[c]1.4	(235)	0.7	-	(249)	-
$[ZnR]^+$	-	(141)	-	3.5	(147)	1.8	2.8	(161)	1.3
$[HL]^+$	2.7	(216)	1.4	5.3	(222)	2.7	15.4	(236)	7.0
$[L-S]^+$	-	(183)	-	[a]5.0	(189)	2.6	10.8	(203)	4.9
$[HL-R']^+$	4.2	(147)	2.1	5.7	(153)	2.9	13.3	(167)	6.0
$[RCO]^+$	100.0	(105)	50.7	*100.0	(111)	51.0	100.0	(125)	45.4
$[RCCH]^+$	1.0	(102)	0.5	1.6	(108)	0.8	0.7	(122)	0.3
$[R]^+$	30.3	(77)	15.4	4.7	(83)	2.4	6.3	(97)	2.9
$[R']^+$	9.0	(69)	4.6	18.2	(69)	9.3	26.1	(69)	11.8
$[CHF_2]^+$	4.8	(51)	2.4	-	(51)	-	-	(51)	-

[a] Identified metastable transitions are indicated by superscripts which relate the daughter ion to its precursor as labelled in column 1.

* daughter ion of (a) and (b).

Table 40. 70 eV-EI mass spectra of compounds **Zn-13a** and **Zn-14a**.

	Zn-13a	**Zn-14a**
R =	$-C_6H_5$	$-C_4H_3S$
R'=	$-C_2F_5$	$-C_2F_5$

ION	%RA	m/z	%TIC	%RA	m/z	%TIC
$[ZnL_2]^+$	15.5	(594)	8.4	19.6	(606)	9.5
$[ZnL(L-R')]^+$	21.3	(475)	11.6	22.3	(487)	10.9
$[ZnLCHCR]^+$	-	(431)	-	0.4	(443)	0.2
$[ZnL]^+$	-	(329)	-	3.8	(335)	1.9
$[ZnR]^+$	2.4	(141)	1.3	6.4	(147)	3.1
$[HL]^+$	-	(266)	-	7.2	(272)	3.5
$[L-S]^+$	-	(233)	-	2.4	(239)	1.2
$[HL-R']^+$	2.2	(147)	1.2	12.6	(153)	6.1
$[RCO]^+$	100.0	(105)	54.4	100.0	(111)	48.7
$[RCCH]^+$	1.3	(102)	0.7	1.6	(108)	0.8
$[R]^+$	30.8	(77)	16.8	4.8	(83)	2.3
$[CF_3]^+$	6.1	(69)	3.3	24.6	(69)	12.0
$[CHF_2]^+$	4.2	(51)	2.3	-	(51)	-

Table 41. 70 eV-EI mass spectra of compounds **Zn-16a** and **Zn-17a**.

	Zn-16a	**Zn-17a**
R =	$-C_6H_5$	$-C_4H_3S$
R'=	$-C_3F_7$	$-C_3F_7$

ION	%RA	m/z	%TIC	%RA	m/z	%TIC
$[ZnL_2]^+$	15.8	(694)	8.9	16.6	(706)	10.0
$[ZnL(L-R')]^+$	26.5	(525)	14.8	22.9	(537)	13.7
$[ZnLCHCR]^+$	-	(481)	-	0.4	(493)	0.2
$[ZnL]^+$	-	(379)	-	3.0	(385)	1.8
$[ZnR]^+$	0.2	(141)	0.1	4.0	(147)	2.4
$[HL]^+$	0.2	(316)	0.1	0.8	(322)	0.5
$[L-S]^+$	-	(283)	-	1.6	(289)	1.0
$[HL-R']^+$	3.9	(147)	2.2	3.1	(153)	1.9
$[RCO]^+$	100.0	(105)	56.0	100.0	(111)	60.0
$[RCCH]^+$	1.2	(102)	0.7	1.4	(108)	0.8
$[R]^+$	21.9	(77)	12.3	3.5	(83)	2.1
$[CF_3]^+$	6.2	(69)	3.5	9.9	(69)	5.9
$[CHF_2]^+$	2.6	(51)	1.5	-	(51)	-

Figure 82.

Normalized 70 eV-EI mass spectrum of

bis[1,1-difluoro-4-phenyl-2,4-butanedionato]Zn(II)

{**Zn-1a**}.

m/z $[M]^{+\cdot}$ = 458, $[L]^{+}$ = 197

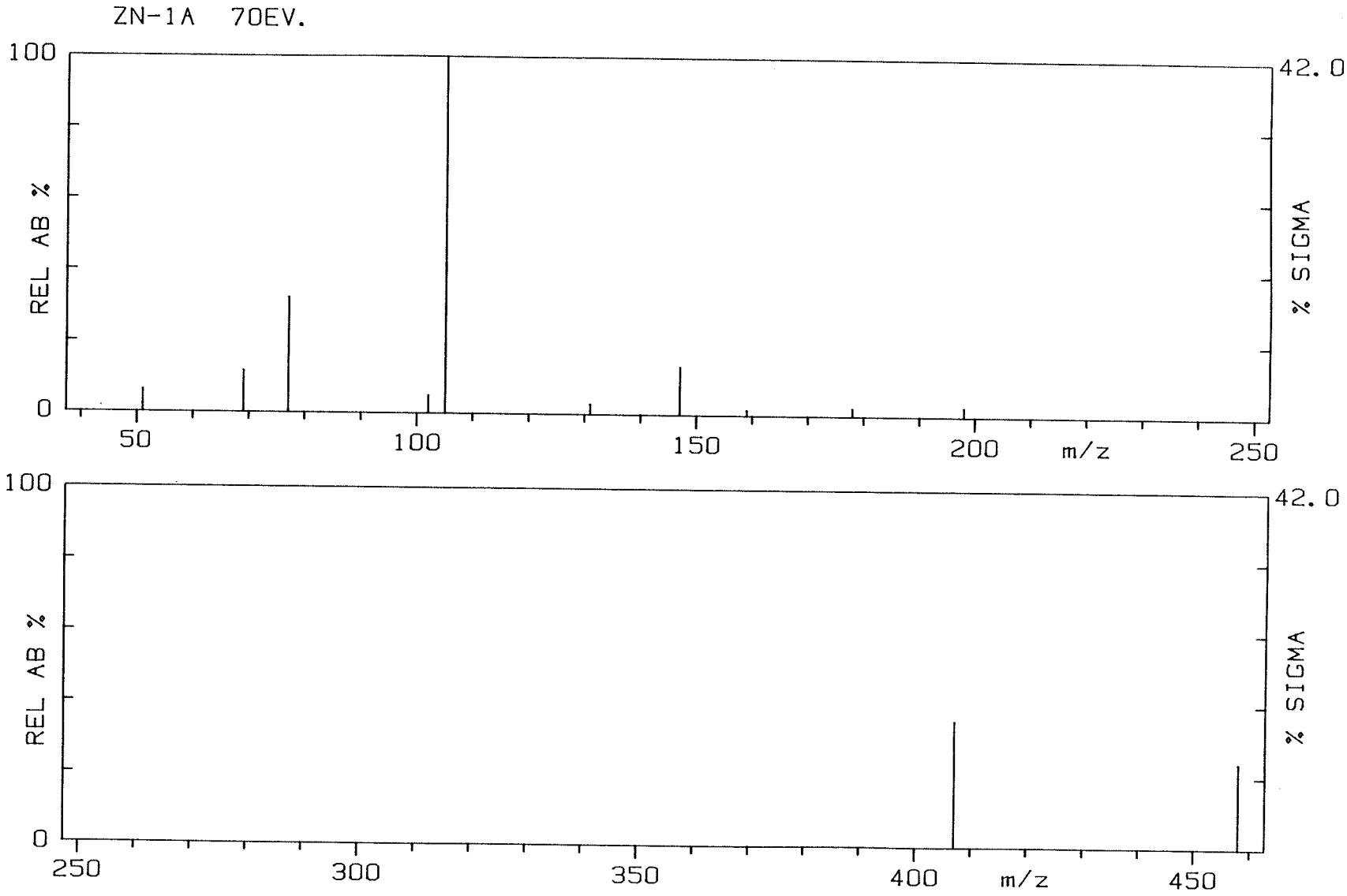
ZN-1A 70EV.
100
REL AB %
0
50
100
150
200
m/z
250
42.0
% SIGMA
100
REL AB %
0
250
300
350
400
m/z
450
42.0
% SIGMA

Figure 83.

Normalized 70 eV-EI mass spectrum of

bis[1,1-difluoro-4-(2'-thienyl)-2,4-butanedionato]Zn(II)

{**Zn-2a**}.

m/z $[M]^{+\cdot}$ = 470, $[L]^{+}$ = 203

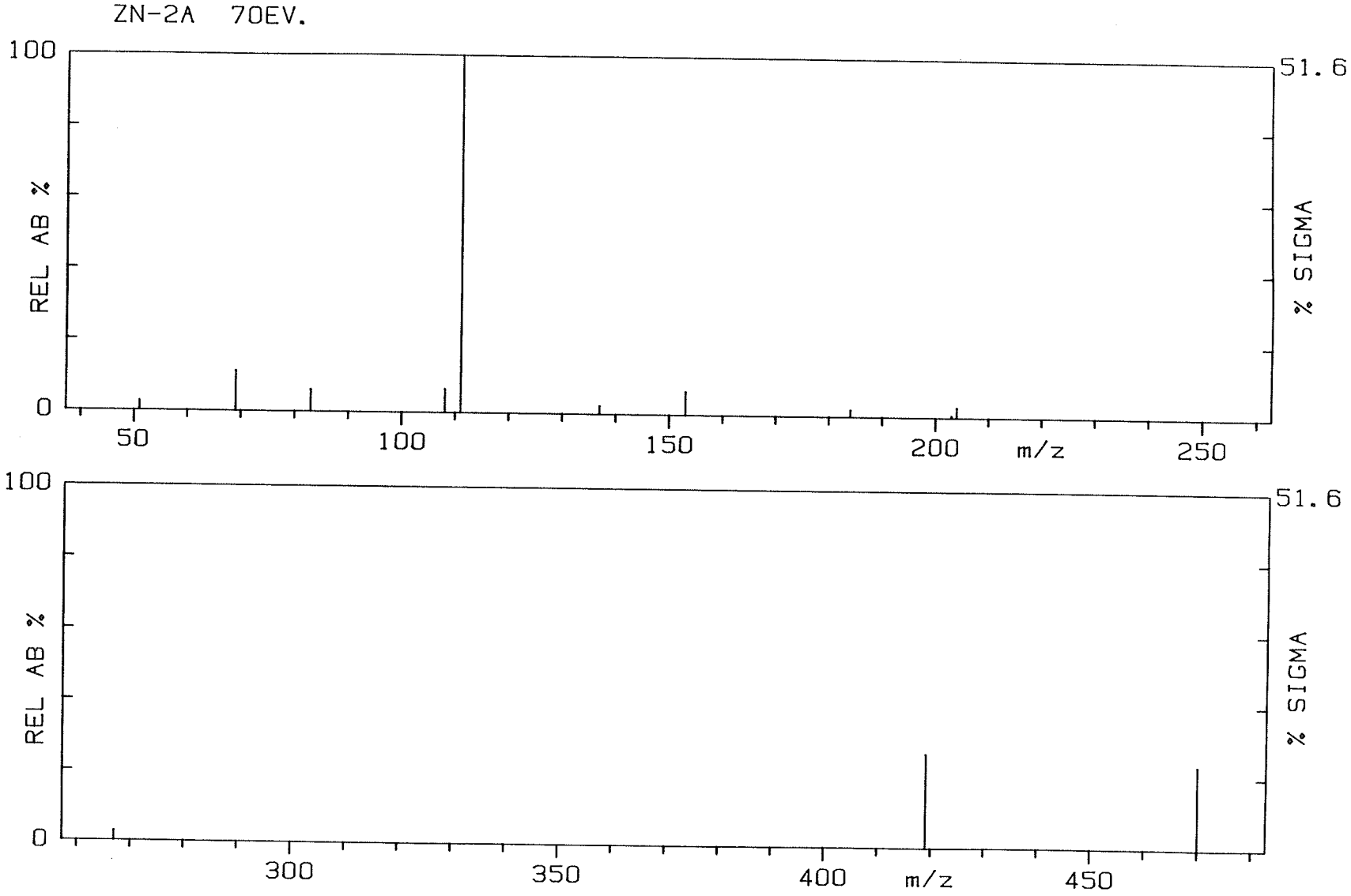
ZN-2A 70EV.
100
REL AB %
0
50
100
150
200
m/z
250
51.6
% SIGMA
100
REL AB %
0
300
350
400
m/z
450
51.6
% SIGMA

Figure 84.

Normalized 70 eV-EI mass spectrum of

bis[1,1,1-trifluoro-4-phenyl-2,4-butanedionato]Zn(II)

{**Zn-3a**}.

m/z $[M]^{+\cdot}$ = 494, $[L]^{+}$ = 215

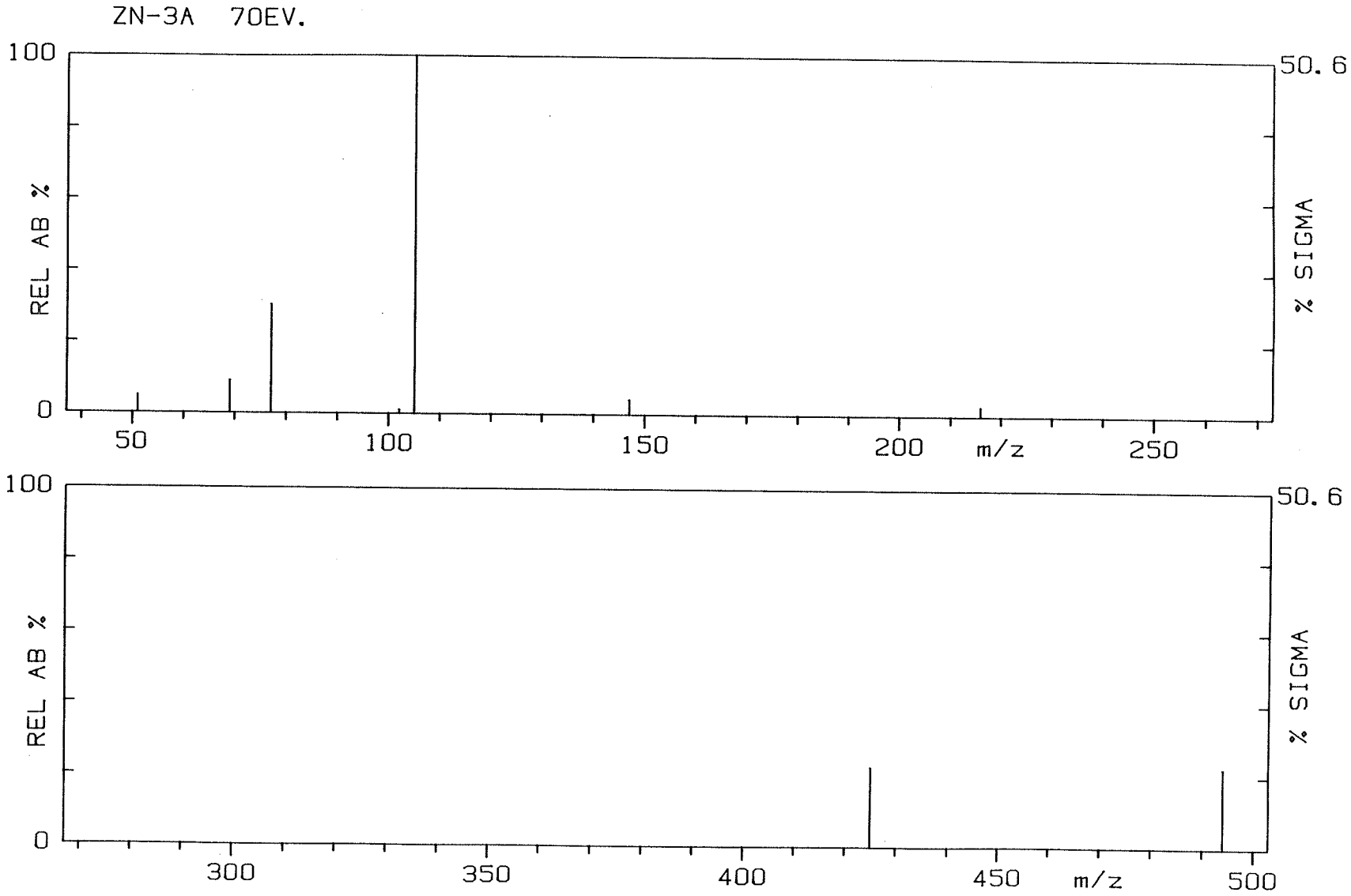
ZN-3A 70EV.
100
REL AB %
0
50.6
% SIGMA
50
100
150
200
m/z
250
100
REL AB %
0
50.6
% SIGMA
300
350
400
450
m/z
500

Figure 85.

Normalized 70 eV-EI mass spectrum of

bis[1,1,1-trifluoro-4-(2'-thienyl)-2,4-butanedionato]Zn(II)

{Zn-8a}.

m/z $[M]^{+\cdot}$ = 506, $[L]^{+}$ = 221

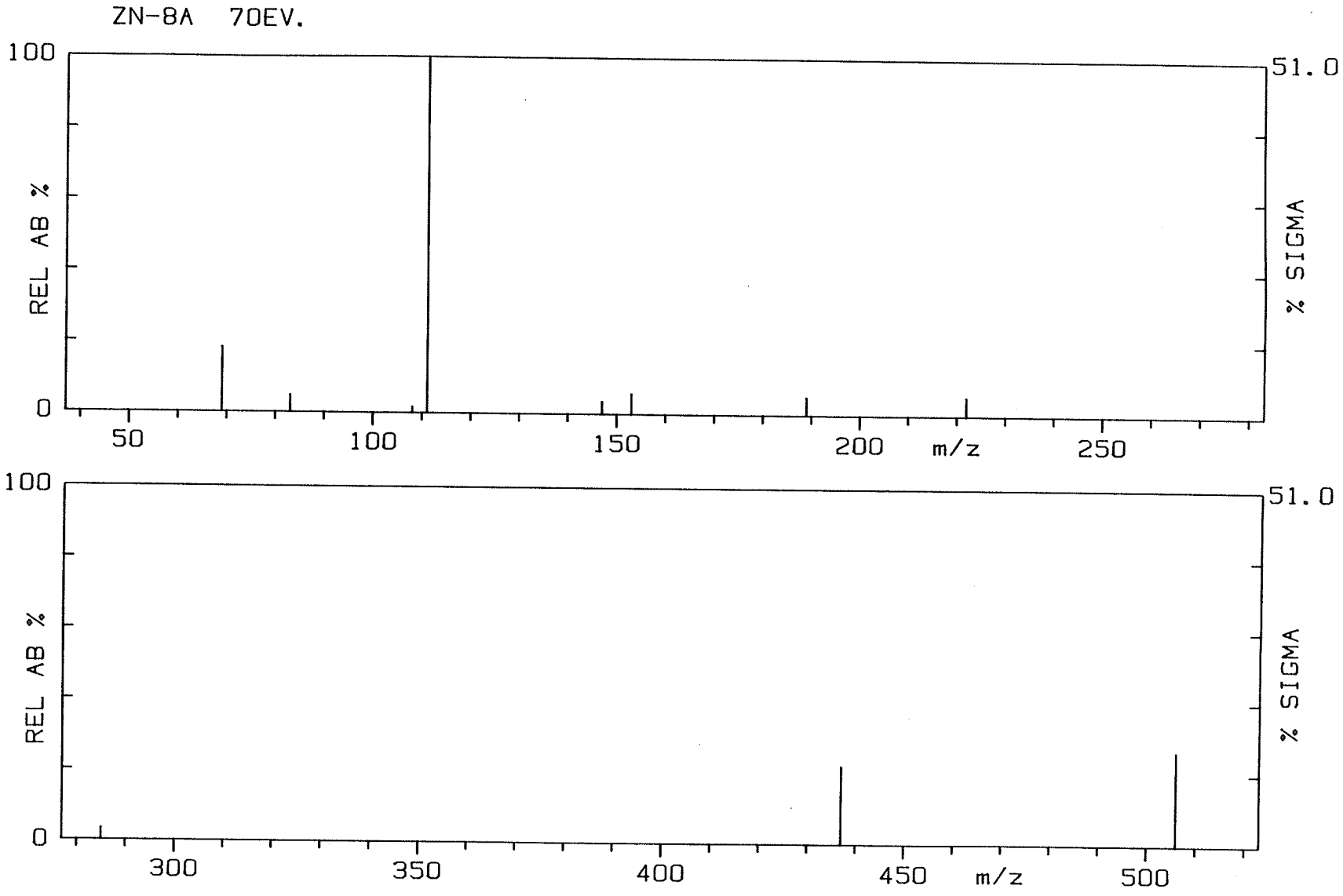
ZN-8A 70EV.
100
REL AB %
0
50
100
150
200
m/z
250
51.0
% SIGMA
100
REL AB %
0
300
350
400
450
m/z
500
51.0
% SIGMA

Figure 86.

Normalized 70 eV-EI mass spectrum of

bis[1,1,1-trifluoro-4-(5'-methyl-2'-thienyl)-2,4-butanedionato]Zn(II)

{**Zn-9a**}.

m/z $[M]^{+\cdot}$ = 534, $[L]^{+}$ = 235

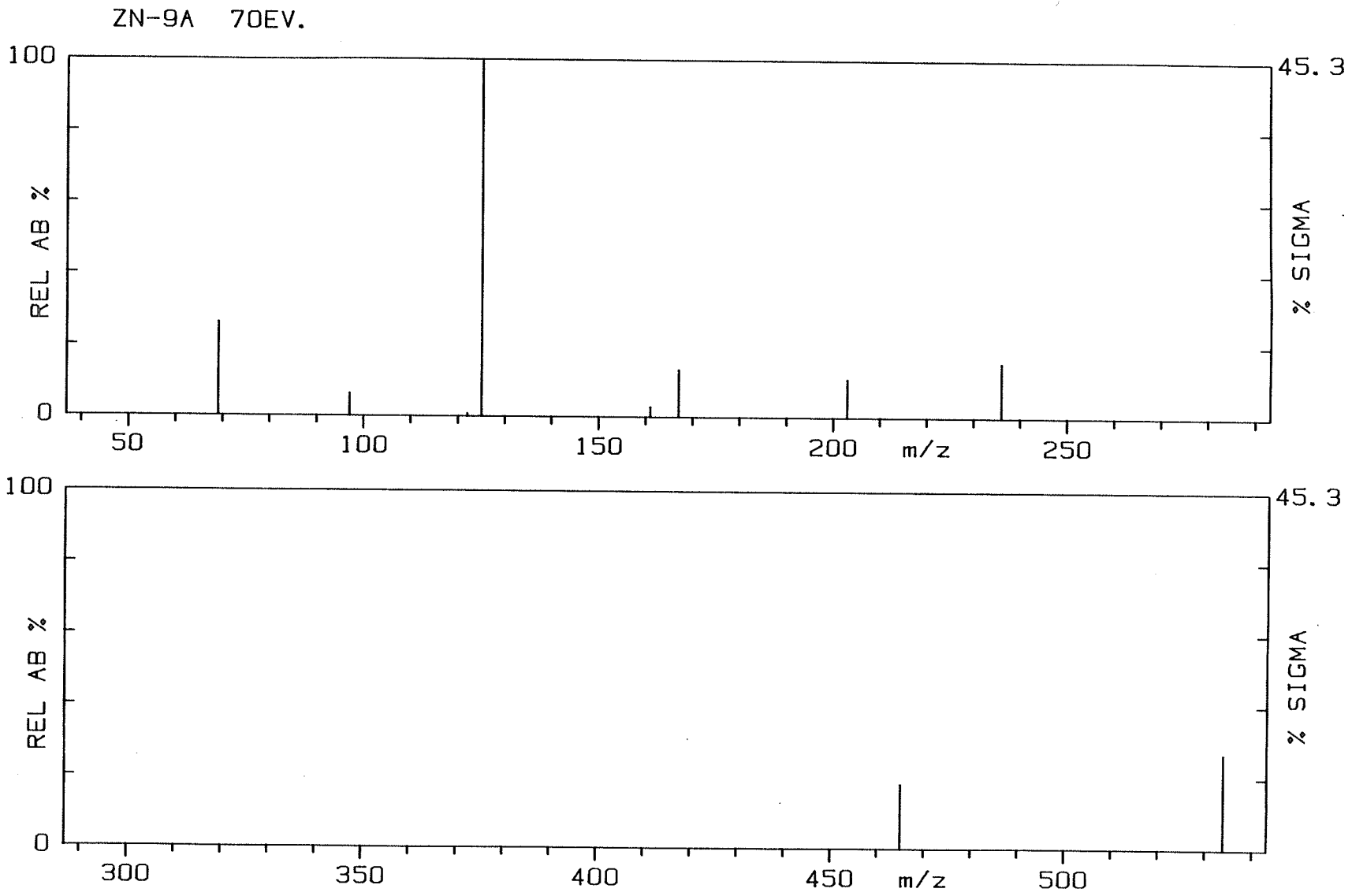
ZN-9A 70EV.
100
REL AB %
0
50
100
150
200
m/z
250
45.3
% SIGMA
100
REL AB %
0
300
350
400
450
m/z
500
45.3
% SIGMA

Figure 87.

Normalized 70 eV-EI mass spectrum of

bis[1,1,1,2,2-pentafluoro-5-phenyl-3,5-pentanedionato]Zn(II)

{**Zn-13a**}.

m/z $[M]^{+\cdot}$ = 594, $[L]^{+}$ = 265

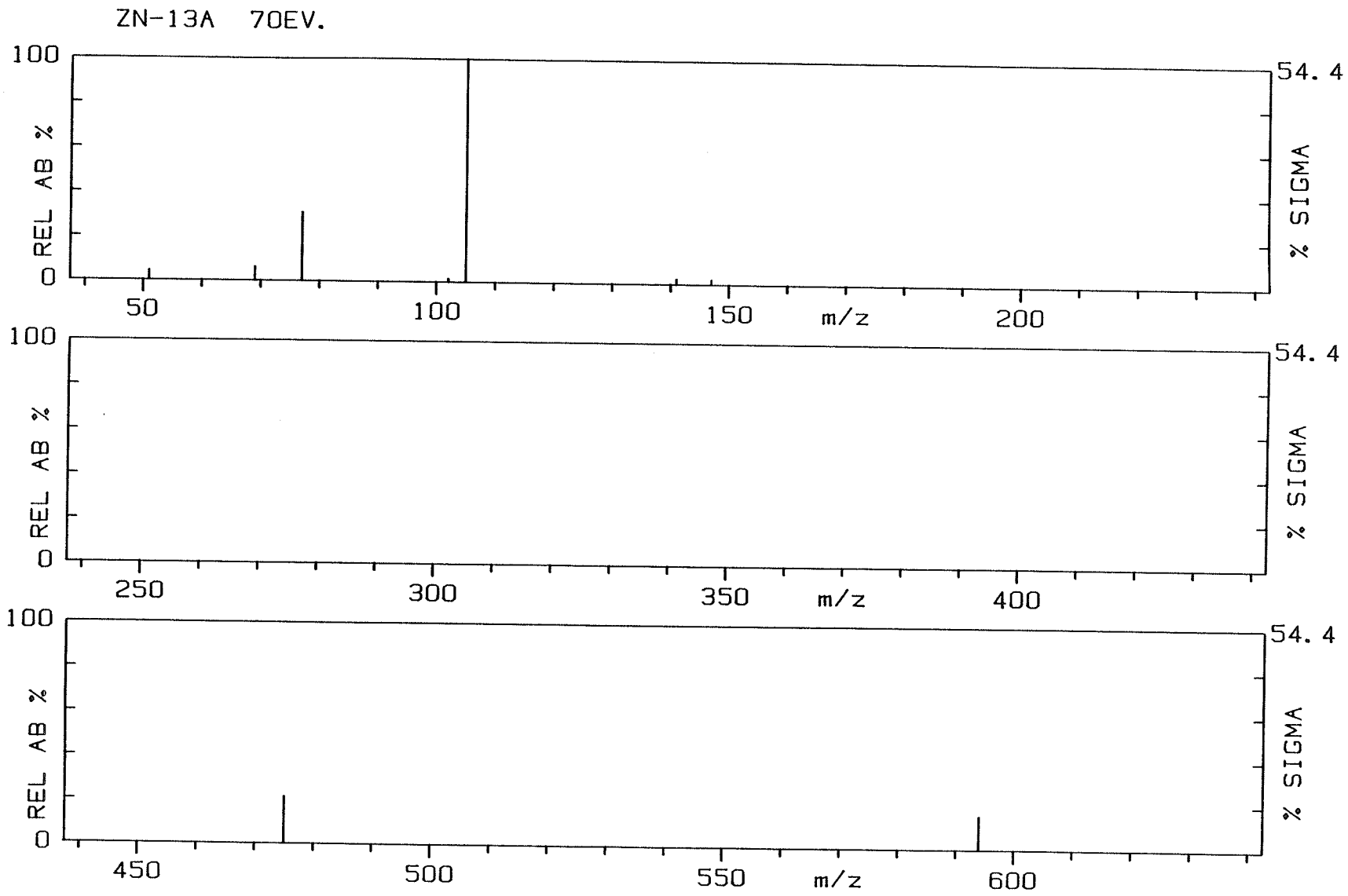
ZN-13A 70EV.
100
0
REL AB %
54.4
% SIGMA
50
100
150
m/z
200
250
300
350
400
450
500
550
600

Figure 88.

Normalized 70 eV-EI mass spectrum of

bis[1,1,1,2,2-pentafluoro-5-(2'-thienyl)-3,5-pentanedionato]Zn(II)

{Zn-14a}.

m/z $[M]^{+\cdot}$ = 606, $[L]^{+}$ = 271

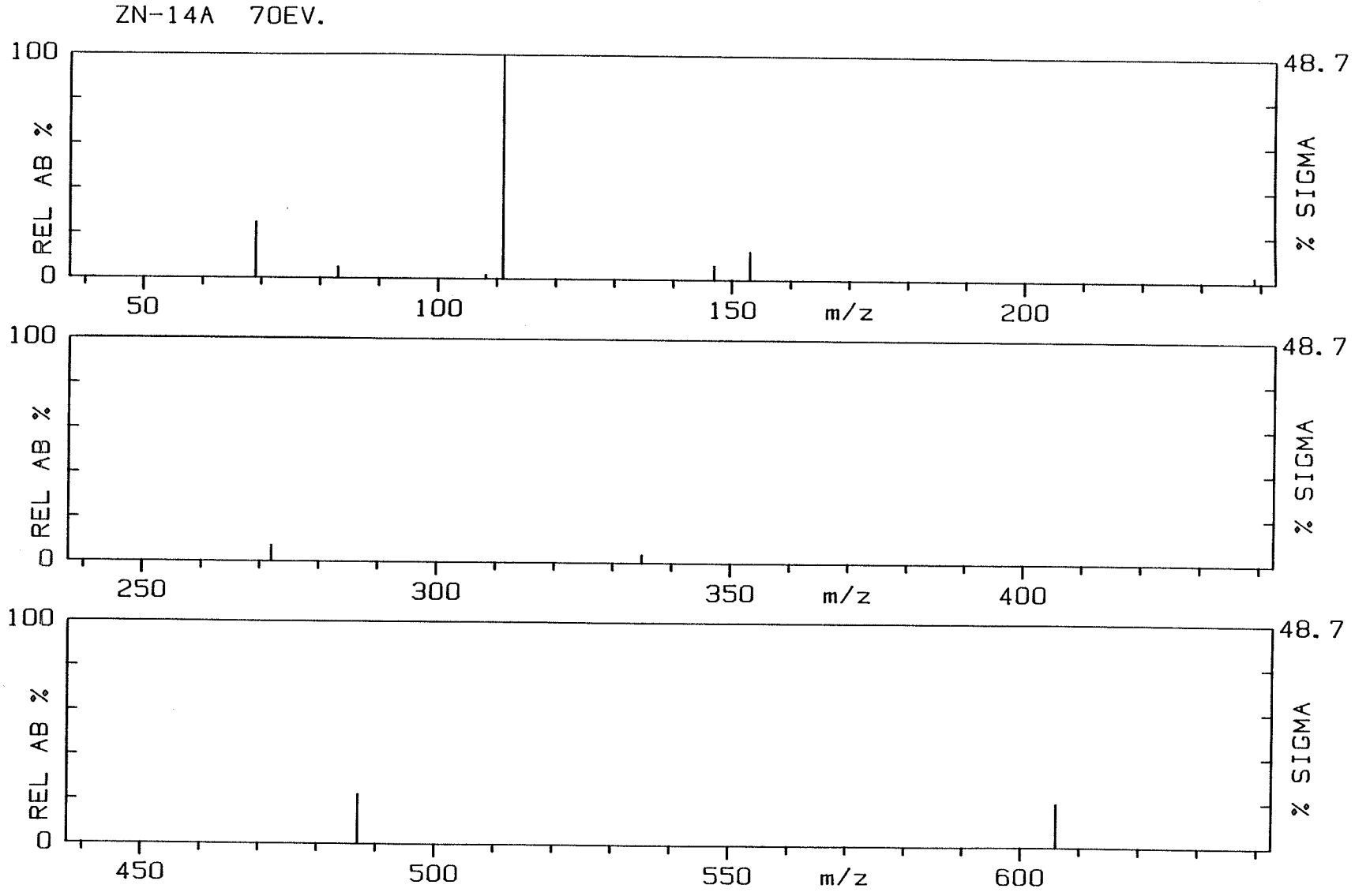
ZN-14A 70EV.
100
REL AB %
0
48.7
% SIGMA
50
100
150
m/z
200
250
300
350
400
450
500
550
600

Figure 89.

Normalized 70 eV-EI mass spectrum of

bis[1,1,1,2,2,3,3-heptafluoro-6-phenyl-4,6-hexanedionato]Zn(II)

{**Zn-16a**}.

m/z $[M]^{+\cdot}$ = 694, $[L]^{+}$ = 315

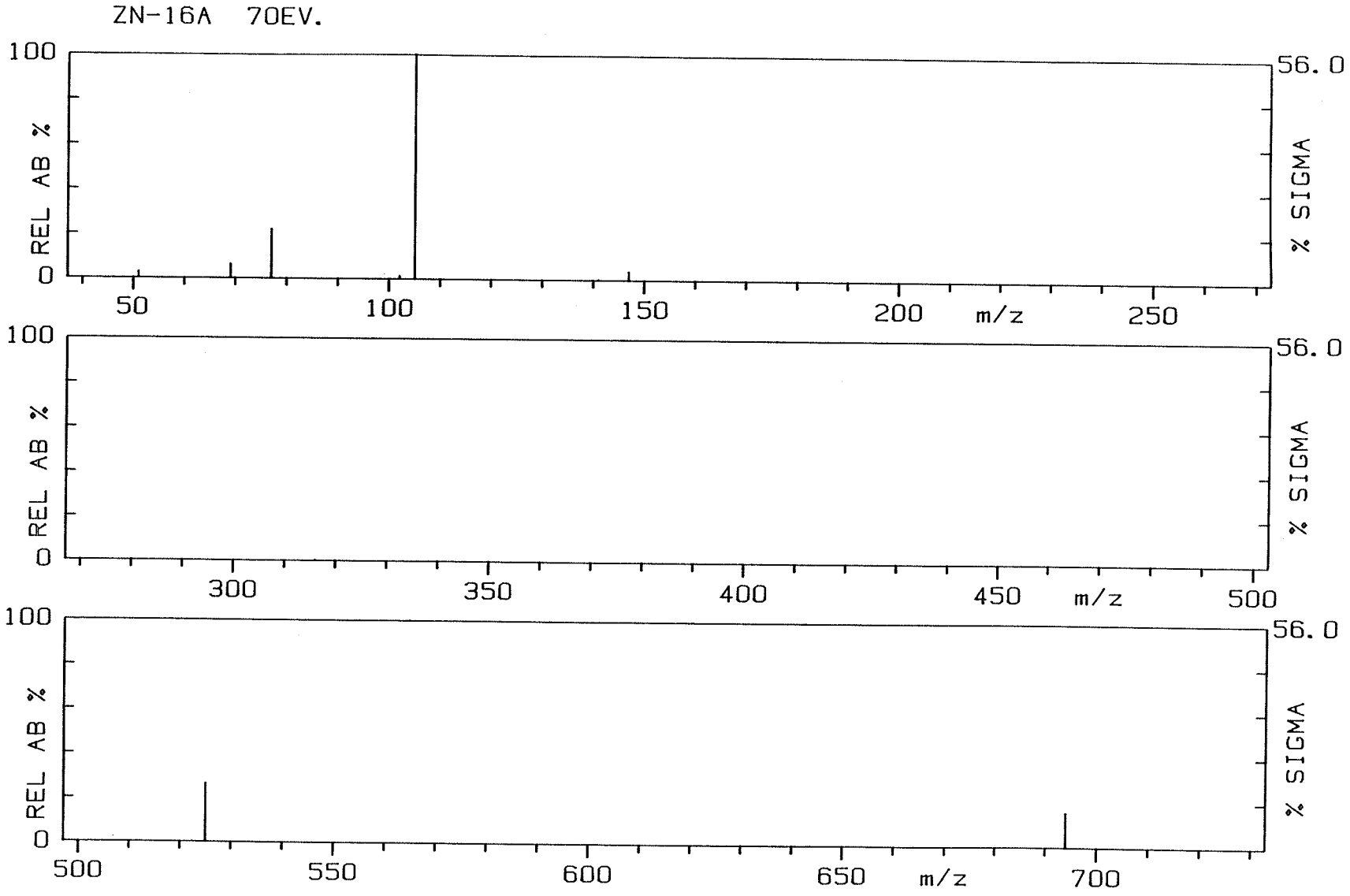
ZN-16A 70EV.
100
REL AB %
0
50
100
150
200
m/z
250
56.0
% SIGMA
100
REL AB %
0
300
350
400
450
m/z
500
56.0
% SIGMA
100
REL AB %
0
500
550
600
650
m/z
700
56.0
% SIGMA

Figure 90.

Normalized 70 eV-EI mass spectrum of

bis[1,1,1,2,2,3,3-heptafluoro-6-(2'-thienyl)-4,6-hexanedionato]Zn(II)

{**Zn-17a**}.

m/z $[M]^{+\cdot}$ = 706, $[L]^{+}$ = 321

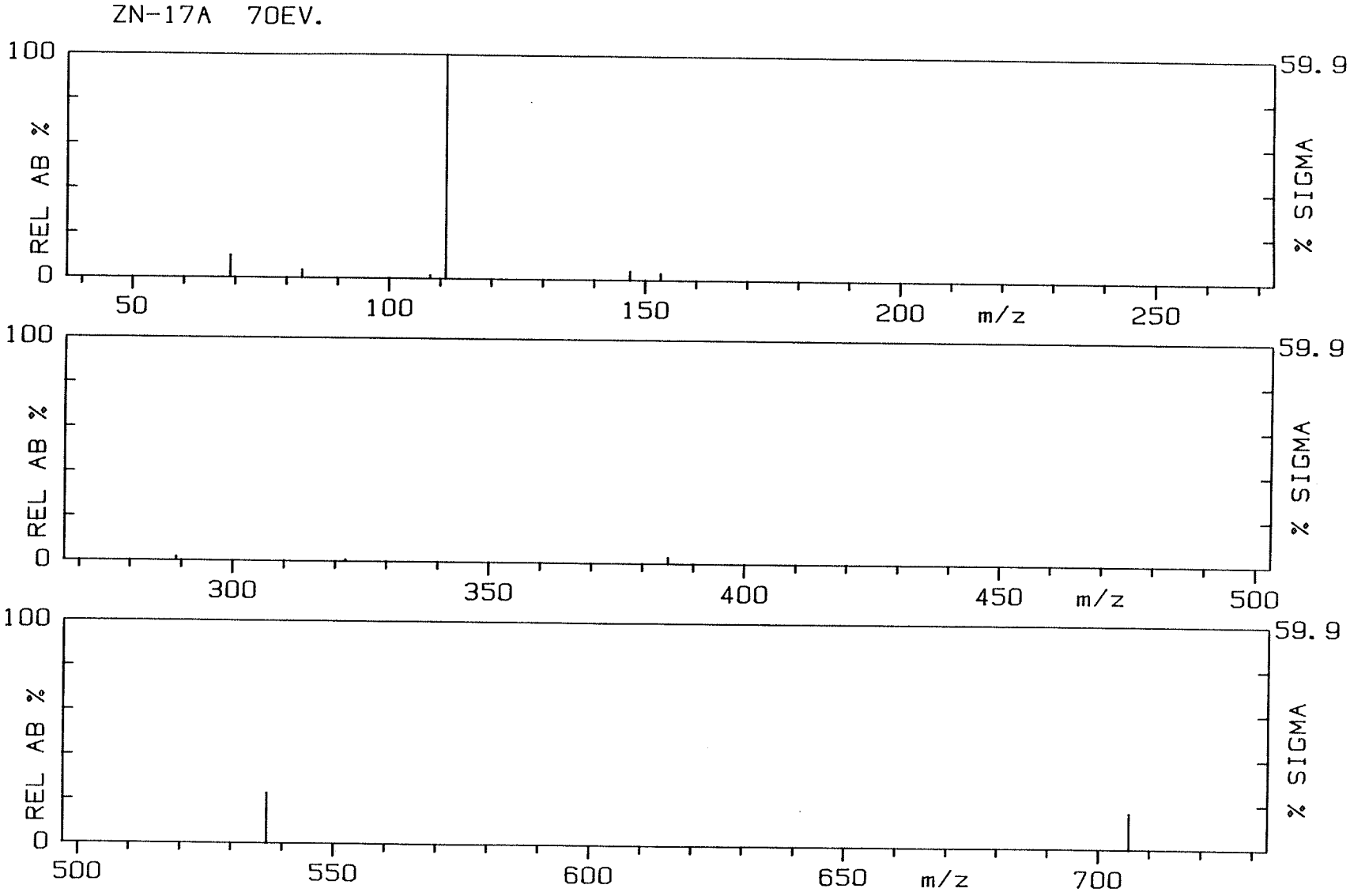
ZN-17A 70EV.
100
0
REL AB %
59.9
% SIGMA
50
100
150
200
m/z
250
300
350
400
450
500
550
600
650
700

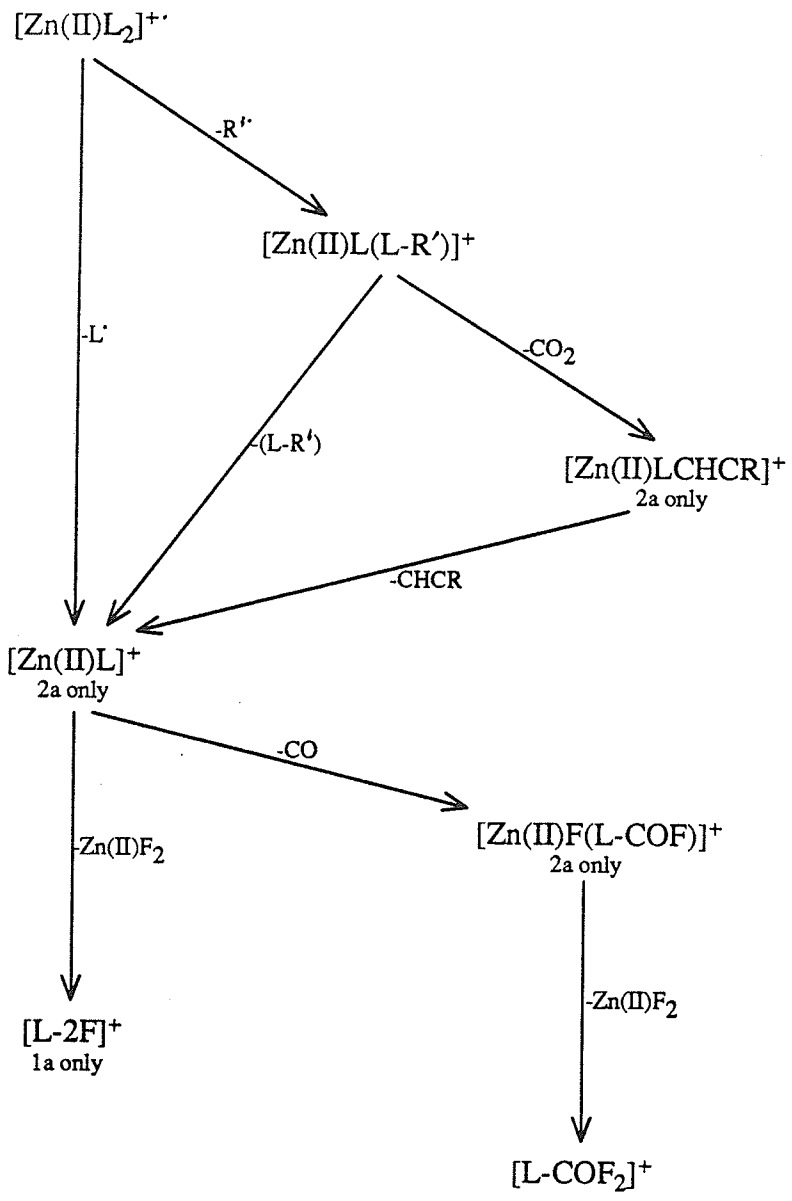

Scheme 59. Proposed fragmentation pathways for Zn(II) β-diketonates where R' = CHF_2 (**Zn-1a** and **-2a**). Pathways are common to both complexes except where noted.

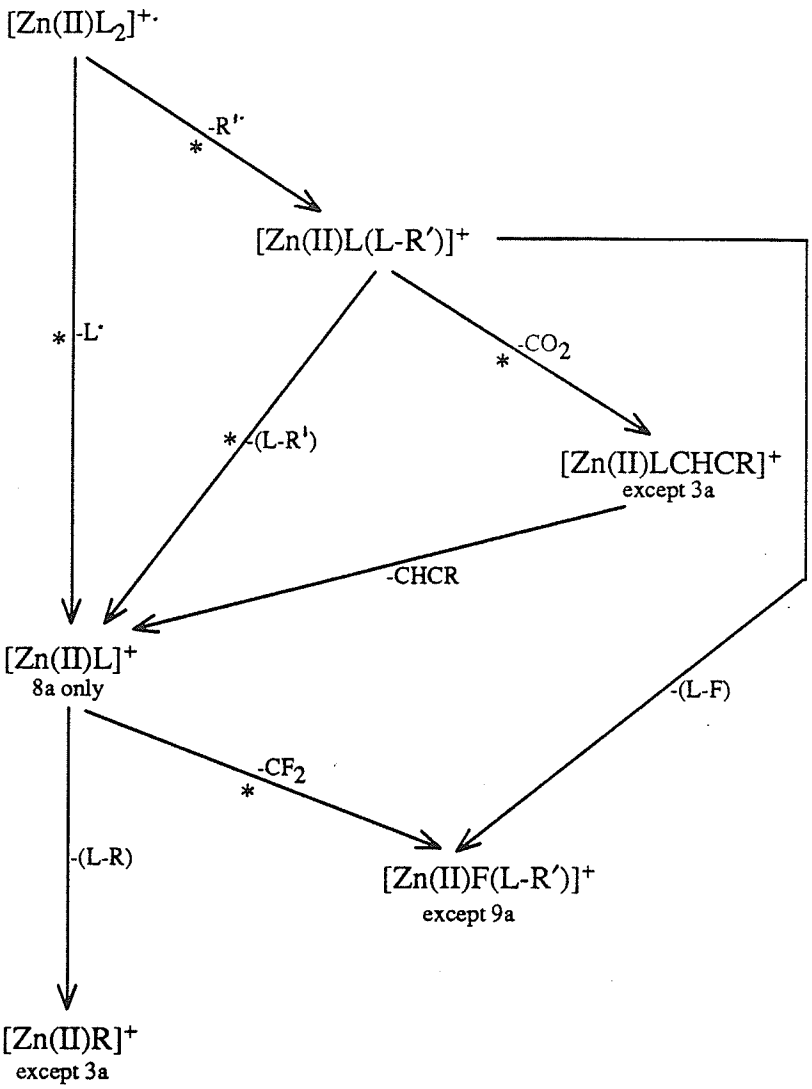

* process confirmed by the observation of a metastable transition in at least one of the complexes.

Scheme 60. Proposed fragmentation pathways for Zn(II) β-diketonates where R' = CF_3 (**Zn-3a, -8a** and **-9a**). Pathways are common to all complexes except where noted.

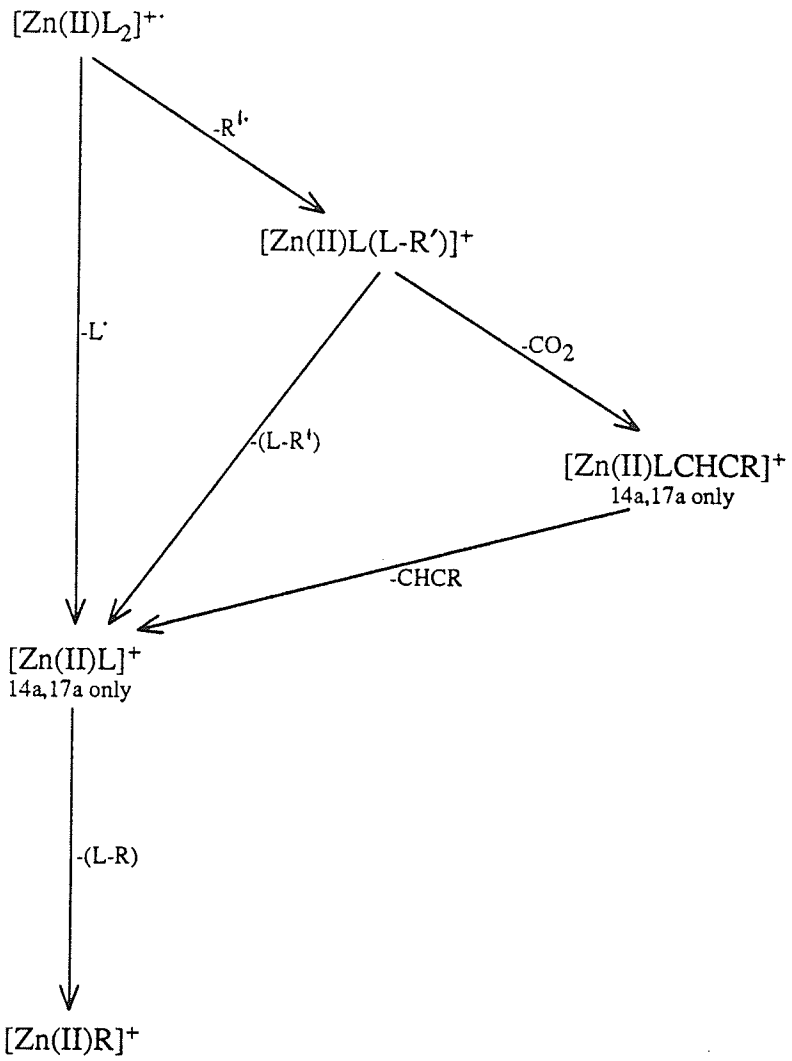

Scheme 61. Proposed fragmentation pathways for Zn(II) β-diketonates where R' = C_2F_5 (**Zn-13a** and **-14a**) or C_3F_7 (**Zn-16a** and **-17a**). Pathways are common to all complexes except where noted.